

**DITHIENOPYRROLE-BASED CONJUGATED MATERIALS FOR  
ORGANIC ELECTRONICS**

**A Dissertation  
Presented to  
The Academic Faculty**

**by**

**Xuan Zhang**

**In Partial Fulfillment  
of the Requirements for the Degree  
Doctor of Philosophy in the  
School of Chemistry and Biochemistry**

**Georgia Institute of Technology**

**December 2009**

# **DITHIENOPYRROLE-BASED CONJUGATED MATERIALS FOR ORGANIC ELECTRONICS**

Approved by:

Dr. Seth R. Marder, Advisor  
School of Chemistry and Biochemistry  
*Georgia Institute of Technology*

Dr. Jean-Luc Brédas  
School of Chemistry and Biochemistry  
*Georgia Institute of Technology*

Dr. Joseph Perry  
School of Chemistry and Biochemistry  
*Georgia Institute of Technology*

Dr. Laren M. Tolbert  
School of Chemistry and Biochemistry  
*Georgia Institute of Technology*

Dr. Bernard Kippelen  
School of Electrical and Computer  
Engineering  
*Georgia Institute of Technology*

Date Approved: October 20, 2009

## ACKNOWLEDGEMENTS

I would like to express my sincerest appreciation to my research advisor, Dr. Seth Marder, for his encouragement, guidance, and support during my study at the Georgia Institute of Technology. What I have learned in these five years is much more than how to perform chemistry experiments; it is about how to think logically and critically, how to take steps to solve problems, and how to be an independent and collaborative researcher. All these aspects will not only be very valuable to my future career, but also to my personal life, no matter where I will be and what type of job I will conduct. I also would like to thank all of my committee members for providing their valuable suggestions to this thesis. I appreciate the help from Dr. Stephen Barlow throughout the years. He reinforced my understanding of fundamental theories and experiments, and taught scientific writing to me by providing suggestions on my manuscripts and this thesis.

I would like to thank all of the collaborators from the Georgia Institute of Technology and other universities. I thank Dr. Bernard Kippelen and some of his group members for their efforts on device fabrication, specifically, William J. Potscavage, Jr. and Jaewon Shim for fabricating and testing OPV devices, Dr. Shree Prakash Tiwari and Dr. Xiaohong Zhang for fabricating and testing OFET devices, and Dr. Séverine Coppée for obtaining AFM data. I also thank Dr. Jean-Luc Brédas and his group members, Dr. Shino Ohira and Dr. Joseph Norton, for the quantum-chemical calculations. I also appreciate the

help with using instruments from various people from different group at Georgia Tech, specifically, Matthew R. Kincer in Dr. Haskell W. Backham's group and Wei Long in Dr. Christopher Jones's group for obtaining GPC data, and Benjamin K. Greve in Dr. August P. Wilkinson's group and for obtaining XRD data.

Collaborators outside Georgia Tech to whom I wish to show appreciation include Dr. Samson A. Jenekhe, and his group members, Pei-Tzu Wu, Dr. Jessica M. Hancock at the University of Washington, for collaborating on polymer synthesis and OFET device fabrication. I would like to thank Dr. John R. Reynolds and his group member, Dr. Timothy T. Steckler, at the University of Florida for the collaboration on polymer synthesis, as well as electrochemistry and spectroelectrochemistry measurements.

I would like to thank all the past and present group members in the Marder group for their great assistance and friendship. Especially, I thank Chun Huang and Anthony J. Giordano for obtaining TGA data, Dr. Raghunath R. Dasari and Dr. Qing Zhang for providing some starting materials as well as synthetic suggestions. I appreciate the help from Dr. Yadong Zhang, Dr. Mariacristina Rumi, Yanrong Shi, Dr. Hsin-Chieh Lin, Dr. Tissa Sajoto, Dr. Yulia Getmanenko, Lauren Hayden, Jonathan D. Matichak, Marsha D. Lamb, Dr. Xiaowei Zhan, Wei Zhang and others either on research or in my personal life.

My deepest gratitude goes to my family, without whose love and support I would not be who I am today. Special thanks go to my parents for their continuous support and

inspiration in my life and finally to my husband Dexing Zeng for always being there for me. This dissertation is dedicated to all of them.

# TABLE OF CONTENTS

ACKNOWLEDGEMENTS.....	iii
LIST OF TABLES.....	ix
LIST OF FIGURES .....	xi
LIST OF SCHEMES.....	xvi
LIST OF ABBREVIATIONS.....	xvii
SUMMARY .....	xviii
CHAPTER 1	
INTRODUCTION .....	1
1.1 Organic Semiconductors.....	1
1.2 Charge Transport in Organic Semiconductors.....	2
1.2.1 Charge-Carrier Mobility .....	2
1.2.2 Theoretical Aspects of Charge Transport in Organic Semiconductors .....	3
1.2.3 Mobility Measurements .....	6
1.3 Organic Electronic Devices Involving Charge Transport.....	9
1.3.1 Organic Field-Effect Transistors.....	10
1.3.2 Organic Photovoltaics .....	13
1.3.3 Organic Light-Emitting Diodes .....	17
1.4 Organic Semiconductors Used in OFETs and OPVs.....	18
1.4.1 Small Molecules as Active Semiconductors in OFETs .....	19
1.4.2 Conjugated Polymers as Active Semiconductors in OFETs .....	27
1.4.3 Small Molecules as Active Semiconductors in OPVs .....	34
1.4.4. Conjugated Polymers as Active Semiconductors in OPVs .....	37
1.5 Organization of the Thesis .....	46
1.6 References.....	48

## CHAPTER 2 N-ARYL DITHIENOPYRROLE

DIMER, TRIMER AND HOMOPOLYMER .....	56
2.1 Introduction.....	56
2.2 Synthesis .....	59
2.3 Density Functional Theory Calculation of Electronic Structure.....	64
2.4 Optical Properties.....	67
2.5 Electrochemical Properties .....	69
2.6 XRD .....	71
2.7 Chemical Oxidation of <b>1-3</b> and <b>P1</b> .....	72
2.8 Electropolymerization and Spectroelectrochemistry of <b>P2</b> .....	77
2.9 Conclusions.....	80
2.10 Experimental Section .....	80
2.11 References.....	93

## CHAPTER 3 N-ALKYL DITHIENOPYRROLE-BASED

DONOR-DONOR COPOLYMERS.....	95
3.1 Introduction.....	95
3.2 Synthesis .....	98
3.3 Density Functional Theory Calculations of Electronic Structure .....	104
3.4 Optical Properties.....	106
3.5 Electrochemical Properties .....	109
3.6 Field-Effect Transistor Characteristics .....	111
3.7 Photovoltaic Cell Characteristics .....	113
3.8 Conclusions.....	117
3.9 Experimental Section .....	118
3.10 References.....	130

## CHAPTER 4 DITHIENOPYRROLE-BENZOTHIADIAZOLE

DONOR-ACCEPTOR COPOLYMERS .....	132
4.1 Introduction.....	132
4.2 Synthesis .....	134
4.3 Density Functional Theory Calculations of Electronic Structure .....	137
4.4 Optical and Electrochemical Properties.....	139
4.5 Aggregation Study of <b>P4</b> .....	144
4.6 Spectroelectrochemistry.....	146
4.7 Field-Effect Transistor Characteristics .....	150
4.8 Photovoltaic Cell Characteristics.....	154
4.9 Conclusions.....	159
4.10 Experimental Section .....	160
4.11 References.....	170

## CHAPTER 5 DITHIENOPYRROLE- QUINOXALINE/PYRIDOPYRAZINE

DONOR-ACCEPTOR COPOLYMERS .....	172
5.1 Introduction.....	172
5.2 Synthesis .....	175
5.3 Density Functional Theory Calculations of Electronic Structure .....	182
5.4 Optical and Electrochemical Properties.....	183
5.5 Field-Effect Transistor Characteristics .....	188
5.6 Photovoltaic Cell Characteristics.....	190
5.7 Conclusions.....	195
5.8 Experimental Section .....	196
5.9 References.....	211
CHAPTER 6 CONCLUSIONS .....	212

## LIST OF TABLES

<b>Table 2.1</b> Optical and redox properties of the compounds in Chapter 2.....	69
<b>Table 3.1</b> Reaction conditions and results for DTP disubstitution optimization .....	100
<b>Table 3.2</b> Yields, molecular weights, and thermal data for <b>P1-P5</b> . ....	103
<b>Table 3.3</b> HOMO, LUMO, $E_g$ , and $S_1$ transition energies extrapolated for $(DTP-X)_\infty$ . ....	105
<b>Table 3.4</b> Optical and redox properties of the polymers. ....	109
<b>Table 3.5</b> Field-effect transistor characteristics of <b>P1-3</b> and <b>P5</b> .....	111
<b>Table 3.6</b> Photovoltaic cell performance of <b>P1-3</b> /PCBM blends.....	113
<b>Table 4.1</b> Yields, molecular weights and thermal properties of the copolymers. ....	136
<b>Table 4.2</b> HOMO, LUMO, $E_g$ , and $S_1$ transition energies extrapolated for $(DTP-X)_\infty$ . ....	139
<b>Table 4.3</b> Optical and redox properties of the polymers. ....	142
<b>Table 4.4</b> Images of colored neutral and redox states of films of <b>P1-5</b> . ....	149
<b>Table 4.5</b> Field-effect transistor characteristics of <b>P1-3</b> . ....	151
<b>Table 4.6</b> Photovoltaic cell performance of <b>P1-3</b> with different conditions. ....	156
<b>Table 5.1</b> Reaction condition and results for preparation of <b>M4</b> .....	177
<b>Table 5.2</b> Yields, molecular weights and thermal properties of the copolymers. ....	181
<b>Table 5.3</b> Extrapolated HOMO, LUMO, $E_g$ , and $S_1$ transition energies.....	183
<b>Table 5.4</b> Optical and redox properties of the polymers .....	186
<b>Table 5.5</b> Field-effect transistor characteristics of <b>P1- 3</b> . ....	189

<b>Table 5.6</b> Photovoltaic cell performance of <b>P1-4</b> blended with PCBM.....	191
--	-----

## LIST OF FIGURES

<b>Figure 1.1</b> Schematic illustration of a) electron transport in the CB of inorganic conductors ( $E_g$ is the energy gap between the CB and VB); b) discrete energy levels in organic semiconductors ( $E_g$ is the energy gap between the HOMO and LUMO levels); c) electron hopping through LUMO levels of organic semiconductors.....	4
<b>Figure 1.2</b> Schematic illustration of the potential energy surfaces for neutral and ionized state in the molecule. (Figure modified from ref 9).....	6
<b>Figure 1.3</b> Schematic illustration of TOF method. ....	7
<b>Figure 1.4</b> Schematic representations of four different OFET geometries. ....	10
<b>Figure 1.5</b> Typical I-V curves of an OFET device: (a) output curve at different constant $V_G$ and (b) transfer curve at a constant $V_{SD}$ . ....	12
<b>Figure 1.6</b> Schematic illustration of an OPV device.....	14
<b>Figure 1.7</b> Schematic illustrations of a) main processes governing the operation of OPVs; b) typical J-V curves in an OPV device under dark (dotted line) and under illumination (solid line) (Figure taken from ref 30). ....	15
<b>Figure 1.8</b> Structures of acenes (compounds <b>1-7</b> ).....	20
<b>Figure 1.9</b> Structures of oligothiophenes (compounds <b>8a-k</b> ). ....	22
<b>Figure 1.10</b> Structures of oligothiophenes (compounds <b>9-14</b> ).....	24
<b>Figure 1.11</b> Structures of other small-molecule systems (compounds <b>15-22</b> ).....	25
<b>Figure 1.12</b> Structures of P3ATs and functionalized polythiophenes (compounds <b>23-26</b> ). ....	28
<b>Figure 1.13</b> Structures of other thiophene-containing polymers (compounds <b>27-34</b> ). ....	31
<b>Figure 1.14</b> Structures of other polymeric systems (compounds <b>35-39</b> ). ....	33
<b>Figure 1.15</b> Structures of small molecules (compounds <b>40-44</b> ) for OPVs. ....	34

<b>Figure 1.16</b> Structures of polythiophenes and other thiophene-containing polymers in OPVs (compounds <b>45-52</b> ).....	40
<b>Figure 1.17</b> Structures of fluorene- and carbazole-based copolymers (compounds <b>53-54</b> ). .....	43
<b>Figure 1.18</b> Structures of other polymeric systems in OPVs (compounds <b>55-57</b> ). ....	45
<b>Figure 2.1</b> Structures of the compounds ( <b>I-IV</b> ) discussed in the text. ....	58
<b>Figure 2.2</b> Target compounds in Chapter 2.....	59
<b>Figure 2.3</b> Representative HOMO/LUMO wavefunctions of a DTP oligomer (n = 6) ..	66
<b>Figure 2.4</b> UV-vis spectra of <b>1-3</b> and <b>P1</b> in a) dilute solutions in dichloromethane and b) thin films. ....	68
<b>Figure 2.5</b> Cyclic voltammogram of <b>1-3</b> at a scan rate of 50 mV/sec. ....	70
<b>Figure 2.6</b> Cyclic voltammogram of <b>P1</b> film at a scan rate of 50 mV/sec.....	71
<b>Figure 2.7</b> XRD pattern (smoothed) of <b>2</b> . ....	72
<b>Figure 2.8</b> Visible-NIR absorption spectra of monocations of <b>1-3</b> in dichloromethane, a) x-axis in wavelength, b) x-axis in eV. The onsets of strong absorption at high energy (at <i>ca.</i> 600 nm) in <b>2</b> correspond to absorption by the excess neutral compound present.....	74
<b>Figure 2.9</b> UV-visible-NIR absorption spectra of <b>P1</b> upon increasing additions of oxidant, a) x-axis in wavelength, b) x-axis in eV.. ....	75
<b>Figure 2.10</b> Polymer growth on Pt working electrode in 0.1 M [ <sup>n</sup> Bu <sub>4</sub> N] <sup>+</sup> [ClO <sub>4</sub> ] <sup>-</sup> solution. ....	78
<b>Figure 2.11</b> Spectroelectrochemistry of <b>P2</b> film on ITO glass. Bold red line = neutral (-0.21 V) and bold black line = oxidized state (1.04V), a) x-axis in wavelength, b) x-axis in eV.....	79
<b>Figure 3.1</b> Structures of some polymers discussed in the text. ....	96

<b>Figure 3.2</b> Structures of target polymers in Chapter 3.....	97
<b>Figure 3.3</b> TGA curves of <b>P1-P5</b> .....	104
<b>Figure 3.4</b> HOMO/LUMO wavefunctions of donor-donor oligomers ( $n = 3$ ) .....	106
<b>Figure 3.5</b> UV-vis spectra of copolymers <b>P1-5</b> in (a) dilute THF and (b) thin film.....	108
<b>Figure 3.6</b> Cyclic voltammogram of <b>P4</b> film at a scan rate of 50 mV/sec.....	110
<b>Figure 3.7</b> Output (left) and transfer (right) characteristics of an OFET of <b>P2</b> under $N_2$ . .....	112
<b>Figure 3.8</b> $J$ - $V$ characteristics of cells made from films of PCBM blended with each of polymers in a 1:1 weight ratio before (left) and after (right) annealing at 100 °C for 10 mins. (Inset shows the same data in a semilogarithmic plot). .....	113
<b>Figure 3.9</b> AFM phase images of the blends of <b>P2</b> /PCBM (1:1 w:w) before (a) and after (b) annealing at 100 °C for 10 mins (vertical scale are 15, 30° for a and b, respectively). .....	115
<b>Figure 3.10</b> XRD Patterns (smoothed) of blends of <b>P2</b> /PCBM (1:1 w:w): a) not annealed, b) after annealing at 100 °C for 10 mins. ....	116
<b>Figure 3.11</b> EQE as a function of wavelength of a device based on a <b>P2</b> /PCBM blend .....	117
<b>Figure 4.1</b> TGA curves of <b>P1-P5</b> .....	137
<b>Figure 4.2</b> Representative HOMO and LUMO wavefunctions of an oligomeric derivative $H(DTP-BThBBT)_2H$ . ....	139
<b>Figure 4.3</b> UV-vis-NIR spectra of copolymers <b>P1-3</b> in THF and in thin films. ....	141
<b>Figure 4.4</b> UV-vis-NIR spectra of copolymers <b>P4-5</b> in THF and in thin films. ....	141
<b>Figure 4.5</b> Representative cyclic voltammograms for the copolymers (left for <b>P1</b> and right for <b>P3</b> ).....	144

<b>Figure 4.6</b> Solution thermochromism of <b>P4</b> in dilute toluene from 10-90 °C. ....	145
<b>Figure 4.7</b> UV-vis-NIR spectra of dilute solution of <b>P4</b> and <b>P6</b> in toluene.....	146
<b>Figure 4.8</b> Oxidative spectroelectrochemistry of <b>P1</b> spray-cast onto ITO from -0.16 V to 1.24 V vs. SCE in 100 mV increments. Bold black line = neutral (-0.16 V) and bold orange line = oxidized state (1.24 V), a) x-axis in wavelength, b) x-axis in eV.. ....	147
<b>Figure 4.9</b> Reductive spectroelectrochemistry of <b>P1</b> spray-cast onto ITO, from -0.92 V to -1.72 V vs. SCE in 100 mV increments. Bold black line = neutral (-0.92 V), bold pink line = beginning of intermediate reduced state (-1.42 V), and bold navy blue line = fully reduced state (-1.72 V), a) x-axis in wavelength, b) x-axis in eV.. ....	148
<b>Figure 4.10</b> Output (a) and transfer (b) characteristics of an OFET based on <b>P1</b> . ....	152
<b>Figure 4.11</b> Output (a) and transfer (b) characteristics of an OFET based on <b>P2</b> . ....	153
<b>Figure 4.12</b> Output characteristics (p-type and n-type) of an OFET based on <b>P3</b> .....	153
<b>Figure 4.13</b> <i>J-V</i> characteristics of multiple cells measured in the dark (dashed line) and under illumination (solid line) for films of PCBM blended with each of the following polymers in a 1:1 weight ratio. (Inset shows the same data in a semilogarithmic plot). ....	157
<b>Figure 4.14</b> AFM tapping-mode height images of <b>P1</b> /PCBM (1:3 weight ratio) film surface processed from a) chlorobenzene, b) <i>o</i> -xylene and c) toluene. The vertical gray scale is 20 nm for a) and b) and 80 nm for c). ....	157
<b>Figure 4.15</b> External quantum efficiency (EQE) as a function of wavelength of a device made from a blend of <b>P1</b> /PCBM (1:1 w:w).....	158
<b>Figure 5.1</b> Structures of some polymers discussed in the text. ....	173
<b>Figure 5.2</b> Structures of the target polymers in Chapter 5. ....	175
<b>Figure 5.3</b> TGA curves of <b>P1-4</b> . ....	181
<b>Figure 5.4</b> HOMO/LUMO wavefunctions of representative oligomers (n=3). ....	183
<b>Figure 5.5</b> UV-vis-NIR spectra of <b>P1-4</b> in (a) dilute THF solution and (b) thin films..	185

<b>Figure 5.6</b> Oxidative (blue line) and reductive (red line) CV of <b>P4</b> film at a scan rate of 50 mV/sec. ....	187
<b>Figure 5.7</b> Output (left) and transfer (right) and characteristics of a OFET of <b>P3</b> . ....	190
<b>Figure 5.8</b> Representative <i>J-V</i> characteristics of multiple cells measured in the dark (dashed line) and under illumination (solid line) for films of PCBM blended with <b>P3</b> in a 1:3 weight ratio. (Inset shows the same data in a semilogarithmic plot).....	192
<b>Figure 5.9</b> AFM images of <b>P3</b> /PCBM blend films (a, 1:1; b, 1:3; c, 1:6) (left, height image, vertical scale is 50 nm for all three images; right, phase image, vertical scale are 70, 80, 45°, respectively for a, b and c).....	194
<b>Figure 5.10</b> EQE spectra as a function of wavelength of devices made from <b>P3</b> /PCBM blends. ....	195

## LIST OF SCHEMES

<b>Scheme 2.1</b> Generic catalytic mechanism of Pd-catalyzed cross-coupling reactions.....	60
<b>Scheme 2.2</b> Synthesis of <b>1</b> , <b>2</b> and <b>P1</b> .....	61
<b>Scheme 2.3</b> Synthesis of dimer <b>3</b> . ....	63
<b>Scheme 3.1</b> Synthesis of DTP-based monomers.....	99
<b>Scheme 3.2</b> Synthesis of TMS-substituted DTP. ....	99
<b>Scheme 3.3</b> Synthesis of other monomers.....	101
<b>Scheme 3.4</b> Synthesis of <b>P1-P5</b> .....	102
<b>Scheme 3.5</b> Attempted polymerizations of DTP and fluorene using Stille and Suzuki couplings. ....	103
<b>Scheme 4.1</b> Synthesis of <b>P1-5</b> .....	135
<b>Scheme 5.1</b> Synthesis of <b>M1-2</b> .....	176
<b>Scheme 5.2</b> Synthesis of <b>M3-4</b> .....	177
<b>Scheme 5.3</b> Trial polymerizations in Chapter 5. ....	179
<b>Scheme 5.4</b> Synthesis of <b>P1-4</b> .....	180

## LIST OF ABBREVIATIONS

AFM	Atom Force Microscopy
Cp	Cyclopentadienyl, C <sub>5</sub> H <sub>5</sub>
DMF	Dimethylformamide
HOMO	Highest Occupied Molecular Orbital
HRMS	High Resolution Mass Spectrometry
LUMO	Lowest Unoccupied Molecular Orbital
NIR	Near Infrared
NMR	Nuclear Magnetic Resonance
THF	Tetrahydrofuran
UV-vis	Ultra Violet-Visible
XRD	X-Ray Diffraction

Other abbreviations and symbols are explained in the text.

## SUMMARY

Dithienopyrrole-based conjugated materials, including oligomers and polymers, for potential organic electronic applications, were designed, synthesized and characterized. The optical and electrochemical properties of these materials were investigated, and their structure-property relationships were studied. Some of the materials can be oxidized (or reduced) chemically or electrochemically. Furthermore, the utility of these materials in organic electronic devices, such as OFETs and OPVs, were assessed. In OFETs, they can function as hole-transport materials with mobilities up to  $4.8 \times 10^{-2} \text{ cm}^2/(\text{Vs})$ , and one example serves as an ambipolar material with comparable hole and electron mobilities of  $1.2 \times 10^{-3}$  and  $5.8 \times 10^{-4} \text{ cm}^2/(\text{Vs})$ , respectively. Some of the materials can also be used as electron donors in OPVs in conjunction with PCBM, and exhibited power conversion efficiencies up to 1.4% after optimizations. They may also be used in other applications such as electrochromic devices, photodetectors, and optical limiting.

# CHAPTER 1

## INTRODUCTION

### 1.1 Organic Semiconductors

Organic charge-transport semiconducting materials have drawn increasing interest due to their potential use in applications including organic light-emitting diodes (OLEDs), organic photovoltaic cells (OPVs), and organic field-effect transistors (OFETs).<sup>1-3</sup> Devices using organic materials are attractive because the optical and electronic properties of the materials can be easily tuned by structural modification; they have the potential to be easily processed and patterned from solution by screen printing, ink-jet printing or other methods; and the low temperature processing techniques allow device fabrication on transparent plastic substrates, leading to the possibility of flexible devices. Therefore, organic semiconductors act as promising candidates for lightweight, low-cost, and flexible electronic and optoelectronic devices.<sup>4,5</sup>

Organic semiconductors have several unique features compared to their inorganic counterparts, such as Si, GaAs.<sup>6,7</sup>  $\pi$ -electrons in organic semiconductors are delocalized on individual molecules (or individual conjugated polymer chains), whereas in traditional inorganic semiconductors, there is considerable delocalization arising from  $\sigma$ -bonded lattice. Also, in contrast to inorganic semiconductors connected by a network of covalent bonds, intermolecular (or interchain) interactions in organic materials are based on weaker interactions, such as van der Waals,  $\pi$ - $\pi$  and dipole-dipole interactions. These characteristics make the charge transporting mechanisms, optical (absorption, emission

*etc.*) and electronic properties of organic semiconductors generally different from traditional inorganic semiconductors.

Organic semiconductors can be classified in different ways. One is distinguished by the molecular weights of the materials; they can be classified into small molecules (or oligomers) and polymers. In general, devices based on small molecules are fabricated by vacuum deposition (although a few examples using solution processing techniques), whereas most of polymers can be processed and patterned from solution. Another way to classify them is based on the types of the charge carriers; they can be divided into hole transporting materials, electron transporting materials, and ambipolar transporting materials, *i.e.*, materials that can transport both electrons and holes. They can also be classified into crystalline, liquid crystal or amorphous materials.

In the following sections, the general background of charge transport in organic materials, the principles of organic electronic devices, and the progress of existing organic materials for OFETs and OPVs are reviewed.

## **1.2 Charge Transport in Organic Semiconductors**

### **1.2.1 Charge-Carrier Mobility<sup>8</sup>**

One of the key parameters to characterize charge-transport materials is the charge-carrier mobility. In the absence of any external potential, the transport of charges is purely diffusive; whereas applying an external electric field can induce a drift of the charge carriers. In this circumstance, the mobility ( $\mu$ ,  $\text{cm}^2/(\text{Vs})$ ) can be defined as the

ratio between the carrier speed ( $v$ , cm/s) and the strength of electric field ( $E$ , V/cm) as expressed in Equation 1.1:

$$\mu = v/E \quad (1.1)$$

High charge-carrier mobilities are generally required in the electronic devices. For examples, in OFETs, high charge-carrier mobility can yield fast switching speed; in OPVs, sufficient charge-carrier mobility is needed to avoid the recombination of the oppositely charged species before they are collected at the electrodes.<sup>9</sup>

### 1.2.2 Theoretical Aspects of Charge Transport in Organic Semiconductors

The charge transport process in traditional inorganic semiconductors, such as single-crystal Si, is usually described by the band model, consisting of a valence band (VB, the highest energy occupied band) and a conduction band (CB, the lowest energy unoccupied band). Charge carriers can be produced by removing electrons from the VB, by adding electrons into the CB, or by promoting electrons from the VB to the CB to generate excitons that can be dissociated into free charge carriers under an applied field at non-zero temperatures. Free charge carriers can move in the highly delocalized states within the bands (Figure 1.1a).<sup>10</sup> As a general rule, bandwidths of at least 0.1 eV are needed to make band transport possible.<sup>11</sup> The charge-transport process in the band model is limited by phonons (lattice vibrations), which scatter the charge carriers. Accordingly, as the temperature increases, the frequency of the lattice vibrations and the scattering of the charge carriers by phonons are increased, and, thus, the charge carrier mobility is decreased.

For disordered organic semiconductors, only weak intermolecular interactions are operative, and usually these materials are described in term of discrete energy levels instead of energy bands.<sup>12</sup> Charge-transport process in those materials is considered as hopping process of charge carriers between the localized states. Compared to the phonon-limited charge-transport process in the band model, the hopping process is phonon-assisted, and usually the charge-carrier mobilities increase with increasing temperatures. However, it is still debated as to whether the charge-transport mechanism in highly ordered molecular crystals should be explained using a band or hopping model.

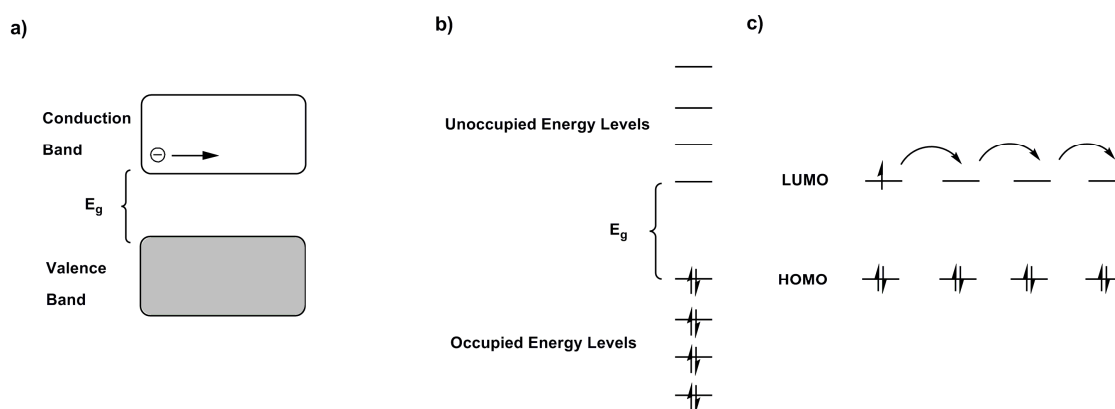


**Figure 1.1** Schematic illustration of a) electron transport in the CB of inorganic semiconductors ( $E_g$  is the energy gap between the CB and VB); b) discrete energy levels in organic semiconductors ( $E_g$  is the energy gap between the HOMO and LUMO levels); c) electron hopping through LUMO levels of organic semiconductors.

At the molecular level, the charge-transport mechanism is considered as a phonon-assisted hopping process involving an electron transfer from a charged molecule to an adjacent neutral molecule.<sup>13</sup> In the context of semi-classical electron-transfer theory, the electron-transfer rate,  $k_{ET}$ , for an electron-transfer with zero free-energy change, can be described as in Equation 1.2:

$$k_{ET} = \frac{4\pi^2}{h} \frac{1}{\sqrt{4\pi k_B T}} t^2 \exp\left(-\frac{\lambda}{4k_B T}\right) \quad (1.2)$$

where  $T$  is the temperature,  $\lambda$  is the reorganization energy,  $t$  is the transfer integral, and  $h$  and  $k_B$  are the Planck and Boltzmann constants, respectively. From this equation, it is seen that both reorganization energy and transfer integral play important roles in the understanding of the charge transport process of organic semiconductors. In order to have a large charge-transfer rate, and thus a high charge-carrier mobility in the material, the reorganization energy should be small and the transfer integral large. The transfer integral reflects the strength of the interaction (electronic coupling) between the two molecules. Large orbital overlap leads to a large intermolecular transfer integral. The reorganization energy  $\lambda$  is the sum of the inner and outer contributions. The internal reorganization energy can be defined as the energy cost due to geometry modifications in the molecule when going from the neutral to the ionized state and vice versa. It can be expressed as the sum of  $\lambda_{i1}$  and  $\lambda_{i2}$  (Figure 1.2), which can be defined as follows:  $\lambda_{i1}$  is the difference between the energies of the neutral molecule in the relaxed charged geometry and the neutral molecule in its equilibrium geometry; and  $\lambda_{i2}$  is the difference between the energy of the charged molecule in the geometry of the neutral species and the charged molecule in its equilibrium geometry. The outer reorganization energy is due to the electronic and nuclear polarization/relaxation of the surrounding media.

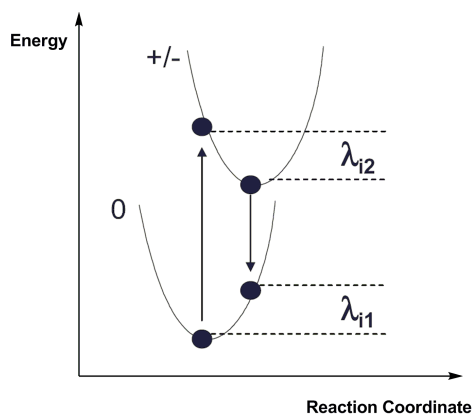


**Figure 1.2** Schematic illustration of the potential energy surfaces for neutral and ionized state in the molecule. (Figure modified from ref 9)

### 1.2.3 Mobility Measurements

Charge-carrier mobility can be determined by various experimental techniques. Commonly used mobility measurements methods include time-of-flight (TOF), field-effect transistor (FET), space-charge limited current (SCLC) method, and pulse-radiolysis time-resolved microwave conductivity (PR-TRMC) techniques. The determination of the charge carrier mobility from FET method will be described later in section 1.3.1.

TOF is one of the most extensively employed methods to determine the carrier mobility. In this method, a thick organic layer (usually 5-20 microns) is sandwiched between a transparent electrode (typically indium tin oxide, ITO) and a metal electrode. The material is irradiated by a laser pulse near one of the electrodes generating excited states that under an applied electric field can dissociate to electrons and holes. The photogenerated holes or electrons migrate towards the second electrode depending on the polarity of the applied bias and the corresponding electric field. The photocurrent is recorded as a function of time and the mobility of the charge carriers is derived via:

$$\mu = \frac{v}{E} = \frac{d}{Et} = \frac{d^2}{Vt} \quad (1.3)$$

where  $d$  is the distance between the electrodes,  $E$  is the electric field strength,  $t$  is the averaged transient time, and  $V$  is the applied voltage. Charge mobilities in organic materials were first measured with the TOF by Kepler<sup>14</sup> and Leblanc.<sup>15</sup> One of the advantages of using TOF is that the electron and hole mobility can be measured separately. However, the low density of charge carriers required by this method make the derived charge carrier mobility highly sensitive to the possible defects and traps present in the material.

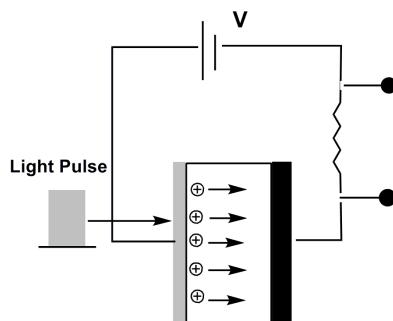


**Figure 1.3** Schematic illustration of TOF method.

In many cases, it is difficult to obtain thick organic films required by TOF, therefore the so-called SCLC technique can be applied in which the mobility is derived from the current-voltage characteristics of thin organic films between two injecting electrodes. According to SCLC theory by Lampert in 1970,<sup>16</sup> the current-voltage characteristics of the sample should be ohmic at low electric fields. When the injected charge density becomes comparable to the charge density on the electrodes, the field between the electrodes is no longer constant and the current becomes space-charge limited (the total

charge  $Q$  becomes limited by the capacitance ( $C$ ) of the material based on  $Q = CV$ , where  $V$  is applied voltage). If the contact is not injection limited and can provide sufficient charges, a trap-free semiconductor will carry a current described as below:

$$J = \frac{9}{8} \epsilon_0 \epsilon_r \mu \frac{V^2}{L^3} \quad (1.4)$$

where  $J$  is the current density,  $V$  is the bias voltage between the electrodes,  $\epsilon_0$  is the free-space permittivity,  $\epsilon_r$  is the dielectric constant of the material,  $L$  is the film thickness, and  $\mu$  is the mobility. This expression is derived for a material in which the mobility is independent of the electric field. In many organic semiconductors, it has been shown that the charge mobility has a field-dependence on the electric field as shown in Equation 1.5:<sup>17</sup>

$$\mu = \mu_0 \exp(\gamma \sqrt{E}) \quad (1.5)$$

Where  $\mu_0$  is the charge mobility at zero electric field, and  $\gamma$  is a constant. In this case, the expression of the SCLC can be approximated by:<sup>18</sup>

$$J \cong \frac{9}{8} \epsilon_0 \epsilon_r \mu_0 \exp\left(0.891 \gamma \sqrt{\frac{V}{d}}\right) \frac{V^2}{L^3} \quad (1.6)$$

In the SCLC method, the possible effects of the traps and imperfect injection are neglected, which means the effective mobility obtained from the measurements will be an underestimation of the bulk mobility under trap-free conditions. However, the types of the charge carriers (hole or electron) cannot be determined, although, in many cases, reasonable assignments can be made based on the relative magnitudes estimated injection barriers for each carrier type between the electrodes and the materials.

PR-TRMC is one of the most widely used methods to determine the charge carrier mobility in liquid crystalline materials.<sup>19</sup> In this method, the material is excited by a high-intensity pulse and leads to the formation of electron-hole pairs. The change in conductivity ( $\Delta\sigma$ ) in the material at microwave frequencies can be expressed by

$$\Delta\sigma = e \sum N_i(t) \mu_i \quad (1.7)$$

Where  $e$  is the elementary charge,  $N_i(t)$  is the time-dependent concentration of a given species  $i$  and  $\mu_i$  is the corresponding mobility. PR-TRMC is a contact-free technique, so that there should be no complications arising from the effects of imperfect injection. The quantity determined is the sum of electron and hole mobilities and the contribution of each charge carriers cannot be distinguished. Moreover, due to the very limited length scales probed by this technique, the mobility values obtained from this method are often considered to be unaffected by the presence of traps, such as grain boundaries. Accordingly, the mobility may be overestimated relative to the values achievable in device geometries, where charge transport occurs over considerably greater length scales. However, on the other hand, the mobilities may be regarded as the “intrinsic” mobility of the material, *i.e.* the maximum values that could potentially be obtained in perfectly oriented materials without defects.

### 1.3 Organic Electronic Devices Involving Charge Transport

OFETs, OPVs and OLEDs are three main organic electronic devices involving charge transport and have been studied extensively over the recent years. In this section, the principles and operation processes of OFETs, OPVs and OLEDs will be described briefly.

### 1.3.1 Organic Field-Effect Transistors

The metal-oxide-semiconductor field-effect transistor (MOSFET), based on inorganic materials, is the crucial building block of today's semiconductor industry. An organic transistor is analogous to the conventional silicon-based MOSFET, with the exception that the semiconductor is an organic material. OFETs can be used for a wide variety of applications, including display backplanes,<sup>20</sup> sensors,<sup>21,22</sup> and any application where logic circuits is used.<sup>22</sup> As mentioned earlier, the OFETs can have advantages over inorganic FETs in terms of compatibility with low-temperature processes, ease of fabrication by printing, *etc.* Furthermore, the existence of organic ambipolar materials that can transport both holes and electrons allows for the possibility of fabricating complementary circuits using only one material instead of using both p- and n-type materials needed in conventional inorganic circuits.

An OFET device has a basic structure consisting of three terminals (source, gate, and drain), a layer consisting of an organic transport material, and an insulating layer (dielectric) that separates the gate from the transport material. Four commonly used device configurations of OFETs are shown in Figure 1.4; these are named according to the relative locations of the gate and the source and drain within the material stack.<sup>4</sup>

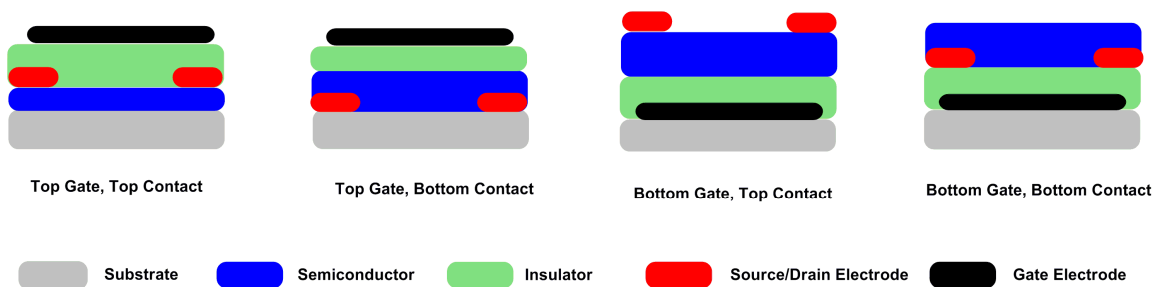


**Figure 1.4** Schematic representations of four different OFET geometries.

In the OFET devices, the current flowing between the source and drain electrodes is modulated by applying a voltage to the gate electrode. There is little to no current flow between the source and drain electrodes when there is no voltage is applied to the gate electrode (“off” state). When a voltage is applied to the gate, electron or holes can be injected from source/drain electrodes and accumulate at the semiconductor-dielectric interface and the source-drain current increases (“on” state). The current that flows from the source to the drain electrode ( $I_{SD}$ ) under a given  $V_G$  is expressed by Equation 1.8. It can be simplified in the linear regime ( $|V_{SD}| \ll |V_G - V_T|$ ) and saturated regime ( $|V_{SD}| > |V_G - V_T|$ ), as described in Equations 1.9 and 1.10, respectively:<sup>8</sup>

$$I_{SD} = \frac{W}{L} \mu C \left[ (V_G - V_T) V_{SD} - \frac{1}{2} V_{SD}^2 \right] \quad (1.8)$$

$$I_{SD,linear} = \frac{W}{L} \mu C (V_G - V_T) V_{SD} \quad (1.9)$$

$$I_{SD,Sat} = \frac{W}{2L} \mu C (V_G - V_T)^2 \quad (1.10)$$

Where  $I_{SD}$  and  $V_{SD}$  are the current and voltage between the source and drain electrodes respectively,  $V_G$  is the gate voltage,  $V_T$  is the threshold gate voltage at which the current starts to rise,  $C$  is the capacitance of the gate dielectric, and  $W$  and  $L$  are the width and length of the conducting channel. On/off ratio ( $I_{on}/I_{off}$ ) is defined as the ratio of the current in the on and off states.

Typical I-V curves of an OFET device are depicted in Figure 1.5. Figure 1.5a is an output characteristic of an OFET that illustrate the change of  $I_{SD}$  vs.  $V_{SD}$  at different constant gate voltages. Figure 1.5b shows the transfer characteristic in the saturated regime of an OFET, which describes the change of  $I_{SD}$  vs.  $V_G$  at a constant  $V_{SD}$ . It is

usually plotted as a semilogarithmic plot of  $I_{SD}$  (as shown here on the left axis) vs.  $V_G$  and as a linear plot of the square root of  $I_{SD}$  (right axis). Important parameters ( $I_{on}/I_{off}$ ,  $V_T$  and  $\mu$ ) can be extracted from the transfer curve.  $I_{on}/I_{off}$  can be obtained from the semilogarithmic plot;  $V_T$  can be obtained by extrapolating the linear fit to zero; the field-effect mobility can be extracted from the slope of the linear plot.

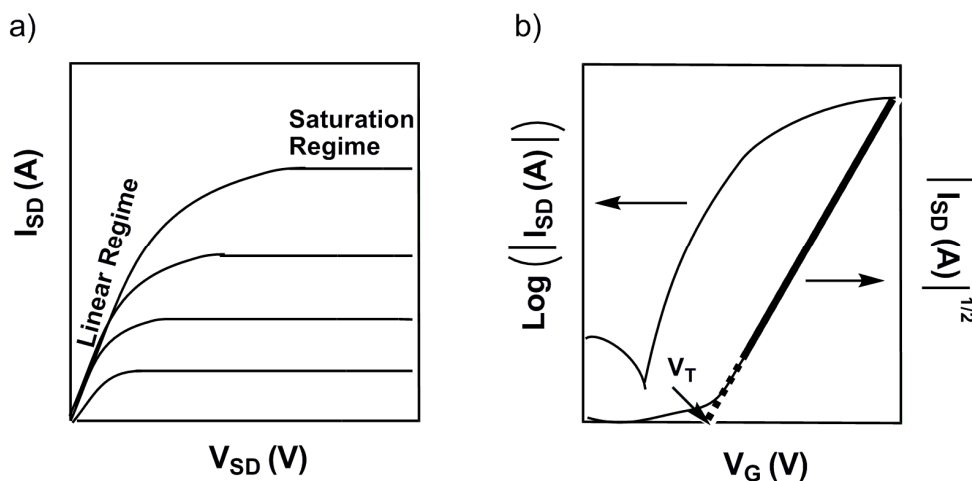


**Figure 1.5** Typical I-V curves of an OFET device: (a) output curve at different constant  $V_G$  and (b) transfer curve at a constant  $V_{SD}$ .

The charge-carrier mobility can be extracted from the OFET I-V curves either from the linear regime or saturated regime. However, the mobility values obtained from OFET measurement are approximated since they are affected by many other parameters which are not included in the above equations. For example, no field dependence of the charge mobility has been taken into account; the mobility measured can be affected by the presence of the traps at the interfaces; contact resistance at the source (drain)/organic semiconductor interface, dielectric constant of the gate electrodes, *etc.*<sup>23,24</sup> High charge-carrier mobility ( $> 1 \text{ cm}^2/(\text{Vs})$ ) in OFETs is desirable, in particular to make these devices

competitive with those based on amorphous Si. Besides the charge-carrier mobility,  $I_{on}/I_{off}$  and  $V_T$  are two of the important parameters to evaluate the performance of OFETs. It is desirable to have little to no current in the off state to eliminate leakage and  $I_{on}/I_{off} > 10^6$  is generally suitable for most applications.<sup>25</sup> Low values (ideally close to zero) of  $V_T$  are desired for low power consumption.<sup>26</sup>

### 1.3.2 Organic Photovoltaics

Solar energy is a potentially inexpensive, clean alternative energy source. Organic photovoltaic devices are potentially a cost-effective, lightweight solar conversion platform. An OPV device is a device can directly convert light energy into electric energy; it consists of thin films of organic materials sandwiched between two electrodes (usually at least two components); the organic materials must be capable of absorbing sunlight, of photogenerating charges, and of transporting these charges to the electrodes. Commonly used architectures of OPV devices are shown in Figure 1.6. Bilayer architecture is a simple architecture that is easy to fabricate, in which the films of two components are sandwiched between contacts in a planar configuration. In contrast, in bulk heterojunction, two components are blended together and create interpenetrating networks. New architectures, such as ordered heterojunction, have been developed over the years.

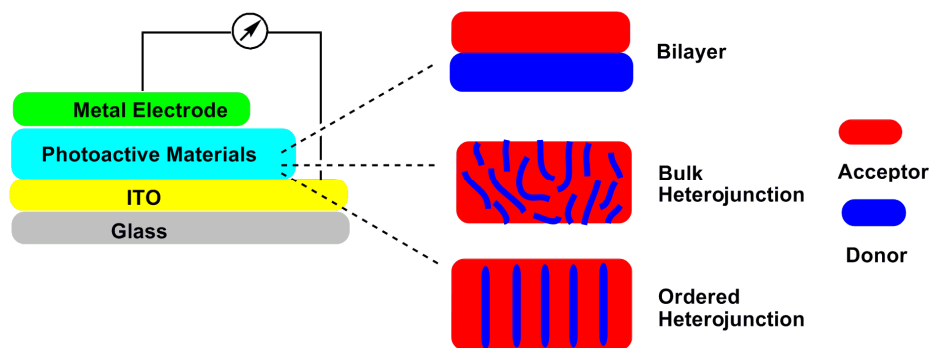


**Figure 1.6** Schematic illustration of an OPV device.

The conversion of light to electricity by OPVs generally has four major steps<sup>27</sup> as shown in Figure 1.7a. 1) Light is absorbed in the photoactive layers, which lead to the formation of the bound electron-hole pair (exciton). 2) Excitons diffuse to a donor/acceptor interface and dissociate into free charge carriers (charge separation). 3) The charge carriers migrate (charge transport). 4) They are collected at the electrodes and produce a current in the external circuit (charge collection). Two components (electron donors and acceptors) are generally used in OPV devices since the most common way to achieve exciton dissociation into free charges is through photo-induced charge transfer process between donors and acceptors; it is generally very difficult to realize efficient photo-dissociation in single-component OPVs. The energetic driving force for an efficient electron transfer from the photoexcited donor to the acceptor can be approximated by the energy difference (offset) between the LUMOs (or, in the case of hole transfer from a photoexcited acceptor to a donor, between the HOMOs) of the two components. It is generally believed that a minimum energy difference of 0.3-0.5 eV is required to overcome the exciton binding energy.<sup>28,29</sup>

Considerable effort is being directed at optimizing the efficiency of each step in order to improve the overall performance of organic solar cells. For example, one of the most

commonly used OPV materials, poly(3-hexylthiophene) (P3HT), is only capable of absorbing about 46% of the available solar photons in the wavelength range between 350 nm and 650 nm. Therefore, new materials are designed to have better light-harvesting ability, specific examples of which will be given later in section 1.4.4.

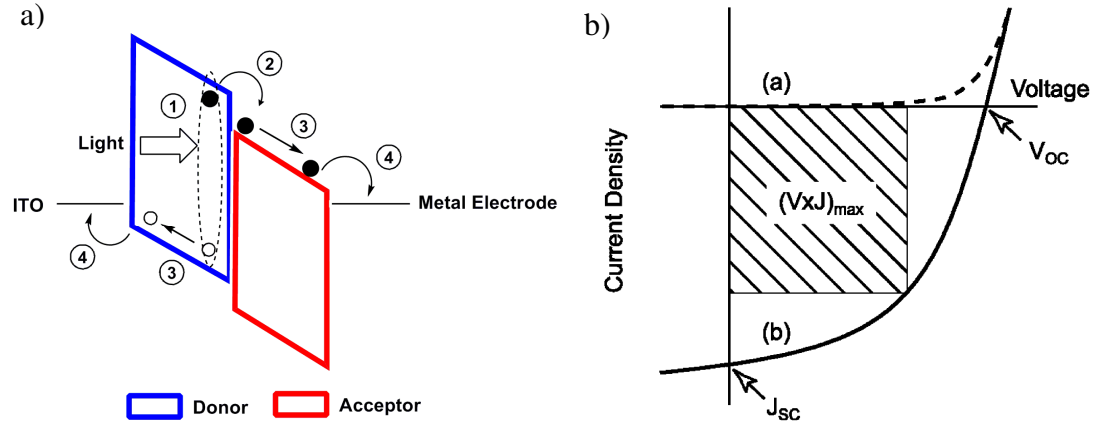


**Figure 1.7** Schematic illustrations of a) main processes governing the operation of OPVs; b) typical J-V curves in an OPV device under dark (dotted line) and under illumination (solid line) (Figure taken from ref 30).

An OPV device is characterized by the current-voltage characteristic of the devices in the dark and under illumination. In the dark, in the reverse bias direction ( $V < 0$ ), little measurable current flows, whereas in the forward bias direction ( $V > 0$ ), current increases with applied voltage. When the OPV is illuminated, the J-V curve is ideally shifted down at all potentials because of the additional photocurrent, and power is generated in the fourth quadrant of the J-V curve (Figure 1.7b)<sup>30</sup> to supply to an external load. There are several critical parameters that determine the OPV efficiency, including open circuit voltage ( $V_{oc}$ ), short circuit current density ( $J_{sc}$ ), power conversion efficiency ( $\eta$ ) and fill

factor ( $FF$ ). The power conversion efficiency ( $\eta$ ) and fill factor ( $FF$ ) are defined as follows:

$$\eta = \frac{P_{\text{out}}}{P_{\text{in}}} = FF \frac{J_{sc} V_{oc}}{P_{\text{in}}} \quad (1.11)$$

$$FF = \frac{J_{\text{max}} V_{\text{max}}}{J_{sc} V_{oc}} \quad (1.12)$$

Where  $V_{oc}$  is the open circuit voltage (the voltage when the current equals to zero),  $J_{sc}$  is the short circuit current density (the current density under zero bias), and  $P_{\text{in}}$  is the incident light power density.  $J_{\text{max}}$  and  $V_{\text{max}}$  are the current density and voltage at the maximum power point (that is, the point at which the absolute value of the product of  $J$  and  $V$  reaches its maximum value), respectively.

Those parameters characterizing OPVs are sensitive to various aspects, such as the energy levels of the donors and acceptors, charge carrier mobilities of the chosen materials, interfaces and morphology.<sup>31</sup> For example, the energy difference between the HOMO of the donor and the LUMO of the acceptor is often found to correlate with the  $V_{oc}$  value, and specific examples to increase  $V_{oc}$  by lowering the HOMO levels of the donors will be discussed in section 1.4. However, the lower the energy of the HOMO, the larger the bandgap (assuming LUMO level unchanged in the donor), the poorer the spectral overlap with the photon flux from the sun. Thus, there will be a trade-off between maximizing photon absorption and maximizing  $V_{oc}$ .<sup>31</sup> On the other hand, if both HOMO and LUMO levels are shifted down at the same time, careful consideration about the energy levels of the materials is needed to maintain an appropriate offset at the interface for charge dissociation while  $V_{oc}$  may be increased.<sup>27</sup>

### 1.3.3 Organic Light-Emitting Diodes

OLEDs have drawn great interest in the field of organic electronics, and have several advantages over their inorganic counterparts including low drive voltage, high brightness, potential for full-color emission, and relatively easy fabrication of thin large-area devices even onto flexible substrates. The first electroluminescent device based on tris(8-hydroxyquinolato) aluminum ( $\text{Alq}_3$ ) and 1,1-bis{4-[di(*p*-tolyl)amino]-phenyl}cyclohexane was reported by Tang and VanSlyke at Kodak.<sup>1</sup> In 1990, Friend and his group discovered electroluminescence (EL) in a conjugated polymer, poly(*p*-phenylenevinylene) (PPV) and thus open the way for the fabrication of polymer light-emitting diodes (PLEDs).<sup>32</sup> OLEDs recently entered the market as active elements in some displays such as in digital cameras by Kodak, in electric shavers by Philips, and in full-color TVs by Sony.

An OLED is a current-driven device that utilizes emissions from the electronically excited states of an organic material. Four main steps are required to generate light from an OLED device, which can be considered as the reverse of the processes found in OPVs:<sup>8</sup> (1) electrons (or holes) are injected at the cathode (or anode) into the LUMO (or HOMO) level of the organic material (charge injection); (2) electrons and holes travel to the opposite directions under the influence of the applied static electric field (charge transport); (3) electrons and holes recombine to lead to the formation of either singlet or triplet excitons (charge recombination); (4) when excitons decay radiatively, the light is generated (excitation decay).

The development of triplet emitters has led to remarkable improvements in the OLED efficiency. When fluorescent emitters are used, only 25% of the generated excitons

(assuming a statistical formation of singlets and triplets) can be utilized, whereas when using phosphorescent emitters, the internal quantum efficiency can theoretically reach 100%.<sup>33</sup>

#### **1.4 Organic Semiconductors Used in OFETs and OPVs**

Remarkable progress has been made in the field of organic electronics, and the continuous effort on the design and synthesis of high-performance active semiconductors is one of the essential aspects that lead to improved performance of the electronic devices.<sup>4,27,31,34</sup> Structure-property relationships among the existing materials may lead to rational design for developing new materials for organic electronics. Here, a few classes of organic semiconductors that have been widely used for the fabrication of OFETs and OPVs are overviewed, with a focus on materials that have been processed from solution. Also, more attention will be paid to thiophene-based materials due to the relevance to the research described in this thesis. In term of OPVs, bulk heterojunction devices based on a fullerene acceptor and donor materials are among the most widely studied systems, and power conversion efficiencies are surpassing 5%. In some cases, devices using other material combinations, such as all-polymer based solar cell, or other device geometries, such as tandem cells, also exhibited high efficiencies. Here the major classes of donor materials that have been used along with fullerene derivatives in bulk heterojunction cells will be the main focus of the survey for organic semiconductors used in OPVs.

### 1.4.1 Small Molecules as Active Semiconductors in OFETs

Small molecules or oligomers, as well as polymers, can be suitable organic semiconductors for OFET applications.<sup>35</sup> Small molecules often have defined and ordered solid-state packing, which sometimes lead to high charge-carrier mobility. However, these materials often have anisotropic mobilities and achieving preferable orientations relative to substrates can be a problem.<sup>36</sup> They are usually easier to synthesize and purify compared to the polymeric counterparts because, for example, some can be repeatedly sublimed. However, in many cases, the utility of those materials is limited by the poor processability from solution due to the low solubility in common organic solvents. The properties and OFET performance of acenes, oligothiophenes, and other classes of small molecules will be discussed in detail in this section.

#### *Acenes*

Acenes, fused polycyclic hydrocarbons, are among the most widely explored small molecules for OFETs.<sup>37</sup> Vapor-grown single crystals of pentacene, **1a**, and rubrene, **2**, (Figure 1.8) show very high field-effect high mobilities. Hole mobilities for vapor-deposited **1a** in thin-film transistors are often larger than  $1 \text{ cm}^2/(\text{Vs})$ ,<sup>38</sup> and values as high as  $5 \text{ cm}^2/(\text{Vs})$  have been reported.<sup>39</sup> Single crystals of **2** have been shown to exhibit field-effect hole mobilities as high as  $20 \text{ cm}^2/(\text{Vs})$  at 300 K.<sup>40</sup> Some acene derivatives containing electron-withdrawing groups (F or  $\text{CF}_3$ ) have been used in n-channel OFETs. For example, electron mobilities of 0.003 and  $0.22 \text{ cm}^2/(\text{Vs})$  have been reported for vapor-deposited films of **1b** and **3**, respectively.<sup>41,42</sup>

Since pentacene is only partially soluble in common organic solvents, soluble precursors have been used in solution-processing film. Films of **1a** have been formed by spin-casting soluble precursors (**4** and **5**) that can be thermally converted to **1a**. Pentacene films have been obtained after heating a film of **4** at 200 °C for 5 seconds.<sup>43</sup> Films of **1** formed from **5a** showed hole mobility as high as 0.9 cm<sup>2</sup>/(Vs) in devices,<sup>44</sup> and a mixture of **5b** and a photoacid allowed photopatterning of **1a** ( $\mu_h = 0.2$  cm<sup>2</sup>/(Vs)).<sup>45</sup>

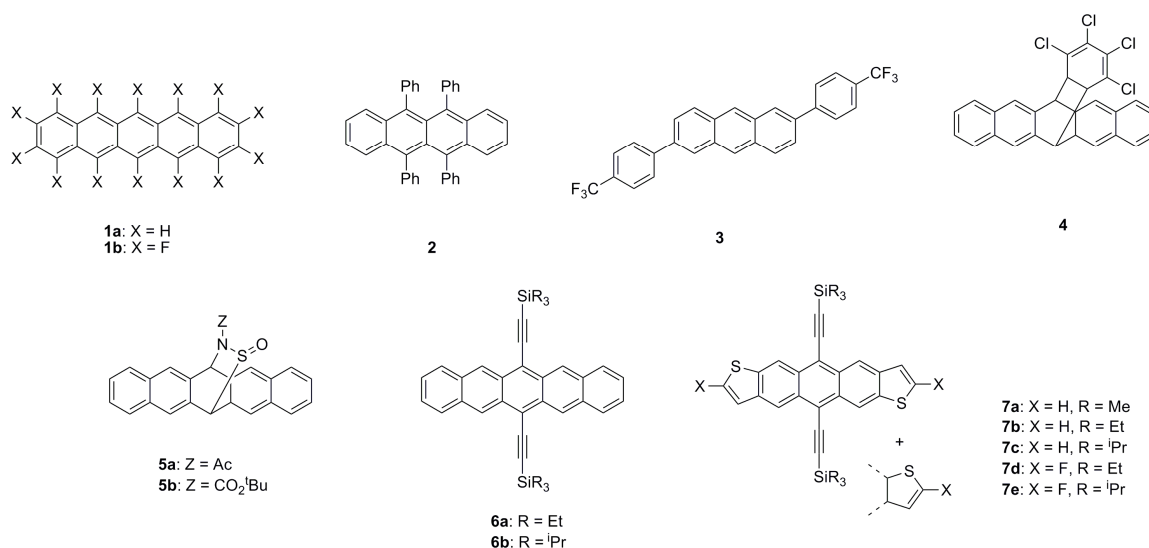


**Figure 1.8** Structures of acenes (compounds **1-7**).

An alternative to the soluble-precursor route is to use pentacenes substituted with solubilizing groups such as the trialkylsilyl ethynyl groups (**6**, Figure 1.8).<sup>46</sup> The substituents not only allow control over the solid-state packing, but also improve the stability and solubility. For films of **6b** formed by vacuum deposition,  $\mu_h = 0.4$  cm<sup>2</sup>/(Vs),<sup>47</sup> whereas solution-processed devices are among the best of solution-processed OFETs, with  $\mu_h = 1.5$  cm<sup>2</sup>/(Vs) and an on/off ratio of 10<sup>7</sup>.<sup>48</sup> The high mobility of this particular derivative, relative to that of **6a**, is attributable to differences in crystal packing.

Anthony and co-workers have also reported solubilized heteoacenes, **7**. **7b** exhibits two-dimensional packing and solution-processed OFETs exhibited  $\mu_h = 1.0 \text{ cm}^2/(\text{Vs})$  with on/off ratio of  $10^7$ , whereas edge-to-face stacked **7a** and 1D stacked **7c** showed  $\mu_h \approx 0.05 \text{ cm}^2/(\text{Vs})$ .<sup>49</sup> However, these materials are rather sensitive to light and must be handled in the dark. The F-substituted derivatives are considerably more thermo- and photostable; films of **7d** showed minimal decomposition over several weeks. OFETs based on **7d** showed  $\mu_h$  as high as  $1.5 \text{ cm}^2/(\text{Vs})$ .<sup>50,51</sup>

### *Oligothiophenes*

Oligothiophenes (**8**, Figure 1.9) represent another group of molecules widely used in OFETs; most studies utilize these materials in p-channel transistors,<sup>35,52</sup> and the achievable  $\mu_h$  have increased dramatically over the years.<sup>24,53-55</sup> Both vacuum deposited and solution-processable oligothiophenes of varying conjugation length and derivatives with substituents at different positions have been developed over the years.

For the unsubstituted oligomers, improved hole mobilities are achieved by controlling the orientation and morphology of the vacuum deposited film. Vacuum deposited OFETs based on the most widely investigated oligothiophene,  $\alpha$ -6T (**8a**), its hole mobilities varied from 0.006 to  $0.025 \text{ cm}^2/(\text{Vs})$  when the substrate temperature during deposition varied from  $-216 \text{ }^\circ\text{C}$  to  $280 \text{ }^\circ\text{C}$ . The authors attributed the differences in charge-carrier mobilities to the influences of the substrate temperature on orientations of the materials relative to substrates, and crystallinity as well as the morphology.<sup>53</sup> Vacuum-deposited OFETs based on for  $\alpha$ -8T (**8b**) have been reported with  $\mu_h$  up to  $0.33 \text{ cm}^2/(\text{Vs})$  when the substrate temperature exceeds  $120 \text{ }^\circ\text{C}$ .<sup>56</sup>

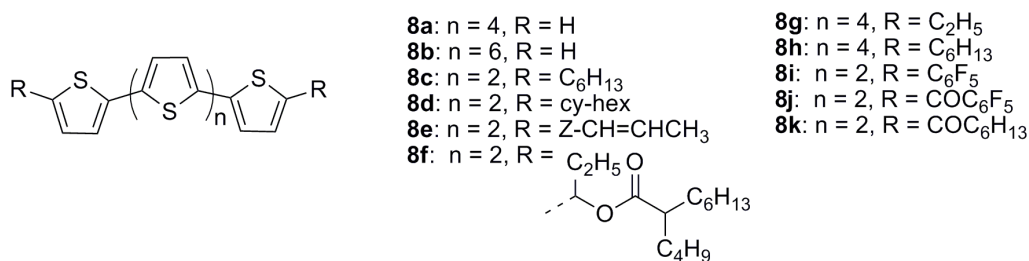


**Figure 1.9** Structures of oligothiophenes (compounds **8a-k**).

Substituted oligothiophenes show significantly increase in solubility and processability compared to the unsubstituted derivatives. Solution-processing has also been applied to some of dialkyl oligothiophenes although the performance is not necessarily better than that of the vapor-deposited devices. In the case of **8c**, both  $\mu_h$  and  $I_{on}/I_{off}$  ( $0.012 \text{ cm}^2/(\text{Vs})$  and  $3 \times 10^4$ ) for solution-processed OFETs are lower than in vapor-deposited devices ( $0.03 \text{ cm}^2/(\text{Vs})$  and  $1 \times 10^5$ ).<sup>57</sup> In the case of **8d** OFETs,  $\mu_h$  ( $0.06 \text{ cm}^2/(\text{Vs})$ ) is higher in solution-processed devices ( $0.038 \text{ cm}^2/(\text{Vs})$  for vacuum-processed devices).<sup>58</sup> Another approach to solublize the unsubstituted oligothiophenes is very similar to that previously discussed for acenes. The thermolysis of solution-processed soluble precursors has been used: films of **8e** have been obtained from pyrolysis of the ester, **8f**.<sup>59</sup> It is believed that the introduction of alkyl side chains at appropriate positions not only help improving the solubility of the materials, but also enhance the molecular ordering in the solid state, which can lead to higher charge-carrier mobilities as well as better processability. The change in orientation induced by alkyl chains leads to a significant increase in the field-effect mobility from  $0.07 \text{ cm}^2/(\text{Vs})$  for the unsubstituted 6T to larger than  $1.0 \text{ cm}^2/(\text{Vs})$  achieved for **8g** and **8h**, respectively with  $I_{on}/I_{off}$  of  $10^4$  in vacuum deposited devices.<sup>60</sup>

Oligothiophenes functionalized with electron-withdrawing groups have been found to function as electron-transport materials. Electron mobility values of  $0.4\text{-}0.6 \text{ cm}^2/(\text{Vs})$

have been reported for OFETs based on vapor-deposited **8i**, **8j** and **8k**.<sup>61-64</sup> Additionally, **8k** has been shown to exhibit ambipolar characteristic with  $\mu_h$  and  $\mu_e$  of 0.01 and 0.1  $\text{cm}^2/(\text{Vs})$ , respectively. Solution-processed n-channel OFETs have been fabricated using **8i**, with  $\mu_e$  (0.21  $\text{cm}^2/(\text{Vs})$ ) comparable to the same material deposited in vacuum.<sup>63</sup>

In recent years, fused thiophene derivatives have been incorporated into the oligomers for OFET applications. Quantum-chemical calculations indicate that the rigid fused-ring units can facilitate the intermolecular  $\pi$ - $\pi$  stacking interactions and lead to higher charge carrier mobilities.<sup>65</sup> This has been demonstrated in the devices based on fused thiophene derivatives. For example, dithienothiophene (DTT) is found to be a good candidate for OFETs. A dimer of DTT (**9**, Figure 1.10) exhibits a mobility of 0.05  $\text{cm}^2/(\text{Vs})$  with  $I_{\text{on}}/I_{\text{off}}$  ratios  $>10^8$ , and the crystal structure of the oligomer reveals a face-to-face  $\pi$ -stacked structure.<sup>66</sup> The dithienothiophene motif was further extended to seven linearly fused rings, and it was also found that this oligomer packs into a face-to-face  $\pi$ -stacking motif. A hole mobility of 0.045  $\text{cm}^2/(\text{Vs})$  with  $I_{\text{on}}/I_{\text{off}}$  ratios up to  $10^3$  was obtained when the OFET devices of **10** were tested in the air.<sup>67</sup> Electron mobilities up to 0.03  $\text{cm}^2/(\text{Vs})$  were observed in compounds **11** when the electron-withdrawing groups were attached to the center core.<sup>68</sup>

Other oligomers containing thiophene have been studied over the years in order to address some specific problems of oligothiophenes. For example, in order to improve the oxidative stability of oligothiophenes, replacing the thiophene with fluorene or phenyl proved to be an effective way to lower the HOMO levels of the materials.<sup>58,69</sup> Several series of materials (**12** and **13**) showed comparable mobilities as oligothiophenes in the range of 0.008-0.17  $\text{cm}^2/(\text{Vs})$ , as well as improved environmental stability.<sup>58,69</sup> Star-

shaped oligothiophenes were synthesized to further increase the solubility by constructing three-dimensional structures. In a solution-processed OFET device of **14**, mobilities up to  $0.025 \text{ cm}^2/(\text{Vs})$  were observed.<sup>70</sup>

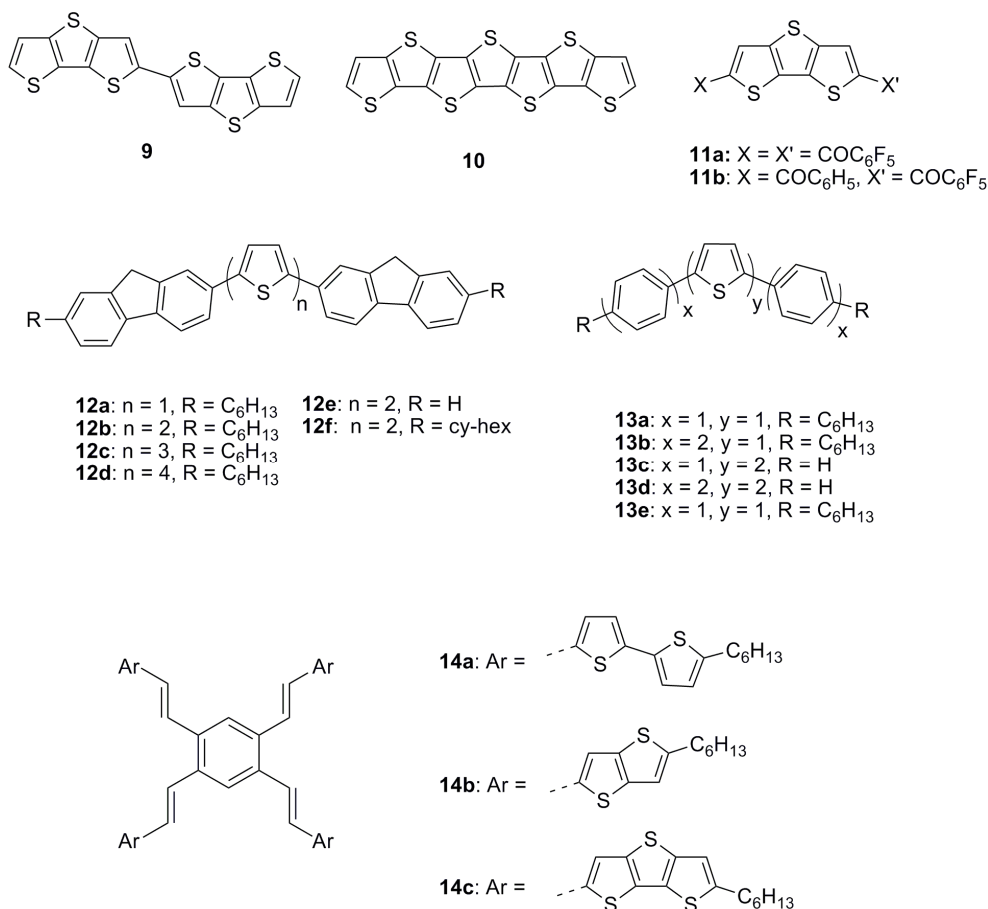


**Figure 1.10** Structures of oligothiophenes (compounds **9-14**).

### *Other Small-molecule Systems*

Acenes, oligothiophenes and their derivatives include many of the best-performing charge transport materials, especially for holes (p-channel). Current research also demonstrated other systems which showed promising hole mobilities in OFETs, such as

phthalocyanines (Pc) (CuPc, **15**),<sup>71,72</sup> tetrathiafulvalene (TTF) derivatives (dithiophene-TTF, **16**)<sup>73,74</sup> *etc.* The structures of the representative compounds are shown in Figure 1.11.

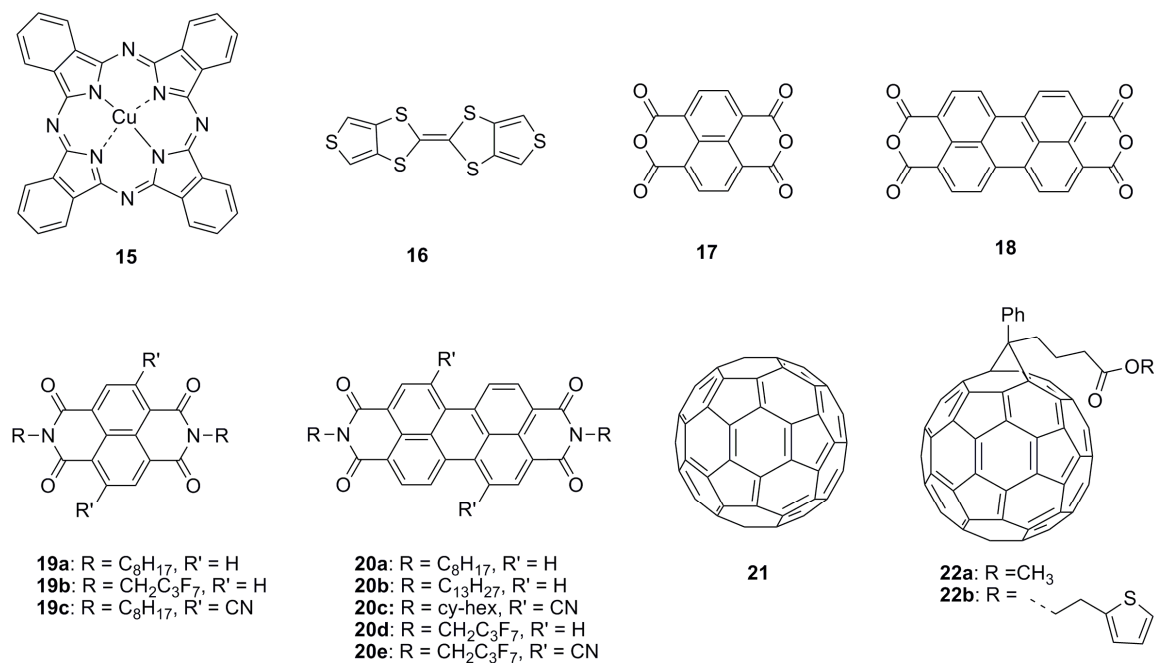


**Figure 1.11** Structures of other small-molecule systems (compounds **15-22**).

The small molecules or oligomers discussed in the previous section are mostly p-channel materials although some of them exhibit n-channel characteristics in OFETs when strong electron-withdrawing groups are introduced lowering the frontier orbitals to facilitate electron injection and to reduce hole injection. Materials based on rylenes (perylene and naphthalene) and fullerenes are considered as the best examples in n-type small-molecule semiconductors. The majority of studies of rylene-based small molecules have focused on vapor-deposited devices, and only few materials with appropriate substitution can be processed from solution. In general, *N,N'*-dialkyl diimides based on

perylene and naphthalene, such as **19a** ( $0.16\text{ cm}^2/(\text{Vs})$ )<sup>75</sup> and **20a** ( $0.60\text{ cm}^2/(\text{Vs})$ ),<sup>76</sup> exhibit better performance in n-channel OFETs than the anhydrides **17** ( $0.003\text{ cm}^2/(\text{Vs})$ )<sup>77</sup> and **18** ( $10^{-4}\text{ cm}^2/(\text{Vs})$ )<sup>78</sup> when vapor deposited and measured in vacuum. A record mobility of  $2.1\text{ cm}^2/(\text{Vs})$  was reported for **19b** after annealing at  $140\text{ }^\circ\text{C}$ .<sup>79</sup> Furthermore, substitution with electron-withdrawing groups on the nitrogen and/or on the aromatic moieties has been found to lead to air-stable electron-transport in examples **19b-c** and **20c-e**,<sup>80-82</sup> whereas the devices are sensitive to air in the previous examples. It is worth noting that **20e** has been processed into OFETs using both vacuum deposition (with top contacts) and drop casting (with bottom contacts); while both types of devices display air-stable operation,  $\mu_e = 0.64$  and  $10^{-3}$ – $10^{-4}\text{ cm}^2/(\text{Vs})$ , respectively.<sup>81</sup>

Fullerene- $\text{C}_{60}$ , **21**, and related compounds represent one of the most widely studied classes of transport materials for the fabrication of n-channel OFETs. Excellent performance has been obtained for these  $\text{C}_{60}$  OFETs using vacuum deposition. Mobilities as high as  $6\text{ cm}^2/(\text{Vs})$  have been reported by Anthopoulos *et al.*<sup>83</sup> Few  $\text{C}_{60}$  derivatives have been used for solution-processed OFETs due to their limited solubility. However, OFETs have been fabricated using solution-based methods with soluble fullerene derivatives, particularly from so-called PCBM, **22a**, for which  $\mu_e$  of 0.01 and  $>0.1\text{ cm}^2/(\text{Vs})$  have been reported.<sup>84, 85</sup> The related thiophene-functionalized derivative **22b** has also been used in spin-coated devices yielding saturation mobilities in the range of  $0.028$ – $0.078\text{ cm}^2/(\text{Vs})$ .<sup>86</sup>

### 1.4.2 Conjugated Polymers as Active Semiconductors in OFETs

Conjugated polymers<sup>3,32</sup> are an attractive class of organic materials for OFETs due to their good solubility in common organic solvents and film-forming properties, which allow them to be deposited from solution and, therefore, patterned by screen printing, ink-jet printing or other methods, whereas most of small molecules or oligomers are processed by vapor deposition. However, the mobilities obtained from the polymers are often lower than the vapor-deposited small molecules or oligomers due to poor intermolecular ordering. Also the purification of the polymers is tedious and sometimes the performance is affected by the batch-to-batch irreproducibility. Some classes of conjugated polymers and their performance in OFETs will be overviewed in the following section.

#### *Polythiophenes*

Polythiophenes are one of most explored polymers for OFETs due to their ease of functionality and good solution processability. Among them, poly(3-hexylthiophene) (P3HT, **23**, Figure 1.12) is the most widely used p-channel organic semiconductor. The 3-alkyl substituents can be incorporated in a polymer backbone, either by head-to-tail (HT), head-to-head (HH) or tail-to-tail (TT) linkages.<sup>26</sup> A polymer with a mixture of different linkages is referred as regiorandom, while one with only HT linkages is referred as regioregular. High  $\mu_h$  in the range 0.05 – 0.1 cm<sup>2</sup>/(Vs) have been obtained for highly regioregular P3HT, with on/off ratio of *ca.* 10<sup>6</sup>, whileas  $\mu_h$  drops to *ca.* 10<sup>-4</sup> cm<sup>2</sup>/(Vs) in regiorandom P3HT.<sup>87,88</sup> Regioregular P3HT (*rr*P3HT) can self-orient into a well-ordered lamellar structure with an edge-on orientation of the thiophene ring relative to the

substrate. The mobility of P3HT depends strongly on the solvent used for spin-coating, with the highest values obtained for 1,2,4-trichlorobenzene.<sup>89</sup> More recent work has addressed the effect of molecular weight, film deposition solvent, and film morphology on P3HT-based OFET performance.<sup>89-91</sup> For example, Zen *et al.* investigated the influence of the molecular weight of P3HT on the OFET charge-carrier mobility. A dramatic increase in the hole mobility was observed with increasing P3HT molecular weights: from  $5.5 \times 10^{-7} \text{ cm}^2/(\text{Vs})$  for the low molecular weight fraction ( $M_n = 2200 \text{ g/mol}$ ) to  $2.6 \times 10^{-3} \text{ cm}^2/(\text{Vs})$  for the high molecular weight fraction ( $M_n = 19000 \text{ g/mol}$ ).<sup>91</sup>

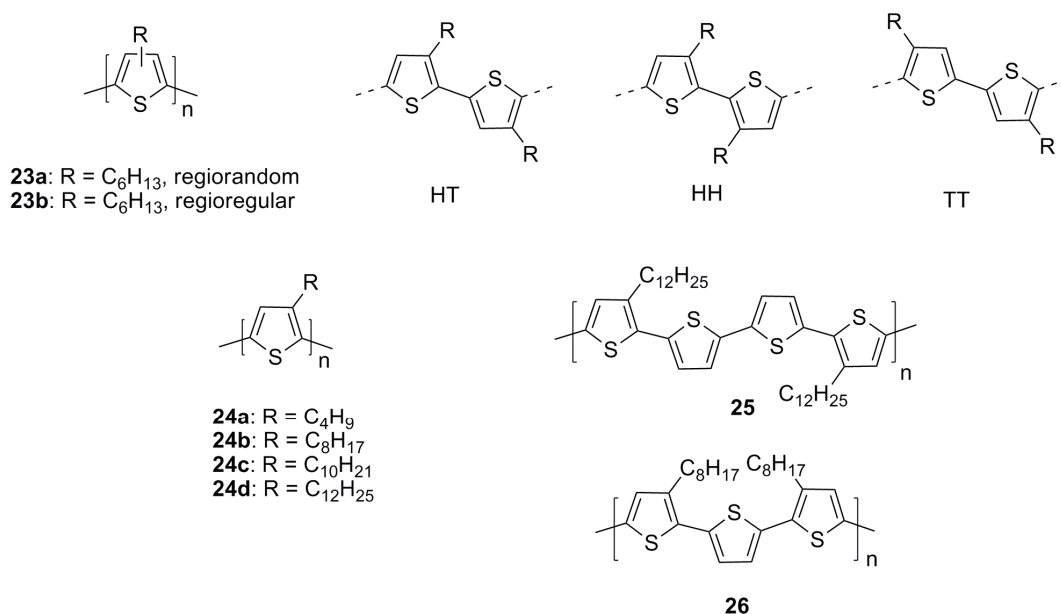


**Figure 1.12** Structures of P3ATs and functionalized polythiophenes (compounds **23-26**).

A systemic study of poly(3-alkylthiophene)s (P3ATs, **24a-d**) with side chains ranging from butyl to decyl was conducted, and the mobilities of P3ATs with different side chains were compared. The mobility values have generally been observed to decrease

with increasing alkyl chain length.  $\mu_{\text{sat}}$  of P3AT films drop from  $2 \times 10^{-4} \text{ cm}^2/(\text{Vs})$  for poly(3-butylthiophene) to  $6 \times 10^{-7} \text{ cm}^2/(\text{Vs})$  for poly(3-decylthiophene).<sup>92</sup>

In recent years, more attention has drawn towards the design and synthesis of new polythiophenes other than P3HT in order to improve the air stability of the materials.<sup>26</sup> Exposure of P3HT film to air usually causes oxidative doping and, therefore, degradation of the transistor performance. In principle, air-stable materials should be realizable by increasing the ionization potential (IP) of the materials. More specifically, increasing IP can be controlled either sterically - by reducing  $\pi$ -overlap between adjacent thiophene rings, or electronically – by introducing less conjugated unit in the backbone. Ong *et al.* have synthesized a new class of polythiophenes with the alkyl side chains strategically placed along the polymer backbone, including poly(3,3'''-bisdodecylquaterthiophene) (PQT-12, **25**) and poly(3,3''-dioctylterthiophene) (PTT-8, **26**) shown in Figure 1.12. Polymer **25** showed a higher mobility of  $0.14 \text{ cm}^2/(\text{Vs})$  along with improved air stability compared to P3HT; the author attributed the latter to the presence of more unsubstituted thienylene moieties and associated rotational freedom reducing the  $\pi$ -conjugation to some extent.<sup>93,94</sup> The same group also reported another class of structurally similar PTT polymers and their use in OFETs. The hole mobilities measured in OFETs are in the range of  $0.015\text{-}0.022 \text{ cm}^2/(\text{Vs})$  with an on/off of  $10^5\text{-}10^6$ .<sup>95</sup> Stability studies after storage for a month under ambient conditions revealed only a slight reduced on/off ratio, whereas P3HT showed a significant degradation on the on/off ratio from  $10^5$  to  $10^2$  under comparable conditions.<sup>96</sup> The increased air stability probably results from the slight twisting of the neighboring thiophene moieties in the polymer backbone, reducing the  $\pi$ -overlap between adjacent thiophene rings.

### ***Other Thiophene-Containing Polymers***

Besides the polythiophenes discussed earlier, a large number of copolymers containing thiophene moieties have been synthesized and studied. There are mainly two principal types: one is the donor-donor type, in which thiophene is coupled with other commonly used donors, such as fluorene; another type is the donor-acceptor type, in which thiophene rings are connected with electron-acceptor moieties, such as quinoxaline or thiadiazole.

Fused thiophene moieties have been incorporated in the polythiophene backbone based on different rationales. It is thought that  $\pi$ - $\pi$  interactions are fundamental for interchain charge propagation and systems which allow aggregation based on  $\pi$ - $\pi$  stacking are attractive candidates as long as one can maintain the balance between the effects of the aliphatic chains and the  $\pi$ - $\pi$  interactions. For example, when thieno[3,2-*b*]thiophene and dithieno[3,2-*b*:2',3'-*d*]thiophene are coupled with alkylthiophenes, the resulting copolymers (**27** and **28**, Figure 1.13) showed relatively high hole mobilities up to 0.6 and 0.3 cm<sup>2</sup>/(Vs), respectively.<sup>26,97</sup> In particular, polymer **28** exhibited liquid-crystalline behavior, highly organized morphology and large crystal domains, which are considered to be important factors for high charge-carrier mobility.<sup>97</sup>

Other thiophene-containing copolymers have been developed by combining thiophene or thienothiophene units with less electron-rich moieties such as fluorene. Copolymers of thiophenes and fluorenes seem to be attractive candidates since polymer and oligomer examples synthesized so far have shown good mobilities of up to 0.1 cm<sup>2</sup>/(Vs), and on/off ratios as high as 10<sup>5</sup>.<sup>98-100</sup> It is worth noting that Sirringhaus *et al.* reported a transistor prepared by inkjet printing of polymer **29** as the active semiconductor material.

A mobility up to  $0.02 \text{ cm}^2/(\text{Vs})$  was obtained by depositing the polymer onto a mechanically rubbed substrate followed by high temperature annealing.<sup>99</sup> Improved stabilities have also been obtained using 9-silafluorenes in place of fluorenes.<sup>101</sup>

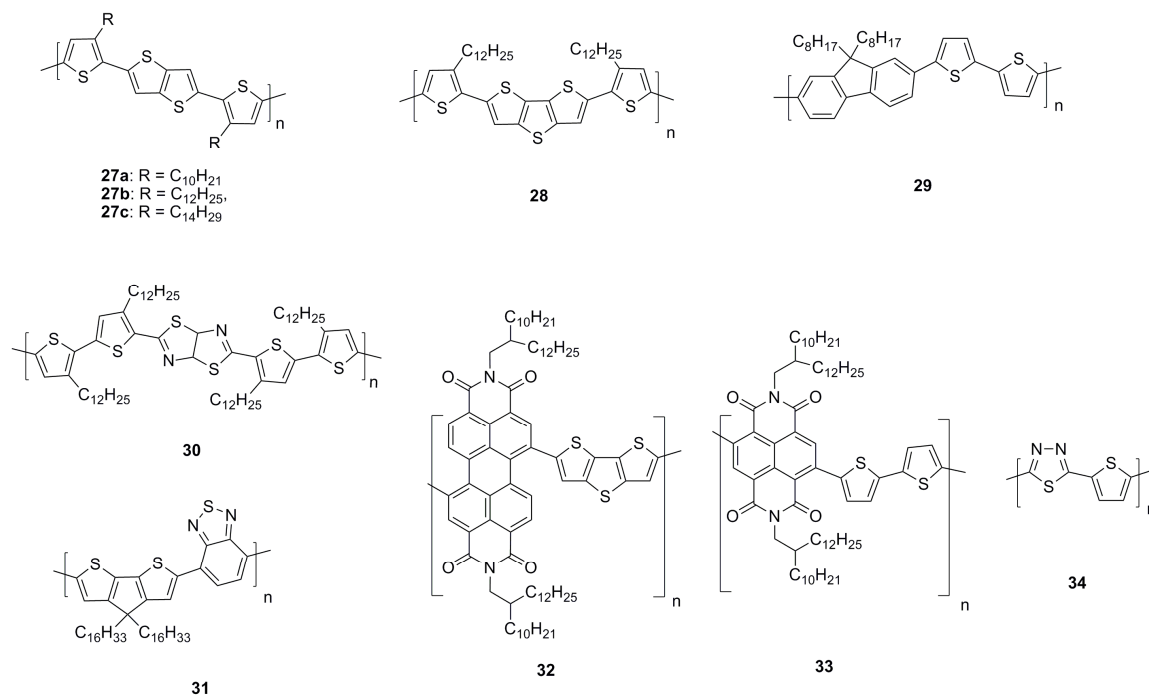


**Figure 1.13** Structures of other thiophene-containing polymers (compounds **27-34**).

Conjugated polymers semiconductors containing both electron donor and acceptor moieties are of growing interests for field-effect transistors due to the potential ambipolar charge transporting characteristics associate with these types of materials. However, only p-channel OFETs have also been obtained from most of the copolymers involving thiophene and electron-poor heterocycles, such as thiazole, quinoxaline, and thienopyrazine.<sup>102-104</sup> Polymer **30**, incorporating a thiazolothiazole unit, functions as a p-channel material with hole mobility up to  $0.14 \text{ cm}^2/(\text{Vs})$  and improved oxidative stability

over *rr*P3HT.<sup>105</sup> Polymer **31** belongs to the same general class and exhibits the highest hole mobility (up to  $0.17\text{ cm}^2/(\text{Vs})$ ) of any donor-acceptor polymer.<sup>106</sup>

In recent years, several solution-processable electron-transport polymers have been developed. They all combined electron-deficient perylene or naphthalene diimide with thiophene derivatives (bithiophene or fused thiophene). In 2007, Zhan *et al.* reported a perylene diimide / dithienothiophene copolymer **32** to be an electron-transport material with an electron mobility of  $1.3 \times 10^{-2}\text{ cm}^2/(\text{Vs})$  in OFETs.<sup>107</sup> More recently, Facchetti *et al.* developed a naphthalene diimide/bithiophene copolymer **33** which is a breakthrough in electron-transport polymeric materials.<sup>108</sup> This polymer is highly soluble ( $\sim 60\text{ g/L}$ ) and exhibits unprecedented OTFT characteristics with electron mobilities up to  $0.85\text{ cm}^2/(\text{Vs})$  under ambient conditions using Au contacts and various polymeric dielectrics. Good processing versatility was demonstrated by fabricating top-gate OTFTs on plastic substrates with the semiconductor-dielectric layers deposited by spin-coating as well as by gravure, flexographic and inkjet printing. Moreover, all-printed polymeric complementary inverters have also been demonstrated, which proved its potential application in practical electronic devices.

A few examples of thiophene-containing polymers have been found to exhibit ambipolar characteristics in OFETs based on a single active semiconductor. A thiophene-based polymer incorporating thiadiazole, **34**, was only poorly soluble in normal organic solvents, requiring use of  $\text{CF}_3\text{CO}_2\text{H}$  as the processing solvent, but was found to be ambipolar.<sup>109</sup> Few other D-A copolymers processed from solution, including one of the copolymers we described in chapter 4, have showed ambipolar characteristics with hole or electron mobility in the range of  $10^{-4}$ - $10^{-3}\text{ cm}^2/(\text{Vs})$ .<sup>110,111</sup>

### Other Polymeric Systems

Other conjugated polymers used in p-channel OFETs include poly(phenylenevinylene) derivatives such as **35**,<sup>112,113</sup> or carbazole-based materials,<sup>114,115</sup> such as **36**, or fluorene-based materials,<sup>116</sup> such as **37**, *etc.* Nevertheless, the performance of those materials is generally not competitive with that obtained from polythiophenes or other thiophene-based copolymers.

There are fewer reports on n-channel OFETs based on polymers. The ladder polymer, **38** exhibited the highest electron mobility of any polymeric material until the recent reported naphthalene/bithiophene copolymer **33** discussed in the previous section; although this is a solution-processed material showing a high OFET mobility, it should be pointed out that the processing solvent was MeSO<sub>3</sub>H, which is a very strong acid.<sup>117</sup> Another example is a fluorene-benzothiadiazole polymer **39** which has been reported to function as an electron-transport material in OFETs with  $\mu_e = 0.6\text{--}4.8 \times 10^{-3} \text{ cm}^2/(\text{Vs})$ , or as an ambipolar material with  $\mu_h \approx \mu_e \approx 8 \times 10^{-4} \text{ cm}^2/(\text{Vs})$ .<sup>118</sup>

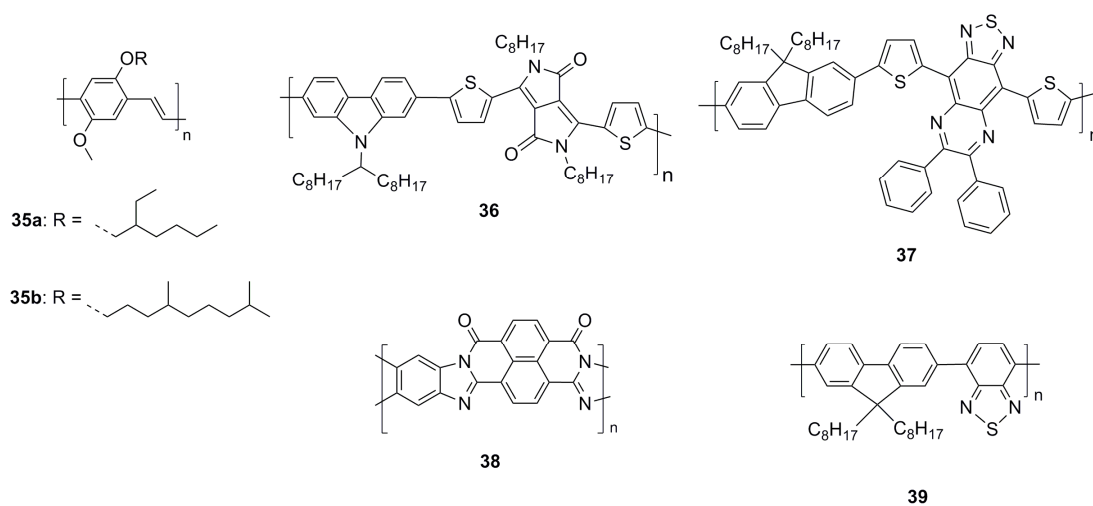


**Figure 1.14** Structures of other polymeric systems (compounds **35**–**39**).

### 1.4.3 Small Molecules as Active Semiconductors in OPVs

Polymeric materials have been the major class of active semiconductors used in OPVs in recent years; however, few classes of small molecules have also been extensively used and studied for many years. Actually the first bilayer device reported by Tang *et al.* in 1986 that considered as groundbreaking discovery in OPVs used two molecular compounds. CuPc (compound **15** in Figure 1.11), the electron donor, and a perylene derivative, 3,4:9,10-perylene tetracarboxylic bis-benzimidazole (PTCBI, compound **40** in Figure 1.15), the electron acceptor, were deposited by sequential thermal vacuum sublimation.<sup>2</sup> A power conversion efficiency approaching 1% was reported in this bilayer device. Most small molecules for OPVs are vapor-deposited onto the substrates, and a few materials processed from solution will be highlighted.

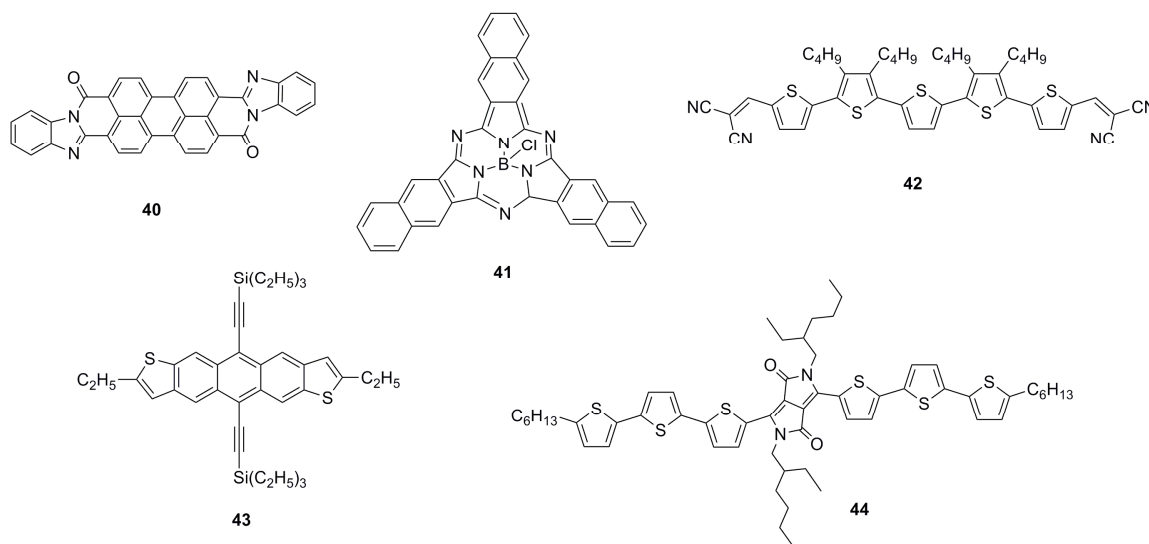


**Figure 1.15** Structures of small molecules (compounds **40-44**) for OPVs.

In the past two decades, CuPc has still been the donor of choice in most small-molecule solar cells due to its high stability, high mobility, and widespread availability.

The original Tang structure was improved by co-sublimation of CuPc and PTCBI leading to a blend structure, and a higher efficiency ( $\eta = 1.5\%$ ) was obtained as a result of improved interfacial area.<sup>119</sup> Later in 2005, a new deposition method called vapour phase deposition (VPE) was used, and the interfacial area was increased by a factor of four compared to a bilayer structure, leading to a power conversion efficiency of 2.2%.<sup>120,121</sup> The efficiencies can be further improved by replacing PTCBI with C<sub>60</sub>, and it is thought that the much larger exciton diffusion length in the fullerene, compared to PTCBI, is beneficial to achieve higher efficiencies. Devices based on incorporating CuPc: C<sub>60</sub> bulk heterojunctions reached power conversion efficiencies of up to 5%.<sup>122-125</sup> The highest efficiency so far for a small molecule based OPV was reached by Xue *et al.*<sup>125</sup> for a stacked solar cell comprising two CuPc: C<sub>60</sub> bulk heterojunction cells separated via a layer of silver nanoclusters. Other phthalocyanine derivatives also have been investigated their use in OPVs. For example, in a boron subphthalocyanine **41**, the HOMO is shifted by *ca.* 400 meV compared to CuPc, which resulted in the  $V_{oc}$  increased by the same amount to nearly 1V.<sup>126</sup> However, overall power conversion efficiency of 2.1% didn't surpass the performance of the combinations of CuPc and C<sub>60</sub>. Another class of promising vapor-deposited small molecules includes oligothiophenes.  $\alpha$ -6T (**8a**) is one of the semiconductors that shows high mobility in OFETs, and it was also found to exhibit relatively high efficiencies up to 2.4% when it is co-deposited with C<sub>60</sub> or C<sub>70</sub> after annealing.<sup>127</sup> Moreover, systematic comparison of  $\alpha$ -6T along with C<sub>60</sub> or C<sub>70</sub> either with or without annealing revealed that the better performance was obtained with the combination with C<sub>70</sub>, and that annealing can in general improve the efficiencies. Schulze *et al.* used  $\alpha,\alpha$ -bis(2,2-dicyanovinyl) quinquethiophene (DCV5T, **42**) as electron donor

in combination with C<sub>60</sub>. Large open circuit voltages of 1.0 V could be obtained since the HOMO level of DCV5T is sufficiently low (−5.6 eV). The IPCE reached values as high as 52%, leading to a high overall efficiency of 3.4%.<sup>128</sup>

Soluble small molecules have attracted more attention since they potentially combined the advantages of small molecules (monodispersity, facile purification, high charge carrier mobility *etc.*) and good film-forming property generally associated with polymeric materials. However, the efficiencies are, in general, lower than those of vapor-deposited small molecule and polymer-based devices. TIPS-pentacene, anthradithiophene are among the best solution-processable materials in OFETs, and devices based on the blends of those acenes and fullerene derivatives have also been investigated in OPVs. In a bilayer configuration based on vacuum-deposited C<sub>60</sub> and spin-coated TIPS-pentacene, the power conversion efficiencies reached a peak value of 0.5%.<sup>129</sup> In a device formed by the blend of an anthradithiophene derivative (**43**) and PCBM, solvent vapor annealing of the blends leads to the formation of spherulites. A correlation between coverage of the device with spherulites and its performance was observed. Devices with high spherulite coverage reach a power conversion efficiency of 1% under illumination of 100 mW/m<sup>2</sup>.<sup>130</sup> Very recently, a solution processable oligothiophene with a dialkylated diketopyrrolopyrrole chromophore (**44**) was used in bulk heterojunction with C<sub>71</sub>-PCBM, and a power conversion efficiency of 3.0% was obtained.<sup>131</sup> Power conversion efficiencies up to 0.8% were observed in the blends of other solution-processable materials and fullerene acceptors, such as star-shape oligothiophenes and triphenylamines.

132,133

#### 1.4.4. Conjugated Polymers as Active Semiconductors in OPVs

Conjugated polymer photovoltaic materials have attracted great attention in recent years, and their advantages and disadvantages in OPVs is somehow similar for OFETs as previously mentioned in section 1.4.2.<sup>31,34</sup> The current state-of-the-art in the organic photovoltaics is represented by bulk heterojunction cells based on P3HT and PCBM, with reproducible power conversion efficiencies approaching 5%.<sup>134,135</sup> Here the optimizations of OPV devices based on P3HT/PCBM blends are summarized, and the progress of OPV materials based on other polymeric systems is also reviewed.

##### *Polythiophenes*

In the last five years, efforts in the field of organic solar cells have been focused on P3HT. In 2002, the first encouraging results for P3HT/PCBM blends (1:3 w:w) was reported with the power conversion efficiency up to 2.8%,<sup>136</sup> since then a rapid development of those blends has occurred with high efficiencies in the range of 3-5%.<sup>134,135,137</sup> Efficiencies of the blends of P3HT/PCBM were found to have correlations with variables either from material or device fabrication, such as molecular weights, regioregularity of P3HT, or annealing conditions of the devices.

The effects of molecular weight and regioregularity have been investigated in films of P3HT/PCBM blends. Although small molecular-weight fractions have low mobility and blue-shifted absorption spectra,<sup>91,138</sup> they are found to initiate or facilitate the growth of crystalline fibrils during the annealing step, leading to a large number of small crystals.<sup>91</sup> On the other hand, high  $M_w$  fractions produced highly entangled, amorphous networks.<sup>139</sup> Some researchers believed that high efficiency was only obtained in high  $M_w$  fractions;<sup>138</sup>

however, other results suggested that the preferred  $M_w$  of P3HT is in the range of 30k-70k with a rather high polydispersity of 2, which gives a mixture of highly crystalline regions formed by low- $M_w$  fractions embedded in and interconnected by a high- $M_w$  P3HT matrix.<sup>140</sup> The influence of regioregularity is also thought to be critical to device performance. Usually a higher RR leads to a higher value of efficiency, mainly because of the better transport property of *rr*P3HT as discussed previously.<sup>141</sup>

The efficiencies of solar cells based on P3HT/PCBM have been dramatically improved by a thermal annealing step. Several studies revealed that the morphology of the blends was changed, and X-ray investigation also suggested a higher crystallinity of the films observed upon annealing.<sup>135,142-144</sup> Savenije *et al.* revealed the relationship between the morphology and charge carrier mobility using the flash photolysis time-resolved microwave conductivity technique (FP-TRMC).<sup>143</sup> Annealing resulted in the formation of crystalline P3HT fibrils and enhanced the hole mobility by more than three orders of magnitude.<sup>144,145</sup> Also upon annealing, an enhanced external quantum efficiency and a pronounced red-shift were observed in the optical spectrum. Mihailetschi *et al.* found the annealed P3HT/PCBM films are capable of absorbing 60% more photons than the unannealed blends.<sup>145</sup>

Other approaches have been used to control the morphology of the P3HT/PCBM blends in order to improve the device performance. For example, additives were used to create better order in the blends. Alkylthiols were added to P3HT/PCBM solution, and a slightly enhanced hole mobility and a significantly longer charge-carrier lifetime were observed in the blends; this is thought to result from the formation of P3HT domains with higher crystallinity.<sup>146</sup>

One of the problems with P3HT as donor materials in bulk heterojunction cells is the mismatching of its absorption spectrum with the solar spectrum as described earlier in section 1.3.2. Poly(thienylenevinylene)s was designed to broaden and intensify the absorption compared to P3HT in the visible region.<sup>147</sup> The incorporation of a bis(thienylenevinylene) side chain that are conjugated to a polythiophene backbone leads to a broadening of the absorption, which results in the improvement in the power conversion efficiencies. Cells with polymer **45c** in combination with PCBM reached 3.2% in efficiency versus 2.4% with P3HT at the same condition.<sup>148</sup> The enhanced performance of this polymer can be attributed to the increased photocurrent in the range of 400-500 nm based on the IPCE results.<sup>148</sup> The same group also reported a series of crosslinked polythiophenes **46** with conjugated bridges,<sup>149,150</sup> in order to improve the interchain charge transport for higher hole mobility. The improved hole mobility is thought to result in higher efficiency in OPVs, and up to 1.7% efficiency was achieved in one of those crosslinked polythiophenes.<sup>150</sup>

### ***Other Thiophene-Containing Copolymers***

Copolymers incorporating thiophene have been widely used in OFETs, and many of them have also been investigated in OPVs, such as polymers **27c**, **29**, and **32** (structures in Figure 1.13) discussed earlier. The most common approach for copolymers used in OPVs is the donor-acceptor type; however, there are also few examples of the donor-donor type copolymers.

Copolymers of thiophene and fluorene/or thienothiophene have been found to exhibit high hole mobility in OFETs described in previous section, and those copolymers have

also been used in OPVs as light absorber and hole transporting materials. Efficiencies up to 2.3% were achieved by using 1:4 blend of a copolymer containing thienothiophene (**27c** in Figure 1.13) with PCBM. The hole mobility measured by SCLC was found to be  $3.8 \times 10^{-4} \text{ cm}^2/(\text{Vs})$ , which is higher than what is reported for P3HT/PCBM blends.<sup>151</sup> The higher hole mobility is thought to be responsible for the relative high efficiency. The similar result was also found in the copolymer of bithiophene and fluorene (**29** in Figure 1.13), which resulted in a high power conversion efficiency of 2.7%.<sup>152</sup>

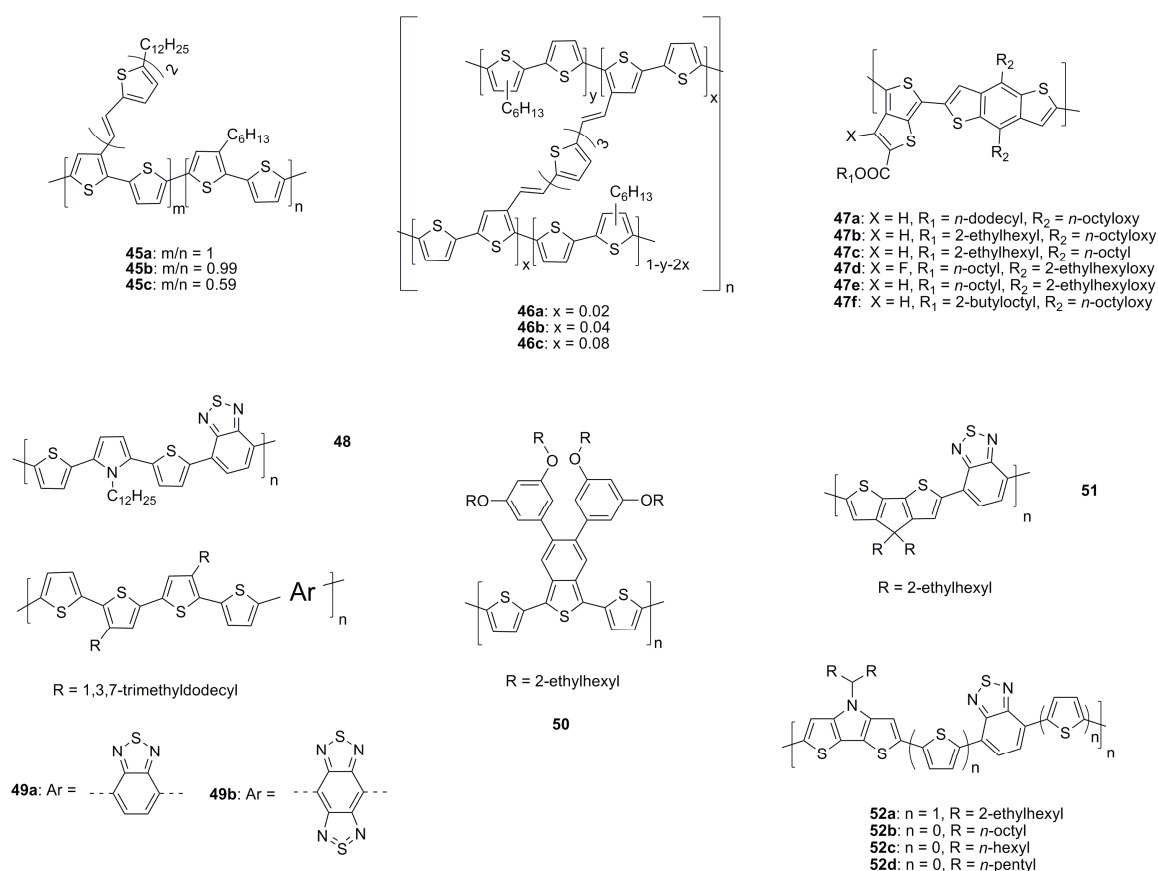


**Figure 1.16** Structures of polythiophenes and other thiophene-containing polymers in OPVs (compounds **45-52**).

Very recently, a series of copolymers (**47**) based on thieno[3,4-*b*]thiophene and

benzodithiophene were reported by Yu *et al.*<sup>153</sup> It is thought that the thieno[3,4-*b*]thiophene moiety can support the quinoidal structure and leads to narrow bandgaps. Also the side chains and substituents affect absorptions and mobilities of the polymers, as well as the miscibilities with the PCBM. Efficiency up to 6.1% has been achieved in devices based on fluorinated **47d**/PCBM films prepared from mixed solvents.

In the so-called donor-acceptor approach, alternating electron-rich and electron-poor units are coupled together to form the copolymer backbone. The intramolecular charge-transfer (ICT) interactions between D and A moieties results in low ionization potentials and high electron affinities in the copolymers, which in turn can lead to the possibility of ambipolar charge transport, and to low-energy absorptions associated with the low bandgap that are attractive for OPVs.

Polymer **48**, incorporating thiophene, pyrrole and benzothiadiazole, is capable of an efficiency of about 1% blended with PCBM in a 1: 3 ratio. The low bandgap (1.6 eV) of this copolymer allows for effective for extension of absorption in the devices out to nearly 800 nm and a broad coverage across much of the visible region.<sup>154</sup> A series of copolymers with thiophene and benzothiadiazole, or bis(benzothiadiazole) acceptors was synthesized by Krebs *et al.*, and has been investigated in OPVs. Efficiencies of 1.0% and 0.6% was obtained for devices based on polymer **49a** with active areas of 0.1 and 3 cm<sup>2</sup>, respectively. The devices based on **49b** were found to give poor devices; this was linked to a poor alignment of the energy levels in **49b** with those of PCBM.<sup>155,156</sup> Another thienopyrazine-thiophene copolymer **50** has also been reported to afford an efficiency of 1.1% with PCBM while exhibiting a bandgap of 1.2 eV; this is the lowest bandgap polymer reported to date that affords an efficiency more than 1%. Photocurrent

production is demonstrated up to 1000 nm in 1:4 blends with PCBM.<sup>157</sup>

In recent years, fused thiophene derivatives have been incorporated into the backbones of a variety of conjugated polymers. In the context of OPV application, planarization of part of polymer chain, relative to that of a polythiophene, leads to reduced bandgaps in those polymers; moreover, these building blocks tend to be stronger electron donors than comparable non-fused species, suggesting the possibility of lower-energy charge-transfer-type absorptions in D-A systems.

Cyclopentadithiophene-based copolymers have attracted considerable attention in the recent years.<sup>158,159</sup> A copolymer of cyclopentadithienophene and benzothiadiazole, **51**, firstly reported in 2006, showed a PCE of 2.7% in a 1:1 blend with PCBM. The good performance of this polymer in organic solar cells can be attributed to its broad absorption spectrum and high hole mobility ( $2 \times 10^{-3} \text{ cm}^2/(\text{Vs})$ , FET method), as well as the good miscibility with PCBM.<sup>158</sup> Using the C<sub>70</sub> analogue of PCBM leads to an even higher efficiency of 3.2% for the device based on the same polymer.<sup>158</sup> In 2007, the PCE of solar cells of the blends of polymer **51** and PCBM have been further increased to 5.5% by using alkanedithiols as solvent additives by Bazan and coworkers.<sup>159</sup>

Dithienothiophene and dithienopyrrole (DTP) are two electron-rich moieties that are more readily oxidized than their unbridged analogue, bithiophene. Perylene diimide-dithienothiophene (**32** in Figure 1.13) and related compounds have also been used as electron-transport materials in single-layer bulk heterojunction solar cells with efficiencies of up to 1.5% in conjunction with polythiophene-based hole-transport materials.<sup>107,160</sup> Very recently, power conversion efficiencies up to 2.8% were reported for organic solar cells based on blends of DTP and benzothiadiazole copolymers, such as

polymer **52**, with PCBM,.<sup>161,162</sup>

### Fluorene-Based Copolymers

In the recent years, several fluorene-based D-A copolymers have been synthesized and tested in OPVs. Andersson *et al.* prepared a variety of them called APFO polymers.<sup>163-165</sup> This class of copolymers is a successful demonstration of the donor-acceptor approach, and the potential of this family for organic solar cells is also illustrated. The highest PCE (4.2 %) of a polyfluorene-based solar cell based on polymer **53a** was reported by ECN (Energy Research Center of the Netherlands). The good performance of fluorene-based copolymers is attributed to the high  $V_{oc}$  of about 1V due to the low-lying HOMO level of the copolymers. Replacing the bridging C atom in the fluorene by a Si atom is designed to lower the HOMO level even further, and better performance (5.4%) was obtained in blends of **53c** with PCBM.<sup>166</sup>

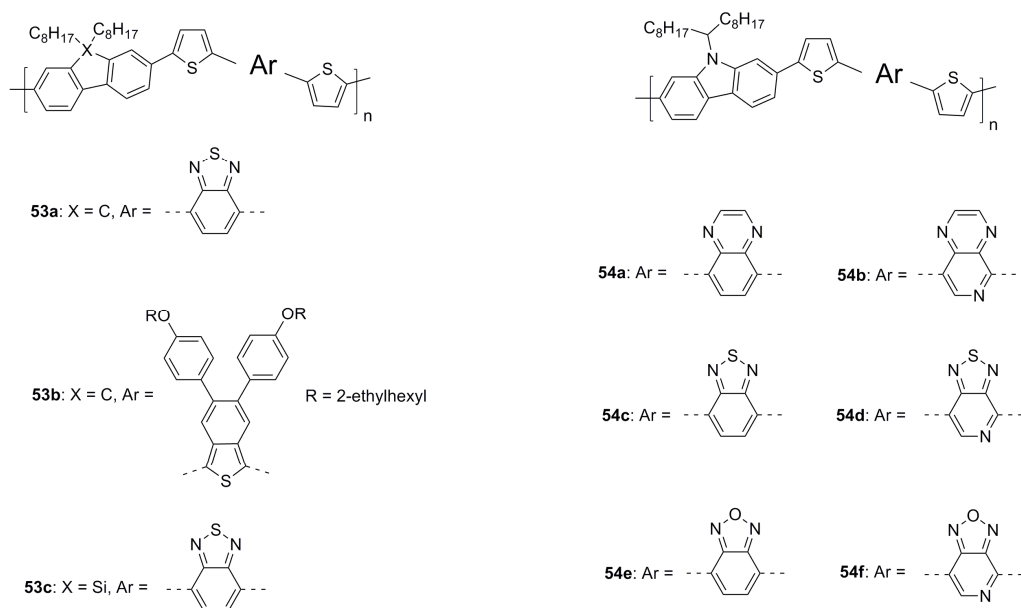


**Figure 1.17** Structures of fluorene- and carbazole-based copolymers (compounds **53-54**).

### ***Carbazole-Based Copolymers***

Carbazole-based copolymers have been investigated in OPVs by the Leclerc group.<sup>167-169</sup> This class of materials has similar optical and electric properties as the polyfluorene copolymers. A series of copolymers based on 2,7-carbazole and various electron-acceptor moieties have been employed in OPVs with efficiencies up to 3.6% found in blends with PCBM.<sup>168</sup> Very recently, a copolymer **54c** containing carbazole and benzothiadiazole was blended with the C<sub>70</sub> analogue of PCBM, and a PCE of 6% was achieved.<sup>170</sup>

### ***Other Polymeric Systems***

Besides the study based on the blends of P3HT/PCBM, the initial study of OPVs were based on blends of poly[2-methoxy-5-(2'-ethyl-hexyloxy)-*p*-phenylene vinylene] (MEH-PPV, **35a**, Figure 1.14)/ C<sub>60</sub> composites, which were later on substituted by the combination of poly[2-methoxy-5-(3',7'-dimethyloctyloxy)-1,4-phenylene vinylene] (MDMO-PPV, **35b**, Figure 1.14) and PCBM.<sup>34</sup> With the relatively large gap and low mobility of the PPV-type polymers, efficiencies of 3% were achieved at best, and the interest in this class of materials faded.<sup>171,172</sup> However, the most thorough morphological study for bulk heterojunction OPVs is based on the blends of MDMO-PPV/PCBM, and the effect of the solvents and weight ratios on the morphology and device performance have been investigated. It was found that blends of MDMO-PPV/PCBM with 1:4 weight ratio processed in chlorobenzene gave the best performance in OPV devices, and the correlation of the morphological changes and the device performance were illustrated by various techniques, such as AFM and TEM (Transmission Electron Microscopy).<sup>172,173</sup>

Metallated conjugated polymers have received some attention in polymer OLEDs

because the incorporation of the metal atom into the polymers can increase the mixing of the first excited singlet and triplet states, thus lead to higher EL quantum yields.<sup>174,175</sup> This type of conjugated polymers has been tested in OPVs in recent years, and the efficiencies below 1% were achieved in the early reports.<sup>176,177</sup> In 2007, a platinum metallopolyne with a low bandgap of 1.85 eV was reported by Wong *et al.*. The solar cells based on the blend of polymer **55c**/ PCBM (1:4, w/w) showed an average PCE of 4.1%.<sup>178</sup> Those results suggested those metallated conjugated polymers in which long-lived triplet excitons are involved in charge generation might be interesting materials for OPVs.

Other polymers used as donors blended with fullerene derivatives in OPVs include indolo[2,3-b]carbazole-based materials such as **56**,<sup>179</sup> or silole-based materials such as polymers **57** *etc.*<sup>180</sup> Devices based on some of the materials when blended with PCBM exhibited relatively high efficiencies up to 3.6%; those materials are thought to be promising new materials for OPV applications.

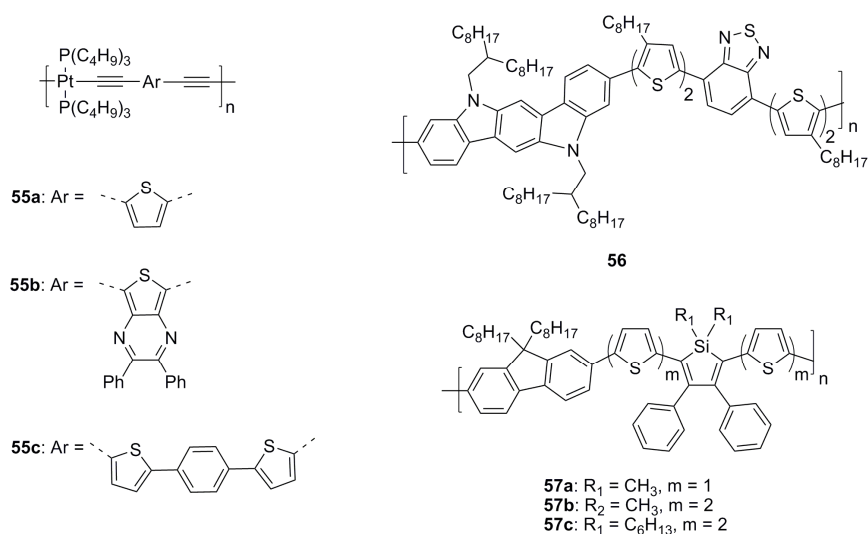


**Figure 1.18** Structures of other polymeric systems in OPVs (compounds **55-57**).

## 1.5 Organization of the Thesis

*N*-Alkyl and aryl dithieno[3,2-*b*:2',3'-*d*]pyrroles (DTPs) have been chosen as the major building block in this research to construct a variety of conjugated materials. The aim of this research is to study the structure-property relationships of the DTP-based materials, and to investigate their potential uses in organic electronic devices. A variety of DTP-based conjugated materials (oligomers and polymers) have been synthesized and characterized. Quantum-chemical calculations on model oligomers have been performed to obtain insight into the experimental optical spectra and electrochemical measurements. In addition, the use of selected materials in OFETs and OPVs has been investigated. For some of the polymers, the spectroelectrochemistry of the materials have also been studied to test their potential use in electrochromic devices.

Specifically, Chapter 1 provides an overview about the general background of charge transport in organic materials, the principles of organic electronic devices, and the progress of existing organic materials for OFETs and OPVs. Chapter 2 describes the syntheses and characterization of *N*-aryl DTP dimers, a trimer, and a homopolymer using Pd-catalyzed coupling chemistry. These compounds have been chemically oxidized and the optical properties of radical ions have been compared. Moreover, the DTP homopolymer has also been obtained by electropolymerization, and the spectroelectrochemistry of the electro-polymerized homopolymer has been compared with the absorption spectra obtained from chemical oxidation of the homopolymer synthesized by Stille coupling. In Chapter 3, a series of *N*-alkyl DTP-based polymers, including a homopolymer and copolymers with some commonly used electron-donating moieties (bithiophene, thiophene and fluorene), have been synthesized and characterized.

Their optical and electrochemical properties are compared. In addition, the OFET and OPV devices from the polymers are also fabricated, and the morphology of blends with PCBM with the DTP-bithiophene copolymer has been studied using AFM and XRD. Both Chapter 4 and Chapter 5 describe the syntheses, characterizations and device performances of DTP-based D-A copolymers. In Chapter 4, the acceptors are all based on the benzothiadiazole moiety, and the effects of their varying acceptor strengths on the optical and electronic properties are compared. Furthermore, the spectroelectrochemistry of the copolymers has been studied to test their potential use in electrochromic devices. Aggregation phenomena have been studied in one of the polymers. Fabrication of OFETs and OPVs from the copolymers is also described along with a film morphology study of selected OPV devices. In Chapter 5, quinoxaline/ pyridopyrazine-containing acceptors have been chosen to couple with a DTP donor, and another series of D-A copolymers have been synthesized and characterized. The OPVs and OFETs based on those copolymers have been tested, and the morphology study of some selected OPV devices has been conducted. Chapter 6 summarizes the research described in this thesis and suggests future directions that may lead to further improvement of the DTP-based research or new applications.

## 1.6 References

- (1) Tang, C. W.; Vanslyke, S. A. *Appl. Phys. Lett.* **1987**, *51*, 913.
- (2) Tang, C. W. *Appl. Phys. Lett.* **1986**, *48*, 183.
- (3) Koezuka, H.; Tsumura, A.; Ando, T. *Synth. Met.* **1987**, *18*, 699.
- (4) Facchetti, A. *Materials Today* **2007**, *10*, 28.
- (5) Winder, C.; Sariciftci, N. S. *J. Mater. Chem.* **2004**, *14*, 1077.
- (6) Bao, Z.; Locklin, J. J. *Organic field-effect transistors*; CRC Press, Boca Raton, FL, 2007.
- (7) Sun, S.-S.; Dalton, L. R. *Introduction to organic electronic and optoelectronic materials and devices*; CRC Press, Boca Raton, FL, 2008.
- (8) Coropceanu, V.; Cornil, J.; da Silva, D. A.; Olivier, Y.; Silbey, R.; Brédas, J. L. *Chem. Rev.* **2007**, *107*, 926.
- (9) Cornil, J.; Brédas, J. L.; Zaumseil, J.; Sirringhaus, H. *Adv. Mater.* **2007**, *19*, 1791.
- (10) Ashcroft, N. W. *Solid state physics*; Saunders College, Philadelphia, 1976.
- (11) Duke, C. B.; Schein, L.B. *Phys. Today* **1980**, *33*, 42.
- (12) Horowitz, G. *Adv. Mater.* **1998**, *10*, 365.
- (13) Brédas, J. L.; Calbert, J. P.; da Silva, D. A.; Cornil, J. *Proc. Natl. Acad. Sci. U. S. A.* **2002**, *99*, 5804.
- (14) Kepler, R. G. *Phys. Rev.* **1960**, *119*, 1226.
- (15) Leblanc, O. H. *J. Chem. Phys.* **1960**, *33*, 626.
- (16) Lampert, M. A.; Mark, P. *Current injection in solids*; Academic Press, New York, 1970.
- (17) Bässler H. *Phys. Status Solidi B* **1993**, *175*, 15.
- (18) Murgatroyd, P. N. *J. Phys.* **1970**, *D3*, 151.
- (19) Schouten, P. G.; Warman, J. M.; Dehaas, M. P.; Fox, M. A.; Pan, H. L. *Nature* **1991**, *353*, 736.
- (20) Gelinck, G. H.; Huitema, H. E. A.; Van Veenendaal, E.; Cantatore, E.; Schrijnemakers, L.; Van der Putten, J.; Geuns, T. C. T.; Beenhakkers, M.; Giesbers, J. B.; Huisman, B. H.; Meijer, E. J.; Benito, E. M.; Touwslager, F. J.; Marsman, A. W.; Van Rens, B. J. E.; De Leeuw, D. M. *Nat. Mater.* **2004**, *3*, 106.
- (21) Roberts, M. E.; Sokolov, A. N.; Bao, Z. N. *J. Mater. Chem.* **2009**, *19*, 3351.
- (22) Smits, E. C. P.; Mathijssen, S. G. J.; van Hal, P. A.; Setayesh, S.; Geuns, T. C. T.; Mutsaers, K.; Cantatore, E.; Wondergem, H. J.; Werzer, O.; Resel, R.; Kemerink, M.; Kirchmeyer, S.; Muzafarov, A. M.; Ponomarenko, S. A.; de Boer, B.; Blom, P. W. M.; de Leeuw, D. M. *Nature* **2008**, *455*, 956.
- (23) Horowitz, G. *J. Mater. Res.* **2004**, *19*, 1946.
- (24) Dodabalapur, A.; Torsi, L.; Katz, H. E. *Science* **1995**, *268*, 270.
- (25) Katz, H. E.; Bao, Z. *J. Phys. Chem. B* **2000**, *104*, 671.
- (26) Ong, B. S.; Wu, Y. L.; Li, Y. N.; Liu, P.; Pan, H. L. *Chem. Eur. J.* **2008**, *14*, 4766.
- (27) de Boer, B.; Facchetti, A. *Polym. Rev.* **2008**, *48*, 423.
- (28) Ohkita, H.; Cook, S.; Astuti, Y.; Duffy, W.; Tierney, S.; Zhang, W.; Heeney, M.; McCulloch, I.; Nelson, J.; Bradley, D. D.; Durrant, J. R. *J. Am. Chem. Soc.* **2008**, *130*, 3030.
- (29) Scharber, M. C.; Wuhlbacher, D.; Koppe, M.; Denk, P.; Waldauf, C.; Heeger, A. J.; Brabec, C. L. *Adv. Mater.* **2006**, *18*, 789.

- (30) Shirota, Y.; Kageyama, H. *Chem. Rev.* **2007**, *107*, 953.
- (31) Thompson, B. C.; Fréchet, J. M. J. *Angew. Chem. Int. Ed.* **2008**, *47*, 58.
- (32) Burroughes, J. H.; Bradley, D. D. C.; Brown, A. R.; Marks, R. N.; Mackay, K.; Friend, R. H.; Burns, P. L.; Holmes, A. B. *Nature* **1990**, *347*, 539.
- (33) Baldo, M. A.; O'Brien, D. F.; You, Y.; Shoustikov, A.; Sibley, S.; Thompson, M. E.; Forrest, S. R. *Nature* **1998**, *395*, 151.
- (34) Dennler, G.; Scharber, M. C.; Brabec, C. J. *Adv. Mater.* **2009**, *21*, 1323.
- (35) Murphy, A. R.; Fréchet, J. M. J. *Chem. Rev.* **2007**, *107*, 1066.
- (36) Shang, L. W.; Liu, M.; Tu, D. Y.; Zhen, L. J.; Liu, G.; Jia, R.; Li, L. Q.; Hu, W. P. *Thin Solid Films* **2008**, *516*, 5093.
- (37) Anthony, J. E. *Angew. Chem. Int. Ed.* **2008**, *47*, 452.
- (38) Lin, Y. Y.; Gundlach, D. J.; Nelson, S. F.; Jackson, T. N. *IEEE Trans. Electron. Dev.* **1997**, *44*, 1325.
- (39) Meijer, E. J.; de Leeuw, D. M.; Setayesh, S.; van Veenendaal, E.; Huisman, B. H.; Blom, P. W. M.; Hummelen, J. C.; Scherf, U.; Kadam, J.; Klapwijk, T. M. *Nat. Mater.* **2003**, *2*, 834.
- (40) Menard, E.; Podzorov, V.; Hur, S. H.; Gaur, A.; Gershenson, M. E.; Rogers, J. A. *Adv. Mater.* **2004**, *16*, 2097.
- (41) Ando, S.; Nishida, J.; Fujiwara, E.; Tada, H.; Inoue, Y.; Tokito, S.; Yamashita, Y. *Chem. Mater.* **2005**, *17*, 1261.
- (42) Inoue, Y.; Sakamoto, Y.; Suzuki, T.; Kobayashi, M.; Gao, Y.; Tokito, S. *Jpn. J. Appl. Phys.* **2005**, *44*, 3663.
- (43) Herwig, P. T.; Müllen, K. *Adv. Mater.* **1999**, *11*, 480.
- (44) Afzali, A.; Dimitrakopoulos, C. D.; Breen, T. L. *J. Am. Chem. Soc.* **2002**, *124*, 8812.
- (45) Weidkamp, K. P.; Afzali, A.; Tromp, R. M.; Hamers, R. J. *J. Am. Chem. Soc.* **2004**, *126*, 12740.
- (46) Anthony, J. E.; Brooks, J. S.; Eaton, D. L.; Parkin, S. R. *J. Am. Chem. Soc.* **2001**, *123*, 9482.
- (47) Sheraw, C. D.; Jackson, T. N.; Eaton, D. L.; Anthony, J. E. *Adv. Mater.* **2003**, *15*, 2009.
- (48) Park, S. K.; Jackson, T. N.; Anthony, J. E.; Mourey, D. A. *Appl. Phys. Lett.* **2007**, *91*, 063514.
- (49) Payne, M. M.; Parkin, S. R.; Anthony, J. E.; Kuo, C. C.; Jackson, T. N. *J. Am. Chem. Soc.* **2005**, *127*, 4986.
- (50) Gundlach, D. J.; Royer, J. E.; Park, S. K.; Subramanian, S.; Jurchescu, O. D.; Hamadani, B. H.; Moad, A. J.; Kline, R. J.; Teague, L. C.; Kirillov, O.; Richter, C. A.; Kushmerick, J. G.; Richter, L. J.; Parkin, S. R.; Jackson, T. N.; Anthony, J. E. *Nat. Mater.* **2008**, *7*, 216.
- (51) Subramanian, S.; Park, S. K.; Parkin, S. R.; Podzorov, V.; Jackson, T. N.; Anthony, J. E. *J. Am. Chem. Soc.* **2008**, *130*, 2706.
- (52) Allard, S.; Forster, M.; Souharce, B.; Thiem, H.; Scherf, U. *Angew. Chem. Int. Ed.* **2008**, *47*, 4070.
- (53) Servet, B.; Horowitz, G.; Ries, S.; Lagorsse, O.; Alnot, P.; Yassar, A.; Deloffre, F.; Srivastava, P.; Hajlaoui, R.; Lang, P.; Garnier, F. *Chem. Mater.* **1994**, *6*, 1809.

- (54) Garnier, F.; Yassar, A.; Hajlaoui, R.; Horowitz, G.; Deloffre, F.; Servet, B.; Ries, S.; Alnot, P. *J. Am. Chem. Soc.* **1993**, *115*, 8716.
- (55) Garnier, F.; Hajlaoui, R.; Yassar, A.; Srivastava, P. *Science* **1994**, *265*, 1684.
- (56) Hajlaoui, M. E.; Garnier, F.; Hassine, L.; Kouki, F.; Bouchriha, H. *Synth. Met.* **2002**, *129*, 215.
- (57) Garnier, F.; Hajlaoui, R.; El Kassmi, A.; Horowitz, G.; Laigre, L.; Porzio, W.; Armanini, M.; Provasoli, F. *Chem. Mater.* **1998**, *10*, 3334.
- (58) Locklin, J.; Li, D. W.; Mannsfeld, S. C. B.; Borkent, E. J.; Meng, H.; Advincula, R.; Bao, Z. *Chem. Mater.* **2005**, *17*, 3366.
- (59) Chang, P. C.; Lee, J.; Huang, D.; Subramanian, V.; Murphy, A. R.; Fréchet, J. M. J. *Chem. Mater.* **2004**, *16*, 4783.
- (60) Halik, M.; Klauk, H.; Zschieschang, U.; Schmid, G.; Ponomarenko, S.; Kirchmeyer, S.; Weber, W. *Adv. Mater.* **2003**, *15*, 917.
- (61) Yoon, M. H.; Facchetti, A.; Stern, C. E.; Marks, T. J. *J. Am. Chem. Soc.* **2006**, *128*, 5792.
- (62) Facchetti, A.; Mushrush, M.; Yoon, M. H.; Hutchison, G. R.; Ratner, M. A.; Marks, T. J. *J. Am. Chem. Soc.* **2004**, *126*, 13859.
- (63) Letizia, J. A.; Facchetti, A.; Stern, C. L.; Ratner, M. A.; Marks, T. J. *J. Am. Chem. Soc.* **2005**, *127*, 13476.
- (64) Yoon, M. H.; DiBenedetto, S. A.; Russell, M. T.; Facchetti, A.; Marks, T. J. *Chem. Mater.* **2007**, *19*, 4864.
- (65) Zhang, X. N.; Johnson, J. P.; Kampf, J. W.; Matzger, A. J. *Chem. Mater.* **2006**, *18*, 3470.
- (66) Li, X. C.; Sirringhaus, H.; Garnier, F.; Holmes, A. B.; Moratti, S. C.; Feeder, N.; Clegg, W.; Teat, S. J.; Friend, R. H. *J. Am. Chem. Soc.* **1998**, *120*, 2206.
- (67) Sirringhaus, H.; Friend, R. H.; Li, X. C.; Moratti, S. C.; Holmes, A. B.; Feeder, N. *Appl. Phys. Lett.* **1997**, *71*, 3871.
- (68) Chen, M. C.; Chiang, Y. J.; Kim, C.; Guo, Y. J.; Chen, S. Y.; Liang, Y. J.; Huang, Y. W.; Hu, T. S.; Lee, G. H.; Facchetti, A.; Marks, T. J. *Chem. Commun.* **2009**, 1846.
- (69) Meng, H.; Zheng, J.; Lovinger, A. J.; Wang, B. C.; Van Patten, P. G.; Bao, Z. N. *Chem. Mater.* **2003**, *15*, 1778.
- (70) Kim, K. H.; Chi, Z. G.; Cho, M. J.; Jin, J. I.; Cho, M. Y.; Kim, S. J.; Joo, J. S.; Choi, D. H. *Chem. Mater.* **2007**, *19*, 4925.
- (71) Bao, Z.; Lovinger, A. J.; Dodabalapur, A. *Appl. Phys. Lett.* **1996**, *69*, 3066.
- (72) Xiao, K.; Liu, Y. Q.; Yu, G.; Zhu, D. B., *Synth. Met.* **2003**, *137*, 991.
- (73) Mas-Torrent, M.; Hadley, P.; Ribas, X.; Rovira, C., *Synth. Met.* **2004**, *146*, 265.
- (74) Leufgen, M.; Rost, O.; Gould, C.; Schmidt, G.; Geurts, J.; Molenkamp, L. W.; Oxtoby, N. S.; Mas-Torrent, M.; Crivillers, N.; Veciana, J.; Rovira, C. *Org. Electron.* **2008**, *9*, 1101.
- (75) Katz, H. E.; Johnson, J.; Lovinger, A. J.; Li, W. J. *J. Am. Chem. Soc.* **2000**, *122*, 7787.
- (76) Malenfant, P. R. L.; Dimitrakopoulos, C. D.; Gelorme, J. D.; Kosbar, L. L.; Graham, T. O.; Curioni, A.; Andreoni, W. *Appl. Phys. Lett.* **2002**, *80*, 2517.
- (77) Laquindanum, J. G.; Katz, H. E.; Dodabalapur, A.; Lovinger, A. J. *J. Am. Chem. Soc.* **1996**, *118*, 11331.

- (78) Ostrick, J. R.; Dodabalapur, A.; Torsi, L.; Lovinger, A. J.; Kwock, E. W.; Miller, T. M.; Galvin, M.; Berggren, M.; Katz, H. E. *J. Appl. Phys.* **1997**, *81*, 6804.
- (79) Tatemichi, S.; Ichikawa, M.; Koyama, T.; Taniguchi, Y. *Appl. Phys. Lett.* **2006**, *89*, 3.
- (80) Katz, H. E.; Lovinger, A. J.; Johnson, J.; Kloc, C.; Siegrist, T.; Li, W.; Lin, Y. Y.; Dodabalapur, A. *Nature* **2000**, *404*, 478.
- (81) Jones, B. A.; Ahrens, M. J.; Yoon, M. H.; Facchetti, A.; Marks, T. J.; Wasielewski, M. R. *Angew. Chem. Int. Ed.* **2004**, *43*, 6363.
- (82) Jones, B. A.; Facchetti, A.; Marks, T. J.; Wasielewski, M. R. *Chem. Mater.* **2007**, *19*, 2703.
- (83) Anthopoulos, T. D.; Singh, B.; Marjanovic, N.; Sariciftci, N. S.; Ramil, A. M.; Sitter, H.; Colle, M.; de Leeuw, D. M. *Appl. Phys. Lett.* **2006**, *89*, 3.
- (84) Anthopoulos, T. D.; de Leeuw, D. M.; Cantatore, E.; Setayesh, S.; Meijer, E. J.; Tanase, C.; Hummelen, J. C.; Blom, P. W. M. *Appl. Phys. Lett.* **2004**, *85*, 4205.
- (85) Singh, T. B.; Marjanovic, N.; Matt, G. J.; Gunes, S.; Sariciftci, N. S.; Ramil, A. M.; Andreev, A.; Sitter, H.; Schwodiauer, R.; Bauer, S. *Org. Electron.* **2005**, *6*, 105.
- (86) Tiwari, S. P.; Nanddas, E. B.; Rao, V. R.; Fichou, D.; Mhaisalkar, S. G. *IEEE Electron Device Lett.* **2007**, *28*, 880.
- (87) Sirringhaus, H.; Brown, P. J.; Friend, R. H.; Nielsen, M. M.; Bechgaard, K.; Langeveld-Voss, B. M. W.; Spiering, A. J. H.; Janssen, R. A. J.; Meijer, E. W.; Herwig, P.; de Leeuw, D. M. *Nature* **1999**, *401*, 685.
- (88) Sirringhaus, H.; Tessler, N.; Friend, R. H. *Science* **1998**, *280*, 1741.
- (89) Chang, J. F.; Sun, B. Q.; Breiby, D. W.; Nielsen, M. M.; Solling, T. I.; Giles, M.; McCulloch, I.; Sirringhaus, H. *Chem. Mater.* **2004**, *16*, 4772.
- (90) Kline, R. J.; McGehee, M. D.; Kadnikova, E. N.; Liu, J. S.; Fréchet, J. M. J.; Toney, M. F. *Macromolecules* **2005**, *38*, 3312.
- (91) Zen, A.; Pflaum, J.; Hirschmann, S.; Zhuang, W.; Jaiser, F.; Asawapirom, U.; Rabe, J. P.; Scherf, U.; Neher, D. *Adv. Funct. Mater.* **2004**, *14*, 757.
- (92) Babel, A.; Jenekhe, S. A. *Synth. Met.* **2005**, *148*, 169.
- (93) Ong, B. S.; Wu, Y. L.; Liu, P.; Gardner, S. *Adv. Mater.* **2005**, *17*, 1141.
- (94) Ong, B. S.; Wu, Y. L.; Liu, P. *Proc. IEEE* **2005**, *93*, 1412.
- (95) Wu, Y. L.; Liu, P.; Gardner, S.; Ong, B. S. *Chem. Mater.* **2005**, *17*, 221.
- (96) Ong, B.; Wu, Y. L.; Jiang, L.; Liu, P.; Murti, K. *Synth. Met.* **2004**, *142*, 49.
- (97) McCulloch, I.; Heeney, M.; Bailey, C.; Genevicius, K.; Macdonald, I.; Shkunov, M.; Sparrowe, D.; Tierney, S.; Wagner, R.; Zhang, W. M.; Chabinyc, M. L.; Kline, R. J.; McGehee, M. D.; Toney, M. F. *Nat. Mater.* **2006**, *5*, 328.
- (98) Sirringhaus, H.; Wilson, R. J.; Friend, R. H.; Inbasekaran, M.; Wu, W.; Woo, E. P.; Grell, M.; Bradley, D. D. C. *Appl. Phys. Lett.* **2000**, *77*, 406.
- (99) Sirringhaus, H.; Kawase, T.; Friend, R. H.; Shimoda, T.; Inbasekaran, M.; Wu, W.; Woo, E. P. *Science* **2000**, *290*, 2123.
- (100) Hamilton, M. C.; Martin, S.; Kanicki, J. *Chem. Mater.* **2004**, *16*, 4699.
- (101) Usta, H.; Lu, G.; Facchetti, A.; Marks, T. J. *J. Am. Chem. Soc.* **2006**, *128*, 9034.
- (102) Yamamoto, T.; Kokubo, H.; Kobashi, M.; Sakai, Y. *Chem. Mater.* **2004**, *16*, 4616.
- (103) Champion, R. D.; Cheng, K. F.; Pai, C. L.; Chen, W. C.; Jenekhe, S. A. *Macromol. Rapid Commun.* **2005**, *26*, 1835.

- (104) Zhu, Y.; Champion, R. D.; Jenekhe, S. A. *Macromolecules* **2006**, *39*, 8712.
- (105) Osaka, I.; Sauve, G.; Zhang, R.; Kowalewski, T.; McCullough, R. D. *Adv. Mater.* **2007**, *19*, 4160.
- (106) Zhang, M.; Tsao, H. N.; Pisula, W.; Yang, C. D.; Mishra, A. K.; Müllen, K. *J. Am. Chem. Soc.* **2007**, *129*, 3472.
- (107) Zhan, X. W.; Tan, Z. A.; Domercq, B.; An, Z. S.; Zhang, X.; Barlow, S.; Li, Y. F.; Zhu, D. B.; Kippelen, B.; Marder, S. R. *J. Am. Chem. Soc.* **2007**, *129*, 7246.
- (108) Yan, H.; Chen, Z. H.; Zheng, Y.; Newman, C.; Quinn, J. R.; Dotz, F.; Kastler, M.; Facchetti, A. *Nature* **2009**, *457*, 679.
- (109) Yamamoto, T.; Yasuda, T.; Sakai, Y.; Aramaki, S.; Ramaw, A. *Macromol. Rapid Commun.* **2005**, *26*, 1214.
- (110) Zaumseil, J.; Donley, C. L.; Kim, J. S.; Friend, R. H.; Sirringhaus, H. *Adv. Mater.* **2006**, *18*, 2708.
- (111) Steckler, T. T.; Zhang, X.; Hwang, J.; Honeyager, R.; Ohira, S.; Zhang, X. H.; Grant, A.; Ellinger, S.; Odom, S. A.; Sweat, D.; Tanner, D. B.; Rinzler, A. G.; Barlow, S.; Brédas, J. L.; Kippelen, B.; Marder, S. R.; Reynolds, J. R. *J. Am. Chem. Soc.* **2009**, *131*, 2824.
- (112) Tanase, C.; Wildeman, J.; Blom, P. W. M.; Mena Benito, M. E.; de Leeuw, D. M.; van Breemen, A. J. J. M.; Herwig, P. T.; Chlon, C. H. T.; Sweelssen, J.; Schoo, H. F. M. *J. Appl. Phys.* **2005**, *97*.
- (113) van Breemen, A. J. J. M.; Herwig, P. T.; Chlon, C. H. T.; Sweelssen, J.; Schoo, H. F. M.; Benito, E. M.; de Leeuw, D. M.; Tanase, C.; Wildeman, J.; Blom, P. W. M. *Adv. Funct. Mater.* **2005**, *15*, 872.
- (114) Zou, Y. P.; Gendron, D.; Badrou-Aich, R.; Najari, A.; Tao, Y.; Leclerc, M. *Macromolecules* **2009**, *42*, 2891.
- (115) Li, Y. N.; Wu, Y. L.; Ong, B. S. *Macromolecules* **2006**, *39*, 6521.
- (116) Miao, X.; Crispin, X.; Perzon, E.; Andersson, M. R.; Pullerits, T.; Andersson, M.; Inganäs, O.; Berggren, M. *Appl. Phys. Lett.* **2005**, *87*, 252105.
- (117) Babel, A.; Jenekhe, S. A. *J. Am. Chem. Soc.* **2003**, *125*, 13656.
- (118) Donley, C. L.; Zaumseil, J.; Andreasen, J. W.; Nielsen, M. M.; Sirringhaus, H.; Friend, R. H.; Kim, J. S. *J. Am. Chem. Soc.* **2005**, *127*, 12890.
- (119) Peumans, P.; Uchida, S.; Forrest, S. R. *Nature* **2003**, *425*, 158.
- (120) Yang, F.; Shtein, M.; Forrest, S. R. *Nat. Mater.* **2005**, *4*, 37.
- (121) Yang, F.; Shtein, M.; Forrest, S. R. *J. Appl. Phys.* **2005**, *98*.
- (122) Uchida, S.; Xue, J. G.; Rand, B. P.; Forrest, S. R. *Appl. Phys. Lett.* **2004**, *84*, 4218.
- (123) Xue, J. G.; Rand, B. P.; Uchida, S.; Forrest, S. R. *J. Appl. Phys.* **2005**, *98*.
- (124) Xue, J. G.; Uchida, S.; Rand, B. P.; Forrest, S. R. *Appl. Phys. Lett.* **2004**, *84*, 3013.
- (125) Xue, J. G.; Uchida, S.; Rand, B. P.; Forrest, S. R. *Appl. Phys. Lett.* **2004**, *85*, 5757.
- (126) Ma, B. W.; Woo, C. H.; Miyamoto, Y.; Fréchet, J. M. J. *Chem. Mater.* **2009**, *21*, 1413.
- (127) Sakai, J.; Taima, T.; Yamanari, T.; Saito, K., *Sol. Energ. Mat. Sol. C.* **2009**, *93*, 1149.

- (128) Schulze, K.; Urich, C.; Schuppel, R.; Leo, K.; Pfeiffer, M.; Brier, E.; Reinold, E.; Bauerle, P. *Adv. Mater.* **2006**, *18*, 2872.
- (129) Lloyd, M. T.; Mayer, A. C.; Tayi, A. S.; Bowen, A. M.; Kasen, T. G.; Herman, D. J.; Mourey, D. A.; Anthony, J. E.; Malliaras, G. G. *Org. Electron.* **2006**, *7*, 243.
- (130) Lloyd, M. T.; Mayer, A. C.; Subramanian, S.; Mourey, D. A.; Herman, D. J.; Bapat, A. V.; Anthony, J. E.; Malliaras, G. G. *J. Am. Chem. Soc.* **2007**, *129*, 9144.
- (131) Tamayo, A. B.; Dang, X. D.; Walker, B.; Seo, J.; Kent, T.; Nguyen, T. Q. *Appl. Phys. Lett.* **2009**, *94*.
- (132) Karpe, S.; Cravino, A.; Frere, P.; Allain, M.; Mabon, G.; Roncali, J. *Adv. Funct. Mater.* **2007**, *17*, 1163.
- (133) Roquet, S.; Cravino, A.; Leriche, P.; Aleveque, O.; Frere, P.; Roncali, J. *J. Am. Chem. Soc.* **2006**, *128*, 3459.
- (134) Kim, J. Y.; Kim, S. H.; Lee, H. H.; Lee, K.; Ma, W. L.; Gong, X.; Heeger, A. J. *Adv. Mater.* **2006**, *18*, 572.
- (135) Ma, W. L.; Yang, C. Y.; Gong, X.; Lee, K.; Heeger, A. J. *Adv. Funct. Mater.* **2005**, *15*, 1617.
- (136) Schilinsky, P.; Waldauf, C.; Brabec, C. J. *Appl. Phys. Lett.* **2002**, *81*, 3885.
- (137) Kim, Y.; Choulis, S. A.; Nelson, J.; Bradley, D. D. C.; Cook, S.; Durrant, J. R. *Appl. Phys. Lett.* **2005**, *86*, 572.
- (138) Schilinsky, P.; Asawapirom, U.; Scherf, U.; Biele, M.; Brabec, C. J. *Chem. Mater.* **2005**, *17*, 2175.
- (139) Hiorns, R. C.; De Bettignies, R.; Leroy, J.; Bailly, S.; Firon, M.; Sentein, C.; Khoukh, A.; Preud'homme, H.; Dagron-Lartigau, C. *Adv. Funct. Mater.* **2006**, *16*, 2263.
- (140) Ma, W.; Kim, J. Y.; Lee, K.; Heeger, A. J. *Macromol. Rapid Commun.* **2007**, *28*, 1776.
- (141) Kim, Y.; Cook, S.; Tuladhar, S. M.; Choulis, S. A.; Nelson, J.; Durrant, J. R.; Bradley, D. D. C.; Giles, M.; McCulloch, I.; Ha, C. S.; Ree, M. *Nat. Mater.* **2006**, *5*, 197.
- (142) Yang, X. N.; Loos, J.; Veenstra, S. C.; Verhees, W. J. H.; Wienk, M. M.; Kroon, J. M.; Michels, M. A. J.; Janssen, R. A. J. *Nano Lett.* **2005**, *5*, 579.
- (143) Savenije, T. J.; Kroeze, J. E.; Yang, X. N.; Loos, J. *Adv. Funct. Mater.* **2005**, *15*, 1260.
- (144) Erb, T.; Zhokhavets, U.; Gobsch, G.; Raleva, S.; Stuhn, B.; Schilinsky, P.; Waldauf, C.; Brabec, C. J. *Adv. Funct. Mater.* **2005**, *15*, 1193.
- (145) Mihailetschi, V. D.; Xie, H. X.; de Boer, B.; Koster, L. J. A.; Blom, P. W. M. *Adv. Funct. Mater.* **2006**, *16*, 699.
- (146) Peet, J.; Soci, C.; Coffin, R. C.; Nguyen, T. Q.; Mikhailovsky, A.; Moses, D.; Bazan, G. C. *Appl. Phys. Lett.* **2006**, *89*.
- (147) Li, Y. F.; Zou, Y. P. *Adv. Mater.* **2008**, *20*, 2952.
- (148) Hou, J. H.; Tan, Z. A.; Yan, Y.; He, Y. J.; Yang, C. H.; Li, Y. F. *J. Am. Chem. Soc.* **2006**, *128*, 4911.
- (149) Zhou, E. J.; Tan, Z.; Yang, C. H.; Li, Y. F. *Macromol. Rapid Commun.* **2006**, *27*, 793.
- (150) Zhou, E. J.; Tan, Z.; Yang, Y.; Huo, L. J.; Zou, Y. P.; Yang, C. H.; Li, Y. F. *Macromolecules* **2007**, *40*, 1831.

- (151) Parmer, J. E.; Mayer, A. C.; Hardin, B. E.; Scully, S. R.; McGehee, M. D.; Heeney, M.; McCulloch, I. *Appl. Phys. Lett.* **2008**, *92*, 113309.
- (152) Schulz, G. L.; Chen, X. W.; Holdcroft, S. *Appl. Phys. Lett.* **2009**, *94*, 3.
- (153) Liang, Y.; Feng, D.; Wu, Y.; Tsai, S. T.; Li, G.; Ray, C.; Yu, L. *J. Am. Chem. Soc.* **2009**, *131*, 7792.
- (154) Brabec, C. J.; Winder, C.; Sariciftci, N. S.; Hummelen, J. C.; Dhanabalan, A.; van Hal, P. A.; Janssen, R. A. J. *Adv. Funct. Mater.* **2002**, *12*, 709.
- (155) Bundgaard, E.; Krebs, F. C. *Sol. Energ. Mater. Sol. C.* **2007**, *91*, 1019.
- (156) Bundgaard, E.; Shaheen, S. E.; Krebs, F. C.; Ginley, D. S. *Sol. Energ. Mater. Sol. C.* **2007**, *91*, 1631.
- (157) Wienk, M. M.; Turbiez, M. G. R.; Struijk, M. P.; Fonrodona, M.; Janssen, R. A. J. *Appl. Phys. Lett.* **2006**, *88*, 3.
- (158) Muhlbacher, D.; Scharber, M.; Morana, M.; Zhu, Z. G.; Waller, D.; Gaudiana, R.; Brabec, C. *Adv. Mater.* **2006**, *18*, 2884.
- (159) Peet, J.; Kim, J. Y.; Coates, N. E.; Ma, W. L.; Moses, D.; Heeger, A. J.; Bazan, G. C. *Nat. Mater.* **2007**, *6*, 497.
- (160) Tan, Z. A.; Zhou, E. J.; Zhan, X. W.; Wang, X.; Li, Y. F.; Barlow, S.; Marder, S. R. *Appl. Phys. Lett.* **2008**, *93*, 3.
- (161) Zhou, E. J.; Nakamura, M.; Nishizawa, T.; Zhang, Y.; Wei, Q. S.; Tajima, K.; Yang, C. H.; Hashimoto, K. *Macromolecules* **2008**, *41*, 8302.
- (162) Yue, W. Z.; Yun; Shao, Shuyan; Tian, Hongkun; Xie, Zhiyuan; Geng, Yanhou; Wang, Fosong *J. Mater. Chem.* **2009**, *19*, 2199.
- (163) Slooff, L. H.; Veenstra, S. C.; Kroon, J. M.; Moet, D. J. D.; Sweelssen, J.; Koetse, M. M. *Appl. Phys. Lett.* **2007**, *90*, 3.
- (164) Gadisa, A.; Mammo, W.; Andersson, L. M.; Admassie, S.; Zhang, F.; Andersson, M. R.; Inganas, O. *Adv. Funct. Mater.* **2007**, *17*, 3836.
- (165) Zhang, F. L.; Mammo, W.; Andersson, L. M.; Admassie, S.; Andersson, M. R.; Inganas, L.; Ingands, O. *Adv. Mater.* **2006**, *18*, 2169.
- (166) Wang, E. G.; Wang, L.; Lan, L. F.; Luo, C.; Zhuang, W. L.; Peng, J. B.; Cao, Y. *Appl. Phys. Lett.* **2008**, *92*, 3.
- (167) Blouin, N.; Leclerc, M. *Acc. Chem. Res.* **2008**, *41*, 1110.
- (168) Blouin, N.; Michaud, A.; Gendron, D.; Wakim, S.; Blair, E.; Neagu-Plesu, R.; Belletete, M.; Durocher, G.; Tao, Y.; Leclerc, M. *J. Am. Chem. Soc.* **2008**, *130*, 732.
- (169) Blouin, N.; Michaud, A.; Leclerc, M. *Adv. Mater.* **2007**, *19*, 2295.
- (170) Park, S. H.; Roy, A.; Beaupre, S.; Cho, S.; Coates, N.; Moon, J. S.; Moses, D.; Leclerc, M.; Lee, K.; Heeger, A. J. *Nat. Photonics* **2009**, *3*, 297.
- (171) Brabec, C. J.; Shaheen, S. E.; Winder, C.; Sariciftci, N. S.; Denk, P. *Appl. Phys. Lett.* **2002**, *80*, 1288.
- (172) Mihailetschi, V. D.; Koster, L. J. A.; Blom, P. W. M.; Melzer, C.; de Boer, B.; van Duren, J. K. J.; Janssen, R. A. J. *Adv. Funct. Mater.* **2005**, *15*, 795.
- (173) Hoppe, H.; Niggemann, M.; Winder, C.; Kraut, J.; Hiesgen, R.; Hinsch, A.; Meissner, D.; Sariciftci, N. S. *Adv. Funct. Mater.* **2004**, *14*, 1005.
- (174) Wittmann, H. F.; Friend, R. H.; Khan, M. S.; Lewis, J. J. *Chem. Phys.* **1994**, *101*, 2693.

- (175) Sandee, A. J.; Williams, C. K.; Evans, N. R.; Davies, J. E.; Boothby, C. E.; Kohler, A.; Friend, R. H.; Holmes, A. B. *J. Am. Chem. Soc.* **2004**, *126*, 7041.
- (176) Guo, F. Q.; Kim, Y. G.; Reynolds, J. R.; Schanze, K. S. *Chem. Commun.* **2006**, 1887.
- (177) Kohler, A.; Wittmann, H. F.; Friend, R. H.; Khan, M. S.; Lewis, J. *Synth. Met.* **1996**, *77*, 147.
- (178) Wong, W. Y.; Wang, X. Z.; He, Z.; Djuricic, A. B.; Yip, C. T.; Cheung, K. Y.; Wang, H.; Mak, C. S. K.; Chan, W. K. *Nat. Mater.* **2007**, *6*, 521.
- (179) Lu, J. P.; Liang, F. S.; Drolet, N.; Ding, J. F.; Tao, Y.; Movileanu, R. *Chem. Commun.* **2008**, 5315.
- (180) Chen, J., Cao, Y. *Acc. Chem. Res.* **2009**, ASAP.

## CHAPTER 2

# N-ARYL DITHIENOPYRROLE DIMER, TRIMER AND HOMOPOLYMER

### 2.1 Introduction

Thiophene-based conjugated materials (oligothiophenes and polythiophenes) are among the most promising materials for OFETs and other electronic devices based on organic semiconductors.<sup>1</sup> Oligothiophenes are one of the most prominent classes of organic semiconducting small molecules and have been widely studied in electronic devices; in many cases these compounds have been deposited from vapor phase. They also serve as models for understanding polythiophenes.<sup>1-3</sup> In recent years, fused thiophene derivatives have been incorporated into the oligomers and polymers for OFETs, and it has been suggested that rigid fused-ring units can facilitate the  $\pi$ - $\pi$  stacking intermolecular interactions and lead to higher charge carrier mobilities.<sup>4-6</sup> For example, [2,2']bi(dithieno[3,2-*b*:2',3'-*d*]thiophenyl) (**9** in Figure 1.11) exhibits a mobility of 0.05 cm<sup>2</sup>/(Vs) with  $I_{\text{on}}/I_{\text{off}}$  ratios  $>10^8$ , and the crystal structure of the oligomer reveals a face-to-face  $\pi$ -stacked structure.<sup>7</sup> Very recently, a dithienothiophene dimer (**I** in Figure 2.1) functionalized with trialkyloxyphenyl group was found to exhibit liquid crystalline behavior and showed hole mobility of  $1.7 \times 10^{-3}$  cm<sup>2</sup>/(Vs) after annealing in a solution-processable OFET.<sup>8</sup> Examples of polymers incorporating fused-thiophene have

been discussed in section 1.4.2, such as **27**, **28** in Figure 1.13.

Dithieno[3,2-*b*:2',3'-*d*]pyrrole (DTP) has been incorporated into oligomers and polymers more recently.<sup>9-15</sup> The rationale for using DTP is, firstly that the *N*-substituents of DTP groups can be used to help improve solubility without leading to large torsion angles between the fused thiophene unit and neighboring monomers in a conjugated polymer chain. In contrast, the dithienothiophene moiety can only be solubilized by the use of 3,5-substitution; this would be anticipated to seriously affect the coplanarity achievable with the neighboring groups. Secondly, DTP-based compounds have also been shown to be more easily oxidized than analogous bithiophene and dithienothiophene compounds; for example, compounds **II-A** and **II-B** (Figure 2.1) are 0.2-0.3 V more readily oxidized than their DTT analogues.<sup>16</sup> Accordingly, DTP-based materials are anticipated to exhibit lower hole injection barriers than their DTT analogues. Other DTP-based materials have been reported, for example, compounds incorporating a central DTP unit (**III** in Figure 2.1) exhibit high fluorescent efficiencies in solution (fluorescent quantum yields up to 53%).<sup>15</sup>

Homopolymers of *N*-alkyl and aryl DTPs (**IV** in Figure 2.1) have been synthesized and studied over the years. Before 2007, most DTP homopolymers (**IV-A**) were obtained by oxidative polymerizations, and their optical properties (absorption, emission) were studied.<sup>14,17</sup> In 2007, Koeckelberghs *et al.* reported a systematic study of coupling methodologies for obtaining DTP homopolymers (**IV-B**); they found that Stille coupling

gave better results, in term of obtaining high molecular weights, than Yamamoto method (reductive homocoupling of aryl halides catalyzed by Ni(0)) or oxidative couplings.<sup>13</sup> Later on the same group also reported the conformation changes in solutions of a chiral DTP homopolymer (**IV-C**).<sup>11</sup>

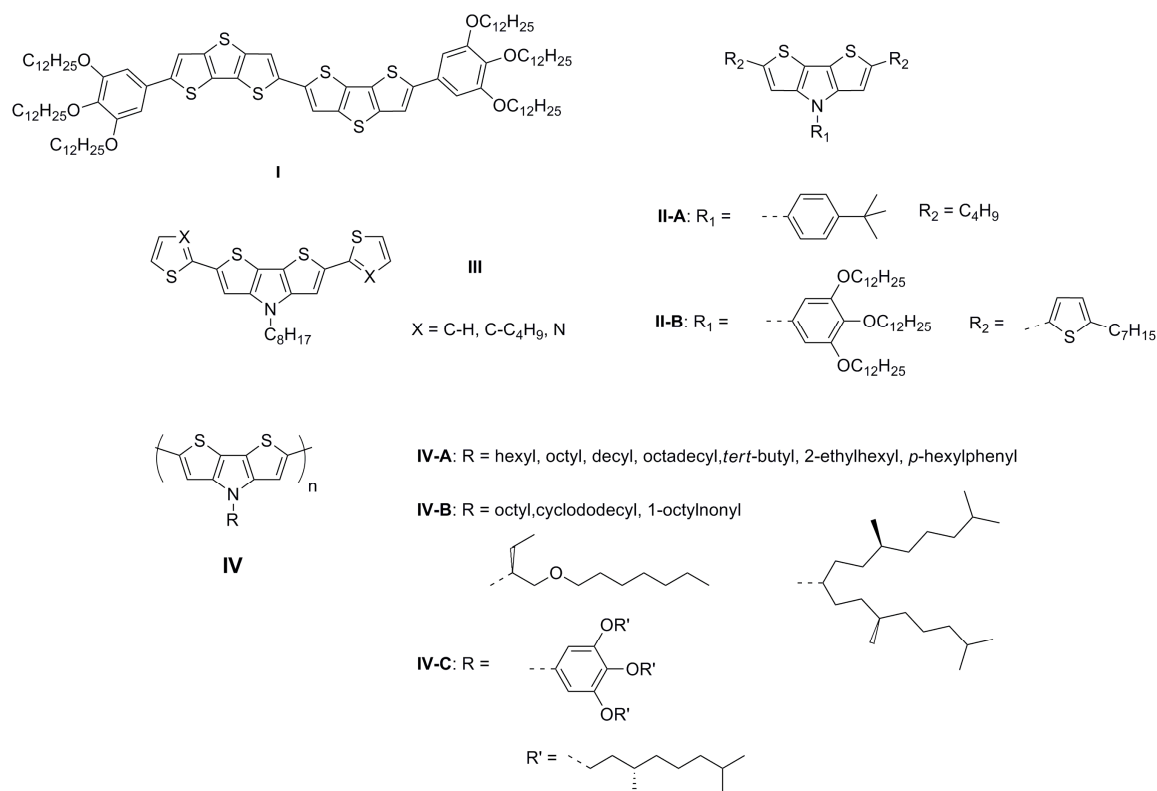


**Figure 2.1** Structures of the compounds (**I-IV**) discussed in the text.

In this chapter, *N*-aryl DTP dimers, a trimer, and a homopolymer (Figure 2.2) have been synthesized by Pd-catalyzed coupling and characterized in order to study the effects of extended conjugation on their optical and electronic properties. They can be

chemically oxidized and the optical properties of radical ions have been compared. In the last portion, a DTP homopolymer has been obtained by electropolymerization, and the spectroelectrochemistry of the electro-polymerized homopolymer has been compared with the absorption spectra obtained from chemical oxidation of the homopolymer synthesized by Stille coupling.

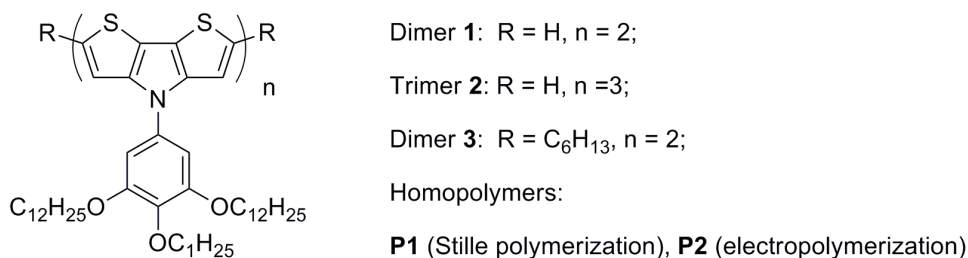
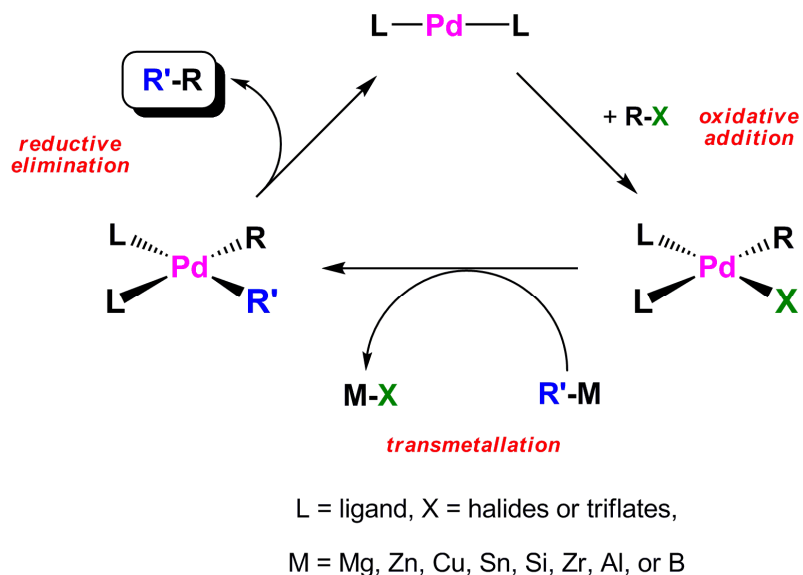


**Figure 2.2** Target compounds in Chapter 2.

## 2.2 Synthesis

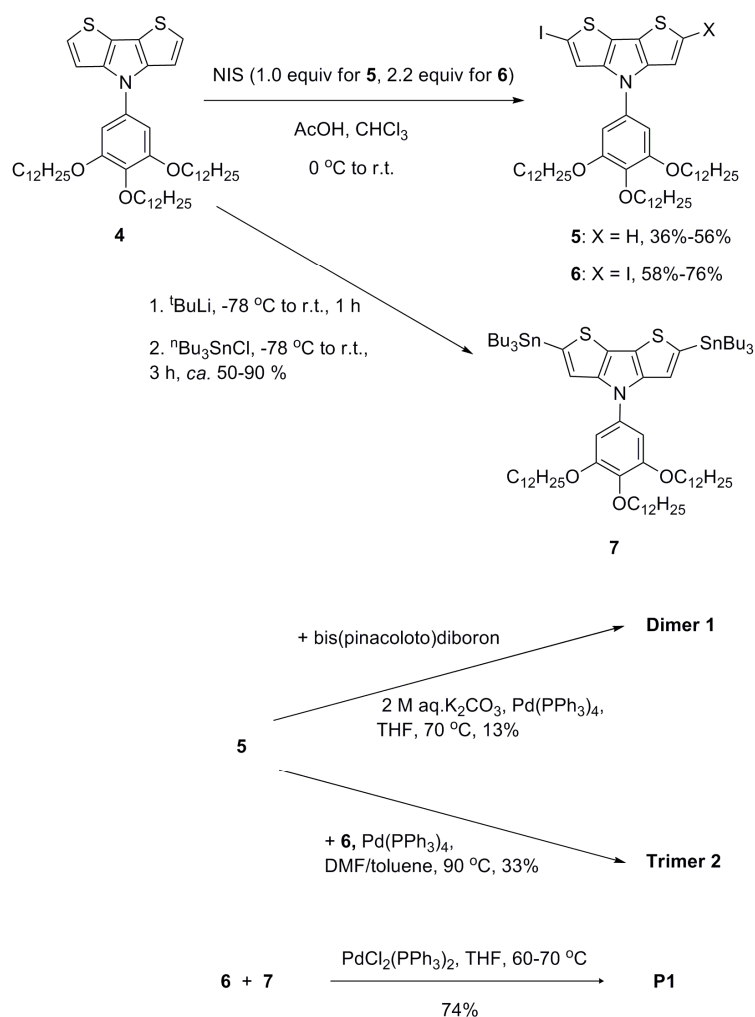
Transition-metal-catalyzed coupling reactions of various organometallic reagents have been widely employed in the synthesis of conjugated materials. Among those, palladium-catalyzed cross-coupling is one of the most widely used methods, including Stille, Suzuki, Sonogashira, Heck couplings, and the generic catalytic mechanism is shown below in Scheme 2.1.<sup>18</sup> In this chapter, both Stille and Suzuki couplings have been used in the synthesis of these oligomers and polymers. In the latter chapters, Stille coupling has been chosen for those polymerizations, as discussed in more detail in Chapter 3.



**Scheme 2.1** Generic catalytic mechanism of Pd-catalyzed cross-coupling reactions.

The synthesis of dimer **1** and trimer **2** is shown in Scheme 2.2. The intermediates, mono and diiodo-substituted DTPs (**5** and **6**), were synthesized by reacting with unsubstituted DTP (**4**) with appropriate quantities of *N*-iodosuccinimide in acetic acid/chloroform. Dimer **1** was synthesized by standard Suzuki coupling of 2-iodo-*N*-(3,4,5-tri-*n*-dodecyloxyphenyl)-dithieno[3,2-*b*:2',3'-*d*]pyrrole (**5**) and bis(pinacolato)diboron. Although the desired product appeared to be one of the major products (based on thin layer chromatography), the isolated yield is low (13%), presumably due to the poor separations of the desired product from other side products either by normal column chromatography using silica gel or alumina, or by size-exclusion column (SEC) chromatography. The desired product was not isolated in a pure form on an over 100 mg scale, even after performing SEC column chromatography

twice, although small amounts can be obtained analytically pure. Trimer **2** was prepared by Stille coupling of *N*-(3,4,5-tri-*n*-decyloxyphenyl)-2,6-di(tri-*n*-butylstannyl)-dithieno[3,2-*b*:2',3'-*d*]pyrrole (**7**) with the monoiodo-substituted DTP (**5**). The condition optimizations to obtain pure distannyl derivatives of DTPs, including compound **7**, will be discussed in detail in section 3.2.

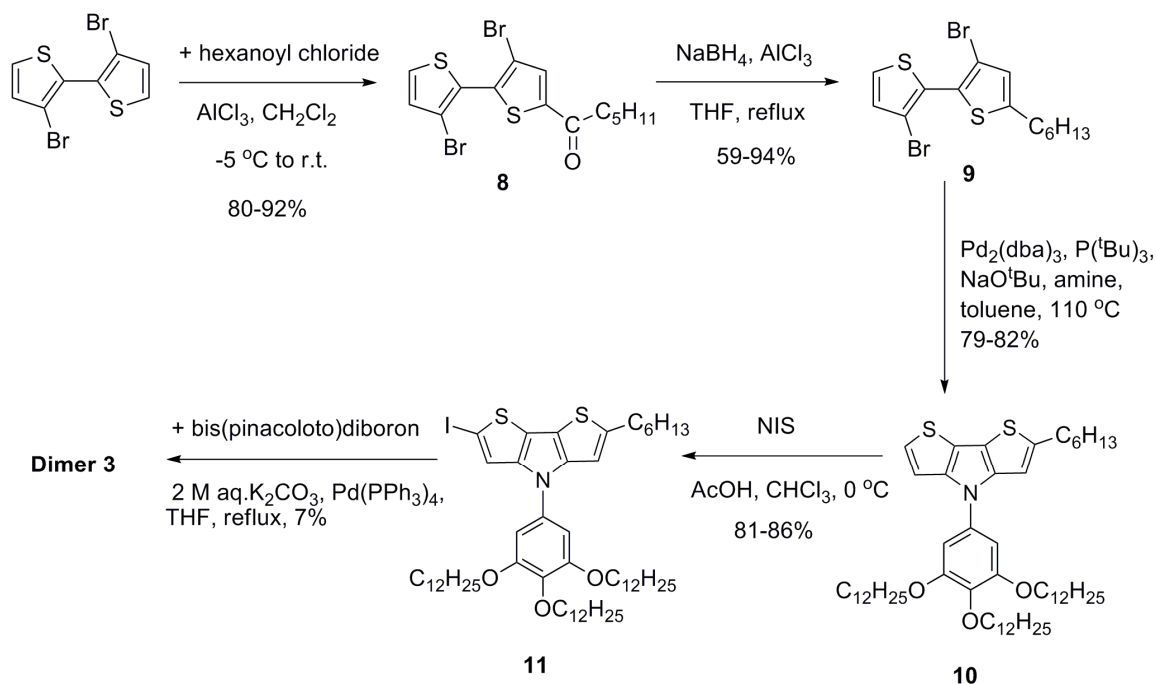


**Scheme 2.2** Synthesis of **1**, **2** and **P1**.

A DTP homopolymer **P1** was obtained by standard Stille polymerization of diiodo-substituted DTP (**6**) and the corresponding bistannyl derivative of DTP (**7**). **P1** is readily soluble in common organic solvents, such as THF, chloroform, and toluene. The weight-average molecular weight ( $M_w$ ) and polydispersity ( $M_w/M_n$ ) were estimated by gel-permeation chromatography (GPC) against polystyrene standards using THF as eluent. The  $M_w$  of the polymer **P1** was 17k, and polydispersity was 2.1.

Dimer **3** was prepared to have the possible reactive sites blocked by the alkyl substituents. Thiophene derivatives with unsubstituted 2 and / or 5 positions often exhibit irreversible oxidative electrochemistry, due to subsequent the chemical instability of the radical cations with respect to dimerization, oligomerization, or polymerization reactions. For examples, polymerization reactions have been shown to occur at the 2- and 5-positions of 3-alkylthiophenes upon oxidation, either using chemical or electrochemical oxidative conditions.<sup>19</sup> Indeed, this process forms the basis of electropolymerization as a preparative method for conjugated polymers. It was previously found that blocking these terminal positions in small-molecule DTP, such as **II-A** in Figure 2.1, led to a reversible oxidation;<sup>16</sup> here **3** was synthesized in case the radical cation of **1** was unstable, leading to irreversible electrochemistry. In this case, the alkyl substituent on the 2-position was installed before constructing the DTP fused ring. The reasons for designing this synthetic route are described as follows. Firstly, attempts at direct mono-substitution on 2-position of *N*-aryl or alkyl DTP with an alkyl chain were not successful. For example, the reaction

of monoiodo *N*-(trialkylsiloxy)phenyl DTP (**5**) with 2-*n*-butyl-4,4,5,5-tetramethyl-1,3,2-dioxaborolane using Suzuki coupling, resulted in the recovery of the starting material based on the  $^1\text{H}$  NMR analysis of crude products from the reaction mixture. Secondly, the synthetic route in Scheme 2.3 can be used as a general method for preparing mono-alkylated fused-thiophene oligomers, not only for DTP derivatives, but also for other fused ring systems, such as dithienothiophene, dithienophosphine. Although the intermediates **8-11** can be obtained in moderate to high yields, the yield of **3** was low, presumably, as with dimer **1**, due to difficulties in purification.



**Scheme 2.3** Synthesis of dimer **3**.

## 2.3 Density Functional Theory of Electronic Structures

Quantum-chemical calculation of the electronic structures of materials can provide predictions of their optical and electrochemical properties.<sup>20a</sup> For conjugated polymers, the so-called oligomer approach is frequently used, in which the properties of oligomers of increasing chain length are first calculated, and then extrapolated to ideal infinite polymers. Different extrapolation methods are used; among them, linear fits and Kuhn fits are two of the mostly used methods. In the linear fits, the properties of the polymers are estimated by linear extrapolation of plots of the calculated parameters for the oligomers vs.  $1/n$ , where  $n$  is the number of repeating units. Another way of extrapolating to the polymer limit is to use a Kuhn fit for the energy values of the transitions in the oligomers vs.  $1/N$ , where  $N$  is the number of double bonds. This model assumes a system of formal double bonds treated as  $N$  identical oscillators, each vibrating at energy  $E_0$ . If  $N$  adjacent double bonds are coupled with a force constant  $k'$ , and the lowest energy can be written as below:<sup>20b</sup>

$$E = E_0 \sqrt{1 + 2 \frac{k'}{k_0} \cos \frac{\pi}{N+1}} \quad (2.1)$$

where  $k_0$  is the force constant of the isolated oscillator.

The energy gaps between HOMO and LUMO levels,  $E_g$ , and the energies of the lowest lying singlet excited states,  $S_1$ , can be obtained from the quantum-chemical calculations. In many cases, the  $S_1$  transition can be well approximated as a HOMO-LUMO transition, however, other configuration changes (HOMO -  $n$  to LUMO +  $n$ ) may also contribute.

Moreover, the calculated HOMO-LUMO gaps are often larger than the calculated  $S_1$  energies, in part due to the need to overcome the exciton binding energy to dissociate holes and electrons. Hence, often  $S_1$  energies follow the same trends to HOMO-LUMO gap,  $E_g$ , but not necessarily have the same values. At the molecular level, optical bandgap is usually considered to be the adiabatic transition energy from  $S_0$  to  $S_1$  states (the energy differences of the molecule in the relaxed geometries in the  $S_0$  and  $S_1$  states). The trend of calculated vertical  $S_1$  transition energy may, therefore, reflect the trend of optical bandgaps. Furthermore, the difference of the vertical and adiabatic  $S_1$  energies is expected to be small for long chain-length conjugated polymers. Since electrochemical experiments involve removal of an electron from the HOMO or addition to the LUMO, the trends in electrochemical estimates of bandgaps are expected to correlate with the HOMO-LUMO gaps. Therefore, the trend of the calculated  $E_g$  can be used to predict the trend of the bandgaps obtained from the electrochemical methods. However, discrepancies are often observed when comparing experimental and calculated data, which may be due to effects that cause changes in both molecular geometry and the environment, such as conformational effects, substitution effects, and both solvent and solid-state effects.<sup>20a</sup>

Optimized geometries and electronic energy levels of the oligomers in this chapter were calculated in the gas phase using DFT at the B3LYP/6-31G(d,p) level of theory. The  $S_1$  energy calculations were performed at the same level of theory using the time-dependent method (TDDFT). All computational results were obtained from Dr.

Joseph Norton in the Brédas group at the Georgia Institute of Technology. Calculations were performed on oligomer structures with lengths of  $n = 1-6$ , from which properties of the polymer were extrapolated using Kuhn fits of energy versus  $1/N$  where  $N$  is the number of double bonds.<sup>20</sup> Representative HOMO/LUMO wavefunctions are shown in Figure 2.3. The trialkoxyphenyl group is replaced by a methyl group for simplicity. From the schematic illustration of wave functions of the representative oligomer, both HOMO and LUMO are delocalized along the conjugated backbone, and HOMOs of the oligomers can be regarded as out-of-phase combinations of the HOMOs of isolated DTP units, and LUMOs of them are in-phase combinations of local LUMOs; those are similar to that observed in the donor-donor copolymers described in Chapter 3. The predicted  $S_1$  values for the oligomers and homopolymer are summarized in Table 2.1, and comparison with the experimental data will be discussed in Section 2.4.

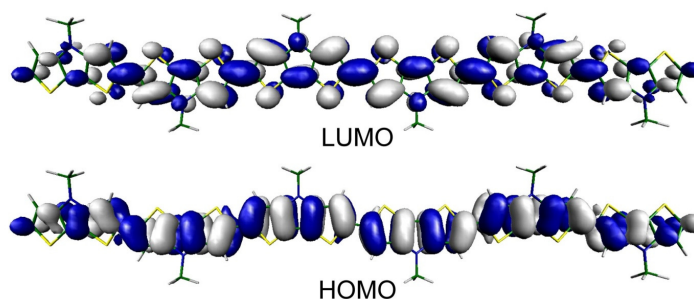


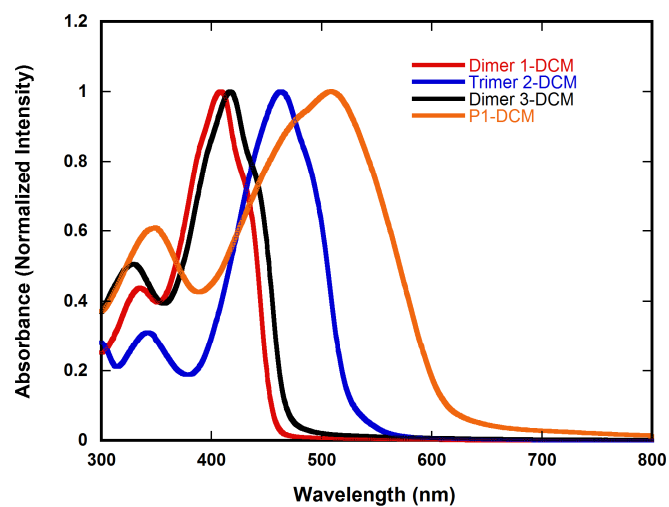
**Figure 2.3** Representative HOMO/LUMO wavefunctions of a DTP oligomer ( $n = 6$ ).

## 2.4 Optical Properties

The normalized optical absorption spectra of the oligomers and polymers in dilute dichloromethane solution are shown in Figure 2.2. The corresponding absorption data are summarized in Table 2.1, and data of monomer **4** is also included as comparison. The oligomers **1-3** and homopolymer **P1** have two major absorption bands, one in the range of 330-350 and another at *ca.* 410-510 nm. It is clearly seen that there is significant red-shifts when the conjugation is extended:  $\lambda_{\text{max}}$  of the compounds in solution vary from 299 nm in monomer **4**, to 410 nm in dimer **1** (417 nm in dimer **3**), then 464 nm in trimer **2**, finally to 510 nm in **P1**. The  $\lambda_{\text{max}}$  and bandgaps of dimers **1** and **3** were very similar, although a slight red-shift was observed from dimer **1** to dimer **3**. The bandgaps for **4**, **1**, **2** and **P1** are 3.54, 2.54, 2.22 and 1.93 eV, estimated from the onsets of the lower energy bands in the solution absorption spectra based on  $E_g \text{ (optical)} = 1240/\lambda_{\text{onset}}$ , follow the trend of the theoretical calculations of the  $S_1$  energy shown in Table 2.1. In thin films, the absorption maxima of **1**, **3** and **P1** were slightly red-shifted and broadened compared to those in solutions. Interestingly, in the thin film of trimer **2**, a significant red-shift in the absorption maxima from 464 nm in solution to 524 nm was observed along with the appearance of a fairly slightly blue-shifted peak at *ca.* 440 nm. This may be due to strong intermolecular interactions in this compound; such interactions are also suggested by XRD data, as discussed in section 2.6. Furthermore, in the thin film spectra, the two

absorption peaks in the range of 480-520 nm in **2** and peaks (400-500 nm) in **3** are presumably due to the vibronic structures (peaks separated by *ca.* 1200-1300  $\text{cm}^{-1}$ ).

a)



b)

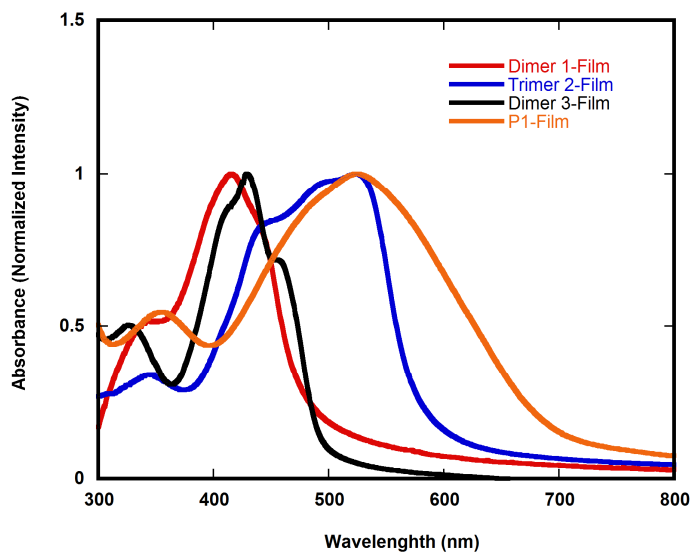


**Figure 2.4** UV-vis spectra of **1-3** and **P1** in a) dilute solutions in dichloromethane and b) in thin films.

**Table 2.1** Optical and redox properties of the compounds in Chapter 2.

Compound	$\lambda_{\max}^{\text{abs}}$ (nm) ( $\epsilon, \times 10^{-4} \text{ M}^{-1} \text{ cm}^{-1}$ or $\alpha, \times 10^{-4} \text{ cm}^{-1}$ )		$E_g^c$ (Optical) (eV)	$S_1^d$ Energy (eV)	$E_{1/2}^{+/0e}$ (CV) (V)	$E_{\text{ox}}^{\text{onset } f}$ (CV) (V)
	Solution <sup>a</sup>	Film <sup>b</sup>				
<b>1</b>	410 (4.24)	416 (2.04)	2.54	3.02	0.21	-
<b>2</b>	464 (7.06)	524 (5.21)	2.22	2.50	0.00	-
<b>3</b>	417 (3.85)	429 (4.09)	2.48	3.02	0.08	-
<b>4</b>	299 (2.88)	-	3.54	4.36	0.38 <sup>g</sup>	
<b>P1</b>	510 (1.54)	526 (1.78)	1.93	1.77	-	0.26 (0.66)

a. measured for diluted solution in dichloromethane (values of molar extinction coefficients,  $\epsilon$ , in the parentheses); b. measured for thin films spin-coated from toluene solution (values of absorption coefficients,  $\alpha$ , in the parentheses); c. values are optical bandgaps estimated from onset absorption edge in solution; d. calculated at B3LYP/6-31G(d,p) level and extrapolated using Kuhn fits; e. measured in 0.1 M <sup>n</sup>Bu<sub>4</sub>NPF<sub>6</sub>/dichloromethane solution and reported vs. [Cp<sub>2</sub>Fe]<sup>+0</sup>; e. measured in 0.1 M <sup>n</sup>Bu<sub>4</sub>NPF<sub>6</sub>/acetonitrile solution and reported vs. [Cp<sub>2</sub>Fe]<sup>+0</sup> (value vs. SCE in the parentheses);<sup>21</sup> g. value for **II-A** in Figure 2.1 obtained in ref 16.

## 2.5 Electrochemical Properties

The electrochemical properties of **1-3** and **P1** have been studied using cyclic voltammetry (CV). From Figure 2.5, the cyclic voltammograms of **1-3** exhibit  $I_{\text{pa}}/I_{\text{pc}}$  (the ratios of the current of oxidative and reductive waves) values of *ca.* 1, and similar profiles to the internal standard, decamethyl ferrocene, indicating chemically reversible oxidations. The half-wave potential ( $E_{1/2}^{+/0}$ ) values (defined as  $(E_{\text{pa}} + E_{\text{pc}})/2$ , where  $E_{\text{pa}}$  and  $E_{\text{pc}}$  are peak oxidation and reduction potentials, respectively) of the first oxidation in **1-3** and 2,6-di-*n*-butyl-*N*-(4-*tert*-butylphenyl)-DTP (**II-A**) are summarized in Table 2.1 (CV of monomer **4** is not reversible). It can clearly be seen that trimer **2** is more easily oxidized than the two dimers, and dimers are more easily oxidized than the analogous

compound **II-A** containing one DTP unit; these results are similar to those observed in other oligomeric systems, such as oligothiophenes or oligo(5,7-bis(thiophen-2-yl)thieno[3,4-*b*]pyrazine)s, when the conjugation length is increased.<sup>22,23</sup> Dimer **3** is more susceptible to oxidation than **1**, presumably due to the inductive electron-donating effect of the terminal hexyl groups. The cyclic voltammogram of a film of **P1** (Figure 2.6) exhibits an onset oxidation peak at +0.26 V vs. [FeCp<sub>2</sub>]<sup>+0</sup> (or +0.66 V vs. SCE,<sup>21</sup> and onset value is defined as the value of the crossing point of two tangent lines in blue). This value falls into the range reported in the literature for other DTP polymers (0.52-0.70 V vs. SCE).<sup>17</sup> The use of CV to characterize the redox properties of polymers will be discussed in detail in section 3.5. Because CV data for oligomers **1-3** and homopolymer **P1** are under different conditions, their CV data cannot be compared directly.

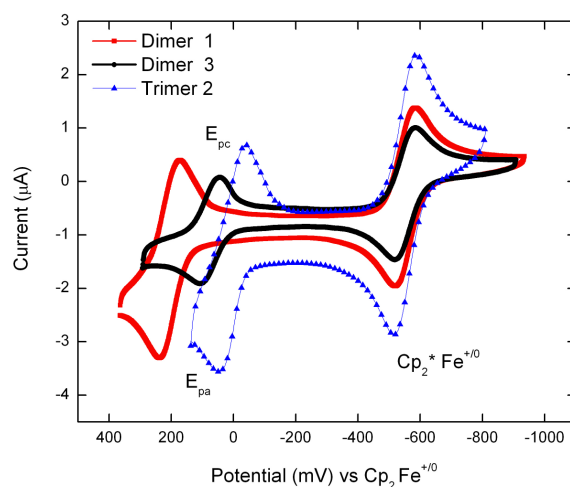


**Figure 2.5** Cyclic voltammogram of **1-3** at a scan rate of 50 mV/sec.

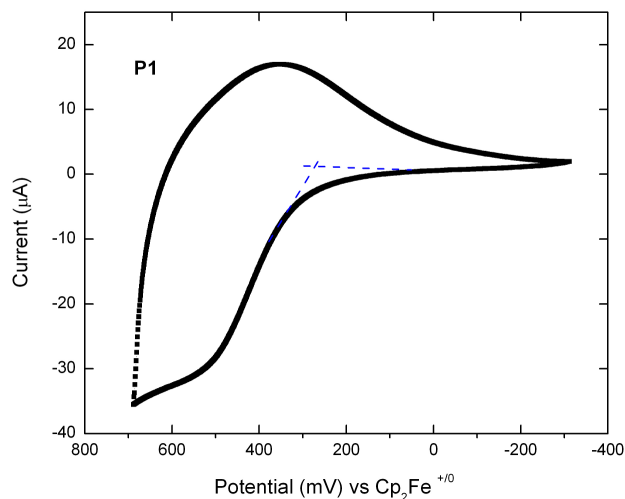


**Figure 2.6** Cyclic voltammogram of **P1** film at a scan rate of 50 mV/sec.

## 2.6 XRD

XRD is a useful tool to obtain valuable information on the molecular packing and crystallinity of organic materials.<sup>24</sup> As previously seen in Figure 2.4, the absorption spectrum of trimer **2** in thin film is significantly different from that in dilute solution; this is assumed to be attributable to strong intermolecular interactions between the individual molecules in the solid state. Therefore, powder XRD of **2** (Figure 2.5) was taken in order to further confirm the assumption. In the diffraction angle,  $2\theta$ , range of  $20\text{--}30^\circ$ , the peak at *ca.*  $20^\circ$  is assigned to a halo peak, which is the characteristic of an amorphous phase, whereas another at *ca.*  $23^\circ$  corresponds to a d-spacing of  $3.9 \text{ \AA}$ , which is close to the  $\pi$ -stacking distances of some other conjugated materials.<sup>9,25</sup> However, it is not clear,

whether the  $\pi$ - $\pi$  interaction formed here arises from the stacking between the DTP units of the conjugated backbone or the phenyl rings of *N*-substituents. In other *N*-alkyl DTP-containing materials, it has been suggested that  $\pi$ - $\pi$  stacks are formed between the DTP cores; this is further supported by a significant red-shift in the solid state UV-vis spectrum compared to that in solution and XRD data.<sup>9</sup> Many other trialkyloxyphenyl-substituted compounds form columnar discotic phases perhaps due to the tendency of trialkyloxyphenyl group to  $\pi$ - $\pi$  stack; however, in many of these discotics stacking is induced between the planar core groups.<sup>26</sup>

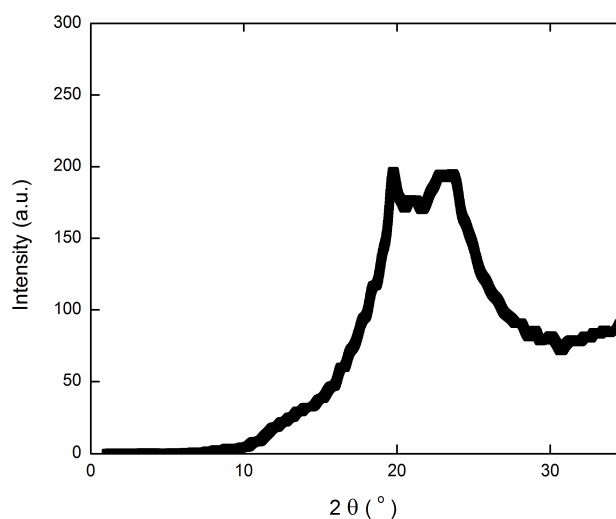


**Figure 2.7** XRD pattern (smoothed) of **2**.

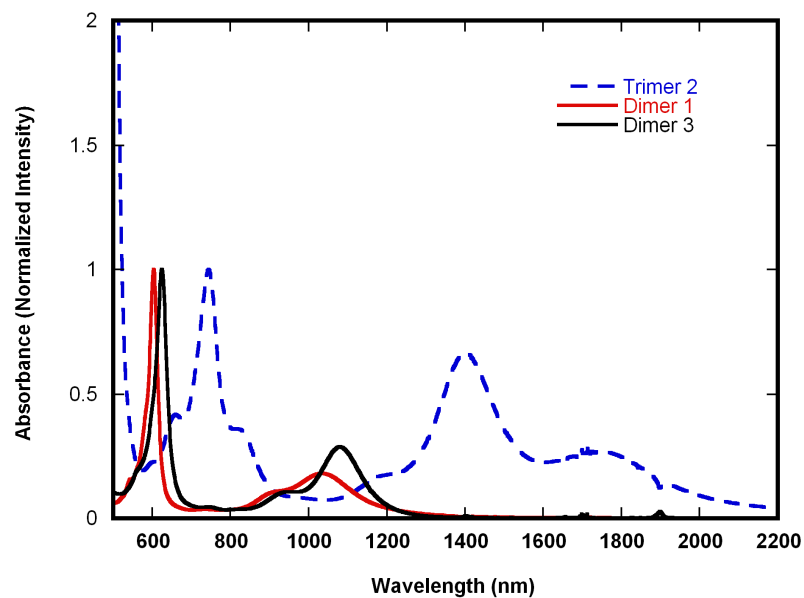
## 2.7 Chemical Oxidations of 1-3 and P1

In hole-transporting materials, the active charge carriers are the radical cations of the

compounds formed upon oxidation.<sup>19,27</sup> Understanding the delocalization of the radical cations along the  $\pi$ -conjugation chain would be useful to afford insight into their charge transport properties. Also, the charged species including cations and dications, often designated as polarons and bipolarons, respectively, have different electronic absorption transitions with their neutral species, which might be useful for other applications, such as electrochromic devices.<sup>27</sup>

Chemical oxidation of the oligomers and homopolymer were carried out by the addition of a strong oxidant, tris(4-bromophenyl)aminium hexachloroantimonate ( $E_{1/2} = 1.36$  V vs.  $\text{Cp}_2\text{Fe}^{+/0}$  in acetonitrile).<sup>21</sup> In the case for **1-3**, *ca.* 0.1 equiv. of oxidant was added to a dilute solution of the neutral compounds in dichloromethane and their monocations were generated. Multiple scans of the solutions showed that the monocations were relatively stable in solution over time. The visible-NIR spectra of monocations of **1-3** are shown in Figure 2.8, normalized to the intensities of their higher energy absorption maxima. It is seen that the spectra of **1**<sup>+</sup> and **3**<sup>+</sup> have similar features with two major absorption bands at *ca.* 600 nm and *ca.* 1000-1100 nm, with slight red-shifts found for **3**<sup>+</sup>. Those spectra are similar as that for a bis(5-alkylthien-2-yl)-substituted DTP oligomer (**II-B** in Figure 2.1) except the low-energy bands is red-shifted.<sup>16</sup> The spectrum of the monocation of **2** is very different with those of the dimers; however, it has some similarities to that of oxidized **P1** (Figure 2.9), and more comparisons will be discussed later.

a)



b)

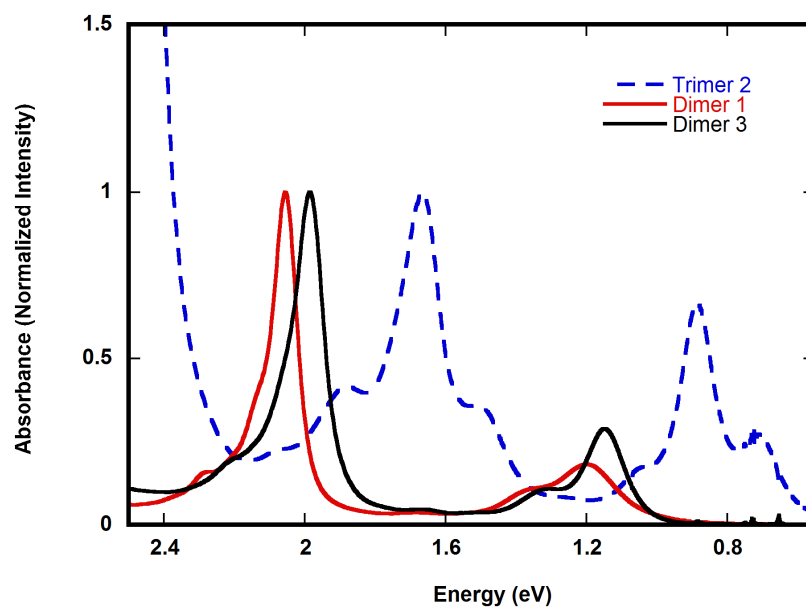
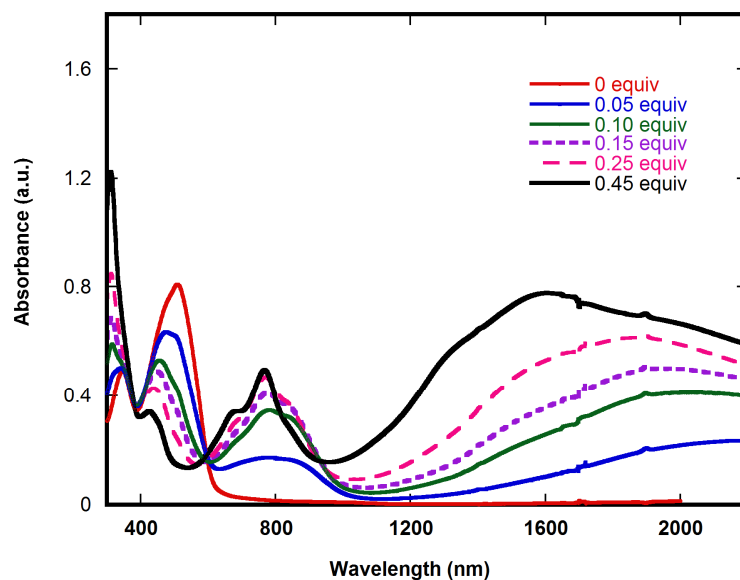


**Figure 2.8** Visible-NIR absorption spectra of monocations of **1-3** in dichloromethane, a) x-axis in wavelength, b) x-axis in eV. The onsets of strong absorption at high energy (at *ca.* 600 nm or 2 eV) in **2** correspond to absorption by the excess neutral compound present.

a)



b)

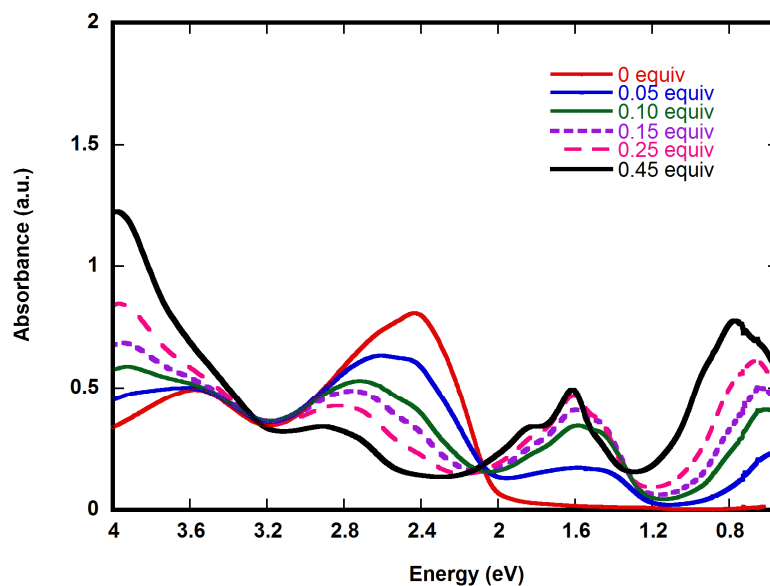


**Figure 2.9** UV-visible-NIR absorption spectra of **P1** upon increasing additions of oxidant, a) x-axis in wavelength, b) x-axis in eV.

For **P1**, tris(4-bromophenyl)aminium hexachloroantimonate was added to a dilute

solution in dichloromethane in small aliquots. It is clearly seen that the peak at *ca.* 500 nm associated with the neutral polymer is diminished, with the growth of peak at *ca.* 800 nm along with appearance of a broad band with an absorption maximum at over 2000 nm when the amounts of the oxidant was increased. When more oxidant was added, the maximum of the peak in the NIR range is shifted to higher energy, from over 2000 nm to *ca.* 1600 nm with the band shape suggesting more than one transition is involved. Those changes are very similar as that seen in the spectroelectrochemistry of the electro-polymerized DTP homopolymer see below (Figure 2.11). The appearance of peaks at *ca.* 800 and 2000 nm upon low levels of oxidant addition (< 0.45 equiv.) is similar to the literature values for radical cation (polaron) in polythiophene (0.65 eV and 1.50 eV, *ca.* 830 and 1900 nm in wavelength).<sup>28,29</sup> There are some further changes upon higher level of doping (> 0.45 equiv), however, it is not clear that whether  $\pi$ -dimers, bipolarons, or both, have started to form in the system; both species have been reported in the literature for oligothiophenes and polythiophenes.<sup>30,31</sup>

In both **2**<sup>+</sup> and oxidized **P1**, one absorption band is seen at *ca.* 800 nm, while other maximum are present in the same NIR region. Both show multiple transitions further out in the NIR region (1200-2000 nm). The similarity in the wavelengths of the absorption maximum may suggest a polaron in **P1** extends over *ca.* three DTP units.<sup>22</sup> This is broadly consistent with results for polythiophenes, in which the literature suggests that a polaron is delocalized over *ca.* five monomer units.<sup>19</sup>

## 2.8 Electropolymerization and Spectroelectrochemistry of P2

Electropolymerization is another attractive method to obtain conjugated polymers, and allows easy and quick characterization of optical and electronic properties.<sup>32</sup> It has been applied to synthesize several conducting polymers, such as polythiophenes, and polypyrroles. In 1992, Berlin *et al.* reported electropolymerization based on 4-*H* (H on nitrogen atom) and *N*-alkyl DTP, but only detailed studies (CV and spectroelectrochemistry) of 4-*H* DTP were carried out. However, the optical absorption of a *N*-alkyl DTP electropolymerized homopolymer was compared with that of 4-*H* DTP in that study.<sup>33</sup> Here, the *N*-(3,4,5-tri-*n*-dodecyloxyphenyl) DTP **4** was electrochemically polymerized in order to compare with the homopolymer synthesized chemically described earlier. Polymer (referred as **P2**) films were deposited from a solution 5 mM in monomer (compound **4**) and 0.1 M in [<sup>n</sup>Bu<sub>4</sub>N]<sup>+</sup>[ClO<sub>4</sub>]<sup>-</sup> on a platinum working electrode or an ITO electrode on glass. Figure 2.10 showed the growth of the polymer film on a platinum working electrode via repeated scan cyclic voltammetry. The resulting film was electrochemically stable, since there is no significant change in CV curves after 50 cycles.

The spectroelectrochemistry (Figure 2.11) was conducted on the electro-polymerized polymer (**P2**) film deposited on an ITO electrode. The absorption maximum of the neutral polymer is seen at the similar wavelength in the literature reported for an *N*-alkyl

DTP electro-polymerized homopolymer.<sup>33</sup> Upon oxidation, the peak at 500-600 nm associated to the neutral polymer was bleached, whereas a peak at *ca.* 750 nm has appeared along the appearance of a broad peak with maximum over 1600 nm, and finally a peak in the IR range (1000 nm to over 1600 nm) was formed. The changes in the spectroelectrochemistry of **P2** are very similar to those upon chemical oxidation of **P1** in solution, which suggested that both chemical and electrochemical methods can lead to similar degrees of oxidation in the DTP homopolymers.

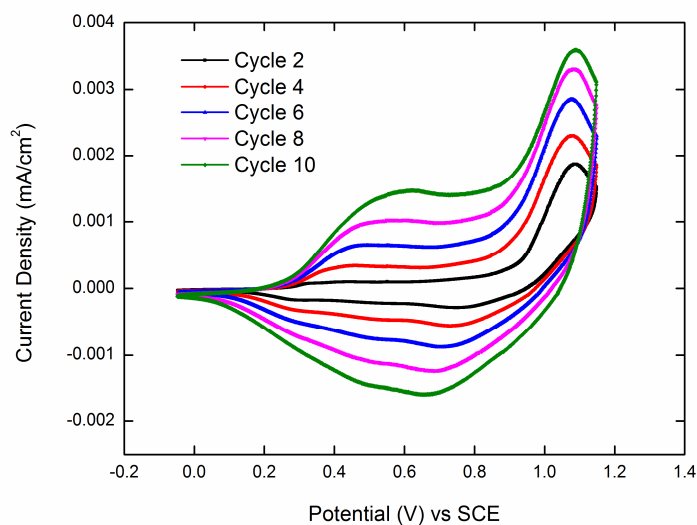
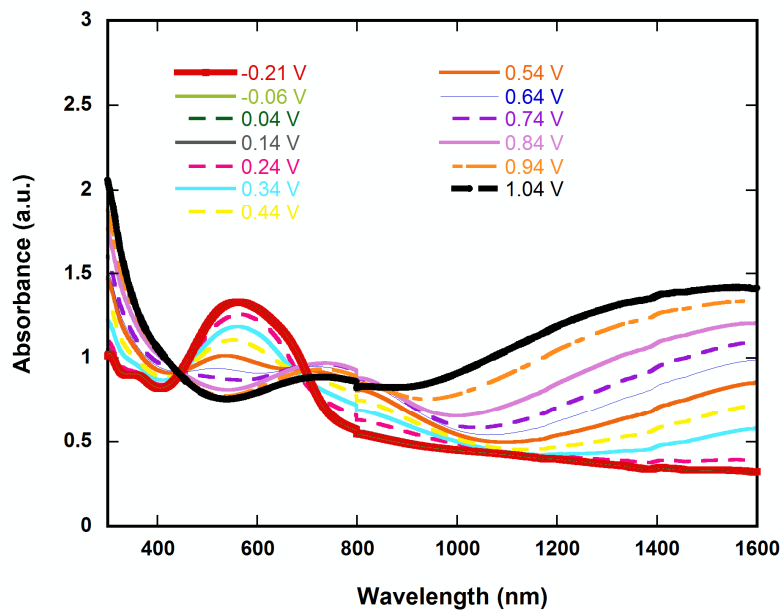


**Figure 2.4** Polymer growth on Pt working electrode in 0.1 M [ $n$ Bu<sub>4</sub>N]<sup>+</sup>[ClO<sub>4</sub>]<sup>-</sup> solution.

a)



b)

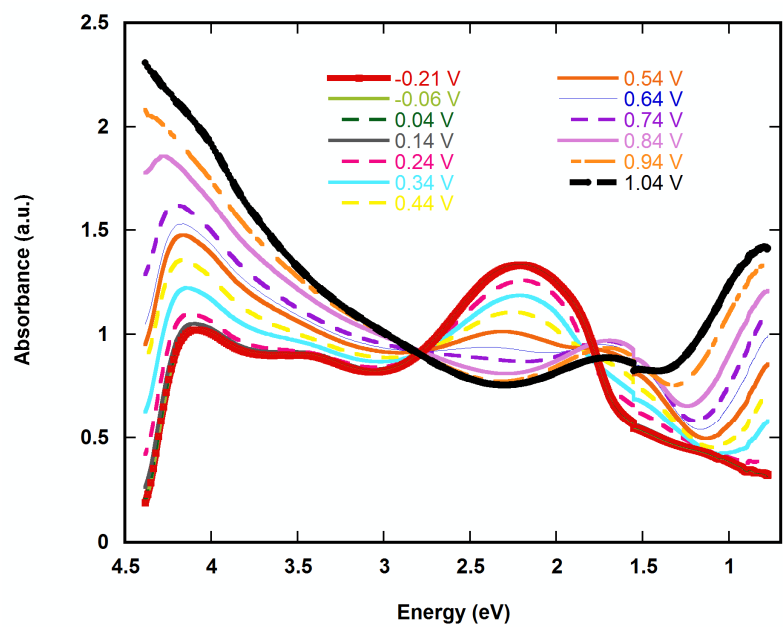


**Figure 2.5** Spectroelectrochemistry of **P2** film on ITO glass. Bold red line = neutral (-0.21 V) and bold black line = oxidized state (1.04V), a) x-axis in wavelength, b) x-axis in eV.

## 2.9 Conclusions

DTP-based oligomers (two dimers and a trimer) along with a homopolymer were synthesized by Pd-catalyzed couplings and characterized. It is clearly seen that the extended conjugation along the DTP main chain can alter their optical and electronic properties. However, the terminal alkyl chain has relatively insignificant effect on those properties. One of the compounds (trimer **3**) exhibited significantly different optical absorption in the thin film from that in solution; this difference was attributed to  $\pi$ - $\pi$  intermolecular interactions in the solid state, which is also supported by XRD data. All of the above compound can be chemically oxidized and their radical cations can be generated. Also a DTP homopolymer was successfully synthesized by electropolymerization, the changes in the spectroelectrochemistry of the electro-polymerized DTP homopolymer is very similar as that observed in the homopolymer synthesized by Stille coupling upon chemical oxidization; this suggested that both chemical and electrochemical methods can lead to similar degrees of oxidation in the DTP homopolymers.

## 2.10 Experimental Section

### Materials.

Unless stated otherwise, starting materials were purchased and were used without further purification. 3,3'-Dibromo-2,2'-bithiophene and 3,4,5-tris(*n*-dodecyloxy)aniline

were prepared by literature procedure<sup>34,35</sup> or provided by Grindus.

### Characterizations.

<sup>1</sup>H NMR and <sup>13</sup>C NMR spectra were measured on a Varian Mercury 300 MHz or Bruker 400 MHz. Mass spectra were measured on a VG Instruments 70-SE using the electron impact (EI) mode or on an Applied Biosystems 4700 Proteomics Analyzer using MALDI mode. Elemental analyses were carried out by Atlantic Microlabs using a LECO 932 CHNS elemental analyzer. A Gel Permeation Chromatography with American Polymer Standards columns (105, 103, 102 Å) was used to determine molecular weights and molecular weight distributions of the polymer; it was equipped with a Waters 510 pump and a Waters 410 differential refractometer, with THF as eluent at a flow rate of 1 mL/min. UV-vis absorption spectra were recorded on a Varian Cary 500 UV/Vis/near IR spectrophotometer. Cyclic voltammetry experiments of **1-3** were performed on an BAS 100B electrochemical analyzer in a three-electrode cell consisting of a glassy carbon working electrode, a platinum wire/flag counter electrode, and a Ag/Ag<sup>+</sup> reference electrode in a 0.1 M [<sup>n</sup>Bu<sub>4</sub>N]<sup>+</sup>[PF<sub>6</sub>]<sup>-</sup>/dichloromethane solution using decamethylferrocene (−0.55 V vs [Cp<sub>2</sub>Fe]<sup>+0</sup> in dichloromethane)<sup>16</sup> as internal standard. Cyclic voltammetry experiments of **P1** was performed on a same instrument in a three-electrode cell consisting of a platinum working electrode, a platinum wire/flag counter electrode, and a Ag/Ag<sup>+</sup> reference electrode in a 0.1 M [<sup>n</sup>Bu<sub>4</sub>N]<sup>+</sup>[PF<sub>6</sub>]<sup>-</sup>/acetonitrile solution using

ferrocene as the internal standard. Obtained values vs  $[\text{Cp}_2\text{Fe}]^{+/0}$  were then converted the value vs. SCE scale assuming the values of  $[\text{Cp}_2\text{Fe}]^{+/0} = 0.40 \text{ V vs SCE}$  (in 0.1 M  $[\text{nBu}_4\text{N}]^+[\text{PF}_6]^-/\text{acetonitrile}$ ).<sup>21</sup> XRD data was collected on a Scintag X1 diffractometer with a Cu K $\alpha$  source ( $\lambda = 1.5406 \text{ \AA}$ ) in a continuous scan mode with a step size of 0.02 degree.

***N*-(3,4,5-Tris(*n*-dodecyloxy)phenyl)-dithieno[3,2-*b*:2',3'-*d*]pyrrole (4).**  $\text{Pd}_2(\text{dba})_3$  (0.45 g, 0.5 mmol), and  $\text{P}(\text{tBu})_3$  (0.40 g, 2.0 mmol) were added to flask and deoxygenated for 30 min, then 3,3'-dibromo-5-hexyl-2,2'-bithiophene (**9**) (4.0 g, 12.3 mmol),  $\text{NaO}^t\text{Bu}$  (9.4 g, 97.9 mmol), 3,4,5-tris(*n*-dodecyloxy)aniline (10.0 g, 15.5 mmol) and dry toluene (*ca.* 100 mL) were added, then heated to 110 °C for 5 h. After the reaction, the mixture was allowed to cool to room temperature. Then water was added, organic layer was separated, and the solvent was removed under reduced pressure. The residue was purified by column chromatography (silica gel, eluent: hexane:  $\text{CH}_2\text{Cl}_2 = 5:1$ ). A yellow solid (5.6 g, 58%) was obtained.  $^1\text{H}$  NMR (300 MHz,  $\text{CD}_2\text{Cl}_2$ ):  $\delta$  7.21 (d,  $J = 5.4 \text{ Hz}$ , 2H), 7.19 (d,  $J = 5.4 \text{ Hz}$ , 2H), 6.76 (s, 2H), 4.00 (m, 6H), 1.80 (m, 6H), 1.44–1.20 (m, 54H), 0.99 (m, 9H). The  $^1\text{H}$  NMR is consistent with that reported in the literature.<sup>16</sup>

**2-Iodo-*N*-(3,4,5-tris(*n*-dodecyloxy)phenyl)-dithieno[3,2-*b*:2',3'-*d*]pyrrole (5).**

*N*-(3,4,5-Tris(*n*-dodecyloxy)phenyl)-dithieno[3,2-*b*:2',3'-*d*]pyrrole (4) (1.5 g, 1.9 mmol),

chloroform (25 mL), and acetic acid (25 mL) were added to a flask. *N*-Iodosuccinimide (0.4 g, 1.9 mmol) was added at 0 °C in small portion. The reaction mixture was then allowed to warm to room temperature and react for 3 h. The solution was diluted with dichloromethane, washed with saturated aq. Na<sub>2</sub>S<sub>2</sub>O<sub>3</sub> and NaHCO<sub>3</sub> solution, and the solvent was removed under reduced pressure. The residue was purified by column chromatography (silica gel, eluent: hexane:CH<sub>2</sub>Cl<sub>2</sub> = 5:1), and a yellow solid (1.0 g, 56%) was obtained. <sup>1</sup>H NMR (300 MHz, CD<sub>2</sub>Cl<sub>2</sub>): δ 7.36 (s, 1H), 7.21 (d, *J* = 5.1 Hz, 1H), 7.15 (d, *J* = 5.1 Hz, 1H), 6.72 (s, 2H), 4.00 (m, 6H), 1.90–1.80 (m, 6H), 1.44–1.21 (m, 54 H), 0.91 (m, 9H). <sup>13</sup>C{<sup>1</sup>H}NMR (75 MHz, CD<sub>2</sub>Cl<sub>2</sub>): δ 154.1, 144.2, 143.7, 136.9, 134.9, 124.3, 121.9, 121.1, 116.4, 112.4, 102.0, 73.7, 70.6, 69.5, 32.2, 30.6, 30.0, 29.9, 29.8, 29.6, 26.4, 26.3, 22.9, 14.1 (14 C are missing presumably due to overlapping peaks). MS (MALDI): *m/z* calcd for C<sub>50</sub>H<sub>80</sub>INO<sub>3</sub>S<sub>2</sub>, 933.4447; found: 933.4369. Anal. Calcd for C<sub>50</sub>H<sub>80</sub>INO<sub>3</sub>S<sub>2</sub>: C, 64.28; H, 8.63; N, 1.50; S, 6.86. Found: C, 64.34; H, 8.46; N, 1.60; S, 6.68.

**2,6-Diiodo-*N*-(3,4,5-tris(*n*-dodecyloxy)phenyl)-dithieno[3,2-*b*:2',3'-*d*]pyrrole (6).**

*N*-(3,4,5-Tris(*n*-dodecyloxy)phenyl)-dithieno[3,2-*b*:2',3'-*d*]pyrrole (**4**) (2.0 g, 2.5 mmol), chloroform (20 mL), and acetic acid (20 mL) were added to a flask. *N*-Iodosuccinimide (1.2 g, 5.5 mmol) was added at 0 °C in small portions. The reaction mixture was allowed to warm to room temperature and react for 3 h. The resulting solution was diluted with

dichloromethane, washed with saturated aq.  $\text{Na}_2\text{S}_2\text{O}_3$  and  $\text{NaHCO}_3$  solution, and the solvent was removed under reduced pressure. The residue was purified by column chromatography (silica gel, hexane as eluent). A yellow solid (1.5 g, 58%) was obtained.  $^1\text{H}$  NMR (300 MHz,  $\text{CD}_2\text{Cl}_2$ ):  $\delta$  7.18 (s, 2H), 6.76 (s, 2H), 4.00 (m, 6H), 1.90–1.80 (m, 6H), 1.44–1.21 (m, 54 H), 0.91 (m, 9H). The  $^1\text{H}$  NMR spectrum is consistent with that reported in the literature.<sup>16</sup>

**2,6-Bis(tri-*n*-butylstannyl)-*N*-(3,4,5-tris(*n*-dodecyloxy)phenyl)-dithieno[3,2-*b*:2',3'-*d*]pyrrole (7).** A deoxygenated solution of

*N*-(3,4,5-tris(*n*-dodecyloxy)phenyl)-dithieno[3,2-*b*:2',3'-*d*]pyrrole (4) (0.34 g, 0.42 mmol) in THF (*ca.* 200 mL) was cooled to  $-78\text{ }^\circ\text{C}$ .  $^t\text{BuLi}$  (1.5 mL, 2.4 mmol, 1.7 M in heptane) solution was added, and the reaction allowed to warm to room temperature and stirred for 1 h, before cooling to  $-78\text{ }^\circ\text{C}$  again;  $^n\text{Bu}_3\text{SnCl}$  (0.25 mL, 0.92 mmol) was then added and the reaction allowed to warm to room temperature and stir for 3 h. The reaction was quenched with addition of water and extracted with dichloromethane; the extracts were dried over  $\text{MgSO}_4$ , concentrated under reduced pressure and stirred with  $\text{NEt}_3$  (50 mL) for 2 h. After removal of the volatiles the residue was purified by column chromatography ( $\text{SiO}_2$ , pretreated with  $\text{NEt}_3$ , eluting with hexanes), after which a pale yellow oil (0.30 g, 52%) was obtained.  $^1\text{H}$  NMR (400 MHz,  $\text{CD}_2\text{Cl}_2$ ):  $\delta$  7.18 (s, 2H), 6.76 (s, 2H), 4.10–3.98 (m, 6H), 1.90–1.80 (m, 6H), 1.70–1.12 (m, 90 H), 0.91 (m, 27H).  $^{13}\text{C}\{^1\text{H}\}$  NMR (100

MHz, CDCl<sub>3</sub>):  $\delta$  153.5, 146.7, 135.7 (two peaks separated by 0.05 ppm), 135.5, 122.1, 119.2, 101.5, 73.7, 69.1, 32.0 (two peaks separated by 0.02 ppm), 30.5, 29.9, 29.8 (two peaks separated by 0.05 ppm), 29.5 (two peaks separated by 0.02 ppm), 29.2, 29.1, 29.0, 27.4, 26.3 (two peaks separated by 0.02 ppm), 22.8, 14.3, 13.8, 11.1 (8 peaks missing, presumably due to overlapping peaks). MS (MALDI):  $m/z$  1388 (M<sup>+</sup>). Anal. Calcd for C<sub>74</sub>H<sub>133</sub>NO<sub>3</sub>S<sub>2</sub>Sn<sub>2</sub>: C, 64.11; H, 9.67; N, 1.01. Found: C, 64.16; H, 9.54; N, 0.98.

**Dimer 1.** 2-Iodo-*N*-(3,4,5-tris(*n*-dodecyloxy)phenyl)-dithieno[3,2-*b*:2',3'-*d*]pyrrole (**5**) (0.63 g, 0.70 mmol), and bis(pinacolato)diboron (0.09 g, 0.35 mmol) were added to flask. Then THF (20 mL) was added, and the mixture was deoxygenated for 30 min. Pd(PPh<sub>3</sub>)<sub>4</sub> (0.04 g, 0.03 mmol) was added under nitrogen, and the mixture was allowed to react at 70 °C for 2 days. After removal of all the solvents under reduced pressure, the residue was purified by a silica gel plug using THF as eluent, followed by two SEC column chromatographies (bio-beads, SX-3 followed by SX-1 using THF as eluent). A dark yellow solid (0.07 g, 13%) was obtained. <sup>1</sup>H NMR (300 MHz, CD<sub>2</sub>Cl<sub>2</sub>):  $\delta$  7.30 (s, 2H), 7.23 (d, *J* = 5.1 Hz, 2H), 7.16 (d, *J* = 5.1 Hz, 2H), 6.78 (s, 4H), 4.02 (m, 12H), 1.83 (m, 12H), 1.55-1.19 (m, 108H), 0.88 (m, 18H). <sup>13</sup>C {<sup>1</sup>H} NMR (100 MHz, CD<sub>2</sub>Cl<sub>2</sub>):  $\delta$  154.3, 144.6, 144.3, 136.9, 136.5, 135.1, 124.3, 116.8, 115.3, 112.6, 108.5, 102.1, 73.9, 69.6, 32.3 (two peaks separated by 0.03 ppm), 30.8, 30.2, 30.1, 30.0, 29.9, 29.8, 29.7, 26.6, 26.5, 23.1, 14.3 (9 C are missing presumably due to overlapping peaks). MS (MALDI):

$m/z$  calcd for  $C_{100}H_{160}N_2O_6S_4$ , 1613.1337; found: 1613.1355. Anal. Calcd for  $C_{100}H_{160}N_2O_6S_4$ : C, 74.39; H, 9.99; N, 1.73; S, 7.94; Found: C, 74.18; H, 9.93; N, 1.76; S, 7.81.

**Trimer 2.** 2-Iodo-*N*-(3,4,5-tris(*n*-dodecyloxy)phenyl)-dithieno[3,2-*b*:2',3'-*d*]pyrrole (**6**)

(0.36 g, 0.40 mmol), and 2,6-bis(*n*-tributylstannyl)-*N*-(3,4,5-tris(*n*-dodecyloxy)phenyl)-dithieno[3,2-*b*:2',3'-*d*]pyrrole (**7**) (0.26 g, 0.20 mmol) were added to flask. Then dry DMF (20 mL) and toluene (20 mL) were added, and the mixture was deoxygenated for 30 min.  $Pd(PPh_3)_4$  (0.01 g, 0.01 mmol) was added under nitrogen, and the mixture was allowed to react at 90 °C for 1 day. After reaction, the crude product was washed with KF solution, and extracted with toluene. After removal of all the solvents under reduced pressure, the residue was purified by a plug (alumina, THF as eluent) followed by a SEC column chromatography (SX-1, bio-beads, THF as eluent). After recrystallization from acetone, a red solid (0.15 g, 33%) was obtained after removing the solvent under reduced pressure.  $^1H$  NMR (300 MHz,  $CD_2Cl_2$ ):  $\delta$  7.29 (s, 2H), 7.26 (s, 2H), 7.23 (d,  $J = 5.4$  Hz, 2H), 7.16 (d,  $J = 5.4$  Hz, 2H), 6.80 (s, 2H), 6.78 (s, 4H), 4.02 (m, 18H), 1.81(m, 18H), 1.55-1.19 (m, 162H), 0.90 (m, 27H).  $^{13}C$  { $^1H$ } NMR (75 MHz,  $CD_2Cl_2$ ):  $\delta$  154.3, 154.2, 144.7, 144.5, 144.3, 137.0, 136.4, 135.1, 124.4, 116.8, 115.4, 112.6, 108.5, 108.2, 102.4, 102.1, 73.9, 69.6, 32.3 (two peaks separated by 0.03 ppm), 30.7, 30.1 (two peaks separated by 0.07 ppm), 30.0, 29.8,

29.7, 26.5 (two peaks apart by 0.05 ppm), 23.0, 14.2 (34C are missing presumably due to overlapping peaks). MS (MALDI):  $m/z$  calcd for  $C_{150}H_{239}N_3O_9S_6$ , 2418.6661; found: 2418.6730. Anal. Calcd for  $C_{150}H_{239}N_3O_9S_6$ : C, 74.42; H, 9.95; N, 1.74; S, 7.95. Found: C, 74.72; H, 10.00; N, 1.76; S, 7.67.

**P1.** To a 50 mL pressure vessel were added 2,6-diiodo-*N*-(3,4,5-tris(*n*-dodecyloxy)phenyl)-dithieno[3,2-*b*:2',3'-*d*]pyrrole (**6**) (0.42 g, 0.40 mmol), 2,6-bis(tri-*n*-butylstannyl)-*N*-(3,4,5-tris(*n*-dodecyloxy)phenyl)-dithieno[3,2-*b*:2',3'-*d*]pyrrole (**7**) (0.56 g, 0.40 mmol), dry THF (20 mL), and  $PdCl_2(PPh_3)_2$  (0.015 g, 0.02 mmol) in a  $N_2$ -filled glove box. The vessel was taken out and heated to 60-70 °C for one week. The solution was washed with aq. KF solution, and extracted with toluene, concentrated to *ca.* 10 mL under reduced pressure. Then it was dropped into methanol (*ca.* 500 mL), and a solid was collected by filtration. The crude product was purified by Soxhlet extraction with methanol, acetone and hexanes, each for 1 day. The extract from hexanes was concentrated under reduced pressure and dropped into methanol (*ca.* 500 mL); a black solid (0.48 g, 74%) was obtained after filtration.  $^1H$  NMR (300 MHz, THF- $d_8$ ):  $\delta$  7.31(br, 2H), 6.89 (br, 2H), 4.05 (br, 6H), 1.85–1.20 (br, 60H), 0.89 (br, 9H). Anal. Calcd. for  $(C_{50}H_{79}NO_3S_2)_n$ : C, 74.48; H, 9.88; N, 1.74. Found: C: 73.70; H: 9.79; N: 1.71.

**1-(3,3'-Dibromo-2,2'-bithiophen-5-yl)hexan-1-one (8).** 3,3'-Dibromo-2,2'-bithiophene (6.1 g, 19 mmol) and AlCl<sub>3</sub> (3.1 g, 23 mmol) were dissolved in dry dichloromethane (200 mL), and stirred at -5 °C for 10 min. Hexanoyl chloride (3.1 g, 21 mmol) was added dropwise, warmed to room temperature, and reacted for 6 h. The solution was diluted with dichloromethane, washed with water, and the solvent was removed under reduced pressure. The residue was purified by column chromatography (silica gel, hexane: CH<sub>2</sub>Cl<sub>2</sub> = 3:1 as eluent). A yellow solid (6.5 g, 81%) was obtained. <sup>1</sup>H NMR (300 MHz, CD<sub>2</sub>Cl<sub>2</sub>): δ 7.68 (s, 1H), 7.53 (d, *J* = 5.4 Hz, 1H), 7.15 (d, *J* = 5.4 Hz, 1H), 2.89 (t, *J* = 7 Hz, 2H), 1.74 (quint, *J* = 7.5 Hz, 2H), 1.41–1.35 (m, 4H), 0.93 (t, *J* = 7.2 Hz, 3H). <sup>13</sup>C{<sup>1</sup>H} NMR (75 MHz, CD<sub>2</sub>Cl<sub>2</sub>): δ 192.6, 144.3, 136.7, 134.6, 131.3, 128.7, 128.4, 113.2, 112.7, 39.1, 31.6, 24.3, 22.7, 13.9. MS (EI): *m/z* calcd for C<sub>14</sub>H<sub>14</sub>Br<sub>2</sub>OS<sub>2</sub>, 419.8852; found 419.8851. Anal. Calcd for C<sub>14</sub>H<sub>14</sub>Br<sub>2</sub>OS<sub>2</sub>: C, 39.83; H, 3.34; S, 15.19. Found: C, 39.88; H, 3.40; N, 15.17.

**3,3'-Dibromo-5-*n*-hexyl-2,2'-bithiophene (9).**

1-(3,3'-Dibromo-2,2'-bithiophen-5-yl)hexan-1-one (**8**) (1.5 g, 3.5 mmol) and NaBH<sub>4</sub> (0.66 g, 18 mmol), AlCl<sub>3</sub> (1.40 g, 11 mmol) were added to a oven-dried flask. Then THF (30 mL, deoxygenated and distilled) was added, and heated it to reflux for 6.5 h. The reaction mixture was diluted with hexanes, washed with water, and the solvent was removed under reduced pressure. The residue was purified by column chromatography

(silica gel, hexane as eluent). A yellow oil (0.90 g, 63%) was obtained.  $^1\text{H}$  NMR (300 MHz,  $\text{CD}_2\text{Cl}_2$ ):  $\delta$  7.44 (d,  $J = 5.4$  Hz, 1H), 7.09 (d,  $J = 5.7$  Hz, 1H), 6.80 (s, 1H), 2.81 (t,  $J = 7.5$  Hz, 2H), 1.70 (quint,  $J = 7.5$  Hz, 2H), 1.42–1.34 (m, 6H), 0.91 (t,  $J = 6.8$  Hz, 3H).  $^{13}\text{C}\{^1\text{H}\}$  NMR (75 MHz,  $\text{CD}_2\text{Cl}_2$ ):  $\delta$  148.7, 130.9, 129.7, 127.8, 127.6, 126.0, 112.4, 111.7, 31.7, 31.3, 30.4, 28.9, 22.8, 14.0. MS (EI):  $m/z$  calcd for  $\text{C}_{14}\text{H}_{16}\text{Br}_2\text{S}_2$ , 405.9060; Found: 405.9043. Anal. Calcd for  $\text{C}_{14}\text{H}_{16}\text{Br}_2\text{S}_2$ : C, 41.19; H, 3.95; S, 15.71. Found: C, 41.40; H, 4.01; S, 15.60.

**2-*n*-Hexyl-*N*-(3,4,5-tris(*n*-dodecyloxy)phenyl)-dithieno[3,2-*b*:2',3'-*d*]pyrrole (10).**

$\text{Pd}_2(\text{dba})_3$  (0.27 g, 0.30 mmol), and  $\text{P}(\text{tBu})_3$  (0.24 g, 1.20 mmol) were added to a flask, which was then deoxygenated for 30 min. Then 3,3'-dibromo-5-*n*-hexyl-2,2'-bithiophene (**9**) (3.00 g, 7.4 mmol),  $\text{NaO}^t\text{Bu}$  (5.65 g, 58.8 mmol), 3,4,5-tris(*n*-dodecyloxy)aniline (5.70 g, 8.2 mmol), and dry toluene (*ca.* 100 mL) were added. The reaction mixture was then heated to 110 °C for 5 h. After cooling to room temperature, water was added, the organic layer was separated, and all the solvents were removed under reduced pressure. The residue was purified by column chromatography (silica gel, hexane as eluent). A yellow solid (5.2 g, 79%) was obtained.  $^1\text{H}$  NMR (300 MHz,  $\text{CD}_2\text{Cl}_2$ ):  $\delta$  7.15 (d,  $J = 5.4$  Hz, 1H), 7.12 (d,  $J = 5.4$  Hz, 1H), 6.90 (s, 1H), 6.74 (s, 2H), 4.02 (m, 6H), 2.89 (t,  $J = 7.5$  Hz, 2H), 1.85 (m, 8H), 1.74–1.26 (m, 60H), 0.91 (m, 12H).  $^{13}\text{C}\{^1\text{H}\}$  NMR (75 MHz,  $\text{CD}_2\text{Cl}_2$ ):  $\delta$  154.3, 145.5, 143.8, 143.2, 136.6, 135.7, 122.8, 117.2, 114.5, 112.7, 110.0,

101.9, 74.0, 69.7, 32.5, 32.4, 32.2, 32.1, 31.9, 30.9, 30.3, 30.2, 30.1, 29.9, 29.8, 29.3, 26.7, 26.6, 23.2, 23.1, 14.4 (11C missing presumably due to overlapping peaks). MS (EI):  $m/z$  calcd for  $C_{56}H_{93}NO_3S_2$ , 891.6596, Found: 891.6629. Anal. Calcd for  $C_{56}H_{93}NO_3S_2$ : C, 75.36; H, 10.50; N, 1.57; Found C, 75.21; H, 10.57; N, 1.54.

**2-*n*-Hexyl-6-iodo-*N*-(3,4,5-tris(*n*-dodecyloxy)phenyl)-dithieno[3,2-*b*:2',3'-*d*]pyrrole**

**(11).** 2-*n*-Hexyl-*N*-(3,4,5-tris(*n*-dodecyloxy)phenyl)-dithieno[3,2-*b*:2',3'-*d*]pyrrole **(10)**

(0.28 g, 0.30 mmol), acetic acid (10 mL), chloroform (10 mL) were added to a flask. *N*-Iodosuccinimide (0.07 g, 0.31 mmol) was added at 0 °C in small portions and allowed to react at 0 °C for 5 h. The solution was diluted with dichloromethane, and washed with saturated aq.  $Na_2S_2O_3$  and  $NaHCO_3$  solution; the solvent was then removed under reduced pressure. The residue was purified by column chromatography (silica gel, hexane:  $CH_2Cl_2$  = 5:1 as eluent). A yellow solid (0.26 g, 85%) was obtained.  $^1H$  NMR (300 MHz,  $CD_2Cl_2$ ):  $\delta$  7.31 (s, 1H), 6.85 (s, 1H), 6.68 (s, 2H), 3.97 (m, 6H), 2.89 (t,  $J$  = 7.5 Hz, 2H), 1.90–1.20 (m, 68H), 0.91 (m, 12H).  $^{13}C\{^1H\}$  NMR (100 MHz,  $CD_2Cl_2$ ):  $\delta$  154.2, 146.2, 143.5, 142.5, 136.9, 135.1, 122.0, 121.5, 114.2, 109.8, 102.1, 73.9, 69.6, 69.3, 32.3, 32.0, 31.9, 31.8, 30.8, 30.1 (two peaks separated by 0.06 ppm), 30.0, 29.8, 29.7, 29.1, 26.5 (two peaks separated by 0.06 ppm), 23.1, 23.0, 14.2 (two peaks apart by 0.04 ppm) (10C are missing presumably due to overlapping peaks). MS (MALDI):  $m/z$  MS (MALDI):  $m/z$  calcd for  $C_{56}H_{92}INO_3S_2$ , 1017.5563, Found 1017.5580. Anal. Calcd. for  $C_{56}H_{92}INO_3S_2$ : C,

66.05; H, 9.11; N, 1.38; S, 6.30; Found: C, 66.16; H, 9.20; N, 1.42; S, 6.26.

**Dimer 3.** 2-Hexyl-6-iodo *N*-(3,4,5-tris(*n*-dodecyloxy)phenyl)-dithieno[3,2-*b*:2',3'-*d*]

pyrrole (1.53 g, 1.50 mmol), and bis(pinacolato)diboron (0.19 g, 0.75 mmol) were added to a flask, then THF (30 mL) was added, and the mixture was deoxygenated for 30 min. Pd(PPh<sub>3</sub>)<sub>4</sub> (0.05 g, 0.04 mmol) were added under nitrogen, and heated to reflux for 2 days. After removal of all the solvents under reduced pressure, the residue was purified by silica gel plug using THF as eluent, followed by SEC column chromatography twice (SX-1 bio-bead, THF as eluent). Dark yellow solid (0.10 g, 7%) was obtained. <sup>1</sup>H NMR (300 MHz, CD<sub>2</sub>Cl<sub>2</sub>): δ 7.22 (s, 2H), 6.86 (s, 2H), 6.74 (s, 4H), 3.99 (m, 12H), 2.88 (t, *J* = 7.5 Hz, 4H), 1.95–1.18 (m, 136H), 0.90 (m, 24H). <sup>13</sup>C{<sup>1</sup>H} NMR (75 MHz, CD<sub>2</sub>Cl<sub>2</sub>): δ 154.1, 146.0, 143.7, 142.9, 136.7, 135.6, 135.2, 115.5, 114.5, 109.8, 108.2, 102.0, 73.9, 69.6, 32.3 (two peaks separated by 0.02 ppm), 32.0, 31.9, 31.8, 30.7, 30.2, 30.1, 30.0, 29.8 (two peaks separated by 0.05 ppm), 29.7, 29.1, 26.5 (two peaks separated by 0.06 ppm), 23.1, 23.0, 14.3 (10C are missing presumably due to overlapping peaks). MS (MALDI): *m/z* calcd for C<sub>112</sub>H<sub>184</sub>N<sub>2</sub>O<sub>6</sub>S<sub>4</sub>, 1781.3037; Found: 1781.3187. Anal. Calcd. for C<sub>112</sub>H<sub>184</sub>N<sub>2</sub>O<sub>6</sub>S<sub>4</sub>: C, 75.45; H, 10.40; N, 1.57; S, 7.19; Found: C, 75.25; H, 10.47; N, 1.64; S, 6.98.

**Chemical Oxidation of 1-3 and P1.**

Monocation solutions (*ca.*  $3\text{--}5 \times 10^{-5}$  M) of **1-3** were generated by addition of *ca.* 0.1 equiv. tris(4-bromophenyl)aminium hexachloroantimonate in dry dichloromethane. Chemical oxidation of **P1** was done by adding small aliquots of concentrated tris(4-bromophenyl)aminium hexachloroantimonate solution (*ca.*  $2 \times 10^{-3}$  M) into a dilute solution (*ca.*  $6 \times 10^{-5}$  M) of **P1**. UV-vis-NIR spectra were recorded on a Cary 500 UV-Vis-NIR spectrophotometer and multiple scans were performed to test the stabilities of the radical cations.

### **Electropolymerization and Spectroelectrochemistry of P2.**

The electropolymerization and spectroelectrochemistry were conducted in the University of Florida with the aid of Timothy Steckler in the Reynolds group. The electrochemical measurements were performed on an EG&G PAR model 273A potentiostat/galvanostat. Electropolymerization was performed in a three electrode cell consisting of a  $0.02\text{ cm}^2$  platinum working electrode (or a ITO/glass electrode), a platinum flag counter electrode, and a silver wire pseudo reference electrode calibrated to the ferrocene-ferrocenium redox couple, assuming the values of  $[\text{Cp}_2\text{Fe}]^{+/0} = 0.38\text{ V}$  (in  $0.1\text{ M } [\text{nBu}_4\text{N}]^+[\text{ClO}_4]^-/\text{acetonitrile}$  solution). Polymer films of **P2** were deposited from a  $5\text{ mM}$  monomer (compound **4**) in  $0.1\text{ M } [\text{nBu}_4\text{N}]^+[\text{ClO}_4]^-$  solution (total  $5\text{ mL}$ ,  $2\text{ mL}$  dichloromethane,  $3\text{ mL}$  acetonitrile) via repeated scan cyclic voltammetry at  $50\text{ mV/s}$  for 10 cycles or galvanostatically until *ca.*  $40\text{ mC}$  of charge had passed. Other polymer

electrochemical characterization was performed in a 0.1 M [ $n$ Bu<sub>4</sub>N]<sup>+</sup>[ClO<sub>4</sub>]<sup>-</sup>/acetonitrile solution unless noted. UV-vis-NIR spectra of the spectroelectrochemistry of **P2** were recorded on a Cary 500 UV-Vis-near IR spectrophotometer.

## 2.11 References

- (1) Ong, B. S.; Wu, Y. L.; Li, Y. N.; Liu, P.; Pan, H. L. *Chem. Eur. J.* **2008**, *14*, 4766.
- (2) Osaka, I.; McCullough, R. D. *Acc. Chem. Res.* **2008**, *41*, 1202.
- (3) Bauerle, P.; Segelbacher, U.; Gaudl, K. U.; Huttenlocher, D.; Mehring, M. *Angew. Chem. Int. Ed.* **1993**, *32*, 76.
- (4) Li, J.; Qin, F.; Li, C. M.; Bao, Q. L.; Chan-Park, M. B.; Zhang, W.; Qin, J. G.; Ong, B. S. *Chem. Mater.* **2008**, *20*, 2057.
- (5) Zhan, X. W.; Tan, Z. A.; Domercq, B.; An, Z. S.; Zhang, X.; Barlow, S.; Li, Y. F.; Zhu, D. B.; Kippelen, B.; Marder, S. R. *J. Am. Chem. Soc.* **2007**, *129*, 7246.
- (6) Zhang, X. N.; Johnson, J. P.; Kampf, J. W.; Matzger, A. J. *Chem. Mater.* **2006**, *18*, 3470.
- (7) Sirringhaus, H.; Friend, R. H.; Li, X. C.; Moratti, S. C.; Holmes, A. B.; Feeder, N. *Appl. Phys. Lett.* **1997**, *71*, 3871.
- (8) Zhang, S. G., Yunlong; Wang, Ling; Li, Qikai; Zheng, Kai; Zhan, Xiaowei; Liu, Yunque; Liu, Ruigang; Wan, Li-Jun. *J. Phys. Chem. C* **2009**, *113*, 16232.
- (9) Zhang, W.; Li, J.; Zou, L.; Zhang, B.; Qin, J. G.; Lu, Z. S.; Poon, Y. F.; Chan-Park, M. B.; Li, C. M. *Macromolecules* **2008**, *41*, 8953.
- (10) Zhang, W.; Li, J.; Zhang, B.; Qin, J. G. *Macromol. Rapid Commun.* **2008**, *29*, 1603.
- (11) Vanormelingen, W.; Van den Bergh, K.; Verbiest, T.; Koeckelberghs, G. *Macromolecules* **2008**, *41*, 5582.
- (12) Odom, S. A.; Lancaster, K.; Beverina, L.; Lefler, K. M.; Thompson, N. J.; Coropceanu, V.; Brédas, J. L.; Marder, S. R.; Barlow, S. *Chem. Eur. J.* **2007**, *13*, 9637.
- (13) Koeckelberghs, G.; De Cremer, L.; Persoons, A.; Verbiest, T. *Macromolecules* **2007**, *40*, 4173.
- (14) Koeckelberghs, G.; De Cremer, L.; Vanormelingen, W.; Verbiest, T.; Persoons, A.; Samyn, C. *Macromolecules* **2005**, *38*, 4545.
- (15) Radke, K. R.; Ogawa, K.; Rasmussen, S. C. *Org. Lett.* **2005**, *7*, 5253.
- (16) Odom, S. A. *Electron transfer and delocalization in mixed-valence monocations*

- of bis- and tris-(diarylamino) derivatives; Ph.D. thesis, Georgia Institute of Technology: Atlanta, GA, 2008.
- (17) Ogawa, K.; Rasmussen, S. C. *Macromolecules* **2006**, *39*, 1771.
  - (18) Babudri, F.; Farinola, G. M.; Naso, F. *J. Mater. Chem.* **2004**, *14*, 11.
  - (19) Fichou, D. *Handbook of oligo- and polythiophenes*; Wiley-VCH: Weinheim, 1999.
  - (20) a) Gierschner, J.; Cornil, J.; Egelhaaf, H. J. *Adv. Mater.* **2007**, *19*, 173; b) Kuhn, W. *Helv. Chim. Acta* **1948**, *31*, 1780.
  - (21) Connelly, N. G.; Geiger, W. E. *Chem. Rev.* **1996**, *96*, 877.
  - (22) Karsten, B. P.; Viani, L.; Gierschner, J.; Cornil, J.; Janssen, R. A. J. *J. Phys. Chem. A* **2008**, *112*, 10764.
  - (23) Diaz, A. F.; Crowley, J.; Bargon, J.; Gardini, G. P.; Torrance, J. B. *J. Electroanal. Chem.* **1981**, *121*, 355.
  - (24) Bao, Z.; Locklin, J. J. *Organic field-effect transistors*; CRC Press, Boca Raton, FL, 2007.
  - (25) Guo, X. G.; Kim, F. S.; Jenekhe, S. A.; Watson, M. D. *J. Am. Chem. Soc.* **2009**, *131*, 7206.
  - (26) An, Z. *Perylene-based materials potential components in organic electronics and optoelectronics*, Ph.D. thesis, Georgia Institute of Technology, Atlanta, GA, 2005.
  - (27) Skotheim, T. A.; Reynolds, J. R. *Handbook of conducting polymers*; 3rd ed., CRC Press, Boca Raton, FL, 2007.
  - (28) Furukawa, Y. *Synth. Met.* **1995**, *69*, 629.
  - (29) Chung, T. C.; Kaufman, J. H.; Heeger, A. J.; Wudl, F. *Phys. Rev. B* **1984**, *30*, 702.
  - (30) Horowitz, G.; Yassar, A.; Vonbardeleben, H. J. *Synth. Met.* **1994**, *62*, 245.
  - (31) Nessakh, B.; Horowitz, G.; Garnier, F.; Deloffre, F.; Srivastava, P.; Yassar, A. *J. Electroanal. Chem.* **1995**, *399*, 97.
  - (32) Mortimer, R. J.; Dyer, A. L.; Reynolds, J. R. *Displays* **2006**, *27*, 2.
  - (33) Berlin, A.; Pagani, G.; Zotti, G.; Schiavon, G. *Makromol. Chem.* **1992**, *193*, 399.
  - (34) Frey, J.; Bond, A. D.; Holmes, A. B. *Chem. Commun.* **2002**, 2424.
  - (35) Percec, V. A.; Emad; Peterca, Mihai; Rudick, Jonathan G.; Lemon, Lance; Ronda, Juan C.; De, Binod B.; Heiney, Paul A.; Meijer, E. W. *J. Am. Chem. Soc.* **2006**, *128*, 16365.

# CHAPTER 3

## N-ALKYL DITHIENOPYRROLE-BASED DONOR-DONOR COPOLYMERS

### 3.1 Introduction

Conjugated polymers are attracting growing interest for organic electronic applications, including OLEDs, OPVs, and OFETs.<sup>1,2</sup> The advantages of using polymers over small molecules and oligomers have been previously discussed in Chapter 1. Polythiophenes and their analogues are among the best performing polymers for p-channel OFETs and for sensitization and hole-transport in OPVs.<sup>3</sup> In recent years, fused thiophene derivatives have been incorporated into the backbones of conjugated polymers. It is believed that rigid fused-ring units can enhance  $\pi$ - $\pi$  stacking intermolecular interactions<sup>4</sup> and lead to higher charge-carrier mobilities,<sup>5,6</sup> and examples of which used as hole-transport materials in OFETs have been described earlier in section 1.4.2, such as polymer **27**, **28** in Figure 1.13.<sup>7,8</sup> Also the planarity of fused rings in the polymer backbone could improve  $\pi$ -electron delocalization, leading to decreased band gaps and broad absorption spectra, which potentially have increased coverage of the solar spectrum, and specific examples using them in OPVs are polymer **27c** (in Figure 1.13) and polymer **47** (in Figure 1.16).<sup>9</sup>

*N*-Alkyl and aryl dithieno[3,2-*b*:2',3'-*d*]pyrroles (DTP) have been incorporated into oligomers and polymers more recently.<sup>10-17</sup> The *N*-substituents of DTP groups can help improve solubility while retaining the planarity of fused-thiophene-type units. DTP-based compounds have also been shown to be more easily oxidized than analogous bithiophene

and dithienothiophene compounds.<sup>14</sup> In 2008, copolymers of dithienopyrrole and thiophene moieties were reported (**I** in Figure 3.1); OFET hole mobilities up to 0.21 cm<sup>2</sup>/Vs suggest the DTP moiety is a promising building block for hole-transport materials.<sup>11,15</sup> More recently, a DTP homopolymer, along with those of copolymers with carbazole, fluorene, and pyridine (**II** in Figure 3.1) were reported; only their optical properties were described.<sup>12</sup> Applications based on DTP-containing polymers in OPVs have not been extensively explored. Organic solar cells based on blends of D-A type DTP-based copolymers (**52** in Figure 1.16) with PCBM was obtained with power conversion efficiencies up to 2.8%,<sup>16,17</sup> however, the donor-donor copolymers have not yet been used in OPV devices. The current research on DTP-based materials suggested that this building block can be useful to construct the polymers for various applications.

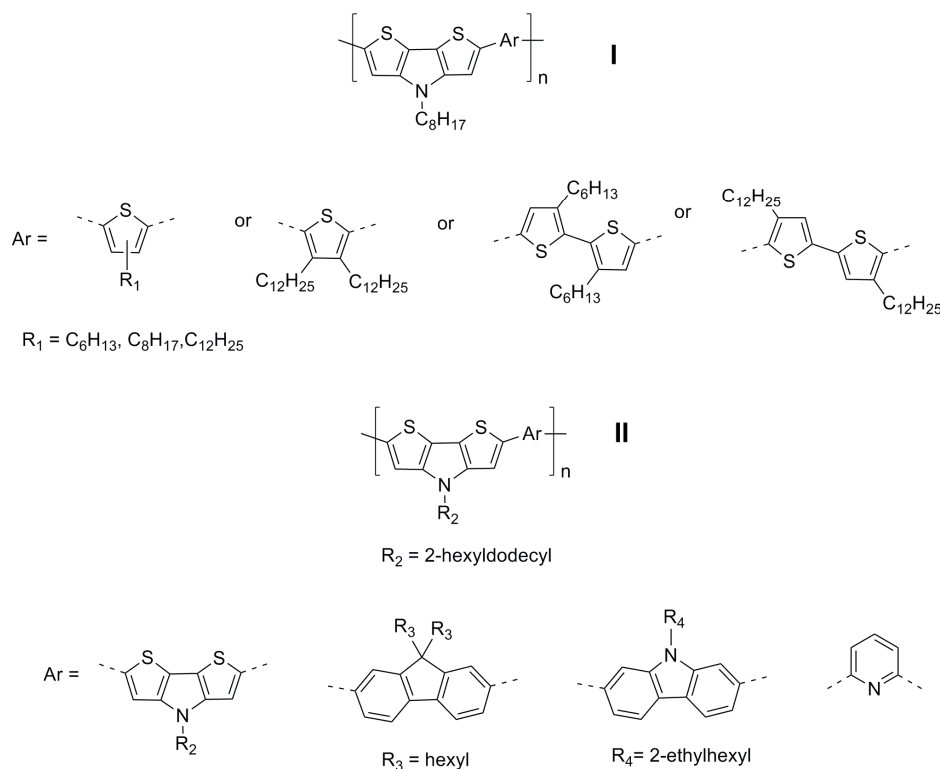


**Figure 3.1** Structures of some polymers discussed in the text.

Although some structurally similar or identical polymers have been reported in the literature recently,<sup>11,12,15</sup> their applications in electronic devices have not been intensively explored. Here a series of *N*-alkyl DTP-based polymers, including a homopolymer and copolymers with some commonly used electron-rich moieties, are synthesized and characterized, and the structures of the target polymers are shown in Figure 3.2. The optical and electronic properties of the copolymers are compared, and quantum-chemical calculations on model oligomers were performed to obtain insight into the experimental optical spectra and electrochemical measurements. In addition, the fabrications of OFETs and OPVs from the polymers are described along with the morphology study of selected OPV devices based on one of the copolymers (DTP-bithiophene) blended with PCBM.

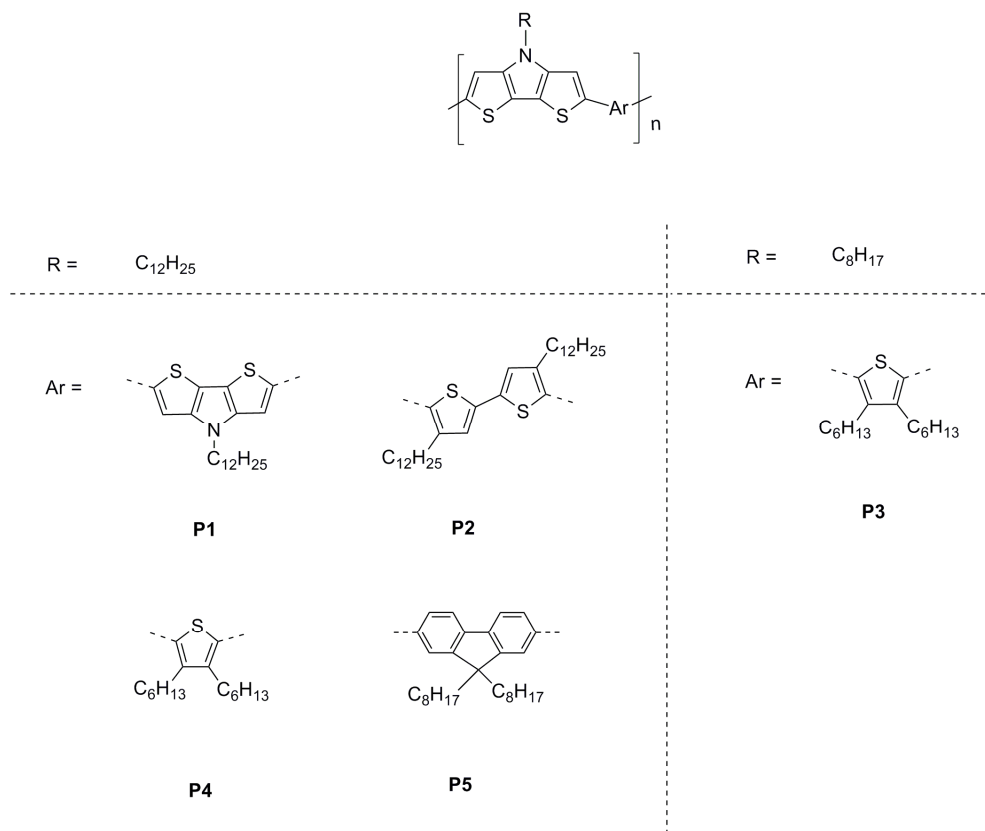


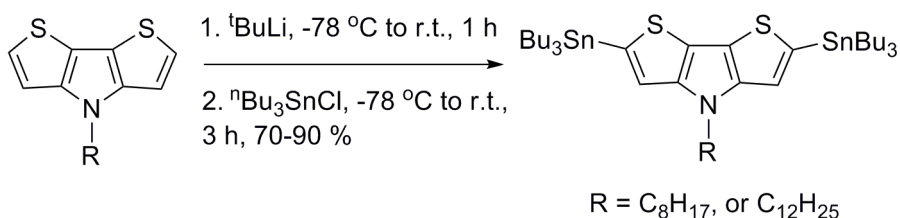
**Figure 3.2** Structures of target polymers in Chapter 3.

### 3.2 Synthesis

Palladium-catalyzed coupling reactions have been widely used in the synthesis of conjugated polymeric materials, and Stille and Suzuki couplings are two of the most commonly used methods.<sup>18</sup> Generally in those polymerizations, aromatic dihalides react with distannyl or diboronic derivatives of another aromatic species, to form the main chains of conjugated polymers. Due to step-growth polymerization nature of these reactions, high purities of monomers, high reaction conversion yields, as well as strict stoichiometric control are required to obtain polymers with high molecular weights.<sup>19</sup> For the polymerizations described in this chapter, a Stille coupling was chosen, as discussed in more detail in section 5.2. Details of the synthesis of the monomers and polymers will be described in the following sub-sections.

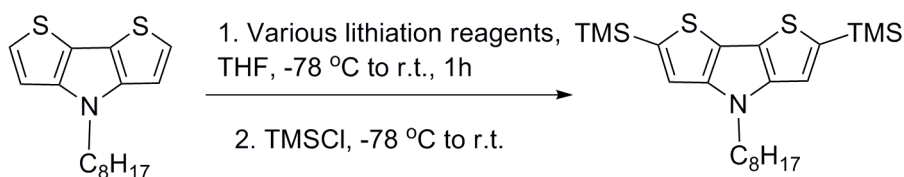
#### *Monomer Synthesis*

For Stille couplings, the distannyl derivatives of DTPs are a key intermediate. The distannyl DTP monomers were obtained by dilithiation of the parent *N*-*n*-octyl or *n*-dodecyl DTP, followed by treatment with <sup>n</sup>Bu<sub>3</sub>SnCl. It has previously been reported that the one of the monomers, 2,6-di(tri-*n*-butylstannyl)-*N*-*n*-octyl-dithieno[3,2-*b*:2',3'-*d*]pyrrole, could not be isolated pure due to its instability;<sup>10</sup> however, the bis(trimethylstannyl) derivative used in the synthesis of a D-A DTP-based copolymer (polymer **52a** in Figure 1.16) has been isolated, although only characterized by <sup>1</sup>H NMR.<sup>17</sup> In contrast, the distannyl monomers in this thesis were obtained analytically pure using optimized preparative conditions and careful purification by column chromatography.



**Scheme 3.1** Synthesis of DTP-based monomers.

Optimizations of the 2,6-disubstitution of DTP were conducted by reacting *N-n*-octyl DTP with various commonly-used lithiating reagents, followed by trapping with trimethylsilyl chloride (TMSCl), as shown in Scheme 3.3. The reactions were monitored by GC-MS, and the reaction conditions (lithiation reagents, reaction scale and molar ratios) and the resulting reaction products are summarized in Table 3.1. As shown in Table 3.1,  $t\text{BuLi}$  was found to be the best lithiation reagent for this specific reaction, and use of extra equivalents (up to 6 equiv) of  $t\text{BuLi}$  can ensure the dilithiation of the DTP precursors. All the DTP distannyl monomers in this thesis, including the two monomers (scheme 3.2) in this chapter were synthesized using this optimized set of conditions, and purified by triethylamine-pretreated silica gel column chromatography.



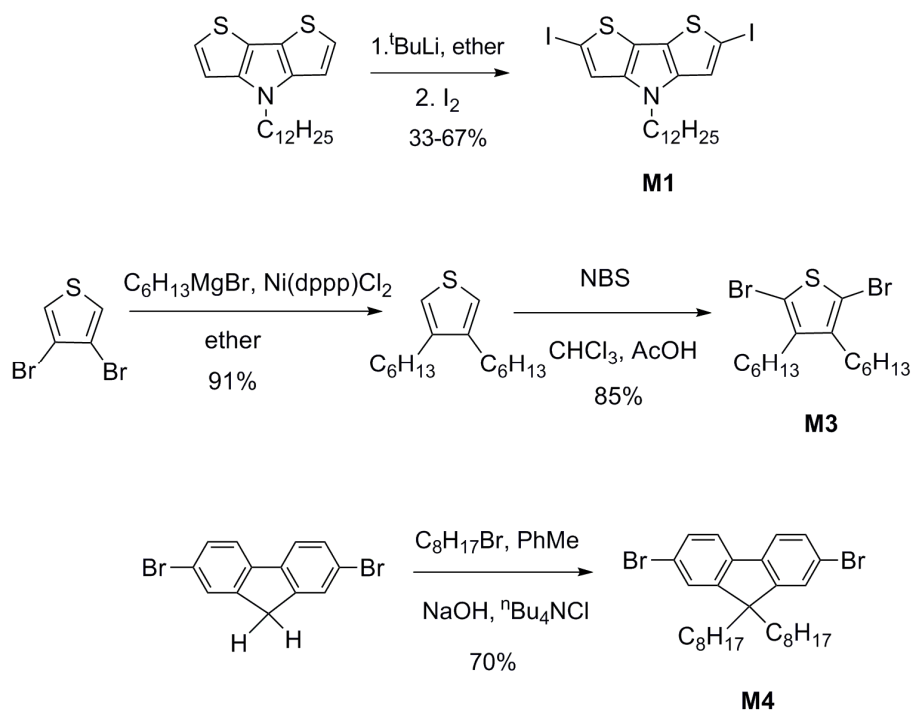
**Scheme 3.2** Synthesis of TMS-substituted DTP.

**Table 3.1** Reaction conditions and results for DTP disubstitution optimization

Lithiation Reagents (molar ratios)	Reaction Scale <sup>c</sup> (mmol) (Concentration, mmol/L)	Reaction Products (relative percentages) <sup>d</sup>		
		DTP	Mono-substituted DTP	Di-substituted DTP
<sup>n</sup> BuLi (3 equiv) & TMEDA <sup>a</sup>	0.1 (6.7)	<i>ca.</i> 100%	-	-
<sup>n</sup> BuLi (3 equiv) & TMEDA <sup>a</sup> (reflux for 30 min after warming to r.t.)	0.1 (6.7)	-	<i>ca.</i> 100%	-
LDA <sup>b</sup> (4 equiv)	0.1 (6.7)	10%	90%	-
<sup>t</sup> BuLi (6 equiv)	0.1 (6.7)	-	60%	40%
<sup>t</sup> BuLi (2 equiv)	1 (5.0)	15%	55%	30%
<sup>t</sup> BuLi (4 equiv)	1 (5.0)	-	25%	75%
<sup>t</sup> BuLi (6 equiv)	1 (5.0)	-	20%	80%

a. TMEDA: *N,N,N',N'*-tetramethylethylenediamine; b. LDA: lithium diisopropylamide; c. based on the molarity of DTP precursor; d. estimations based on GC-MS results.

All the other monomers (monomer **M2**, 5,5'-dibromo-4,4'-di-*n*-dodecyl-2,2'-bithiophene was provided by the Jenekhe group at the University of Washington) were prepared according to the literature methods,<sup>20-23</sup> and the synthetic routes are shown below (Scheme 3.3).

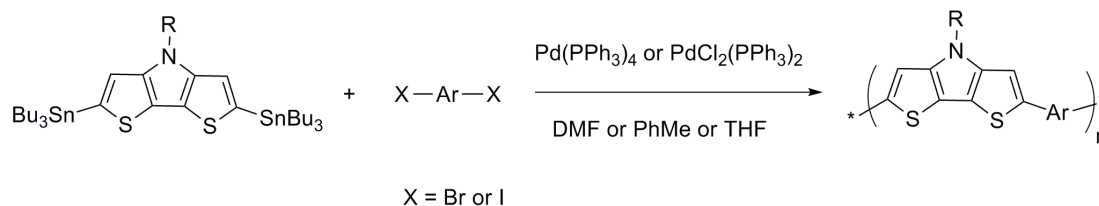


**Scheme 3.3** Synthesis of other monomers.

### Polymer Synthesis

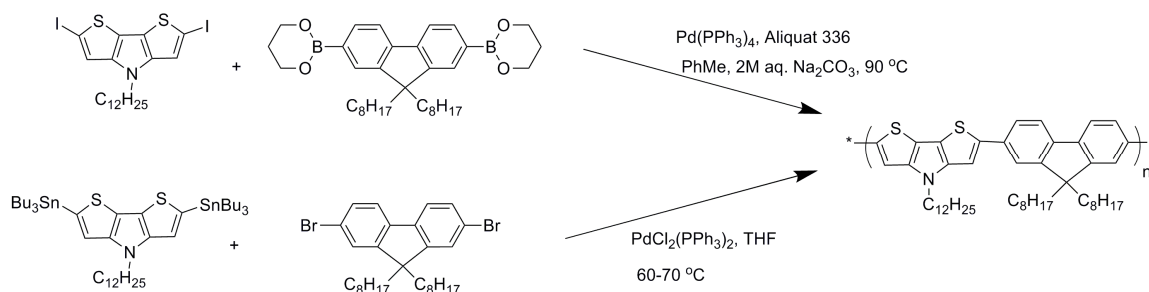
The target polymers shown in Figure 3.2 were prepared by standard Stille coupling polymerizations of *N-n*-dodecyl- or *N-n*-octyl-2,6-di(tri-*n*-butylstannyl)-dithieno[3,2-*b*:2',3'-*d*]pyrrole with different dihalo-functionalized moieties (Scheme 3.4). The polymerizations were carried out in anhydrous solvents under an inert atmosphere over approximately three to four days, and the crude polymers were isolated by precipitation into methanol. The crude polymers were then purified by Soxhlet extractions with a variety of solvents. In some cases, the solids obtained after Soxhlet extractions were re-dissolved in THF, precipitated into methanol again, and collected by filtration yielding black solids. However, the catalyst/solvent combinations (Pd(0) or Pd(II) catalyst), reaction systems (3-neck flask or pressure vessel), as well as purification procedures have been varied for **P1-5**, because during the process, the reaction conditions have been

optimized, and purification procedures have been standardized. More details about optimization of the conditions of Stille polymerizations based on distannyl DTP derivatives will be discussed later in detail in Chapter 5.



**Scheme 3.4** Synthesis of **P1-P5**.

It is worth noting that both Stille and Suzuki coupling reactions have been attempted for the polymerizations; however, Stille coupling has been chosen here for several reasons. The boron-containing DTP monomers could not readily be obtained pure in our hands (several attempts were made), although the synthesis of DTP boronates has been reported recently by Zhang *et al.*<sup>12</sup> An alternative approach is to use boronate derivatives of the co-monomers in conjunction with a diiodo-DTP. However, a few attempted trial polymerizations, in which diiodo-DTPs were coupled with some commercially available boronic esters, such as 2,2'-bithiophene-5,5'-diboronic acid bis(pinacol) ester, suggested Suzuki coupling is not advantageous over Stille coupling in terms of achieving high molecular weights (or large DP, degree of polymerization). For example in synthesizing a copolymer of DTP and fluorene, slightly higher molecular weights ( $M_n = 8.5\text{k}$ ,  $M_w = 30\text{k}$ , DP = 12) were obtained from the Stille coupling of the distannyl DTP and dibromofluorene derivatives, compared to the values from the same polymer using Suzuki coupling of the diiodo DTP and diboronato fluorene derivatives ( $M_n = 6.3\text{k}$ ,  $M_w = 11\text{k}$ , DP = 9).



**Scheme 3.5** Attempted polymerizations of DTP and fluorene using Stille and Suzuki couplings.

The Stille-coupled polymers **P1-5** are soluble in many common organic solvents, such as THF, chloroform, and toluene. Weight average molecular weights ( $M_w$ ) and the polydispersity ( $M_w/M_n$ ) were estimated by GPC against polystyrene standards using toluene as eluent (Table 3.2).  $M_w$  of the copolymers varies from 30k-9k, and polydispersities are in the range of 1.7-3.6.

The thermal properties of all of the polymers were determined by TGA; the TGA plots of the polymers are shown in Figure 3.3. The polymers all showed good thermal stability with 5% wt loss over 300 °C, and the decomposition temperatures of the polymers are listed in Table 3.2.

**Table 3.2** Yields, molecular weights, and thermal data for **P1-P5**.

Polymer	Yield	$M_w^a$	$M_w/M_n^a$	DP <sup>b</sup>	$T_d(^{\circ}\text{C})^c$
<b>P1</b>	51%	9k	1.8	14	339
<b>P2</b>	79%	22k	1.8	14	375
<b>P3</b>	69%	19k	1.7	21	402
<b>P4</b>	66%	28k	2.3	20	369
<b>P5</b>	71%	30k	3.6	12	384

a.  $M_w$  and  $M_w/M_n$  determined by means of GPC with toluene as eluent vs. polystyrene standards; b. degree of polymerization,  $DP = M_n/M_0$ ,  $M_0$  is the molecular weight of the repeating unit; c. decomposition temperature, defined as 5% weight loss, estimated using TGA under  $N_2$  at 10°C/min (20 °C/min for **P2**).

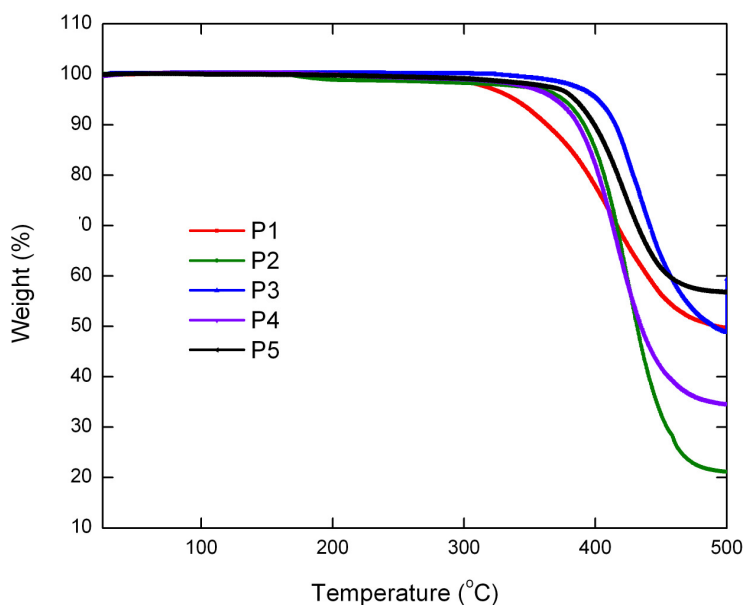


**Figure 3.3** TGA curves of **P1-P5**.

### 3.3 Density Functional Theory Calculations of Electronic Structure

Optimized geometries and electronic energy levels were calculated in the gas phase using DFT at the B3LYP/6-31G(d,p) level of theory. Excited-state energy calculations were performed at the same level of theory using the time-dependent method (TDDFT). (obtained by Dr. Joeseeph Norton in the Brédas group at the Georgia Institute of Technology). Calculations were performed on model donor-donor oligomers constructed from a DTP donor unit coupled with DTP, bithiophene, thiophene, and fluorene moieties, shown in Figure 3.2. Extended alkyl chains were replaced by methyl groups for simplicity.

Calculations were performed on oligomer structures of length  $n = 1-3$  ( $n = 1-6$  oligomers for the DTP homopolymer); the properties of the polymers were extrapolated from those of the oligomers using Kuhn fits of energy versus  $1/N$  where  $N$  is the number

of double bonds.<sup>24</sup> The HOMO/LUMO wave functions are shown in Figure 3.4. From the schematic illustration of wave functions of the oligomers, HOMOs of the oligomers are out-of-phase combinations of local HOMOs of each moiety, and LUMOs of them are in-phase combinations of local LUMOs. Moreover, it can be seen that both HOMO and LUMO levels of the DTP homopolymer and donor-donor copolymers are delocalized along the polymer backbone; this differs from the pattern observed in related donor-acceptor copolymers (copolymers in the literature<sup>17</sup> and in Chapter 4 & 5) in which the HOMO levels are delocalized, while the LUMO levels are localized on the acceptor moieties. The extrapolated values of HOMO and LUMO orbital energies,  $E_g$  and the energies of the lowest lying singlet excited states,  $S_1$ , are summarized in Table 3.3. Based on the computational results below, the HOMO and LUMO levels have slight variations when coupled with different donating moieties, which result in the differences in the bandgaps from 2.1 to 2.8 eV. The comparison of computational values with experimental estimates from UV-vis spectra will be discussed in section 3.4.

**Table 3.3** HOMO, LUMO,  $E_g$ , and  $S_1$  transition energies extrapolated for (DTP-X)<sub>∞</sub>.<sup>a</sup>

Polymers	HOMO (eV)	LUMO (eV)	$E_g$ (eV)	$S_1$ (eV)
<b>P1</b>	−4.08	−1.98	2.10	1.77
<b>P2</b>	−4.31	−2.09	2.22	1.88
<b>P3 (or P4)</b>	−4.48	−1.72	2.76	2.35
<b>P5</b>	−4.52	−1.79	2.73	2.35

a. Calculated at the B3LYP/6-31G(d,p) level and extrapolated using Kuhn fits

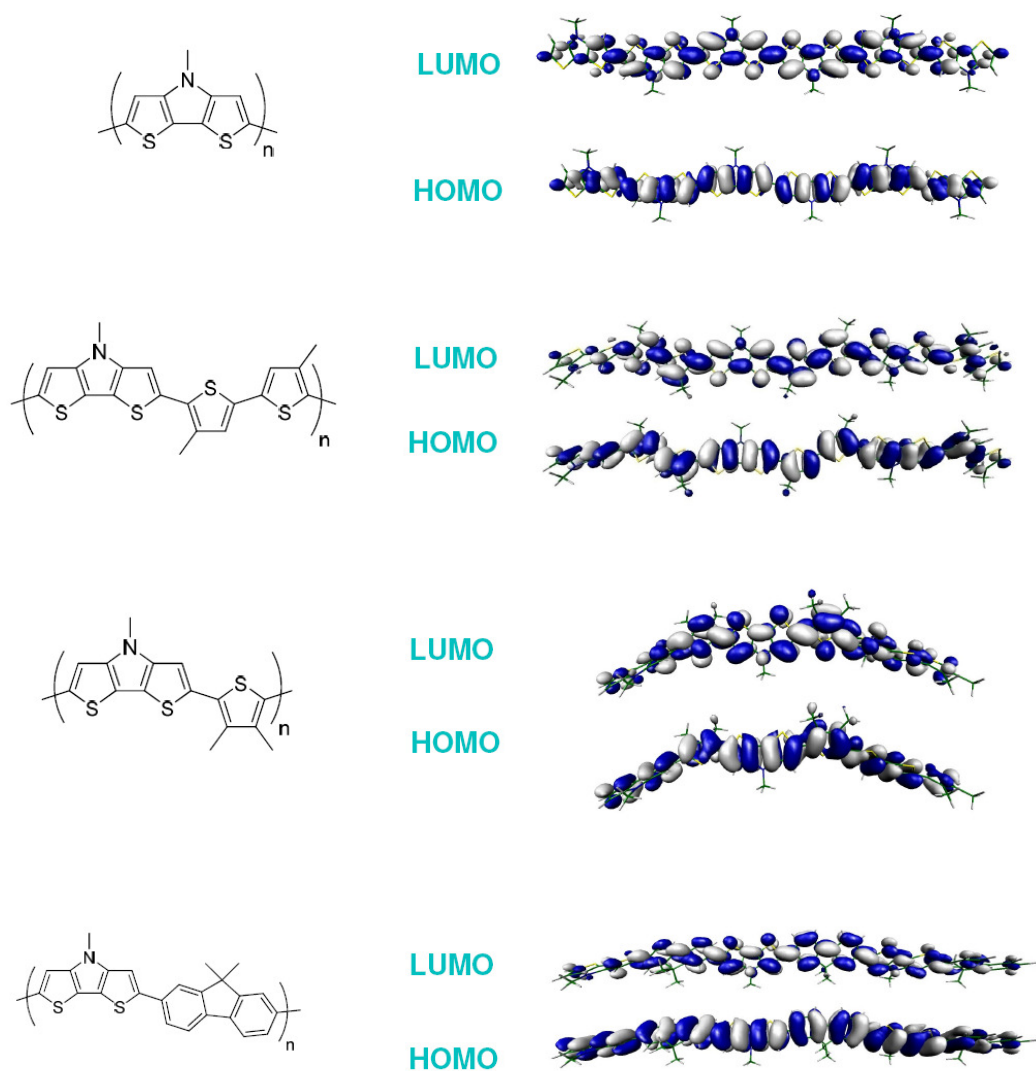


**Figure 3.4** HOMO/LUMO wavefunctions of donor-donor oligomers ( $n = 3$ ) ( $n = 6$  for homopolymer).

### 3.4 Optical Properties

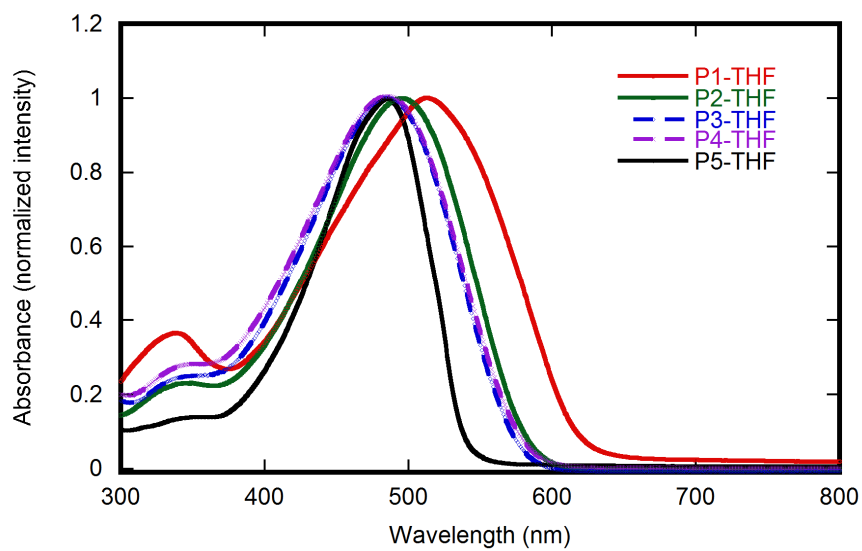
The normalized optical absorption spectra of the polymers in dilute THF solution and thin films are shown in Figure 3.5, and corresponding absorption properties are summarized in Table 3.4.

All the polymers show a major absorption band in the range of 470-520 nm in the

dilute solution, and the absorption maxima of polymers vary only slightly with the choice of co-monomers. However,  $\lambda_{\text{max}}^{\text{abs}}$  of the copolymers (**P2-P5**) is blue-shifted with respect to that of homopolymer **P1**, presumably, at least in part, due to decreased planarity in the polymer backbone. In thin films,  $\lambda_{\text{max}}^{\text{abs}}$  of **P2** is significantly red-shifted to 581 nm, which can be attributed to strong interchain  $\pi$ - $\pi$  stacking interactions in the solid state.<sup>11</sup> The UV-vis spectra of **P3** and **P4** are almost identical either in solution or thin film, which indicated that the length of the alkyl chains attached to the N atom does not affect their optical properties.

The optical band gaps estimated from the absorption edges of the polymers varied from 1.94 to 2.19 eV. **P1** has the smallest bandgap (1.94 eV) and **P5** has the largest one (2.19 eV), and **P2** and **P3** (or **P4**) have the similar bandgaps (2.06 eV) estimated from the UV-vis spectra, which suggested that the incorporation of different donor moieties affect the HOMO-LUMO gaps in the polymers. However, the trends of the increasing bandgaps from **P1** to **P5** did not follow the same trend as the quantum chemical calculation predicted. The inconsistencies between theory and experiment are possibly due to effects that cause changes in both molecular geometry and the environment. Since the calculations were performed in the gas phase, effects such as solvent or solid-state effects are neglected.

a)



b)

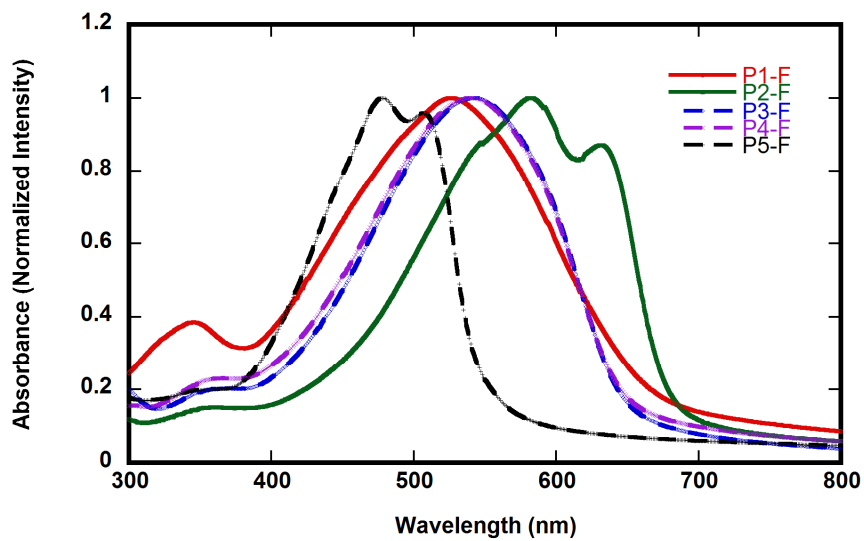


**Figure 3.5** UV-vis spectra of copolymers **P1-5** in (a) dilute THF and (b) thin film.

**Table 3.4** Optical and redox properties of the polymers.

Polymer	$\lambda_{\max}^{\text{abs}}$ (nm) ( $\epsilon, \times 10^{-4} \text{ M}^{-1} \text{ cm}^{-1}$ or $\alpha, \times 10^{-4} \text{ cm}^{-1}$ )		$E_g^c$ (optical) eV	$E_{\text{ox}}^d$ onset (CV) V	IP <sup>e</sup> (CV) eV
	Solution <sup>a</sup>	Film <sup>b</sup>			
<b>P1</b>	513 (1.85)	527 (2.92)	1.94	0.51	4.9
<b>P2</b>	495 (4.43)	582 (6.62), 631 (5.76)	2.06	0.59	5.0
<b>P3</b>	485 (3.39)	543 (4.39)	2.06	0.49	4.9
<b>P4</b>	485 (2.89)	541 (5.82)	2.06	0.51	4.9
<b>P5</b>	486 (5.12)	478 (7.02), 507 (6.67)	2.19	0.69	5.1

a. measured for diluted solution in THF (values of molar extinction coefficients,  $\epsilon$ , in the parentheses); b. measured for thin films spin-coated from toluene solution (values of absorption coefficients,  $\alpha$ , in the parentheses); c. values are optical bandgaps estimated from onset absorption edge in solution; d. measured in 0.1 M [<sup>n</sup>Bu<sub>4</sub>N]<sup>+</sup>[PF<sub>6</sub>]<sup>−</sup> /acetonitrile solution and reported vs SCE, using [Cp<sub>2</sub>Fe]<sup>+0</sup> as internal reference; e. values were estimated based on IP =  $E_{\text{ox}}^{\text{onset}} + 4.4 \text{ eV}$ .<sup>24</sup>

### 3.5 Electrochemical Properties

The electrochemical redox properties of **P1-5** were characterized by CV *via* drop-casting the polymer films on platinum disk (or Pt wire) working electrode. A representative oxidative cyclic voltammogram (that of **P4**) is shown in Figure 3.6. Ideally when reversible peaks are observed in CV, the half-wave potential ( $E_{1/2}$ ) of a process can be expressed as the average of the peak reduction potential ( $E_{\text{pc}}$ ) and the peak oxidation potential ( $E_{\text{pa}}$ ). This value is dependent only on the thermodynamics of the electron transfer in question and, unlike peak and onset potentials, is not dependent upon the scan rate.<sup>25</sup> However,  $E_{1/2}$  cannot be obtained for electrochemically irreversible processes. Non-reversible broad waves are often observed in CV plots of polymer films, as is the case in the plot shown in Figure 3.6. Moreover, the signals observed in the cyclic voltammograms of conjugated polymers often consist of multiple overlapping potentials arising from successive oxidations (or reductions) at slightly different potentials, further complicating definition of  $E_{1/2}$  for the first oxidation.<sup>25</sup> Accordingly, oxidation (or

reduction) onsets are usually used to characterize the redox properties of the polymers, with the recognition that these values are only an estimate for the thermodynamic redox potential of interest. The solid-state IP of the polymers were estimated from the oxidation onsets ( $E_{\text{ox}}^{\text{onset}}$ , the crossing point of two tangent lines in blue as shown in Figure 3.6) respectively based on  $\text{IP} = E_{\text{ox}}^{\text{onset}} + 4.4 \text{ eV}$ .<sup>26</sup>

All of the estimated IP values are in the range of 4.9-5.1 eV, and the IP of **P5** is a little higher than the others probably due to the less electron-rich nature of fluorene moiety; this is similar as in the other structurally similar copolymers of thiophene (or fused thiophene) with fluorene, such as polymer **29** in Figure 1.13.<sup>27-29</sup> The IP values of **P1-P4** are somewhat less than those from an estimate performed in the same manner for P3HT (*ca.* 5.0 eV),<sup>15</sup> which can be attributed to the incorporation of the electron-rich DTP moiety. These results suggest that **P1-P4** might be more susceptible to aerial oxidation, which might result in decreased stability in the devices.

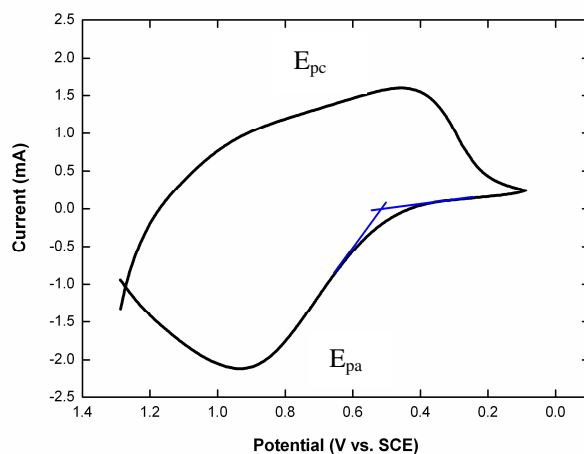


**Figure 3.6** Cyclic voltammogram of **P4** film at a scan rate of 50 mV/sec.

### 3.6 Field-Effect Transistor Characteristics

Charge-carrier transport in the copolymers were explored directly by investigating their use as the active layer in organic field-effect transistors (OFETs) fabricated from gold source/drain electrodes and SiO<sub>2</sub> gate dielectric layer in the Kippelen group at the Georgia Institute of Technology or in the Jenekhe group at the University of Washington. Field-effect mobilities ( $\mu$ ) and threshold voltages ( $V_T$ ) were measured in the saturation regime from the saturation region current equation of a standard MOSFET, using highest slope of  $|I_{DS}|^{1/2}$  vs.  $V_{GS}$  plot.

$$I_{DS} = \frac{1}{2} \mu C_i \frac{W}{L} (V_{GS} - V_T)^2 \quad (3.1)$$

where  $C_i$  is the capacitance per unit area of the gate dielectric [F/cm<sup>2</sup>], and  $W$  (width) and  $L$  (length) are the dimensions of the semiconductor channel defined by the source and drain electrodes of the transistor. Characteristics of OFETs based on polymers **P1-3** and **P5**, including mobilities ( $\mu$ ), threshold voltages ( $V_T$ ), and current on/off ratios ( $I_{on}/I_{off}$ ), are summarized in Table 3.5.

**Table 3.5** Field-effect transistor characteristics of **P1-3** and **P5**

Polymers	$\mu_h$ (cm <sup>2</sup> /(Vs))	$V_T$ (V)	$I_{on}/I_{off}$	Operation Atmosphere	Device Geometry
<b>P1</b>	$2.2 \times 10^{-5}$	-20	$1.2 \times 10^3$	N <sub>2</sub>	top
<b>P2</b>	$1.5 \times 10^{-2}$	-5	$9.3 \times 10^4$	N <sub>2</sub>	top
<b>P5</b>	$2.3 \times 10^{-6}$	-16	50	N <sub>2</sub>	top
<b>P2</b>	$4.8 \times 10^{-2}$	45	1000	Air	bottom
<b>P3</b>	$1.8 \times 10^{-3}$	22	65	Air	bottom

The devices based on the polymers showed typical p-channel field-effect transistor characteristics. A representative output and transfer curve (a device based on **P2** under N<sub>2</sub>) is shown in Figure 3.7. The devices exhibited low to moderate mobilities in the range of

$10^{-6}$  to  $10^{-2}$   $\text{cm}^2/\text{Vs}$  depending on the choices of the co-monomers. Devices with **P2** exhibited the best performance up to  $4.8 \times 10^{-2}$   $\text{cm}^2/(\text{Vs})$  with threshold voltages around 45 V and on/off ratios about  $10^3$  in air. Devices based on the same material (**P2**) has also been fabricated and tested in the glove box under  $\text{N}_2$ . Although the different device geometries precludes direct comparisons of the effects of the fabrication and operation atmosphere, significant differences are observed between the two types of devices and are likely to be primarily due to the different atmosphere: the threshold voltage is significantly changed from positive to negative and the on/off ratios are significantly increased in the inert conditions compared to those in air. The relatively low on-off ratios in the devices measured in air might be due to adventitious doping from aerial oxidation of the materials. Also the positive values of  $V_T$  in the devices operated in air indicates that they are always "on" without applying any external field, and application of a gate voltage of opposite sign is needed to turn the device off, again presumably as a result of adventitious doping from oxidation of the materials in the air.

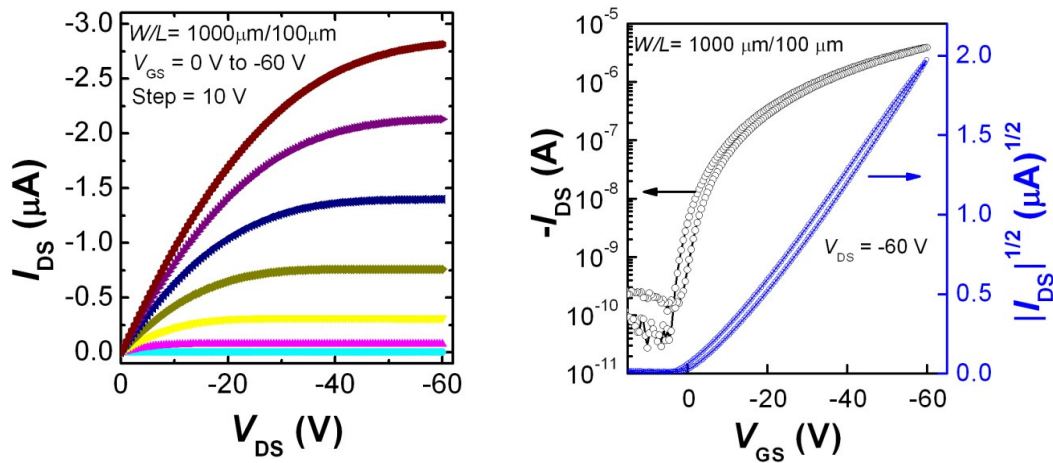


**Figure 3.7** Output (left) and transfer (right) characteristics of an OFET of **P2** under  $\text{N}_2$ .

### 3.7 Photovoltaic Cell Characteristics

Bulk heterojunction photovoltaic devices were constructed based on blends of the polymers **P1-P3** with the soluble fullerene, PCBM. They were fabricated and tested in the Kippelen group at the Georgia Institute of Technology. The  $J$ - $V$  characteristics of the devices based on **P1-P3** are shown in Figure 3.6; the device performances of each polymer are summarized in Table 3.6.

**Table 3.6** Photovoltaic cell performance of **P1-3/PCBM** blends.

Annealed	Polymers <sup>a</sup>	$V_{oc}$ (mV)	$J_{sc}$ (mA/cm <sup>2</sup> )	$FF$	$\eta$ <sup>b</sup> (%)	$P_{in}$ (mW/cm <sup>2</sup> )
No	<b>P1</b>	328 ± 4	0.50 ± 0.01	0.25 ± 0.01	0.05	81
	<b>P2</b>	367 ± 19	1.00 ± 0.04	0.31 ± 0.01	0.15 ± 0.01	73
	<b>P3</b>	462 ± 5	0.99 ± 0.02	0.33 ± 0.01	0.18 ± 0.01	87
Yes (100 °C, 10 min)	<b>P1</b>	301 ± 20	0.89 ± 0.01	0.30 ± 0.02	0.10	81
	<b>P2</b>	413 ± 5	3.38 ± 0.12	0.50 ± 0.01	0.95 ± 0.05	73
	<b>P3</b>	370 ± 38	1.34 ± 0.06	0.30 ± 0.01	0.17 ± 0.01	87

a. processing solvents for the blends films is chlorobenzene; b. power conversion efficiencies  $\eta$  was calculated using the equation 1.11.

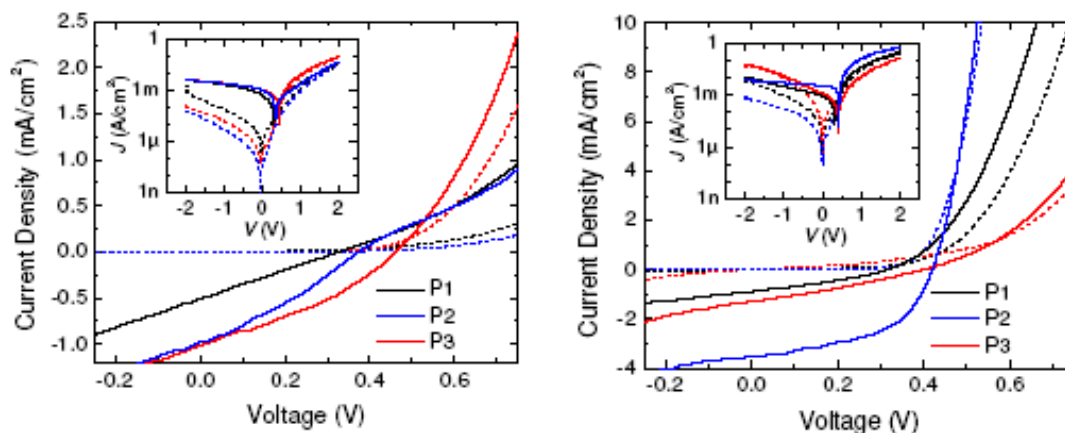
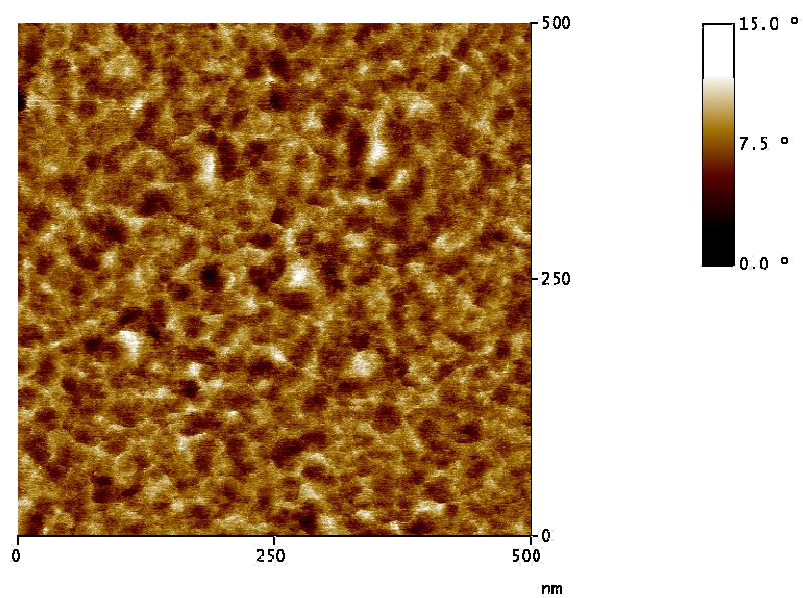


**Figure 3.8**  $J$ - $V$  characteristics of cells made from films of PCBM blended with each of polymers in a 1:1 weight ratio before (left) and after (right) annealing at 100 °C for 10 mins. (Inset shows the same data in a semilogarithmic plot).

Without annealing, the power conversion efficiencies of **P1**- **P3** are all low. However, although there are no significant differences for the blends containing **P1** or **P3** after annealing, the **P2**/PCBM cells show significant improvement, and a power conversion efficiency of  $0.95 \pm 0.05\%$  was obtained after annealing at 100 °C for 10 min. The improvement of efficiency upon annealing was previously reported in P3HT/PCBM blends, and it has been suggested that annealing process leads to higher degree of crystallinity and increased hole mobility.<sup>30,31</sup> In order to further investigate the effect of annealing step in the blends of **P2** and PCBM, several techniques have been used in this study.

Both AFM and XRD were used to investigate the morphology changes before and after annealing for the blends of **P2**/PCBM. AFM images of the blends before and after annealing were shown in Figure 3.9. From the phase images, it is seen that the blend film without annealing has small and homogeneous domains, whereas after annealing, slightly larger domains were observed. These domains may be crystalline; this is supported by XRD patterns. As seen in Figure 3.10, no obvious peaks were observed before annealing, suggesting an amorphous polymer, whereas sharp diffraction peaks were appeared in the XRD patterns after annealing indicating the increased crystallinity of the films. The peaks at  $2\theta = 4.6$  and  $9.2^\circ$  in the XRD patterns may correspond to an inter-chain distance of 1.92 nm, which is same as that reported in the literature for **P2** itself,<sup>11</sup> which suggests that the annealing step facilitates the crystallization of the polymer domains. The increased crystallinity after annealing in the blends of **P2** and PCBM are very similar to the reported phenomena in the P3HT/PCBM blends.<sup>32</sup>

a)



b)

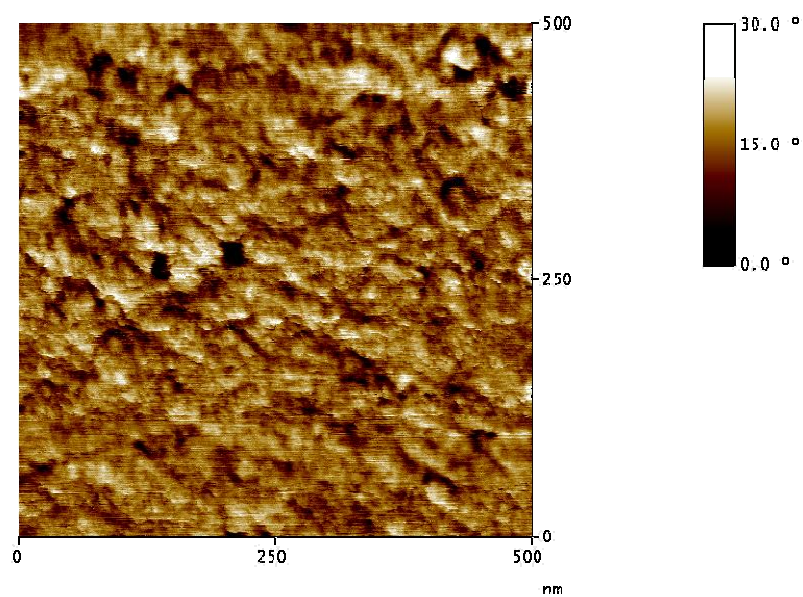


**Figure 3.9** AFM phase images of the blends of **P2/PCBM** (1:1 w:w) before (a) and after (b) annealing at 100 °C for 10 mins (vertical scale are 15, 30° for a and b, respectively).

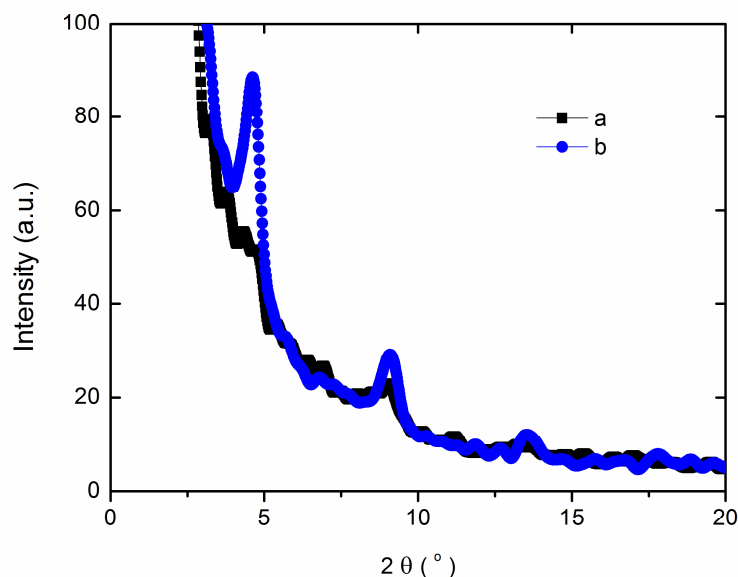


**Figure 3.10** XRD Patterns (smoothed) of blends of **P2**/PCBM (1:1 w:w): a) not annealed, b) after annealing at 100 °C for 10 mins.

Moreover, the external quantum efficiency (EQE) spectra of the blends of **P2**/PCBM were measured (Figure 3.11). It is clearly seen that EQE was also dramatically improved upon annealing. Again, the enhancement in EQE was very similar as what was observed in P3HT/PCBM blends reported in the literature.<sup>33</sup> Although the efficiency is moderate, the blend exhibits a broad incident photon-to-current conversion efficiency spectrum with a maximum at 550 nm, which is red-shifted compared to the blends of P3HT and PCBM.<sup>34</sup> From the measurement of the spectrum of the EQE, a power conversion efficiency of 0.5% can be estimated at this stage for the annealed devices under standardized AM1.5 G illumination.

In summary, the best performance in the photovoltaic cells based on the blends of **P2**/PCBM could be the combined results of a relatively high mobility, as seen in the OFETs, significant enhancement in EQE and a favorable morphology after annealing.

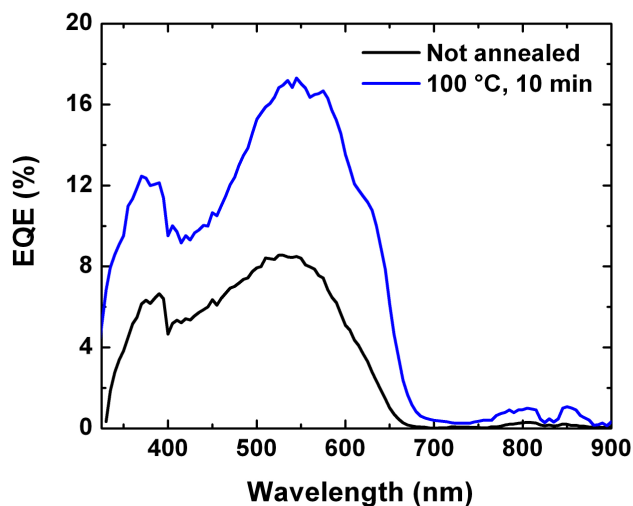


**Figure 3.11** EQE as a function of wavelength of a device based on a **P2**/PCBM blend before and after annealing at 100°C for 10 min.

### 3.7 Conclusions

A series of DTP-based donor-donor copolymers have been synthesized and characterized. The optical and electronic properties of the polymers have been varied with different co-monomers. The potential uses of those polymers in OFETs and OPVs were also investigated. One of the polymers, **P2** has shown relatively high mobility (up to  $4.8 \times 10^{-2} \text{ cm}^2/(\text{Vs})$  under ambient conditions), as well as moderate performance ( $\eta = 0.95\%$ ) in OPV devices when **P2** was blended with PCBM (1:1 w:w) and annealed at 100°C for 10 min under illumination of a broadband Xenon lamp at an irradiance of 73 mW/cm<sup>2</sup>. The relatively good performance in the OPV devices based on the blends of **P2**/PCBM could be due to the combination of a relatively high mobility in the OFET devices, significant enhancement in EQE, and the increased crystallinity after annealing based on morphology studies from AFM and XRD.

### 3.8 Experimental section

#### Materials.

Unless stated otherwise, starting materials were purchased and were used without further purification. 3,3'-Dibromo-2,2'-bithiophene was prepared by literature procedure<sup>35</sup> or provided by Grindus. Monomer **M2** was prepared using the literature procedure<sup>21</sup> and provided by Pei-Tzu Wu in the Jenekhe group in the University of Washington (UW). Monomer **M3** is initially synthesized by Pei-Tzu Wu and re-synthesized here according to the literature procedure.<sup>20</sup> Polymer **P3** was synthesized and characterized by Pei-Tzu Wu in UW.

#### Characterization.

<sup>1</sup>H NMR and <sup>13</sup>C NMR spectra were measured on a Varian Mercury 300 MHz or Bruker-AF300. Mass spectra were measured on a VG Instruments 70-SE using the electron impact (EI) mode or on an Applied Biosystems 4700 Proteomics Analyzer using MALDI mode. Elemental analyses were carried out by Atlantic Microlabs using a LECO 932 CHNS elemental analyzer. Gel permeation chromatography (GPC) analysis was performed on a Waters styragel HR 4, 3, and 1, columns coupled with a Waters 2410 Refractive Index detector and 2690 separations module, using toluene as eluent, against polystyrene standards, and a flow rate of 1mL/min. UV-vis absorption spectra were recorded on Varian Cary 500 UV/Vis/near-IR spectrophotometer. Cyclic voltammetry experiments of polymers were carried out using an EG&G Princeton Applied Research Potentiostat/Galvanostat (Model 273A) or BAS 100B electrochemical analyzer using 0.1 [nBu<sub>4</sub>N]<sup>+</sup>[PF<sub>6</sub>]<sup>-</sup>/in acetonitrile as electrolyte. The Ag<sup>+</sup>/Ag (AgNO<sub>3</sub>) reference electrode

was calibrated at the beginning of the experiments by running cyclic voltammetry using ferrocene as the internal standard. The potential values obtained in reference to  $\text{Ag}^+/\text{Ag}$  electrode were then converted to the saturated calomel electrode (SCE) scale, assuming the values of  $[\text{FeCp}_2]^{+/0} = 0.40 \text{ V}$  in  $0.1 \text{ M } [\text{nBu}_4\text{N}^+][\text{PF}_6^-]/\text{acetonitrile}$  solution.<sup>36</sup> Thermogravimetric analysis (TGA) analysis was conducted with a TA instrument Q50 TGA at a heating rate of  $20 \text{ }^\circ\text{C}/\text{min}$  under a nitrogen gas flow or with a NETZSCH thermogravimetric analyzer (model STA 449C) under a nitrogen flow at a heating rate of  $10 \text{ }^\circ\text{C}/\text{min}$ . AFM images were taken on a Digital Instruments NanoScope™ Scanning Probe Microscope and obtained from Séverine Coppée in the Kippelen group at the Georgia Institute of Technology. XRD data was collected on a Scintag X1 diffractometer with a  $\text{Cu K}\alpha$  source ( $\lambda = 1.5406 \text{ \AA}$ ) in a continuous scan mode with a step size of  $0.02$  degree.

***N-n-Octyl-dithieno[3,2-*b*:2',3'-*d*]pyrrole.*** 3,3'-Dibromo-2,2'-bithiophene (2.8 g, 8.6 mmol),  $\text{NaO}^t\text{Bu}$  (2.0 g, 20.8 mmol),  $\text{Pd}_2(\text{dba})_3$  (0.21 g, 0.23 mmol), 2,2'-bis(diphenylphosphino)-1,1'-binaphthyl (BINAP) (0.54 g, 0.86 mmol) and dry toluene were added to 3-neck flask and purged with nitrogen for 30 min, and 1-octylamine (1.1 g, 8.6 mmol) was added and reaction mixture was heated to  $110 \text{ }^\circ\text{C}$  for 7 h. After reaction, the resulting solution was washed with water, extracted with diethyl ether and the organic layer was separated. The solution was dried over  $\text{MgSO}_4$ , and all the solvents were removed under reduced pressure. The residue was purified by column chromatography (silica gel, eluent: hexane:  $\text{CH}_2\text{Cl}_2 = 9:1$ ). A grey solid (1.5 g, 60%) was obtained.  $^1\text{H}$  NMR (300 MHz,  $\text{CDCl}_3$ )  $\delta$  7.12 (d,  $J = 5.4 \text{ Hz}$ , 2H), 6.99 (d,  $J = 5.4 \text{ Hz}$ , 2H), 4.17 (t,  $J =$

6.9 Hz, 2H), 1.85 (quint,  $J = 6.9$  Hz, 2H), 1.30-1.23 (m, 10H), 0.85 (t,  $J = 6.6$  Hz, 3H). The  $^1\text{H}$  NMR spectrum is consistent with that reported in the literature.<sup>37</sup>

***N-n*-Dodecyl-dithieno[3,2-*b*:2',3'-*d*]pyrrole.** 3,3'-dibromo-2,2'-bithiophene (4.0 g, 12.0 mmol), NaO<sup>t</sup>Bu (2.8 g, 29 mmol), Pd<sub>2</sub>(dba)<sub>3</sub> (0.23 g, 0.25 mmol), BINAP (0.62 g, 1.0 mmol) and dry toluene were added to 3-neck flask and purged with nitrogen for 30 min, and 1-dodecylamine (2.3 g, 12.0 mmol) was added and reaction mixture was heated to 110 °C for 7 h. After reaction, the resulting solution was washed with water, extracted with diethyl ether and the organic layer was separated. The organic solution was dried over MgSO<sub>4</sub>, and all the solvents were removed under reduced pressure. The residue was purified by column chromatography (silica gel, elute: hexane: CH<sub>2</sub>Cl<sub>2</sub> = 9:1). A white solid (2.4 g, 58%) was obtained.  $^1\text{H}$  NMR (300 MHz, CDCl<sub>3</sub>)  $\delta$  7.12 (d,  $J = 5.4$  Hz, 2H), 7.00 (d,  $J = 5.4$  Hz, 2H), 4.18 (t,  $J = 6.9$  Hz, 2H), 1.86 (quint,  $J = 6.9$  Hz, 2H), 1.33-1.21 (m, 18H), 0.90 (t,  $J = 6.7$  Hz, 3H).  $^{13}\text{C}\{^1\text{H}\}$  NMR (75 MHz, CDCl<sub>3</sub>)  $\delta$  144.9, 122.7, 114.5, 110.9, 47.3, 31.9, 30.3, 29.6, 29.5, 29.4, 29.3, 29.2, 26.9, 22.7, 14.1 (1C missing due to overlaps). HRMS(EI): 347.1726 (Calcd for C<sub>20</sub>H<sub>29</sub>NS<sub>2</sub>, M<sup>+</sup>, 347.1741). Elemental Analysis: (Calculated) C, 69.11; H, 8.41; N, 4.03; (Found) C, 69.28; H, 8.47; N, 4.15. The  $^1\text{H}$  and  $^{13}\text{C}$  NMR spectra are consistent with that reported in the literature.<sup>15</sup>

**2,6-Di(tri-*n*-butylstannyl)-*N-n*-octyl-dithieno[3,2-*b*:2',3'-*d*]pyrrole.** A deoxygenated solution of *N*-octyl-dithieno[3,2-*b*:2',3'-*d*]pyrrole (0.50 g, 1.7 mmol) in THF (400 mL) was cooled to -78 °C; <sup>t</sup>BuLi (6 mL, 10 mmol, 1.7 M in heptane) solution was added, and the reaction was allowed to warm to room temperature and stirred for 1 h, before cooling

to  $-78\text{ }^{\circ}\text{C}$  again.  $^n\text{Bu}_3\text{SnCl}$  (1 mL, 3.7 mmol) was then added and the reaction allowed to warm to room temperature and stir for 3 h. The reaction was quenched with addition of water and extracted with dichloromethane; the extracts were dried over  $\text{MgSO}_4$ , concentrated under reduced pressure and stirred with  $\text{NEt}_3$  (50 mL) for 2 h. After removal of the volatiles under reduced pressure, the residue was purified by column chromatography (silica gel, pretreated with  $\text{NEt}_3$ , eluting with hexanes), after which a pale yellow oil (1.2 g, 80%) was obtained.  $^1\text{H}$  NMR (300 MHz,  $\text{CDCl}_3$ )  $\delta$  6.98 (s, 2H), 4.21 (t,  $J = 7.2$  Hz, 2H), 1.88 (m, 2H), 1.62–1.10 (m, 46H), 0.90 (m, 21H).  $^{13}\text{C}\{^1\text{H}\}$  NMR (75 MHz,  $\text{CDCl}_3$ ):  $\delta$  148.2, 134.9, 120.4, 118.3, 47.6, 32.1, 30.7, 29.3, 27.5, 22.9, 14.3, 14.0, 11.2 (3C missing presumably due to overlaps) HRMS(EI): 871.3219 (Calcd for  $\text{C}_{40}\text{H}_{73}\text{NS}_2\text{Sn}_2$ ,  $\text{M}^+$ , 871.3228). Elemental Analysis: (Calculated) C, 55.25; H, 8.46; N, 1.61; (Found) C, 55.38; H, 8.48; N, 1.57.

**2,6-Di(tri-*n*-butylstannyl)-*N*-*n*-dodecyl-dithieno[3,2-*b*:2',3'-*d*]pyrrole.**

A

deoxygenated solution of *N*-dodecyl-dithieno[3,2-*b*:2',3'-*d*]pyrrole (0.68 g, 2 mmol) in THF (400 mL) was cooled to  $-78\text{ }^{\circ}\text{C}$ ;  $^t\text{BuLi}$  (7.2 mL, 12 mmol, 1.7 M in heptane) solution was added, and the reaction allowed to warm to room temperature and stirred for 1 h, before cooling to  $-78\text{ }^{\circ}\text{C}$  again.  $^n\text{Bu}_3\text{SnCl}$  (1.2 mL, 4.4 mmol) was then added and the reaction allowed to warm to room temperature and stir for 3 h. The reaction was quenched with addition of water and extracted with dichloromethane; the extracts were dried over  $\text{MgSO}_4$ , concentrated under reduced pressure and stirred with  $\text{NEt}_3$  (50 mL) for 2 h. After removal of the volatiles under reduce pressure, the residue was purified by column chromatography (silica gel, pretreated with  $\text{NEt}_3$ , eluting with hexanes), after

which a pale yellow oil (1.5 g, 81%) was obtained.  $^1\text{H}$  NMR (300 MHz,  $\text{CDCl}_3$ )  $\delta$  6.96 (s, 2H), 4.21 (t,  $J = 7.2$  Hz, 2H), 1.88 (m, 2H), 1.62–1.10 (m, 54H), 0.90 (m, 21H).  $^{13}\text{C}\{^1\text{H}\}$  NMR (75 MHz,  $\text{CDCl}_3$ )  $\delta$  147.9, 134.7, 120.1, 118.0, 47.4, 31.9, 30.4, 29.6, 29.5, 29.4, 29.3, 29.0, 27.3, 27.1, 22.7, 14.1, 13.7, 10.9 (2C missing presumably due to overlaps). HRMS(EI): 927.3841 (Calcd for  $\text{C}_{44}\text{H}_{81}\text{NS}_2\text{Sn}_2$ ,  $\text{M}^+$ , 927.3854). Elemental Analysis: (Calculated) C, 57.09; H, 8.82; N, 1.51; (Found) C, 57.22; H, 8.90; N, 1.50.

**2,6-Diiodo-*N*-*n*-dodecyl-dithieno[3,2-*b*:2',3'-*d*]pyrrole. (M1)** The title compound was synthesized in the same way as its *N*-(1-octylnonyl) analogues published in the literature.<sup>23</sup> A solution of *N*-dodecyl-dithieno[3,2-*b*:2',3'-*d*]pyrrole (0.7 g, 2.0 mmol) in diethyl ether (100 mL) was cooled to 0 °C.  $^t\text{BuLi}$  (2.5 mL, 4.2 mmol, 1.7 M in heptane) solution was added, and the reaction allowed to warm to room temperature and stirred for 1 h. Before cooling to 0 °C again, a solution of  $\text{I}_2$  (1.27 g, 5.0 mmol) was then added and the reaction allowed to warm to room temperature and stir for 2 h. The reaction was washed with aq.  $\text{Na}_2\text{S}_2\text{O}_3$  solution and aq.  $\text{NaHCO}_3$  solution, and organic layer was dried over  $\text{MgSO}_4$ . After removal of the volatiles under reduce pressure, the residue was purified by column chromatography (silica gel, eluting with hexanes), after which a pale yellow solid (0.4 g, 33%) was obtained.  $^1\text{H}$  NMR (300 MHz,  $\text{CD}_2\text{Cl}_2$ )  $\delta$  7.22 (s, 2H), 4.10 (t,  $J = 7.2$  Hz, 2H), 1.81 (quint,  $J = 7.2$  Hz, 2H), 1.34–1.25 (m, 18H), 0.89 (t,  $J = 6.6$  Hz, 3H).  $^{13}\text{C}\{^1\text{H}\}$  NMR (75 MHz,  $\text{CD}_2\text{Cl}_2$ )  $\delta$  144.2, 120.9, 119.3, 100.2, 70.8, 48.0, 32.3, 30.5, 30.0, 29.9, 29.8, 29.7, 29.5, 27.2, 23.1, 14.3. HRMS(EI): 598.9681 (Calcd for  $\text{C}_{20}\text{H}_{27}\text{I}_2\text{NS}_2$ ,  $\text{M}^+$ , 598.9675). Elemental Analysis: (Calculated) C, 40.08; H, 4.54; N, 2.34; S, 10.70; (Found) C, 40.24; H, 4.39; N, 2.36; S, 10.62.

**3,4-Di-*n*-hexylthiophene.** Hexyl magnesium bromide (31 mL, 62 mmol, 2.0M in diethyl ether) was added dropwise to a stirred solution of 3,4-dibromothiophene (3 g, 24 mmol) and 1,3-bis(diphenylphosphino) propane nickel(II) chloride (NiCl<sub>2</sub>(dppp)) (0.68 g, 1.2 mmol) at 0 °C under N<sub>2</sub>. After completing the addition, the mixture was heated to refluxed overnight. After cooling to r.t., the mixture was extracted with hexanes; organic layer was separated, and then all the solvents were removed under reduced pressure. The residue was purified by column chromatography (silica gel, eluting with hexanes), after which a pale yellow oil (5.5 g, 91%) was obtained. <sup>1</sup>H NMR (300 MHz, CD<sub>2</sub>Cl<sub>2</sub>) δ 6.89 (s, 2H), 2.51 (t, *J* = 7.5 Hz, 4H), 1.54-1.28 (m, 16H), 0.90 (t, *J* = 6.6 Hz, 6H). MS(GC-MS): 252 (M<sup>+</sup>). The <sup>1</sup>H NMR spectrum is consistent with that reported in the literature.<sup>20</sup>

**2,5-Dibromo-3,4-di-*n*-hexylthiophene. (M3)** 3,4-Di-*n*-hexylthiophene (2.52 g, 10 mmol) and a mixture of acetic acid/chloroform (1:1, 40 mL) were added to a flask, and *N*-bromosuccinimide (3.73 g, 21 mmol) was added slowly. After completing addition, the solution was heated to 70 °C for 30 min, then cooled down and washed with aq. NaHCO<sub>3</sub> solution three times. The organic layer was separated and evaporated under reduced pressure. The residue was purified by column chromatography (silica gel, eluting with hexanes), after which a pale yellow oil (3.5 g, 85%) was obtained. <sup>1</sup>H NMR (300 MHz, CD<sub>2</sub>Cl<sub>2</sub>) δ 2.54 (t, *J* = 7.2 Hz, 4H), 1.54-1.28 (m, 16H), 0.91 (t, *J* = 6.6 Hz, 6H). Elemental Analysis: (Calculated) C, 46.84; H, 6.39; S, 7.82; (Found) C, 46.94; H, 6.46; S, 7.65. The <sup>1</sup>H NMR spectrum is consistent with that reported in the literature.<sup>20</sup>

**2,7-Dibromo-9,9-di-*n*-octyl-9*H*-fluorene. (M4)** The title compound was synthesized in an analogous fashion to the literature procedure for 2-bromo-9,9-di-*n*-octyl-9*H*-fluorene.<sup>22</sup> 2,7-Dibromo-9*H*-fluorene (3.0 g, 9.3 mmol), 1-bromo-*n*-octane (4.0 g, 21 mmol), tetra-*n*-butylammonium chloride (0.13 g, 0.45 mmol), 50 wt % aq. NaOH solution (8 mL), and toluene (*ca* 50 mL) were added to a flask, and stirred at 70 °C overnight. After cooling to r.t., water was added to the reaction mixture, extracted with hexanes, and the organic layer was separated. The residue was purified by flash column chromatography (silica gel, eluting with hexanes), and was recrystallized from ethanol, after which a white solid (3.5 g, 70%) was obtained. <sup>1</sup>H NMR (300 MHz, CD<sub>2</sub>Cl<sub>2</sub>)  $\delta$  7.56 (dd, *J* = 7.8, 0.9 Hz, 2H), 7.48-7.45 (m, 4H), 1.94 (m, 4H), 1.23-1.05 (m, 20H), 0.82 (t, *J* = 6.6 Hz, 6H), 0.56 (m, 4H). Elemental Analysis: (Calculated) C, 63.51; H, 7.35; (Found) C, 63.72; H, 7.29. The <sup>1</sup>H NMR spectrum is consistent with that reported in the literature.<sup>38</sup>

**P1.** To a 100 mL 3-neck round-bottomed flask were added 2,6-diiodo-*N*-(*n*-dodecyl)dithieno[3,2-*b*:2',3'-*d*]pyrrole (0.39 g, 0.65 mmol), 2,6-di(tri-*n*-butylstannyl)-*N*-*n*-dodecyl-dithieno[3,2-*b*:2',3'-*d*]pyrrole (0.61 g, 0.65 mmol) and dry toluene (20 mL). The flask was pump-filled with nitrogen (3 cycles), and the solution was deoxygenated with nitrogen for 30 min. Pd(PPh<sub>3</sub>)<sub>4</sub> (0.038 g, 0.033 mmol) was added, and the solution was deoxygenated with nitrogen for another 20 min. The solution was stirred at 90 °C for 4 days. The reaction mixture was cooled to r.t., and dropped into methanol (*ca.* 500 mL), and the solid was filtered. The crude product was purified by Soxhlet extraction with methanol and acetone each for *ca.* 1 day. A black solid (0.23 g, 51%) was obtained. <sup>1</sup>H

NMR (300 MHz, CD<sub>2</sub>Cl<sub>2</sub>):  $\delta$  7.18 (br, 2H), 4.21 (br, 2H), 1.92 (br, 2H), 1.44–1.21 (br, 18 H), 0.91 (br, 3H). Elemental Analysis: (Calculated) C, 69.11; H, 8.41; N, 4.03; (Found): C, 68.53; H, 7.70; N, 3.84.

**P2.** To a 100 mL 3-neck round-bottomed flask were added 5,5'-dibromo-4,4'-di-*n*-dodecyl-2,2'-bithiophene (0.33 g, 0.50 mmol), 2,6-di(tri-*n*-butylstannyl)-*N*-*n*-dodecyl-dithieno[3,2-*b*:2',3'-*d*]pyrrole (0.46 g, 0.50 mmol) and dry DMF (20 mL). The flask was pump-filled with nitrogen (3 cycles), and deoxygenated with nitrogen for 20 min. Then Pd(PPh<sub>3</sub>)<sub>4</sub> (0.029 mg, 0.025 mmol) was added under nitrogen, and the reaction mixture was heated to 85-90 °C for 3 days. Additional portion of dry THF (10 mL each) were added to the reaction mixture after 24 h and 48 h, respectively. The product was precipitated out upon the addition of methanol, filtered, and sequentially washed with dilute aqueous HCl, dilute aqueous NH<sub>3</sub>, water, methanol and acetone. The crude product was purified by Soxhlet extraction with acetone. A black solid (0.37 g, 79%) was obtained. <sup>1</sup>H NMR (300 MHz, CDCl<sub>3</sub>)  $\delta$  7.05 (br, 4H), 4.22 (br, 2H), 2.85 (br, 4H), 1.93-1.29 (br, 60 H), 0.90 (br, 9H). Elemental Analysis: (Calculated) C, 73.61; H, 9.62; N, 1.65; (Found): C, 72.63; H, 9.28; N, 1.56.

**P3.** To a 100 mL 3-neck round-bottomed flask were added 2,5-dibromo-3,4-di-*n*-hexylthiophene (0.23 g, 0.55 mmol), 2,6-di(tri-*n*-butylstannyl)-*N*-*n*-octyl-dithieno[3,2-*b*:2',3'-*d*]pyrrole (0.48 g, 0.55 mmol) and dry DMF (20 mL), and deoxygenated with nitrogen for 20 min. Pd(PPh<sub>3</sub>)<sub>4</sub> (0.032 g, 0.030 mmol) was added, and deoxygenated with nitrogen for another 20 min. The solution was stirred at 90 °C for 4 days. The solution

was dropped into methanol (*ca.* 200 mL), and the solid was filtered. The crude product was purified by Soxhlet extraction with acetone for 24 h. A black solid (0.20 g, 69%) was obtained. <sup>1</sup>H NMR (300 MHz, CD<sub>2</sub>Cl<sub>2</sub>):  $\delta$  7.09 (br, 2H), 4.21 (br, 2H), 2.80 (br, 4H), 1.91–1.29 (br, 28 H), 0.92 (br, 9H). Elemental Analysis: (Calculated) C: 70.92; H: 8.74; N: 2.58; (Found): C: 71.28; H: 8.40; N: 2.58.

**P4.** To a 100 mL pressure vessel were added 2,5-dibromo-3,4-di-*n*-hexylthiophene (0.39 g, 0.97 mmol), 2,6-di(tri-*n*-butylstannyl)-*N*-*n*-dodecyl-dithieno[3,2-*b*:2',3'-*d*]pyrrole (0.90 g, 0.97 mmol), dry THF (40 mL), and PdCl<sub>2</sub>(PPh<sub>3</sub>)<sub>2</sub> (0.033 g, 0.050 mmol) in a N<sub>2</sub>-filled glove box. The vessel was sealed and taken out the glove box, and the solution was heated to 60-70 °C for 4 days. The solution was washed with aq. KF solution, and extracted with toluene, and then all of the solvents were removed under reduced pressure. The solid was dissolved into THF (*ca.* 50 mL), then was dropped into methanol (*ca.* 500 mL), and the solid was filtered. The crude product was purified by Soxhlet extraction with methanol, acetone and hexanes each for 1 day. After extraction, the solid was dissolved in THF again, and was precipitated from methanol, filtered, and a black solid (0.38 g, 66%) was obtained. <sup>1</sup>H NMR (300 MHz, CDCl<sub>3</sub>):  $\delta$  7.05 (br, 2H), 4.18 (br, 2H), 2.78 (br, 4H), 1.90–1.23 (br, 32 H), 0.87 (br, 9H). Elemental Analysis: (Calculated) C: 71.19; H: 8.40; N: 2.59; (Found): C: 71.77; H: 8.97; N: 2.32.

**P5.** To a 100 mL pressure vessel were added 2,7-dibromo-9,9-di-*n*-octyl-9*H*-fluorene (0.57 g, 1.0 mmol), 2,6-di(tri-*n*-butylstannyl)-*N*-*n*-dodecyl-dithieno[3,2-*b*:2',3'-*d*]pyrrole (0.97 g, 1.0 mmol), dry THF (50 mL), and PdCl<sub>2</sub>(PPh<sub>3</sub>)<sub>2</sub> (0.035 g, 0.050 mmol) in a N<sub>2</sub>-

filled glove box. The vessel was sealed and taken out of the glove box, and the solution was heated to 60-70 °C for 4 days. The solution was washed with aq. KF solution, and extracted with toluene. Then the organic layer was separated, concentrated to *ca.* 10 mL under reduced pressure. The concentrated solution was dropped in methanol (*ca.* 500 mL), and the solid was filtered. The crude product was purified by Soxhlet extraction with methanol, acetone and hexanes each for 1 day. After extraction, the solid was dissolved in THF again, and was precipitated from methanol, filtered, and a dark red solid (0.52 g, 71%) was obtained. <sup>1</sup>H NMR (300 MHz, CD<sub>2</sub>Cl<sub>2</sub>): 7.70 (br, 6H), 7.41 (br, 2H), 4.32 (br, 2H), 1.90–1.80 (br, 6H), 1.44–1.21 (br, 42 H), 0.91 (br, 9H). Elemental Analysis: (Calculated) C, 80.16; H, 9.20; N, 1.91; (Found): C, 79.17; H, 9.01; N, 1.88.

## **Fabrication and Characterization of Thin Film Transistors.**

### **a. Fabrication procedures of transistors tested under N<sub>2</sub>**

OFETs were fabricated and tested by Shree Prakash Tiwari in the Kippelen group at the Georgia Institute of Technology. OFETs were fabricated on heavily doped n-type silicon substrates (which also serve as gate electrodes) with 200 nm thick thermally grown SiO<sub>2</sub> as the gate dielectric, in top contact configuration. Ti/Au (10 nm/100 nm) metallization on the backside of the substrate was performed to enhance the gate electrical contact. The substrates were cleaned by O<sub>2</sub> plasma for three minutes. Octyltrichlorosilane (OTS) treatment (with 5mM in toluene) was done by soaking the substrates in the OTS solution for 15 h in a N<sub>2</sub>-filled dry box. The substrates were rinsed with toluene, and annealed at 60 °C for 5 min. The capacitance of the OTS treated SiO<sub>2</sub> was about 16.2 nF/cm<sup>2</sup>. A thin layer of polymer was formed on the substrates by spin

coating with a solution (10 mg/mL) in chlorobenzene. To remove solvent, the films were annealed at 90°C for 30 minutes. 50 nm-thick Au was deposited through a shadow mask to act as top source/drain electrode. The prepared devices were post-annealed at 130 °C for 35 min inside a N<sub>2</sub> glove box.

#### **b. Fabrication procedures of transistors tested under ambient condition**

OFETs were fabricated and tested by Jessica M. Hancock in the Jenekhe group at the University of Washington. Bottom-contact geometry was used to fabricate the thin-film field-effect transistors. Heavily n-doped Si with a conductivity of 10<sup>3</sup> S/cm was used as a gate electrode with 300 nm thick SiO<sub>2</sub> layer as the gate dielectric. Using photolithography and a vacuum sputtering system ( $2 \times 10^{-6}$  Torr), two 90 nm thick gold electrodes (source and drain) with a 10 nm thick adhesive layer of TiW alloy were fabricated onto the SiO<sub>2</sub> layer. A channel length ( $L$ ) of 5-25  $\mu\text{m}$  and a channel width ( $W$ ) of 200-500  $\mu\text{m}$  were used. The gate electrode launching pad was placed on top of the Si gate electrode after the SiO<sub>2</sub> gate dielectric had been mechanically etched away. On the top of this device structure, thin films (~ 40 nm) of the polymers were spin-cast from 2mg/mL chloroform solutions. Electrical characteristics of the devices were measured using a Keithley 4200 semiconductor parameter analyzer (Keithley Instruments, Inc., Cleveland, OH). All the measurements were done under ambient laboratory conditions.

#### **Fabrication and Characterization of Photovoltaic Cells.**

Photovoltaic cell were fabricated and tested by William J. Potscavage Jr. in the Kippelen group at the Georgia Institute of Technology. Photovoltaic cells were fabricated

by blending one of the three copolymers with the acceptor 3'-phenyl-3'*H*-cyclopropa[1,9](C<sub>60</sub>-I<sub>h</sub>)[5,6]fullerene-3'-butanoic acid methyl ester (PCBM) (MTR Ltd., PCBM). Solutions of a polymer and PCBM were made in chlorobenzene (1:1 weight ratio, 20 mg/mL) for each of the polymers. ITO-coated glass (Colorado Concept Coatings LLC) with a sheet resistance of ~15 Ω/sq. was used as the substrates for the solar cells. The substrates were cleaned in an ultrasonic bath of detergent water, rinsed with deionized water, and then cleaned in sequential ultrasonic baths of deionized water, acetone, and isopropanol. Nitrogen was used to dry the substrates after each of the last three baths. A 300-nm-thick layer of SiO<sub>x</sub> was deposited on the cleaned ITO by e-beam deposition (AXXIS, Kurt J. Lesker) to pattern the anode. Next, the substrates were ultrasonicated in isopropanol for 10 min, blown dry with nitrogen, and air-plasma treated for 2 min. A hole-conducting layer of PEDOT:PSS (CLEVIOS P VP AI 4083, H. C. Starck) was filtered through a 0.45-μm-pore PVDF filter and spin coated on the substrates at 5,000 rpm for 1 min, and the substrates were annealed at 140 °C for 10 min in atmosphere. After loading into a nitrogen-filled glove box, 80-90-nm-thick films of the polymer mixtures were deposited on the substrates by spin coating for 1 min at speeds of 1500, 1400 and 1000 rpm, for the **P1-P3**/PCBM mixture, respectively. The polymers were filtered through 0.2-μm-pore PTFE filters prior to spin coating. The substrates were then loaded into a vacuum thermal evaporation system (SPECTROS, Kurt J. Lesker) connected to the glove box, and 200 nm of Al was deposited through a shadow mask at a rate of 1 – 3 Å/s and a base pressure of ~7 × 10<sup>-8</sup> Torr to define the cathodes. The completed devices were transferred in a sealed container to another nitrogen-filled glove box for electrical measurements. Current-voltage characteristics were measured using a

source meter (2400, Keithley) controlled by a LabVIEW program. When testing the solar cells under illumination, filtered light from a 175 W Xenon lamp (ASB-XE-175EX, CVI) was used as a broadband light source with an irradiance of  $\sim 73\text{--}87\text{ mW/cm}^2$  to simulate sunlight. A monochromator and calibrated photodiode were used to measure EQE.

### 3.9 References

- (1) Facchetti, A. *Materials Today* **2007**, *10*, 28.
- (2) de Boer, B.; Facchetti, A. *Polym. Rev.* **2008**, *48*, 423.
- (3) Ong, B. S.; Wu, Y. L.; Li, Y. N.; Liu, P.; Pan, H. L. *Chem. Eur. J.* **2008**, *14*, 4766.
- (4) Zhang, X. N.; Johnson, J. P.; Kampf, J. W.; Matzger, A. J. *Chem. Mater.* **2006**, *18*, 3470.
- (5) Sirringhaus, H.; Friend, R. H.; Li, X. C.; Moratti, S. C.; Holmes, A. B.; Feeder, N. *Appl. Phys. Lett.* **1997**, *71*, 3871.
- (6) Zhan, X. W.; Tan, Z. A.; Domercq, B.; An, Z. S.; Zhang, X.; Barlow, S.; Li, Y. F.; Zhu, D. B.; Kippelen, B.; Marder, S. R. *J. Am. Chem. Soc.* **2007**, *129*, 7246.
- (7) McCulloch, I.; Heeney, M.; Bailey, C.; Genevicius, K.; Macdonald, I.; Shkunov, M.; Sparrowe, D.; Tierney, S.; Wagner, R.; Zhang, W. M.; Chabinyc, M. L.; Kline, R. J.; McGehee, M. D.; Toney, M. F. *Nat. Mater.* **2006**, *5*, 328.
- (8) Li, J.; Qin, F.; Li, C. M.; Bao, Q. L.; Chan-Park, M. B.; Zhang, W.; Qin, J. G.; Ong, B. S. *Chem. Mater.* **2008**, *20*, 2057.
- (9) Parmer, J. E.; Mayer, A. C.; Hardin, B. E.; Scully, S. R.; McGehee, M. D.; Heeney, M.; McCulloch, I. *Appl. Phys. Lett.* **2008**, *92*.
- (10) Radke, K. R.; Ogawa, K.; Rasmussen, S. C. *Org. Lett.* **2005**, *7*, 5253.
- (11) Zhang, W.; Li, J.; Zou, L.; Zhang, B.; Qin, J. G.; Lu, Z. S.; Poon, Y. F.; Chan-Park, M. B.; Li, C. M. *Macromolecules* **2008**, *41*, 8953.
- (12) Zhang, W.; Li, J.; Zhang, B.; Qin, J. G. *Macromol. Rapid Commun.* **2008**, *29*, 1603.
- (13) Pappenfus, T. M.; Hermanson, B. J.; Helland, T. J.; Lee, G. G. W.; Drew, S. M.; Mann, K. R.; McGee, K. A.; Rasmussen, S. C. *Org. Lett.* **2008**, *10*, 1553.
- (14) Odom, S. A.; Lancaster, K.; Beverina, L.; Lefler, K. M.; Thompson, N. J.; Coropceanu, V.; Brédas, J. L.; Marder, S. R.; Barlow, S. *Chem. Eur. J.* **2007**, *13*, 9637.
- (15) Liu, J. Y.; Zhang, R.; Sauve, G.; Kowalewski, T.; McCullough, R. D. *J. Am. Chem. Soc.* **2008**, *130*, 13167.
- (16) Yue, W. Z.; Yun; Shao, Shuyan; Tian, Hongkun; Xie, Zhiyuan; Geng, Yanhou; Wang, Fosong. *J. Mater. Chem.* **2009**, *19*, 2199.
- (17) Zhou, E. J.; Nakamura, M.; Nishizawa, T.; Zhang, Y.; Wei, Q. S.; Tajima, K.; Yang, C. H.; Hashimoto, K. *Macromolecules* **2008**, *41*, 8302.
- (18) Babudri, F.; Farinola, G. M.; Naso, F. *J. Mater. Chem.* **2004**, *14*, 11.

- (19) Sakamoto, J.; Rehahn, M.; Wegner, G.; Schluter, A. D. *Macromol. Rapid Commun.* **2009**, *30*, 653.
- (20) Banishoeib, F.; Henckens, A.; Fourier, S.; Vanhooyland, G.; Breselge, M.; Manca, J.; Cleij, T. J.; Lutsen, L.; Vanderzande, D.; Nguyen, L. H.; Neugebauer, H.; Sariciftci, N. S. *Thin Solid Films* **2008**, *516*, 3978.
- (21) Zagorska, M.; Krische, B. *Polymer* **1990**, *31*, 1379.
- (22) Li, T. X.; Yamamoto, T.; Lan, H. L.; Kido, J. J. *Poly. Adv. Tech.* **2004**, *15*, 266.
- (23) Koeckelberghs, G.; De Cremer, L.; Persoons, A.; Verbiest, T. *Macromolecules* **2007**, *40*, 4173.
- (24) Gierschner, J.; Cornil, J.; Egelhaaf, H. J. *Adv. Mater.* **2007**, *19*, 173.
- (25) Skotheim, T. A., Reynolds, John R. *Handbook of conducting polymers*; 3rd ed; CRC: Boca Raton, FL., 2007.
- (26) Micaroni, L.; Nart, F. C.; Hummelgen, I. A. *J. Solid State Electrochem.* **2002**, *7*, 55.
- (27) Sirringhaus, H.; Wilson, R. J.; Friend, R. H.; Inbasekaran, M.; Wu, W.; Woo, E. P.; Grell, M.; Bradley, D. D. C. *Appl. Phys. Lett.* **2000**, *77*, 406.
- (28) Lim, E.; Jung, B. J.; Shim, H. K. *Macromolecules* **2003**, *36*, 4288.
- (29) Lim, E.; Jung, B. J.; Lee, J.; Shim, H. K.; Lee, J. I.; Yang, Y. S.; Do, L. M. *Macromolecules* **2005**, *38*, 4531.
- (30) Woo, C. H.; Thompson, B. C.; Kim, B. J.; Toney, M. F.; Frechet, M. J. *J. Am. Chem. Soc.* **2008**, *130*, 16324.
- (31) Li, G.; Shrotriya, V.; Yao, Y.; Huang, J. S.; Yang, Y. *J. Mater. Chem.* **2007**, *17*, 3126.
- (32) Vanlaeke, P.; Swinnen, A.; Haeldermans, I.; Vanhoyland, G.; Aernouts, T.; Cheyns, D.; Deibel, C.; D'Haen, J.; Heremans, P.; Poortmans, J.; Manca, J. V. *Sol. Energy Mater. Sol. Cells* **2006**, *90*, 2150.
- (33) Mihailetchi, V. D.; Xie, H. X.; de Boer, B.; Koster, L. J. A.; Blom, P. W. M. *Adv. Func. Mater.* **2006**, *16*, 699.
- (34) Al-Ibrahim, M.; Ambacher, O.; Sensfuss, S.; Gobsch, G. *Appl. Phys. Lett.* **2005**, *86*, 201120.
- (35) Frey, J.; Bond, A. D.; Holmes, A. B. *Chem. Commun.* **2002**, 2424.
- (36) Connelly, N. G.; Geiger, W. E. *Chem. Rev.* **1996**, *96*, 877.
- (37) Koeckelberghs, G.; De Cremer, L.; Vanormelingen, W.; Dehaen, W.; Verbiest, T.; Persoons, A.; Samyn, C. *Tetrahedron* **2005**, *61*, 687.
- (38) Cho, S. Y.; Grimsdale, A. C.; Jones, D. J.; Watkins, S. E.; Holmes, A. B. *J. Am. Chem. Soc.* **2007**, *129*, 11910.

## CHAPTER 4

### DITHIENOPYRROLE-BENZOTHIADIAZOLE

### DONOR-ACCEPTOR COPOLYMERS

#### 4.1 Introduction

Conjugated polymers in which the main chain consists of alternating electron donor (D) and acceptor (A) moieties are of growing interest because the optical and electronic properties of the polymers can be easily tuned by the ground- and excited-state intramolecular charge-transfer (ICT) interactions between D and A moieties, resulting in their possible utilities for a variety of device applications. The advantages of using D-A type copolymers in OFETs and OPVs have been mentioned earlier in Chapter 1, and few examples were discussed in sections 1.4.2 and 1.4.4.<sup>1-18</sup> For example, a series of copolymers (**54** in Figure 1.17) based on 2,7-carbazole and various electron-acceptor moieties have been studied in OPVs with efficiencies of up to 3.6% being found in blends with PCBM,<sup>5</sup> while a thiophene-based polymer incorporating thiadiazole (**34** in Figure 1.13) was used to fabricate ambipolar OFETs.<sup>19</sup> The use of alternative donor and / or acceptor building blocks for constructing D-A copolymers may lead to improved device performance or even lead to new properties and, possibly, new applications.

In recent years, fused thiophene derivatives have been incorporated into the backbones of a variety of conjugated polymers. The reasons and specific examples of which have been discussed in Chapter 1.<sup>7-9,20,21</sup> Several D-A polymers based on fused-ring donors have been reported and exhibit a range of properties depending on the choice of D and A. For example, a perylene diimide / dithienothiophene copolymer (**32** in Figure 1.13) was

found to be an electron-transport material with an electron mobility of  $1.3 \times 10^{-2} \text{ cm}^2/(\text{Vs})$ .<sup>21</sup> Furthermore, polymer **32** and related compounds have been used as electron-transport materials in single-layer bulk heterojunction solar cells with efficiencies of up to 1.5% in conjunction with polythiophene-based hole-transport materials.<sup>8,9,22</sup> More recently, *N*-alkyl and *N*-aryl dithieno[3,2-*b*:2',3'-*d*]pyrroles (DTPs) have been incorporated into conjugated oligomers and polymers,<sup>20,23,24</sup> with OFET hole mobilities of up to  $0.21 \text{ cm}^2/(\text{Vs})$  for DTP-thiophene copolymers (**I** in Figure 3.1) suggesting that this group is a promising building block for hole-transport materials.<sup>20</sup> DTP-based compounds have been shown to be more easily oxidized than analogous bithiophene and dithienothiophene compounds,<sup>25</sup> suggesting that this moiety will act as a strong  $\pi$ -donor when incorporated into D-A polymers.

The acceptor building blocks that are used in this chapter, [2,1,3]-benzothiadiazole (BTd), [1,2,5]-thiadiazolo[3,4-*g*]quinoxaline (TQ) and benzo[1,2-*c*:4,5-*c'*]bis[1,2,5]thiadiazole (BBT), have previously been incorporated into various D-A conjugated oligomers and polymers. Polymers based on [2,1,3]-benzothiadiazole copolymerized with thiophene, fluorene, silafluorene, carbazole, cyclopentadithiophene, and dithienosilole groups, such as **48**, **49a**, **51** and **52** in Figure 1.15, have previously been reported; OPV devices made from blends with soluble fullerenes show power conversion efficiencies ranging from 0.2 to 5.4%.<sup>10-12,26,27</sup> For example, very recently, power conversion efficiencies up to 2.8% were reported for solar cells based on blends of a DTP-BThBTd polymer or DTP-BTd copolymers with PCBM (**52** in Figure 1.16).<sup>28,29</sup> [1,2,5]Thiadiazolo[3,4-*g*]quinoxaline derivatives have been used in a variety of D-A polymers,<sup>13,14</sup> including a fluorene-based D-A copolymer (**37** in Figure 1.14) shown to

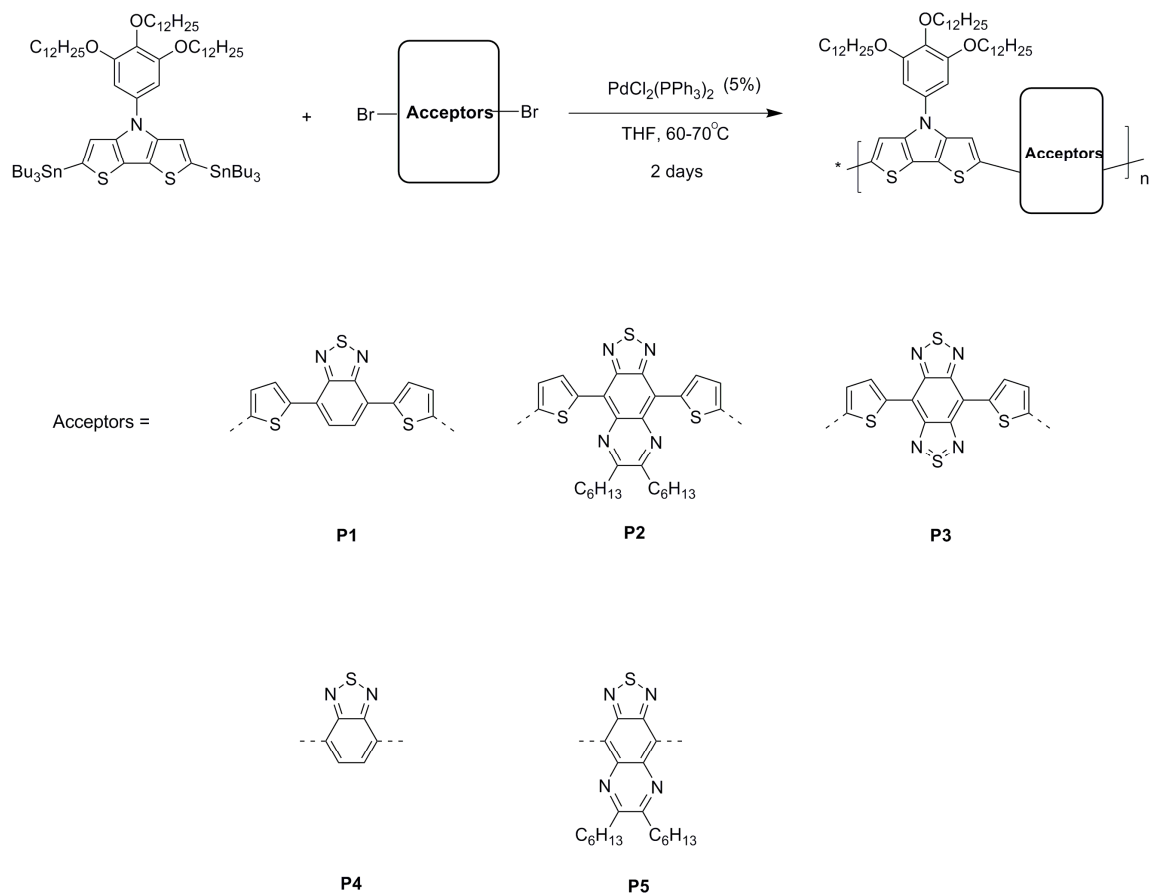
have a hole mobility of  $0.03 \text{ cm}^2/(\text{Vs})$  in an OFET.<sup>14</sup> Although there are a few reports on the synthesis of oligomers and polymers incorporating BBT,<sup>10,16,17</sup> such as **49b** in Figure 1.15, their use in device applications has not been extensively explored.

In this chapter, the synthesis, characterization, and optical and electronic properties of a series of D-A copolymers incorporating a *N*-aryl DTP as a donor co-monomer and five BTD-containing acceptor moieties are described (collaborative work with the Reynolds group at University of Florida), and the effects of their varying acceptor strengths on the optical and electronic properties are compared. In addition, the spectroelectrochemistry of the copolymers has been studied to test their potential use in electrochromic devices. Aggregation phenomena have been studied in one of the polymers (DTP-BTD). Fabrication of OFETs and OPVs from the copolymers is also described along with film morphology study of selected OPV devices.

## 4.2 Synthesis

Five copolymers **P1-5** incorporating DTP-based donors and BTD-based acceptors were synthesized. They were prepared by a standard Stille coupling polymerization of 2,6-di(tri-*n*-butylstannyl)-*N*-(3,4,5-tri-*n*-dodecyloxyphenyl) DTP with five different di(bromothienyl)- (BTh) or dibromo-substituted acceptor derivatives (Scheme 4.1). Initially, a few attempts were made to polymerize the *N*-*n*-alkyl DTP monomers with dibromo-benzothiadiazole or di(bromothienyl)-benzothiadiazole; these resulted in completely insoluble solids or in products with very limited solubilities in common organic solvents, which prevented further characterizations. Therefore, in this chapter and

in chapter 5, the *N*-trialkyloxyphenyl DTP monomer was used in order to obtain solution-processable copolymers.



**Scheme 4.1** Synthesis of **P1-5**.

The *N*-aryl distannyl DTP monomer was obtained as the same fashion as the *N*-alkyl distannyl DTP monomers described in Chapter 3, and again, it can be obtained analytically pure after careful purification. The acceptor monomers were synthesized using reported procedures for the identical compounds or close analogues.<sup>16,17</sup>

The polymerizations were carried out in THF at reflux over approximately two days, and the polymers were isolated by reduction of the solvent volume, followed by

precipitation into methanol. In each case, the crude polymer was then purified by Soxhlet extraction with methanol, hexane, acetone, and chloroform. The chloroform fraction was then reduced in volume, precipitated into methanol, and collected by filtration yielding a black solid.

The copolymers are readily soluble in many common organic solvents including THF, chloroform, and toluene. Weight-average molecular weights ( $M_w$ ) and polydispersities ( $M_w/M_n$ ) were estimated by gel-permeation chromatography (GPC) against polystyrene standards using THF as eluent (Table 4.1). The  $M_w$  values for the copolymers vary from 147 k to 28 k. In particular, **P1** has a relatively high  $M_w$  and low polydispersity compared to a recently reported structurally similar copolymer (polymer **52a** in Figure 1.16) also synthesized using Stille chemistry.<sup>28</sup> This is perhaps attributable to improved solubility arising from use of the long-chain alkoxy substituents on the DTP moiety, although the degree of polymerization is highly sensitive to the monomer purity and the reaction conditions, as would be expected for a condensation polymerization.

**Table 4.1** Yields, molecular weights and thermal properties of the copolymers.

Polymers	Yield	$M_w^a$	$M_w/M_n^a$	DP <sup>b</sup>	T <sub>d</sub> (°C) <sup>c</sup>
<b>P1</b>	95%	147k	1.4	96	368
<b>P2</b>	46%	28k	2.9	7	367
<b>P3</b>	88%	51k	3.6	12	331
<b>P4</b>	95%	53k	2.2	25	353
<b>P5</b>	83%	38k	2.0	16	340

a. Weight average molecular weight ( $M_w$ ) and polydispersity index ( $M_w/M_n$ ) determined by GPC with THF as eluent vs. polystyrene standards. b. degree of polymerization, DP =  $M_n/M_0$ ,  $M_0$  is the molecular weight of the repeating unit; c. Temperature at which 5% weight loss is observed using TGA under N<sub>2</sub> at heating rate of 10 °C/min.

The thermal properties of all the polymers were determined by thermal gravimetric analysis (TGA), as shown in Table 4.1 and Figure 4.1. Copolymers **P1-5** showed good thermal stability with 5% weight loss occurring only at temperatures in excess of 300 °C. Other small weight loss is observed at *ca.* 175 °C for **P3** may be attributable to the presence of low molecular weight oligomers, which is consistent with the relatively high polydispersity (3.6) found for this material.

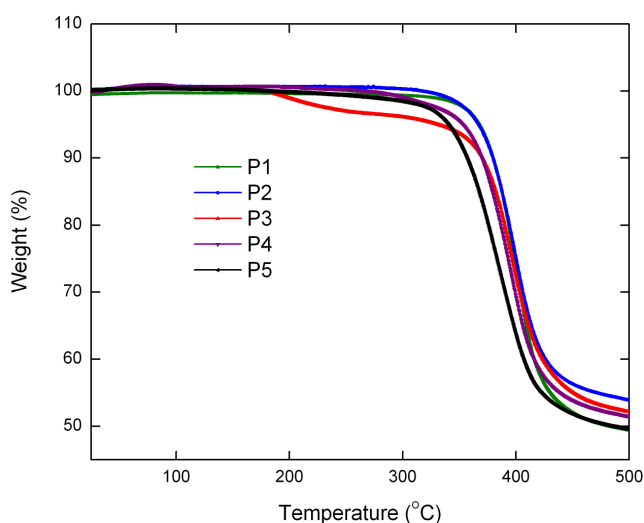


**Figure 4.1** TGA curves of **P1-P5**.

### 4.3 Density Functional Theory Electronic Structure Calculations

The geometries of model oligomers  $H(DTP-X)_nH$  ( $X = BThBTD, BThTQ, BThBBT, BTD,$  and  $TQ, n = 1, 2,$  and  $3$ ) in which the dodecyloxy groups of the DTP *N*-aryl substituents of **P1-P5** are replaced with methoxy groups, and in which the *n*-hexyl acceptor substituents on the acceptor of **P2** and **P5** were replaced with hydrogen atoms, were minimized at the Density Functional Theory B3LYP/3-21G\* (obtained by Dr. Shino

Ohira in the Brédas group at the Georgia Institute of Technology). The energy gaps between highest occupied and lowest unoccupied molecular orbitals,  $E_g$ , and the energies of the lowest lying singlet excited states,  $S_1$ , were computed at B3LYP/6-31G\*\* and INDO/S levels, respectively. Values of  $E_g$  and the  $S_1$  energy for the polymers were estimated by extrapolation of plots of the calculated parameters for the oligomers vs.  $1/n$  to  $n = \infty$ . The HOMO and LUMO wavefunctions of the representative oligomer H(DTP-BThBBT)<sub>2</sub>H are illustrated in Figure 4.2. As in several similar polymers with alternating donor and acceptor units,<sup>14,28,30</sup> the HOMO wavefunction is delocalized over the entire conjugated backbone, while the LUMO wavefunction is strongly localized on the acceptor units. The calculated LUMO energies and band gaps strongly decrease in the order BTB > TQ > BBT, suggesting that the acceptor strengths increase in the order BTB < TQ < BBT. In contrast, the HOMO energies are more-or-less independent of the identity of the acceptor. The trends in the calculated HOMO and LUMO energies are consistent with those suggested by the electrochemical oxidation and reduction potentials (see section 4.3 below). In addition, the calculated band gaps for **P1-5** (Table 4.2) are in good agreement with experimental estimates (Table 4.3). However, the extrapolated values of  $S_1$  energy are slightly larger than the values of the extrapolated  $E_g$  values, which is somehow different with the trends of the calculated values of  $S_1$  energy and  $E_g$  in other chapters, possibly in part due to the uses of different levels of computations here as indicated in Table 4.2.

**Table 4.2** HOMO, LUMO,  $E_g$ , and  $S_1$  transition energies extrapolated for  $(DTP-X)_\infty$ .

X	HOMO <sup>a</sup>	LUMO <sup>a</sup>	$E_g$ <sup>a</sup>	$S_1$ <sup>b</sup>
BThBTD	-4.36	-2.93	1.44	1.47
BThTQ	-4.04	-3.35	0.70	0.97
BThBBT	-4.16	-3.67	0.47	0.50
BTD	-4.21	-3.35	1.31	1.45
TQ	-4.01	-3.54	0.47	0.71

a. calculated at B3LYP/6-31G\*\* level and extrapolated using linear fits; b. calculated at INDO/S level and extrapolated using linear fits.

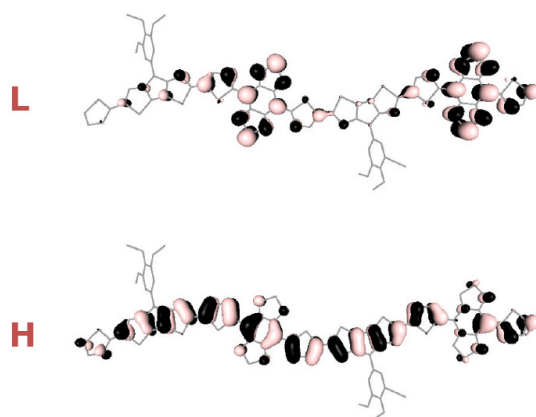


**Figure 4.2** Representative HOMO and LUMO wavefunctions of an oligomeric derivative  $H(DTP-BThBBT)_2H$ .

#### 4.4 Optical and Electrochemical Properties

Normalized optical absorption spectra of the copolymers in dilute THF solution and thin films are shown in Figure 4.3 and 4.4, respectively, and the corresponding absorption maxima are summarized in Table 4.3. All the copolymers except **P4** show two prominent absorption bands: a band in the range of 420-520 nm is relatively insensitive to the acceptor strength, while a lower energy band is strongly dependent on the acceptor. The lowest energy bands presumably involve considerable donor-to-acceptor charge-transfer

(CT) character and, accordingly, the energies of these bands are strongly dependent on the acceptor strength (see below). In thin films, the absorption spectra of the copolymers are similar to those in solution, with slight red-shifts observed in some cases. The solution absorption maximum of **P1** (674 nm) is similar as that of the recently reported closely analogous polymer **52a** (Figure 1.16,  $\lambda_{\text{max}}^{\text{abs}}$  at 671 nm);<sup>32</sup> however, it is seen at much lower energy than those obtained for other structurally similar D-A copolymers with donors including carbazole (polymer **54c** in Figure 1.17,  $\lambda_{\text{max}}^{\text{abs}}$  at *ca.* 550 nm) and thiophene or bithiophene ( $\lambda_{\text{max}}^{\text{abs}}$  at 435-479 nm),<sup>16,31</sup> consistent with the expectation that DTP acts as a stronger donor. Similar observations are seen for **P2** or **P3** compared with the other D-A copolymers containing the same or similar acceptor moieties. For examples, copolymers of BThBBT with thiophene or bithiophene have absorption maxima at 770 and 902 nm respectively ( $\lambda_{\text{max}}^{\text{abs}}$  of **P3** at 1154 nm).<sup>16</sup> In the case of **P4** and **P5**, in which there is a direct link between the DTP donor and the acceptor, absorption peaks are considerably red-shifted into the NIR range compared to those seen for their analogues in which thienylene bridges are interposed between donor and acceptor, **P1** and **P2**, respectively. In **P4**, there is a peak seen at 682 nm, which is similar to the the peak position seen in **P1**, along with an additional peak at 1050 nm presumably due to aggregation; this spectrum will be discussed in more detail the section 4.5. There is a significant red-shift observed in the long wavelength peak from **P2** ( $\lambda_{\text{max}}^{\text{abs}}$  at 930 nm) to **P5** ( $\lambda_{\text{max}}^{\text{abs}}$  at 1298 nm), which could be due to either stronger intramolecular interaction between the donor and the acceptor, as predicted in section 4.2 or aggregation effects, as seen in **P4**, or both.

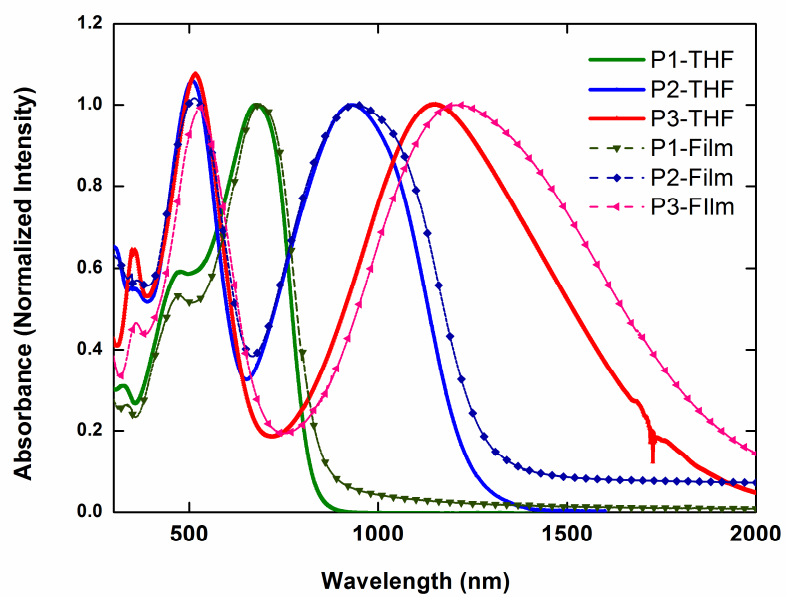


**Figure 4.3** UV-vis-NIR spectra of copolymers **P1-3** in THF and in thin films.

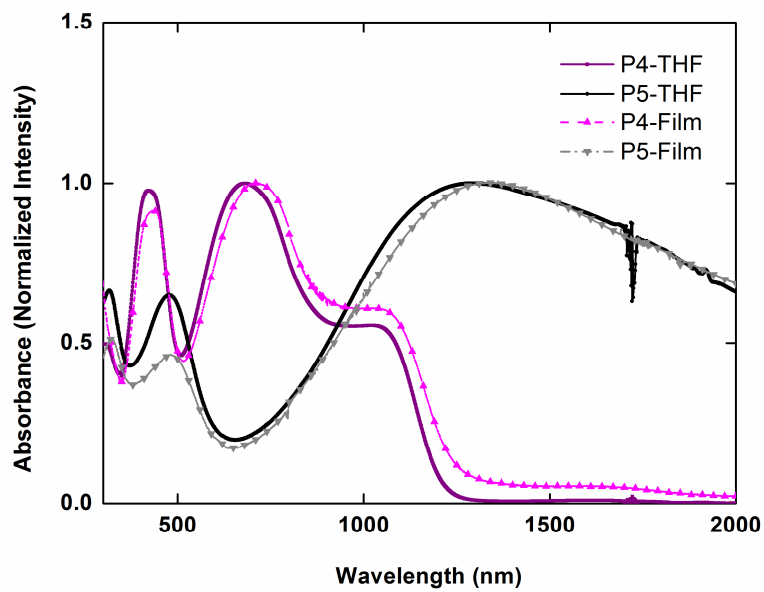


**Figure 4.4** UV-vis-NIR spectra of copolymers **P4-5** in THF and in thin films.

**Table 4.3** Optical and redox properties of the polymers.

Polymer	$\lambda_{\max}^{\text{abs}}$ (nm) ( $\epsilon, \times 10^{-4} \text{ M}^{-1} \text{ cm}^{-1}$ or $\alpha, \times 10^{-4} \text{ cm}^{-1}$ )		$E_g^c$ (opt) eV	$E_{\text{ox}}^d$ onset (CV) V	IP <sup>e</sup> (CV) eV	$E_{\text{red}}^d$ onset (CV) V	EA <sup>e</sup> (CV) eV	$E_g^f$ (CV) eV
	Solution <sup>a</sup>	Film <sup>b</sup>						
<b>P1</b>	472 (2.31), 674 (3.92)	470 (1.13), 686 (2.13)	1.41	0.60	5.0	-1.31	3.1	1.9
<b>P2</b>	508 (3.11), 931 (2.93)	514 (2.04), 941 (2.01)	0.87	0.52	4.9	-0.81	3.6	1.3
<b>P3</b>	516 (2.69), 1154 (2.49)	526 (3.51), 1206 (3.53)	0.56	0.44	4.8	-0.50	3.9	0.9
<b>P4</b>	422 (1.70), 682 (1.74), 1048 (0.96)	435 (3.17), 699 (3.47), 1049 (2.08)	0.97	0.49	4.9	-1.30	3.1	1.8
<b>P5</b>	477 (1.37), 1298 (2.12)	483 (1.26), 1310 (2.72)	–	0.46	4.9	-0.83	3.6	1.3

a. measured for diluted solution in THF (values of molar extinction coefficients,  $\epsilon$ , in the parentheses); b. measured for thin films spin-coated from toluene solution (values of absorption coefficients,  $\alpha$ , in the parentheses); c. values are optical bandgaps estimated from onset absorption edge in solution; d. measured in 0.1 M [<sup>n</sup>Bu<sub>4</sub>N]<sup>+</sup>[ClO<sub>4</sub>]<sup>-</sup>/ propylene carbonate and reported vs. SCE.<sup>32</sup> e. values were estimated based on  $\text{IP} = E_{\text{ox}}^{\text{onset}} + 4.4 \text{ eV}$ ,  $\text{EA} = E_{\text{red}}^{\text{onset}} + 4.4 \text{ eV}$ .<sup>33,34</sup> f.  $E_g$  (CV) is the differences of IP and EA values.

The electrochemical properties of the polymers were characterized by CV using films of the polymers drop-cast from chloroform solution onto platinum button working electrodes are summarized in Table 4.3. Representative oxidative and reductive CV curves of the copolymers are shown in Figure 4.5. The electrochemical oxidation and reduction onsets ( $E_{\text{ox}}^{\text{onset}}$  and  $E_{\text{red}}^{\text{onset}}$  vs. SCE) were also used to obtain estimates of solid-state ionization potential (IP) and electron affinity (EA) according to  $\text{IP} = E_{\text{ox}}^{\text{onset}} + 4.4 \text{ eV}$ ,  $\text{EA} = E_{\text{red}}^{\text{onset}} + 4.4 \text{ eV}$ ,<sup>33,34</sup> the electrochemical band gaps were obtained from the difference between the  $E_{\text{ox}}^{\text{onset}}$  and  $E_{\text{red}}^{\text{onset}}$ . The oxidation potentials have shown relatively little variation with the choice of acceptor. The estimated values of ionization potentials in these polymers (4.7-4.9 eV) are similar as those obtained in electrochemical

estimates for other DTP-containing polymers (4.7-5.0 eV),<sup>20,28,29</sup> although a detailed direct comparison is not possible due to the use of different electrochemical methods in different studies (onset vs. peak potentials, varying scan rates). On the other hand, the reduction potentials change significantly when the acceptors in the polymer backbone were varied. The trends mirror those obtained for small molecules related to the present monomers; solution CV peak reduction potentials of -1.22, -0.72 and -0.53 V vs. SCE have been reported for isolated small-molecule acceptors BThX, X = BTd, TQ and BBT, respectively.<sup>17</sup> The increase in ease of reduction from **P1** to **P2** to **P3** is consistent with the trends of red-shifts in their low-energy CT-type bands, and provides further evidence for the increase of electron-accepting strengths in the order BTd < TQ < BBT. The same trend was also observed from **P4** to **P5** when the acceptor was varied from BTd to TQ.

The optical and electrochemical data are generally in good agreement with the calculations described in the previous section. Experimental electrochemical band gaps are similar in magnitude to the respective DFT-extrapolated bandgaps (Table 4.2) and show the same trends. Similar trends are also observed when comparing the calculated  $S_1$  energies and optical bandgaps. The experimental sensitivity of the low-energy absorption to the acceptor is consistent with the molecular orbitals shown in Figure 4.2, in which the LUMOs are strongly acceptor-localized, indicating that a HOMO-LUMO transition would have substantial DTP to acceptor CT character. The variation of the reduction potentials with acceptor, and the relative invariance of the oxidation potentials, are also consistent with the trends in calculated orbital energies.

Although experimental optical and electrochemical bandgaps follow the same trend, the values obtained from electrochemical method are different from the bandgaps

estimated from the absorption spectra, mainly because optical bandgaps are related to the energy differences of the ground and excited states of the molecules, whereas the bandgaps obtained from electrochemical methods are the energy differences between the oxidized and reduced molecules. Moreover, the bandgaps estimated from electrochemistry are often larger than the values estimated from the optical spectra, in part due to the need to overcome the exciton binding energy to dissociated holes and electrons. Other factors may also cause the differences of the bandgaps estimated using different methods, such as solvent and solid-state effects. The optical and electronic properties of the polymers suggest some possible applications: the broad low-energy absorption bands suggest use in OPVs and photodetectors, while the estimated IP and EA values suggest the possibility of facile injection of both holes and electrons from commonly used electrode materials, which is a prerequisite for use as ambipolar charge-transport materials.

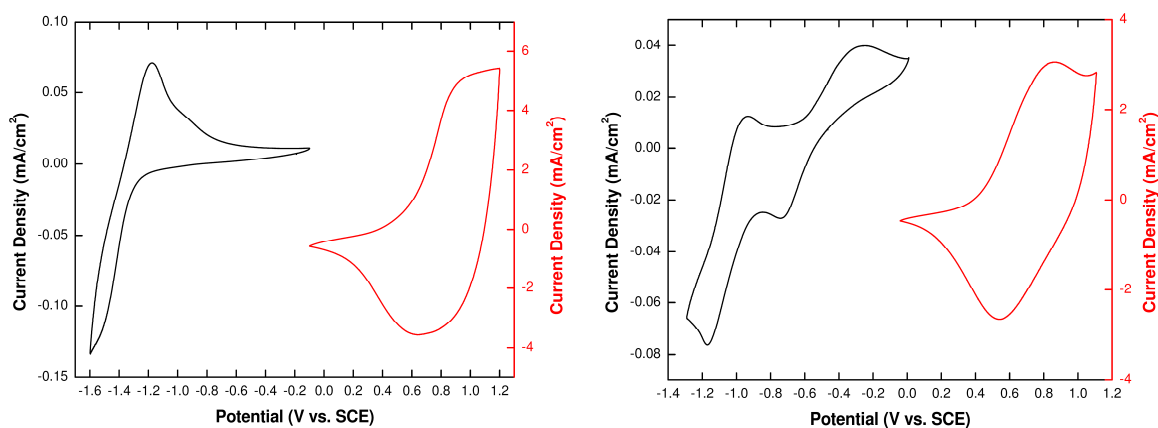


**Figure 4.5** Representative cyclic voltammograms for the copolymers (left for **P1** and right for **P3**)

#### 4.5 Aggregation Study of P4

As can be seen in Figure 4.4, **P4**, in addition to the peaks at *ca.* 420 and 680 nm, which are at similar wavelengths to those seen for **P1**, exhibits an additional peak at *ca.* 1050 nm, which may be due to the aggregation induced by the trialkyoxyl side group. Although the shapes of the UV-vis-NIR spectrum of **P4** were found not to change with different concentrations at room temperature, but there are noticeable changes observed when the temperatures were varied (see Figure 4.6), which is similar as the observations in other conjugated polymers that have been claimed to aggregate.<sup>30,35</sup> Also the UV-vis-NIR spectrum of an analogous polymer **P6** with branched alkyl side chain (synthesized by Raghunath Dasari in the Marder group), shown below in Figure 4.7, does not show a peak at *ca.* 1050 nm, which might suggest the presence of aggregation in **P4** is indeed induced by the trialkyoxyl side group.

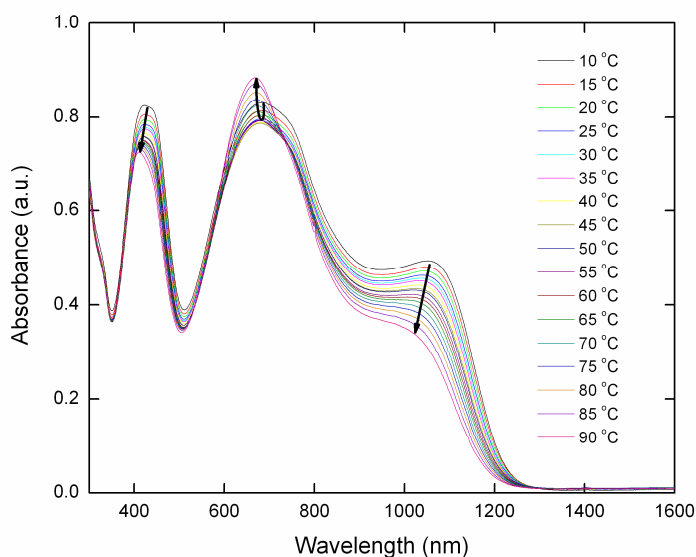


**Figure 4.6** Solution thermochromism of **P4** in dilute toluene from 10-90 °C.

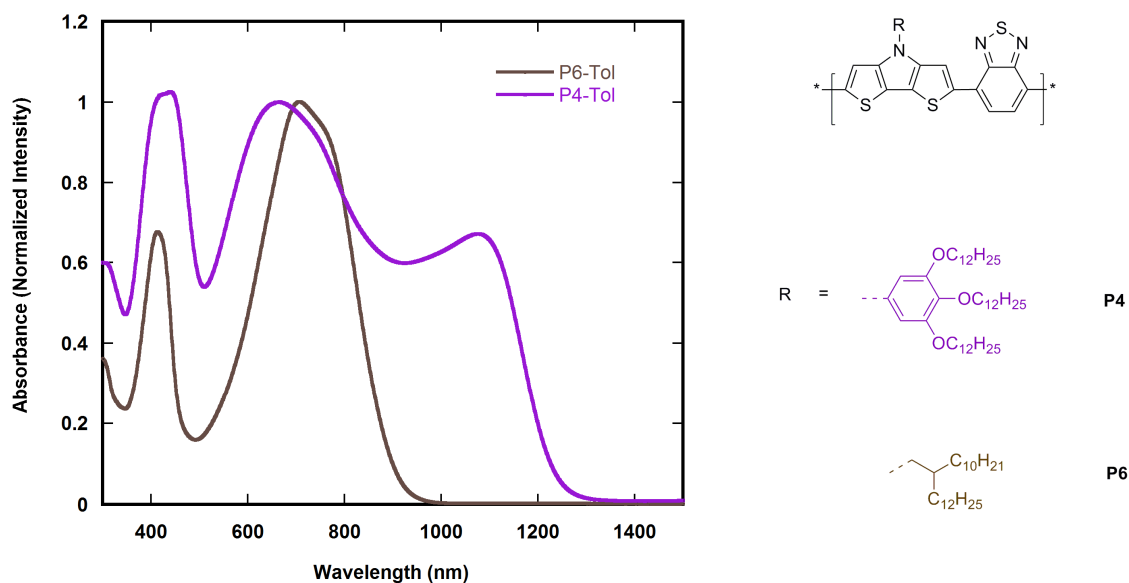


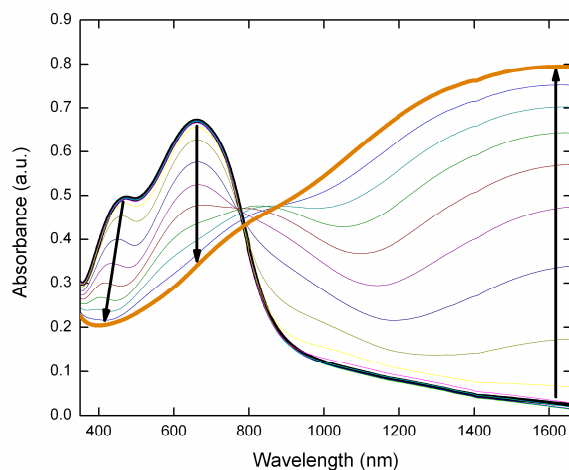
**Figure 4.7** UV-vis-NIR spectra of dilute solution of **P4** and **P6** in toluene.

## 4.6 Spectroelectrochemistry

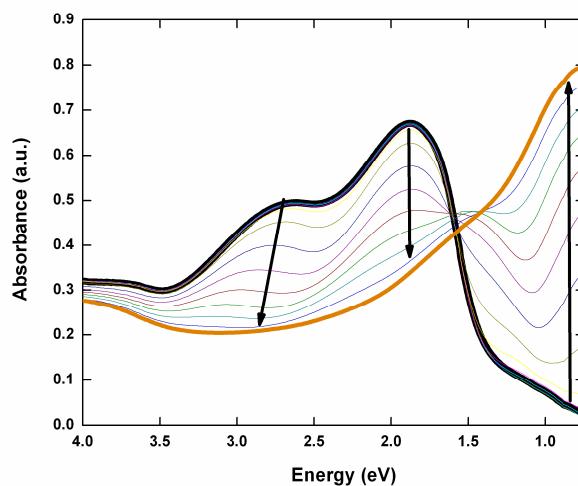
Spectroelectrochemical measurements offer a direct means of evaluating the electrochromic properties of the materials. The electrochromic devices could have applications in smart windows, protective eyewears, displays, *etc.* Conjugated polymers are increasingly used in electrochromic applications due to their multicolor control, ease in processability and structural modifications.<sup>33,36,37</sup> The spectroelectrochemical measurements were carried out by Timothy Steckler in the Reynolds group at the University of Florida. All the polymers **P1-5** undergo similar spectral changes on oxidation; the oxidative spectrum of **P1** is shown in Figure 4.8. As described above, the neutral states of all the copolymers except **P4** show two peaks, one at 420-520 nm and another in the low-energy portion of the visible or in near-IR, with the appearance of neutral polymers varied (see photographs in Table 4.4). For example, upon incremental

oxidation of **P1**, there is a bleaching of both neutral peaks (473 nm and 660 nm) with concomitant formation of charge carrier peaks around 800 nm and beyond 1600 nm in the near-IR. Upon full oxidation, the charge carrier band beyond 1600 nm tails through the visible portion of the spectrum resulting in a more visibly transparent gray/blue film.

a)

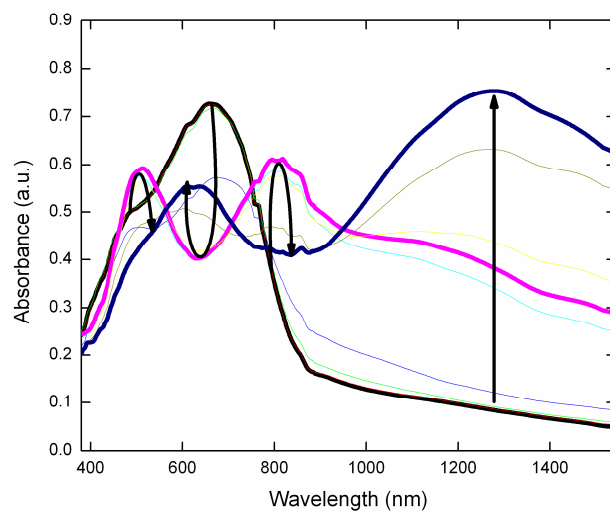


b)

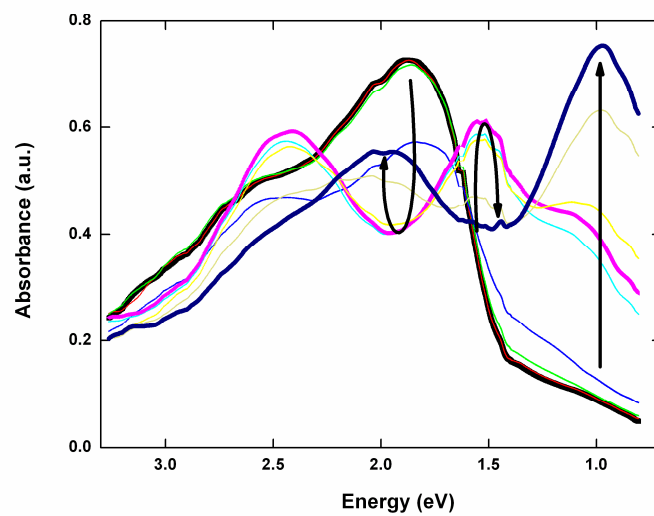


**Figure 4.8** Oxidative spectroelectrochemistry of P1 spray-cast onto ITO from -0.16 V to 1.24 V vs. SCE in 100 mV increments. Bold black line = neutral (-0.16 V) and bold orange line = oxidized state (1.24 V), a) x-axis in wavelength, b) x-axis in eV.

a)




















b)



**Figure 4.9** Reductive spectroelectrochemistry of **P1** spray-cast onto ITO, from -0.92 V to -1.72 V vs. SCE in 100 mV increments. Bold black line = neutral (-0.92 V), bold pink line = beginning of intermediate reduced state (-1.42 V), and bold navy blue line = fully reduced state (-1.72 V), a) x-axis in wavelength, b) x-axis in eV.

**Table 4.4** Images of colored neutral and redox states of films of **P1-5**.

	P1	P2	P3	P4	P5
Ox					
Neut					
Red 1					
Red 2					

In the reductive spectroelectrochemistry, there are slight differences between the copolymers. In **P1**, **P4** and **P5**, only one reduced state could be accessed in the measured range, whereas **P2** and **P3** show successive formation of two different reduced states. During incremental reduction of **P1** (Figure 4.9) there is a sharp decrease in the low-energy absorption at 660 nm at intermediate reduction potentials (−1.32 to −1.52 V), along with the formation of bands at 500 nm and *ca.* 810 nm tailing further into the near-IR. Upon complete reduction, there is an intense lower energy transition that develops at *ca.* 1280 nm and a smaller peak at *ca.* 625 nm and the film appears light purple. In **P2** and **P3** incremental potential stepping from the neutral state to the first reduced state induces a decrease in intensity of the near-IR bands of the neutral polymers along with

the formation of a band at even longer wavelength (*ca.* 1300 nm in **P2**, *ca.* 1500 nm in **P3**). There is a concomitant increase in the intensity of the high-energy band at *ca.* 520 nm (with a 10-15 nm red shift) along with the development of a shoulder at *ca.* 700 nm. This results in a darker purple film in the first reduced state. When the potential is stepped to the second reduction, the band at *ca.* 1500 nm is fully bleached, while the shoulder from the first reduction develops into new peaks at 800-900 nm. This results in the polymers yielding a bright blue/purple film with saturated color.

The spectroelectrochemical measurements indicate that each of the polymers can be either p-doped or n-doped at moderate potentials, with three or four differently colored redox states being accessible in each case (Table 4.4).

#### 4.7 Field-Effect Transistor Characteristics

Charge-carrier transport in the copolymers was explored directly by investigating their use as the active layer in top-contact organic field-effect transistors (OFETs) fabricated from gold source/drain electrodes and SiO<sub>2</sub> as a gate dielectric layer and fabricated in the Kippelen group at the Georgia Institute of Technology. Field-effect mobilities ( $\mu$ ) and threshold voltages ( $V_T$ ) were measured in the saturation regime from the saturation region current equation for standard MOSFET, using the highest slope of the  $|I_{DS}|^{1/2}$  vs.  $V_{GS}$  plot:

$$I_{DS} = \frac{1}{2} \mu C_i \frac{W}{L} (V_{GS} - V_T)^2 \quad (4.1)$$

, where  $C_i$  is the capacitance per unit area of the gate dielectric [F/cm<sup>2</sup>], and  $W$  (width) and  $L$  (length) are the dimensions of the semiconductor channel defined by the source and drain electrodes of the transistor. Characteristics of OFETs based on copolymers **P1-3**,

including mobilities ( $\mu$ ), threshold voltages ( $V_T$ ), and current on/off ratios ( $I_{on}/I_{off}$ ), are summarized in Table 4.5.

**Table 4.5** Field-effect transistor characteristics of **P1-3**.

Polymers	Operation mode	$\mu$ (cm <sup>2</sup> /(Vs))	$V_T$ (V)	$I_{on}/I_{off}$
<b>P1</b>	p-type	$1.2 \times 10^{-4}$	2.2	$10^2 \sim 10^3$
<b>P2</b>	p-type	$2.2 \times 10^{-3}$	-8.2	$10^3 \sim 10^4$
<b>P3</b>	p-type	$1.6 \times 10^{-3}$	-16	-
	n-type	$7.9 \times 10^{-4}$	37.4	-

Figures 4.10 and 4.11 show the output and transfer characteristics of OFETs ( $W/L=1000 \mu\text{m}/100 \mu\text{m}$ ) with **P1** and **P2**. The devices based on **P1** and **P2** showed typical p-channel field-effect transistor characteristics. Devices with **P1** exhibited an average hole mobility of about  $1.2 \times 10^{-4} \text{ cm}^2/(\text{Vs})$  with threshold voltages around 2.2 V and on/off ratios around  $10^2 \sim 10^3$ . These relatively low on-off ratios might be due to adventitious doping since the materials are easily oxidized; indeed such doping has been suggested to result in low on/off ratios in other low-IP DTP materials.<sup>20</sup> OFETs based on **P2** show higher p-channel average hole mobilities of about  $2.2 \times 10^{-3} \text{ cm}^2/(\text{Vs})$  along with threshold voltages around -8V and current on/off ratios of about  $10^3 \sim 10^4$ . It was also found that annealing could lead to improved device performance; for instance, the average hole mobilities of the devices of **P2** before and after post-annealing were  $1.2 \times 10^{-3}$  and  $2.2 \times 10^{-3} \text{ cm}^2/(\text{Vs})$ , respectively.

Since quantum-chemical calculations, electrochemistry, and spectroelectrochemistry suggest the possibility of both hole and electron injection into **P3** at moderate potentials, it was thought that this polymer might serve as a candidate ambipolar charge-transport

material. Figure 4.12 shows the output characteristics of an OFET ( $W/L = 1000 \mu\text{m}/100 \mu\text{m}$ ) in which **P3** is the active material and in which the source and drain electrodes are Au. These OFETs show ambipolar behavior with the hole and electron mobilities of similar magnitude,  $1.6 \times 10^{-3} \text{ cm}^2/(\text{Vs})$  and  $7.9 \times 10^{-4} \text{ cm}^2/(\text{Vs})$  for p- and n-channel, respectively. Those values are slightly higher than those we reported previously ( $1.2 \times 10^{-3} \text{ cm}^2/(\text{Vs})$  and  $5.8 \times 10^{-4} \text{ cm}^2/(\text{Vs})$  for p- and n-channel) when using Al source and drain electrodes.<sup>18</sup> Few low band-gap polymers have been used in the fabrication of ambipolar OFETs,<sup>6,19</sup> and the obtained hole and electron mobilities have been of similar magnitude to those reported here. Although the hole and electron mobilities obtained in **P3** is moderate, this polymer is one of very few examples of the materials that have been found to exhibit ambipolar characteristics in OFETs processed from solution.

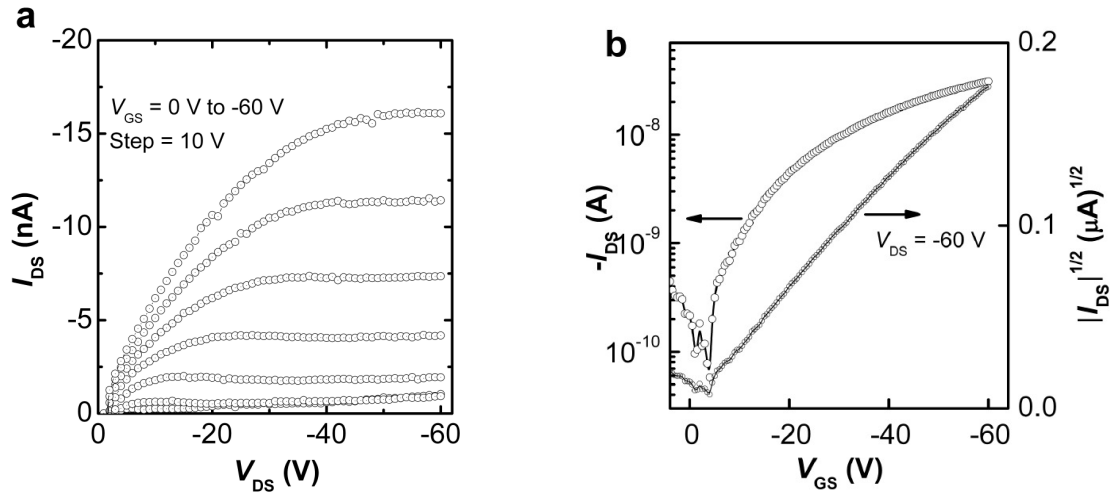


**Figure 4.10** Output (a) and transfer (b) characteristics of an OFET based on **P1**.

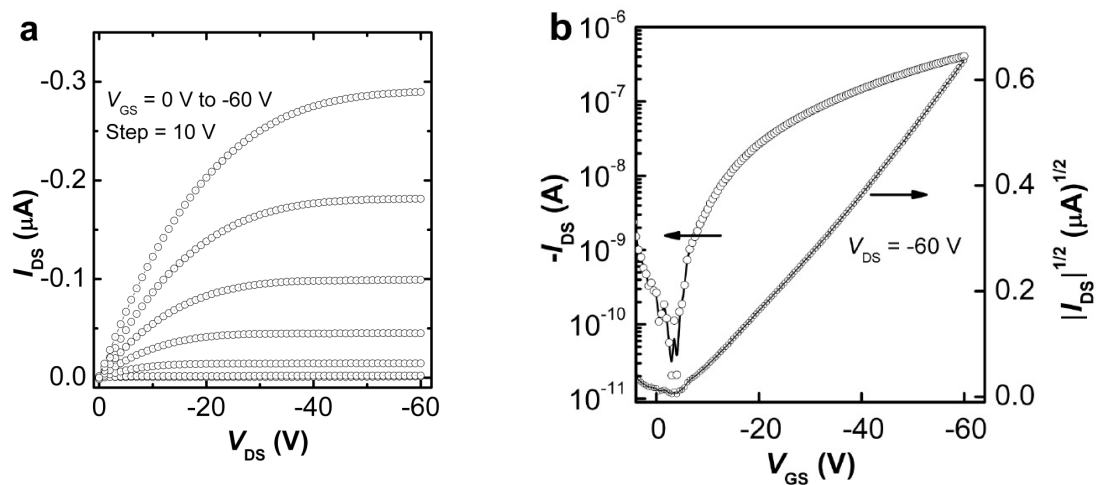


**Figure 4.11** Output (a) and transfer (b) characteristics of an OFET based on **P2**.

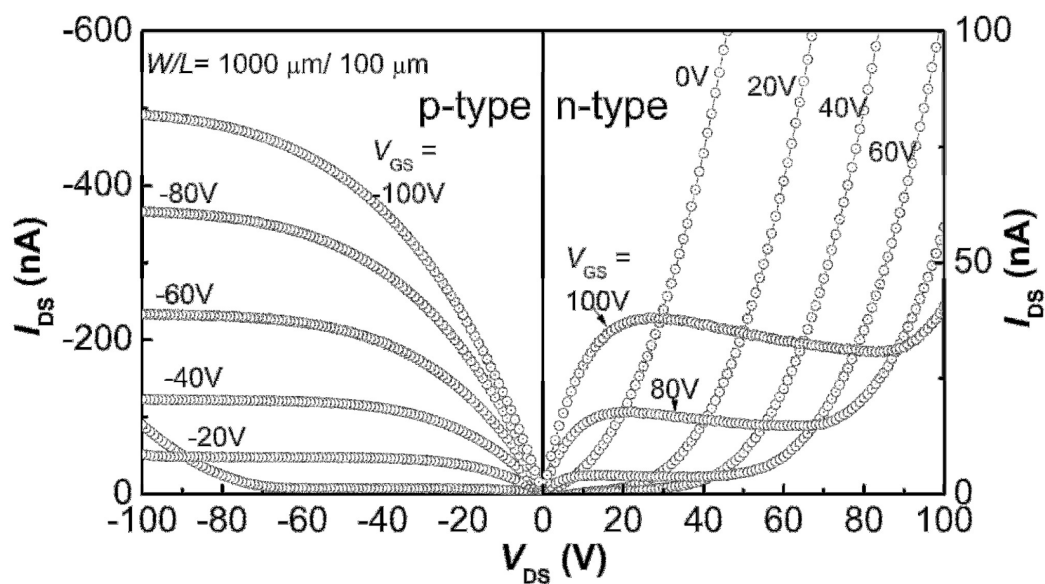


**Figure 4.12** Output characteristics (p-type and n-type) of an OFET based on **P3**.

#### 4.8 Photovoltaic Cell Characteristics

Bulk heterojunction photovoltaic devices were fabricated based on blends of each polymer with the soluble fullerene PCBM in the Kippelen group at the Georgia Institute of Technology. The *J-V* characteristics of the devices are shown in Figure 4.13; the performance of devices with different polymers and under different conditions is summarized in Table 4.6.

Based on the optical, electrochemical, and OFET data of **P1** described in the previous sections, **P1** has good spectral coverage of the visible spectrum and reasonable hole mobility. Moreover, the estimated IP and EA for **P1** suggest the best energy-level alignment with PCBM of the three copolymers; the estimated EA of **P1** (*ca.* 3.2 eV) is 0.7 eV lower in magnitude than that of PCBM (3.9 eV),<sup>38</sup> an offset which the literature suggests should be sufficient for achieving high yields of charge separation in a blend.<sup>39</sup> Therefore, it was thought to be a good candidate for a donor in photovoltaic applications in combination with fullerene acceptors. Indeed, in preliminary studies, cells with blends of PCBM and **P1** yielded better OPV performance than cells fabricated with the other copolymers. Some studies on bulk-heterojunction solar cells fabricated from conjugated polymers and fullerenes have suggested that different weight ratios as well as solvents can affect the nanoscale morphology of the films.<sup>40</sup> Optimizations of the devices of **P1** blended with PCBM were carried out by varying the weight ratio of polymer and PCBM and/or changing the processing solvent. The best performance was observed when the polymer was spin-coated using chlorobenzene and blended with PCBM in a 1:3 weight ratio, which showed a power conversion efficiency,  $\eta$ , under broadband light of  $1.3 \pm 0.1\%$ .

AFM images of the blends processed using different solvents have been obtained and compared. The height images (Figure 4.14) of the blends of **P1**/PCBM (1:3) films fabricated from chlorobenzene, toluene, and *o*-xylene showed that the film fabricated from chlorobenzene gave the morphology with the smoothest surface and smallest domain size compared to films fabricated from toluene or *o*-xylene. RMS (root mean square) roughness values for the blends of **P1**/PCBM (1:3 weight ratio) films processed from chlorobenzene, *o*-xylene, and toluene are 1.3, 3.5 and 12.7 nm, respectively. Our observation of different morphologies when processed from different solvents is somewhat similar to what has been observed and reported in the literature on processing other polymer, such as MDMO-PPV, blended with PCBM from different solvents, and the brighter domains (with larger height values) are probably PCBM-rich domains based on the literature reports for the MDMO-PPV/PCBM blends.<sup>40</sup>

Although our efficiencies on solar cells based on **P1** are not as high as those based upon the structurally similar copolymer **52a** (Figure 1.15) reported very recently,<sup>16</sup> the optimization of the devices by varying the weight ratio with PCBM as well as changing the solvents could provide useful information for further studies of the photovoltaic applications of DTP-based copolymers.

Devices with **P2** and **P3** were also made and measured using the same fabrication methods. The lowest photocurrent coupled with the smallest open-circuit voltage lead to the lowest power conversion efficiency in **P3**. The devices incorporating **P2**, the estimated EA of which lies between that of **P1** and **P3**, gave photovoltaic performance intermediate between that of **P1** and **P3**. Nevertheless, the similarity of the estimated EA of 3.7 eV in **P2** (or 4.0 eV in **P3**) and 3.9 eV in PCBM,<sup>38</sup> might be one of the reasons for

low efficiency since a driving force of 0.3-0.5 eV is generally required to achieve efficient charge separation.<sup>39,43</sup>

**Table 4.6** Photovoltaic cell performance of **P1-3** with different conditions.

Polymers (X: PCBM weight ratio)	Spin- coating Solvent <sup>a</sup>	$V_{OC}$ (mV)	$J_{SC}$ (mA/cm <sup>2</sup> )	$FF$	$\eta$ <sup>b</sup> (%)
<b>P1</b> (1:1)	CB	500 ± 4	4.3 ± 0.1	0.37 ± 0.01	1.1 ± 0.1
<b>P1</b> (1:2)	CB	511 ± 6	4.1 ± 0.1	0.43 ± 0.01	1.2 ± 0.1
<b>P1</b> (1:3)	CB	510 ± 2	3.9 ± 0.2	0.47 ± 0.01	1.3 ± 0.1
<b>P1</b> (1:3)	<i>O</i> -XY	523 ± 2	3.6 ± 0.1	0.39 ± 0.01	0.9 ± 0.1
<b>P1</b> (1:3)	DCB	436 ± 4	1.7 ± 0.2	0.54 ± 0.01	0.56 ± 0.1
<b>P1</b> (1:3)	TOL	394 ± 48	1.6 ± 0.4	0.25 ± 0.01	0.19 ± 0.1
<b>P2</b> (1:1)	CB	268 ± 3	1.7 ± 0.01	0.36 ± 0.01	0.22 ± 0.01
<b>P3</b> (1:1)	CB	109 ± 4	0.20 ± 0.01	0.29 ± 0.01	0.007 ± 0.001

a. Abbreviations for solvents: CB = chlorobenzene, *O*-XY = *o*-xylene, DCB = dichlorobenzene, TOL = toluene. b.  $\eta$  was calculated using the equation 1.11 using a broadband light source with  $P_{in} = \sim 73\text{-}76 \text{ mW/cm}^2$ .

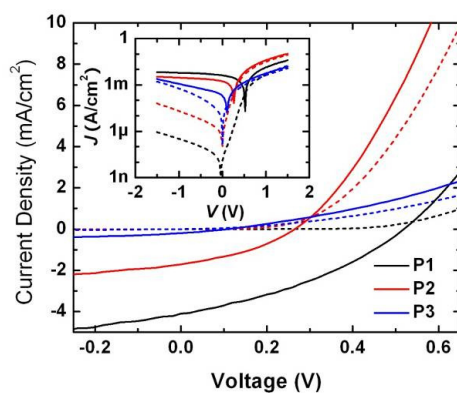


**Figure 4.13** *J-V* characteristics of multiple cells measured in the dark (dashed line) and under illumination (solid line) for films of PCBM blended with each of the following polymers in a 1:1 weight ratio. (Inset shows the same data in a semilogarithmic plot)

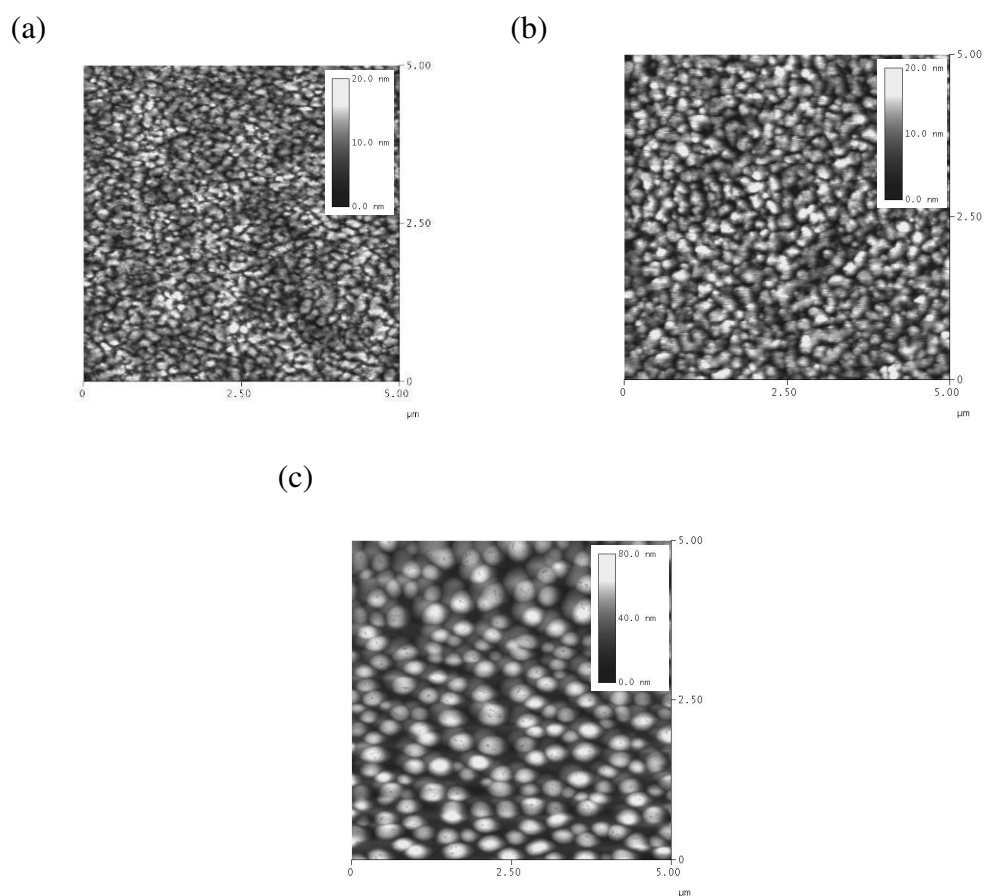


**Figure 4.14** AFM tapping-mode height images of **P1/PCBM** (1:3 weight ratio) film surface processed from a) chlorobenzene, b) *o*-xylene and c) toluene. The vertical gray scale is 20 nm for a) and b) and 80 nm for c).

The external quantum efficiency (EQE) spectrum for a **P1** device with PCBM in a 1:1 weight ratio is shown in Figure 4.15 and indicates that there is absorption of photons and conversion into current out to wavelengths of ~800 nm. While the broad spectrum is encouraging, photocurrent is limited by the maximum EQE of ~30%. From the EQE, the AM1.5 G efficiency for this device is estimated to be ~0.9%.

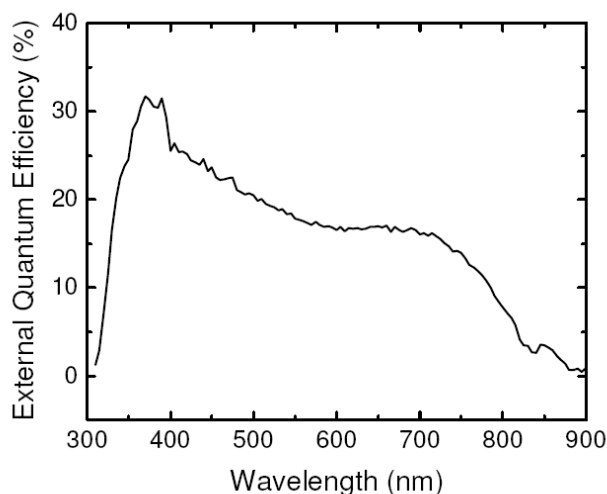


**Figure 4.15** External quantum efficiency (EQE) as a function of wavelength of a device made from a blend of **P1**/PCBM (1:1 w:w).

Although the photovoltaic cell performance of **P1** / PCBM devices is moderate, and the performance of devices based on **P2** and **P3** are relatively low, the device optimizations on **P1** revealed the effects of donor / acceptor ratio and of different processing solvents. Device performance might be further improved by annealing and/or control of the film morphology. Moreover, devices based on **P2** and **P3** might be useful as active components in tandem cells due to their broad absorbance in the near-IR range, as well as potentially serving as near-IR photodetectors.

## 4.9 Conclusions

A series of D-A copolymers have been synthesized and characterized based on dithieno[3,2-*b*:2',3'-*d*]pyrrole donors linked to benzothiadiazole-based acceptors, either directly or through thienylene bridges. Both quantum-chemical calculations and the optical and electrochemical properties of these copolymers suggest that the HOMO energy is only weakly dependent upon the choice of the acceptors, while the LUMO energy and the energy of the low-energy absorption band is strongly influenced by the acceptor. Both theory and experiment indicate that the acceptor strength increases in the order benzothiadiazole < thiadiazolo[3,4-*g*]quinoxaline < benzobisthiadiazole. The low-energy absorption bands have considerable donor-to-acceptor charge-transfer character and, in the case of the compound with a benzobisthiadiazole acceptor, this band is found at *ca.* 1.2  $\mu\text{m}$ , making this material one of the lowest bandgap solution-processible polymers reported to date. An aggregation study for one of the polymers suggested the substituent on the DTP moieties plays an important role on the optical properties of the copolymers. Furthermore, their potential utilities in electrochromic devices, OFETs, and OPVs were tested. Spectroelectrochemical measurements indicated they can be either electrochemically p-doped or n-doped at moderate potentials, suggesting that the polymers could have potential use in electrochromic devices. Two of the polymers functioned as hole-transport materials in OFETs with mobilities as high as  $2.2 \times 10^{-3} \text{ cm}^2/(\text{Vs})$ , while the example with the strongest acceptor exhibited ambipolar field-effect characteristics. In the OPV devices made from the copolymers/PCBM blends, the example with the weakest acceptor (benzothiadiazole) exhibited the best performance with a power conversion efficiency up to  $1.3 \pm 0.1\%$ . Devices based on the other

acceptors exhibit significantly lower efficiencies, presumably in part due to reduced driving forces for charge-transfer to PCBM; however, they might act as active components in tandem cells due to their broad absorbance in the near-IR, especially in conjunction with more electron-accepting electron-transport materials than PCBM. In summary, the present study demonstrated that optical and electronic properties of this series of D-A copolymers can be easily manipulated through the acceptor strength, and also resulted in their potential uses in various applications, such as electrochromic devices, OFETs and OPVs.

#### 4.10 Experimental Section

##### Materials.

Unless stated otherwise, starting materials were purchased and were used without further purification. The synthesis of 2,6-bis(tri-*n*-butylstannyl)-*N*-(3,4,5-tris(*n*-dodecyloxy)phenyl)-dithieno[3,2-*b*:2',3'-*d*]pyrrole was described in experimental section of Chapter 2. 4,7-Bis(5-bromothiophen-2-yl)-[2,1,3]-benzothiadiazole, 4,7-dibromo-[2,1,3]-benzothiadiazole, 4,7-bis(5-bromothiophen-2-yl)-2 $\lambda^4$  $\delta^2$ -benzo[1,2-*c*;4,5-*c'*]bis[1,2,5]thiadiazole, and 4,7-dibromo-2 $\lambda^4$  $\delta^2$ -benzo[1,2-*c*;4,5-*c'*]bis[1,2,5]thiadiazole were prepared according to the published procedures<sup>16</sup> and provided by Timothy Steckler in UF. 6,7-di(*n*-hexyl)-4,9-di(thien-2yl)-[1,2,5]thiadiazolo[3,4-*g*]quinoxaline was prepared according to literature procedure<sup>17</sup> and provided by Timothy Steckler in UF or Raghunath Dasari in the Marder group. *N*-(2-Decyltetradecyl)-dithieno[3,2-*b*:2',3'-*d*]pyrrole, 2,6-bis(tri-*n*-butylstannyl)-*N*-(2-decyltetradecyl)-dithieno[3,2-*b*:2',3'-*d*]pyrrole,

and **P6** were synthesized using the same methods as the analogous *N*-(3,4,5-tris(*n*-dodecyloxy)phenyl) compounds<sup>18</sup> by Raghunath Dasari in the Marder group.

### Characterization.

The <sup>1</sup>H and <sup>13</sup>C NMR spectra were measured on a Varian Mercury 300 MHz spectrometer. Mass spectra were measured on an Applied Biosystems 4700 Proteomics Analyzer using MALDI mode. Elemental analyses were carried out by Atlantic Microlabs using a LECO 932 CHNS elemental analyzer. UV-vis-NIR absorption spectra were recorded on a Varian Cary 500 UV-Vis-NIR spectrophotometer. Electrochemistry and spectroelectrochemistry were conducted by Timothy Steckler in UF. It was performed in a three-electrode cell consisting of an ITO-coated glass or platinum button working electrode, a platinum wire/flag counter electrode, and a Ag/Ag<sup>+</sup> reference electrode or a silver wire pseudo-reference electrode in a 0.1 M [<sup>n</sup>Bu<sub>4</sub>N]<sup>+</sup>[ClO<sub>4</sub>]<sup>-</sup>/propylene carbonate or 0.1 M [<sup>n</sup>Bu<sub>4</sub>N]<sup>+</sup>[PF<sub>6</sub>]<sup>-</sup>/acetonitrile solution calibrated to the ferrocene-ferrocenium redox couple, assuming the values of [FeCp<sub>2</sub>]<sup>+0</sup> = 0.34 V (for 0.1 M [<sup>n</sup>Bu<sub>4</sub>N]<sup>+</sup>[ClO<sub>4</sub>]<sup>-</sup>/propylene carbonate solution) or 0.40 V (0.1 M [<sup>n</sup>Bu<sub>4</sub>N]<sup>+</sup>[PF<sub>6</sub>]<sup>-</sup>/acetonitrile solution).<sup>32</sup> Polymer films were spray cast onto ITO-coated glass working electrodes or drop cast onto platinum button (0.02 cm<sup>2</sup>) working electrodes from a chloroform solution. Electrochemical measurements were made with an EG&G PAR model 273A potentiostat/galvanostat or BAS 100B electrochemical analyzer, and optical data was measured with a Cary 500 UV-VIS-NIR spectrophotometer or a StellarNet Diode Array UV-VIS-NIR. Thermal gravimetric analysis (TGA) measurements were performed on NETZSCH thermogravimetric analyzer (model STA 449C) under a

nitrogen flow at a heating rate of 10 °C/min. Gel permeation chromatography (GPC) was performed using a Waters Associates GPCV2000 liquid chromatography system with its internal differential refractive index detector (DRI) at 40 °C, using two Waters Styragel HR-5E columns (10 µm PD, 7.8 mm i.d., 300 mm length) with HPLC grade THF as the mobile phase at a flow rate of 1.0 mL / min. Injections were made at 0.05 - 0.07% w/v sample concentration using a 220.5 µL injection volume. Retention times were calibrated against a minimum of nine narrow molecular weight polystyrene standards (Polymer Laboratories; Amherst, MA). AFM images were taken on a Digital Instruments NanoScope™ Scanning Probe Microscope and obtained from Séverine Coppée in the Kippelen group at the Georgia Institute of Technology.

**4,9-Bis(5-bromothiophen-2-yl)-6,7-di-*n*-hexyl-[1,2,5]thiadiazolo[3,4-*g*]quinoxaline.**

6,7-Di-*n*-hexyl-4,9-di(thiophen-2yl)-[1,2,5]thiadiazolo[3,4-*g*]quinoxaline<sup>17</sup> (1.1 g, 2.1 mmol) was dissolved in 170 mL DMF and *N*-bromosuccinimide (0.78 g, 4.4 mmol) were added in the absence of light. The solution was stirred for 10 h, then methanol was added and the precipitate was filtered off, washed with cold methanol and dried to obtain of a blue solid (1.1 g, 76 %). <sup>1</sup>H NMR (300 MHz, C<sub>2</sub>D<sub>2</sub>Cl<sub>4</sub>): δ 8.73 (d, *J* = 3.8 Hz, 2H), 7.14 (d, *J* = 3.8 Hz, 2H), 2.92 (t, *J* = 7.4 Hz, 4H), 1.94 (t, *J* = 7.0 Hz, 4H), 1.59-1.35 (m, 12H), 0.94 (t, *J* = 7.0 Hz, 6H). <sup>13</sup>C{<sup>1</sup>H} NMR (300 MHz, C<sub>2</sub>D<sub>2</sub>Cl<sub>4</sub>): δ 159.3, 152.4, 139.1, 136.1, 134.6, 131.1, 121.9, 121.5, 37.0, 33.3, 30.8, 29.6, 24.1, 15.7. HRMS (ESI TOF) *m/z* calcd. for C<sub>28</sub>H<sub>30</sub>Br<sub>2</sub>N<sub>4</sub>S<sub>3</sub> (M<sup>+</sup>): 676.0049, found 675.9999; Anal. calcd. for C<sub>28</sub>H<sub>30</sub>Br<sub>2</sub>N<sub>4</sub>S<sub>3</sub>: C 49.56, H 4.46, N 8.26 found C 49.64, H 4.44, N 8.23.

***N*-(2-Decyltetradecyl)-dithieno[3,2-*b*:2',3'-*d*]pyrrole.** A solution of 3,3'-dibromo-2,2'-bithiophene (2.0 g, 6.0 mmol), NaO<sup>t</sup>Bu (1.4 g, 15 mmol), Pd<sub>2</sub>(dba)<sub>3</sub> (0.24 mmol) and 2,2'-bis(diphenylphosphino)-1,1'-binaphthyl (BINAP, 0.60 g, 0.96 mmol) in dry toluene (25 mL) was purged with argon for 20 min. Then was added 2-decyltetradecan-1-amine (2.3 g, 6.5 mmol) *via* syringe, and the mixture was stirred at 110 °C under an argon atmosphere for 12 h. Reaction mixture poured into water and extracted twice with ethyl acetate solvent. The combined organic layers were dried over Na<sub>2</sub>SO<sub>4</sub> and the solvent was removed under reduced pressure. Crude product was purified through column chromatography (silica gel, 95:5 v/v hexanes/ethyl acetate) to afford a colorless liquid (1.2 g, 62%). <sup>1</sup>H NMR (CDCl<sub>3</sub>, 300MHz): δ 7.14 (d, *J* = 2.5 Hz, 2H), 6.95 (d, *J* = 2.4Hz, 2H), 4.03 (d, *J* = 4.2 Hz, 2H), 1.97 (s ,br, 1H), 1.56 (s, 2H), 1.38-1.05 (m, 38H), 0.92-0.80 (m, 6H). <sup>13</sup>C NMR (CDCl<sub>3</sub>, 75 MHz): δ 145. 2, 122.5, 114.3, 111.0, 51.6, 39.0, 31.9, 31.5, 29.8, 29.7, 29.6, 29.5, 29.4, 29.3, 26.4, 22.7, 14.1. MS (FAB) *m/z*: 515 (MH<sup>+</sup>). Anal Calcd. For C<sub>32</sub>H<sub>53</sub>NS<sub>2</sub>: C, 75.50; H, 10.35; N, 2.72, Found C, 74.40; H, 10.55; N, 2.78.

**2,6-Bis(tri-*n*-butylstannyl)-*N*-(2-decyltetradecyl)-dithieno[3,2-*b*:2',3'-*d*]pyrrole.** At -78 °C, under an argon atmosphere <sup>t</sup>BuLi (3.6 mL, 5.4 mmol, 1.5 M in pentane) was added *via* syringe to the solution of 4-(2-decyltetradecyl)-4*H*-dithieno[3,2-*b*:2',3'-*d*]pyrrole (1.1 g, 2.2 mmol) in dry tetrahydrofuron (30 mL). The reaction mixture was stirred for 1 h at room temperature, cooled reaction mixture to -78 °C and a solution of <sup>n</sup>Bu<sub>3</sub>SnCl (1.9 mL, 6.0 mmol) in dry THF (10 mL) was added dropwise *via* syringe. After stirring for another 3 h at room temperature, water was added and the layers were separated. The water phase extracted twice with ethyl acetate. The combined organic

layers were dried over Na<sub>2</sub>SO<sub>4</sub>, and the solvents were removed under reduced pressure. The crude compound was purified through silica gel column chromatography (pretreated with triethylamine, eluting with hexanes). Upon removal of solvent under reduced pressure, a pale yellow oil (2.1 g, 89%) was obtained. <sup>1</sup>H NMR (CDCl<sub>3</sub>, 300 MHz):  $\delta$  6.92 (s, 2H), 4.03 (d, *J* = 6 Hz, 2H), 1.97 (s, br, 1H), 1.65-1.50 (m, 12H), 1.40-1.20 (m, 46H), 1.19-1.10 (m, 10H), 0.92-0.80 (m, 24H). <sup>13</sup>C NMR (CDCl<sub>3</sub>, 75 MHz):  $\delta$  148.3, 134.2, 120.4, 118.2, 51.8, 39.3, 31.9, 31.6, 29.9, 29.7, 29.6, 29.4, 29.0, 27.2, 26.5, 22.7, 14.1, 13.7, 10.9. MS (MALDI) *m/z*: 1094 (MH<sup>+</sup>). Anal Calcd. For C<sub>56</sub>H<sub>105</sub>NS<sub>2</sub>Sn<sub>2</sub>: C, 61.48; H, 9.67; N, 1.28, Found C, 61.69; H, 9.94; N, 1.34.

**P1.** To a 100 mL 3-neck round bottom flask were added 4,7-bis(5-bromothiophen-2-yl)-[2,1,3]-benzothiadiazole (0.35 g, 0.76 mmol), 2,6-bis(tri-*n*-butylstannyl)-*N*-(3,4,5-tris(*n*-dodecyloxy)phenyl)-dithieno[3,2-*b*:2',3'-*d*]pyrrole (1.11 g, 0.80 mmol) and dry THF (100 mL), vacuum pump filled for 5-6 times, and deoxygenated with argon for 30 min. PdCl<sub>2</sub>(PPh<sub>3</sub>)<sub>2</sub> (0.027 g, 0.04 mmol) was added, and the solution was stirred at 60-70 °C for 2 days. The solution was dropped into methanol (*ca.* 500 mL), and the solid was filtered. The crude product was purified by Soxhlet washings with methanol, acetone and hexanes each for 1 day, and extraction with chloroform for 1 day. The chloroform fraction was concentrated, precipitated from methanol again, and a black solid (0.80 g, 95%) was obtained. <sup>1</sup>H NMR (300 MHz, THF-*d*<sub>8</sub>, 60 °C, ppm):  $\delta$  8.20-7.80 (br, 4H), 7.51-7.02 (br, 4H), 6.83 (br, 2H), 4.11 (br, 6H), 1.94-1.21 (br, 60 H), 0.91 (br, 9H). Anal. Calcd for (C<sub>64</sub>H<sub>85</sub>N<sub>3</sub>O<sub>3</sub>S<sub>5</sub>)<sub>n</sub>: C, 69.58; H, 7.76; N, 3.80. Found: C, 69.72; H, 7.77; N, 3.69.

**P2.** To a 100 mL 3-neck round bottom flask were added 2,6-bis(tri-*n*-butylstannyl)-*N*-(3,4,5-tris(*n*-dodecyloxy)phenyl)-dithieno[3,2-*b*:2',3'-*d*]pyrrole (0.56 g, 0.40 mmol), PdCl<sub>2</sub>(PPh<sub>3</sub>)<sub>2</sub> (0.014 g, 0.02 mmol) and dry THF (50 mL), vacuum pump filled for 5 times, and deoxygenated with argon for 60 min. 4,9-Bis(5-bromothiophen-2-yl)-6,7-dihexyl-[1,2,5]thiadiazolo[3,4-*g*]quinoxaline (0.23 g, 0.39 mmol) was added, and the solution was stirred at 60-70 °C for 2 days. The solution was dropped into methanol (*ca.* 700 mL), and the solid was filtered. The crude product was purified by Soxhlet washings with methanol, acetone and hexanes each for 1 day, and extraction with chloroform for 1 day. The chloroform fraction was concentrated, precipitated from methanol again, and a black solid (0.23 g, 46%) was obtained. <sup>1</sup>H NMR (300 MHz, 1,1,2,2-tetrachloroethane-*d*<sub>2</sub>, 60 °C):  $\delta$  9.02 (br, 2H), 7.60-6.78 (br, 6H), 4.12 (br, 6H), 3.21 (br, 4H), 1.94–1.21 (br, 76 H), 0.91 (br, 15H). Anal. Calcd for (C<sub>78</sub>H<sub>109</sub>N<sub>5</sub>O<sub>3</sub>S<sub>5</sub>)<sub>n</sub>: C, 70.70; H, 8.29; N, 5.29. Found: C, 70.63; H, 8.30; N, 4.90.

**P3.** To a 100 mL 3-neck round-bottomed flask were added 2,6-bis(tri-*n*-butylstannyl)-*N*-(3,4,5-tris(*n*-dodecyloxy)phenyl)-dithieno[3,2-*b*:2',3'-*d*]pyrrole (0.66 g, 0.48 mmol), PdCl<sub>2</sub>(PPh<sub>3</sub>)<sub>2</sub> (0.016 g, 0.02 mmol) and dry THF (50 mL), vacuum pump-filled for 5 times, and deoxygenated with argon for 60 min. 4,7-bis(5-bromothiophen-2-yl)-2 $\lambda^4$  $\delta^2$ -benzo[1,2-*c*;4,5-*c'*]bis[1,2,5]thiadiazole (0.23 g, 0.45 mmol) was added, and the solution was stirred at 60-65 °C for 2 days. The solution was dropped into methanol (*ca.* 600 mL), and the solid was filtered. The crude product was purified by Soxhlet washings with methanol, acetone and hexanes each for 1 day, and extraction with chloroform for 1 day. After the second precipitation of the chloroform extracts into methanol, a black solid

(0.47 g, 88%) was obtained.  $^1\text{H}$  NMR (300 MHz,  $\text{THF-}d_8$ , 60 °C):  $\delta$  9.02 (br, 2H), 7.55-5.78 (br, 6H), 4.15 (br, 6H), 1.94–1.21 (br, 60 H), 0.91 (br, 9H). Anal. Calcd for  $(\text{C}_{64}\text{H}_{83}\text{N}_5\text{O}_3\text{S}_6)_n$ : C, 66.11; H, 7.19; N, 6.02; Found: C, 65.23; H, 7.30; N, 5.60.

**P4.** To a 100 mL 3-neck round bottom flask were added 2,6-bis(tributylstannyl)-*N*-(3,4,5-tris(dodecyloxy)phenyl)-dithieno[3,2-*b*:2',3'-*d*]pyrrole (0.32 g, 0.23 mmol),  $\text{PdCl}_2(\text{PPh}_3)_2$  (0.008 g, 0.01 mmol) and dry THF (30 mL). The flask was then pump-filled for 5 times, and deoxygenated with argon for 60 min. 4,7-Dibromo-[2,1,3]-benzothiadiazole (0.06 g, 0.22 mmol) was added, and the solution was stirred at 60-70 °C for 2 days. The solution was dropped into methanol (*ca.* 500 mL), and the solid was filtered. The crude product was purified by Soxhlet washings with methanol, acetone and hexanes each for 1 day, and extraction with chloroform for 1 day. After the second precipitation of the chloroform extracts into methanol, a black solid (0.20 g, 95%) was obtained.  $^1\text{H}$  NMR (300 MHz, 1,1,2,2-tetrachloroethane- $d_2$ , 40 °C):  $\delta$  8.40 (br, 2H), 7.78 (br, 2H), 7.22-6.78 (br, 2H), 4.01 (br, 6H), 2.10–1.10 (br, 60H), 0.90 (br, 9H). Anal. Calcd for  $(\text{C}_{56}\text{H}_{81}\text{N}_3\text{O}_3\text{S}_3)_n$ : (Calculated) C, 71.52; H, 8.68; N, 4.47; Found C, 70.82; H, 8.62; N, 4.12.

**P5.** To a 100 mL 3-neck round bottom flask were added 2,6-bis(tri-*n*-butylstannyl)-*N*-(3,4,5-tris(dodecyloxy)phenyl)-dithieno[3,2-*b*:2',3'-*d*]pyrrole (0.57 g, 0.40 mmol),  $\text{PdCl}_2(\text{PPh}_3)_2$  (0.014 g, 0.02 mmol) and dry THF (50 mL). The flask was pump filled 5 times, and further deoxygenated with argon for 60 min. 4,9-Dibromo-6,7-dihexyl-[1,2,5]thiadiazolo[3,4-*g*]quinoxaline (0.20 g, 0.39 mmol) was added, and the solution was

stirred at 60-70 °C for 2 days. The solution was dropped into methanol (*ca.* 600 mL), and the solid was filtered. The crude product was purified by Soxhlet washings with methanol, acetone and hexanes each for 1 day, and extraction with THF and chloroform each for 1 day. After the second precipitation of the chloroform extracts into methanol, a black solid (0.38 g, 83%) was obtained. <sup>1</sup>H NMR (300 MHz, 1,1,2,2-tetrachloroethane-*d*<sub>2</sub>, 60 °C):  $\delta$  9.40 (br, 2H), 7.09-6.90 (br, 2H), 4.21 (br, 6H), 3.18 (br, 4H), 1.91–1.29 (br, 76H), 0.92 (br, 15H). Anal. Calcd for (C<sub>70</sub>H<sub>105</sub>N<sub>5</sub>O<sub>3</sub>S<sub>3</sub>)<sub>n</sub>: C 72.43, H 9.12, N 6.03; found C 71.93, H 9.07, N 5.42.

**P6.** To a 100 mL 3-neck round bottom flask were added 4,7-dibromo-[2,1,3]-benzothiadiazole (0.24 g, 0.80 mmol), 2,6-bis(tri-*n*-butylstannyl)-*N*-(2-decyltetradecyl)-dithieno[3,2-*b*:2',3'-*d*]pyrrole (0.88 g, 0.80 mmol) and dry THF (15 mL). The flask was then pump-filled, and deoxygenated with argon for 30 min. Pd(PPh<sub>3</sub>)<sub>2</sub>Cl<sub>2</sub> (0.029 g, 0.05 mmol) was added, and the solution was stirred at 60-70 °C for 2 days. 1-Bromobenzene (0.16 mL, 1.60 mmol) was added and the reaction continued for another 12 h, then phenylboronic acid (0.19 g, 1.60 mmol) was added and the reaction continued for another 12 h. The solution was dropped in methanol (*ca.* 300 mL), and the solid was filtered. The crude product was purified by Soxhlet washings successively with methanol, acetone and chloroform. After the second precipitation of the chloroform extracts into methanol, a dark reddish black solid (0.67 g, 62%) was obtained. <sup>1</sup>H NMR (300 MHz, 1,1,2,2-tetrachloroethane-*d*<sub>2</sub>, 80 °C, ppm):  $\delta$  9.02 (br, 2H), 8.10-7.35 (br, 2H), 4.05 (br, 2H), 2.13 (br, 4H), 1.94–1.10 (br, 40 H), 0.89 (br, 6H). Anal Calcd. For (C<sub>76</sub>H<sub>106</sub>N<sub>6</sub>S<sub>6</sub>)<sub>n</sub>: C, 70.43; H, 8.24; N, 6.48, Found C, 69.83; H, 8.27; N, 5.96.

### **Fabrication and Characterization of Thin Film Transistors.**

OFETs were fabricated and tested by Shree Prakash Tiwari in the Kippelen group at the Georgia Institute of Technology. OFETs were fabricated on heavily n-doped silicon substrates (also serving as the gate electrodes) with 200 nm-thick thermally grown SiO<sub>2</sub> as the gate dielectric in top contact configuration. Ti/Au (10 nm/100 nm) metallization on the backside of the substrate was done to enhance the gate electrical contact. OTS treatment (with 5mM in toluene) was done by soaking the substrates in the OTS solution for overnight (15 hours) in a N<sub>2</sub>-filled dry box. The substrates were rinsed with toluene and annealed at 60 °C for 5 minutes. The capacitance of the OTS treated SiO<sub>2</sub> was about 16.2 nF/cm<sup>2</sup>. A thin layer of organic semiconductor was formed on the substrates by spin coating with a solution (10-20 mg/mL) in chlorobenzene. To remove the solvent from the film, a pre-annealing is done at 90 °C for 30 minutes. 50 nm-thick Au was deposited through a shadow mask to act as top source/drain electrode. The prepared devices were post-annealed at 130 °C for 35 minutes (followed by 150 °C for 30 minutes for **P3**) inside another N<sub>2</sub> glove box with I-V characterization setup.

### **Fabrication and Characterization of Photovoltaic Cells.**

Photovoltaic cell were fabricated and tested by William J. Potscavage Jr. in the Kippelen group at the Georgia Institute of Technology. Photovoltaic cells were fabricated by blending one of the three copolymers with the acceptor PCBM (MTR Ltd., PCBM). Solutions of a polymer and PCBM were made in chlorobenzene (1:1 weight ratio, 20 mg/mL) for each of the polymers. ITO-coated glass (Colorado Concept Coatings LLC) with a sheet resistance of ~15 Ω/sq. was used as the substrates for the solar cells. The

substrates were cleaned in an ultrasonic bath of detergent water, rinsed with deionized water, and then cleaned in sequential ultrasonic baths of deionized water, acetone, and isopropanol. Nitrogen was used to dry the substrates after each of the last three baths. A 300-nm-thick layer of  $\text{SiO}_x$  was deposited on the cleaned ITO by e-beam deposition (AXXIS, Kurt J. Lesker) to pattern the anode. Next, the substrates were ultrasonicated in isopropanol for 10 min, blown dry with nitrogen, and air-plasma treated for 2 min. A hole-conducting layer of PEDOT:PSS (CLEVIOS P VP AI 4083, H. C. Starck) was filtered through a 0.45- $\mu\text{m}$ -pore PVDF filter and spin coated on the substrates at 5,000 rpm for 1 min, and the substrates were annealed at 140 °C for 10 min in atmosphere. After loading into a nitrogen-filled glove box, 80-90-nm-thick films of the polymer mixtures were deposited on the substrates by spin coating for 1 min at speeds of 1000 rpm for the **P3**/PBCM mixture and 1500 rpm for the **P1**(or **P2**)/PCBM mixtures. The polymers were filtered through 0.2- $\mu\text{m}$ -pore PTFE filters prior to spin coating (samples containing **P2** easily clogged the filter, so no filter was used). The substrates were then loaded into a vacuum thermal evaporation system (SPECTROS, Kurt J. Lesker) connected to the glove box, and 200 nm of Al was deposited through a shadow mask at a rate of 1 – 3 Å/s and a base pressure of  $\sim 7 \times 10^{-8}$  Torr to define the cathodes. The completed devices were transferred in a sealed container to another nitrogen-filled glove box for electrical measurements. Current-voltage characteristics were measured using a source meter (2400, Keithley) controlled by a LabVIEW program. When testing the solar cells under illumination, filtered light from a 175 W Xenon lamp (ASB-XE-175EX, CVI) was used as a broadband light source with an irradiance of  $\sim 73\text{-}76 \text{ mW/cm}^2$  to simulate

sunlight. A monochromator and calibrated photodiode were used to measure external quantum efficiency (EQE).

#### 4.11 References

- (1) Facchetti, A. *Materials Today* **2007**, *10*, 28.
- (2) Salleo, A. *Materials Today* **2007**, *10*, 38.
- (3) Zhou, E. J.; Tan, Z.; Yang, Y.; Huo, L. J.; Zou, Y. P.; Yang, C. H.; Li, Y. F. *Macromolecules* **2007**, *40*, 1831.
- (4) Ong, B. S.; Wu, Y. L.; Li, Y. N.; Liu, P.; Pan, H. L. *Chem. Eur. J.* **2008**, *14*, 4766.
- (5) Blouin, N.; Michaud, A.; Gendron, D.; Wakim, S.; Blair, E.; Neagu-Plesu, R.; Belletete, M.; Durocher, G.; Tao, Y.; Leclerc, M. *J. Am. Chem. Soc.* **2008**, *130*, 732.
- (6) Zaumseil, J.; Donley, C. L.; Kim, J. S.; Friend, R. H.; Sirringhaus, H. *Adv. Mater.* **2006**, *18*, 2708.
- (7) Gadisa, A.; Mammo, W.; Andersson, L. M.; Admassie, S.; Zhang, F.; Andersson, M. R.; Inganas, O. *Adv. Funct. Mater.* **2007**, *17*, 3836.
- (8) Osaka, I.; Sauve, G.; Zhang, R.; Kowalewski, T.; McCullough, R. D. *Adv. Mater.* **2007**, *19*, 4160.
- (9) Tan, Z. A.; Zhou, E. J.; Zhan, X. W.; Wang, X.; Li, Y. F.; Barlow, S.; Marder, S. R. *Appl. Phys. Lett.* **2008**, *93*, 073309.
- (10) Bundgaard, E.; Krebs, F. C. *Sol. Energy Mater. Sol. Cells* **2007**, *91*, 1019.
- (11) Hou, Q.; Zhou, Q. M.; Zhang, Y.; Yang, W.; Yang, R. Q.; Cao, Y. *Macromolecules* **2004**, *37*, 6299.
- (12) Wang, E. G.; Wang, L.; Lan, L. F.; Luo, C.; Zhuang, W. L.; Peng, J. B.; Cao, Y. *Appl. Phys. Lett.* **2008**, *92*, 033307.
- (13) Cheng, K.-F.; Chueh, C.-C.; Lin, C.-H.; Chen, W.-C. *J. Polym. Sci. B* **2008**, *46*, 6305.
- (14) Chen, M. X.; Crispin, X.; Perzon, E.; Andersson, M. R.; Pullerits, T.; Andersson, M.; Inganas, O.; Berggren, M. *Appl. Phys. Lett.* **2005**, *87*, 252105.
- (15) Hou, J.; Zhang, S.; Chen, T. L.; Yang, Y. *Chem. Commun.* **2008**, 6034.
- (16) Bundgaard, E.; Krebs, F. C. *Macromolecules* **2006**, *39*, 2823.
- (17) Kitamura, C.; Tanaka, S.; Yamashita, Y. *Chem. Mater.* **1996**, *8*, 570.
- (18) Steckler, T. T.; Zhang, X.; Hwang, J.; Honeyager, R.; Ohira, S.; Zhang, X.-H.; Grant, A.; Ellinger, S.; Odom, S. A.; Sweat, D.; Tanner, D. B.; Rinzler, A. G.; Barlow, S.; Brédas, J. L.; Kippelen, B.; Marder, S. R.; Reynolds, J. R. *J. Am. Chem. Soc.* **2009**, *131*, 2824.
- (19) Yamamoto, T.; Yasuda, T.; Sakai, Y.; Aramaki, S.; Ramaw, A. *Macromol. Rapid Commun.* **2005**, *26*, 1214.
- (20) Liu, J. Y.; Zhang, R.; Sauve, G.; Kowalewski, T.; McCullough, R. D. *J. Am. Chem. Soc.* **2008**, *130*, 13167.
- (21) Zhan, X. W.; Tan, Z. A.; Domercq, B.; An, Z. S.; Zhang, X.; Barlow, S.; Li, Y. F.; Zhu, D. B.; Kippelen, B.; Marder, S. R. *J. Am. Chem. Soc.* **2007**, *129*, 7246.

- (22) Zhan, X.; Tan, Z. A.; Zhou, E.; Li, Y.; Misra, R.; Grant, A.; Domercq, B.; Zhang, X.-H.; An, Z.; Zhang, X.; Barlow, S.; Kippelen, B.; Marder, S. R. *J. Mater. Chem.* **2009**, *19*, 5794.
- (23) L. U. Lehmann, *U. S. Pat. Appl. Publ.*, 2008, 2008262183.
- (24) Radke, K. R.; Ogawa, K.; Rasmussen, S. C. *Org. Lett.* **2005**, *7*, 5253.
- (25) Odom, S. A.; Lancaster, K.; Beverina, L.; Lefler, K. M.; Thompson, N. J.; Coropceanu, V.; Brédas, J. L.; Marder, S. R.; Barlow, S. *Chem. Eur. J.* **2007**, *13*, 9637.
- (26) Mühlbacher, D.; Scharber, M.; Morana, M.; Zhu, Z.; Waller, D.; Gaudiana, R.; Brabec, C. *Adv. Mater.* **2006**, *18*, 2884.
- (27) Peet, J.; Kim, J. Y.; Coates, N. E.; Ma, W. L.; Moses, D.; Heeger, A. J.; Bazan, G. C. *Nature Mater.* **2007**, *6*, 497.
- (28) Zhou, E. J.; Nakamura, M.; Nishizawa, T.; Zhang, Y.; Wei, Q. S.; Tajima, K.; Yang, C. H.; Hashimoto, K. *Macromolecules* **2008**, *41*, 8302.
- (29) Yue, W. Z., Y.; Shao, S.; Tian, H.; Xie, Z.; Geng, Y.; Wang, F. *J. Mater. Chem.* **2009**, *19*, 2199.
- (30) Karsten, B. P.; Viani, L.; Gierschner, J.; Cornil, J.; Janssen, R. A. J. *J. Phys. Chem. A* **2008**, *112*, 10764.
- (31) Blouin, N.; Leclerc, M. *Acc. Chem. Res.* **2008**, *41*, 1110.
- (32) Connelly, N. G.; Geiger, W. E. *Chem. Rev.* **1996**, *96*, 877.
- (33) Micaroni, L.; Nart, F. C.; Huemmelgen, I. A. *J. Solid State Electrochem.* **2002**, *7*, 55.
- (34) We have previously reported slightly different estimated IP and EA values for **P3**, the differences being due to different assumptions being used in the estimates. Of course, the trends in the electrochemically estimated IP and EA values for the series of polymers will be the same regardless of the method used to estimate these values.
- (35) Brookins, R. N.; Berda, E.; Reynolds, J. R. *J. Mater. Chem.* **2009**, *19*, 4197.
- (36) Thompson, B. C.; Kim, Y. G.; McCarley, T. D.; Reynolds, J. R. *J. Am. Chem. Soc.* **2006**, *128*, 12714.
- (37) Beaujuge, P. M.; Ellinger, S.; Reynolds, J. R. *Nat. Mater.* **2008**, *7*, 795.
- (38) Akaike, K.; Kanai, K.; Yoshida, H.; Tsutsumi, J.; Nishi, T.; Sato, N.; Ouchi, Y.; Seki, K. *J. Appl. Phys.* **2008**, *104*, 023710.
- (39) Ohkita, H.; Cook, S.; Astuti, Y.; Duffy, W.; Tierney, S.; Zhang, W.; Heeney, M.; McCulloch, I.; Nelson, J.; Bradley, D. D. C.; Durrant, J. R. *J. Am. Chem. Soc.* **2008**, *130*, 3030.
- (40) Hoppe, H.; Niggemann, M.; Winder, C.; Kraut, J.; Hiesgen, R.; Hinsch, A.; Meissner, D.; Sariciftci, N. S. *Adv. Funct. Mater.* **2004**, *14*, 1005.

## CHAPTER 5

### DITHIENOPYRROLE- QUINOXALINE/PYRIDOPYRAZINE

### DONOR-ACCEPTOR COPOLYMERS

#### 5.1 Introduction

As discussed in Chapter 1 and 4, “the donor-acceptor approach” can be an effective route obtaining low bandgap copolymers for OFET and OPV applications. Quinoxaline (Qx) and pyrido[3,4-*b*]pyrazine (PPz) are two of the acceptors that have previously been incorporated into D-A copolymers due to their high electron affinities and ease of structural modifications;<sup>1-10</sup> some of them have previously been used in OPV applications. For example, carbazole-quinoxaline/pyridopyrazine copolymers (polymer **54a** and **54b** in Figure 1.17) have been used in OPVs, and power efficiencies of 1.8% and 1.1% were achieved in conjunction with PCBM.<sup>7</sup> Very recently, a fluorene-quinoxaline copolymer (**I** in Figure 5.1), was blended with the C<sub>70</sub> analogue of PCBM yielding a high power conversion efficiency of 5.5%.<sup>3</sup> Quinoxaline/pyridopyrazine acceptors have also been used to construct conjugated polymers for OFETs. In 2005, a thiophene-quinoxaline copolymer (**II** in Figure 5.1), was reported to have a hole mobility of  $3.6 \times 10^{-3} \text{ cm}^2/(\text{Vs})$  by Jenekhe *et al.*<sup>9</sup> A series of pyridopyrazine-based copolymers (**III** in Figure 5.1) have been synthesized and used in field-effect transistors by the same group; hole mobilities of  $4.1 \times 10^{-4}$  -  $4.4 \times 10^{-3} \text{ cm}^2/(\text{Vs})$  were observed in the devices.<sup>8</sup> However, many of the

quinoxaline or pyridopyrazine-containing copolymers reported to date have poor solubility in common organic solvents; for instance, the copolymer of diheptyl-pyridopyrazine with thiophene was only soluble in acidic solvents (formic acid and trifluoroacetic acid).<sup>10</sup>

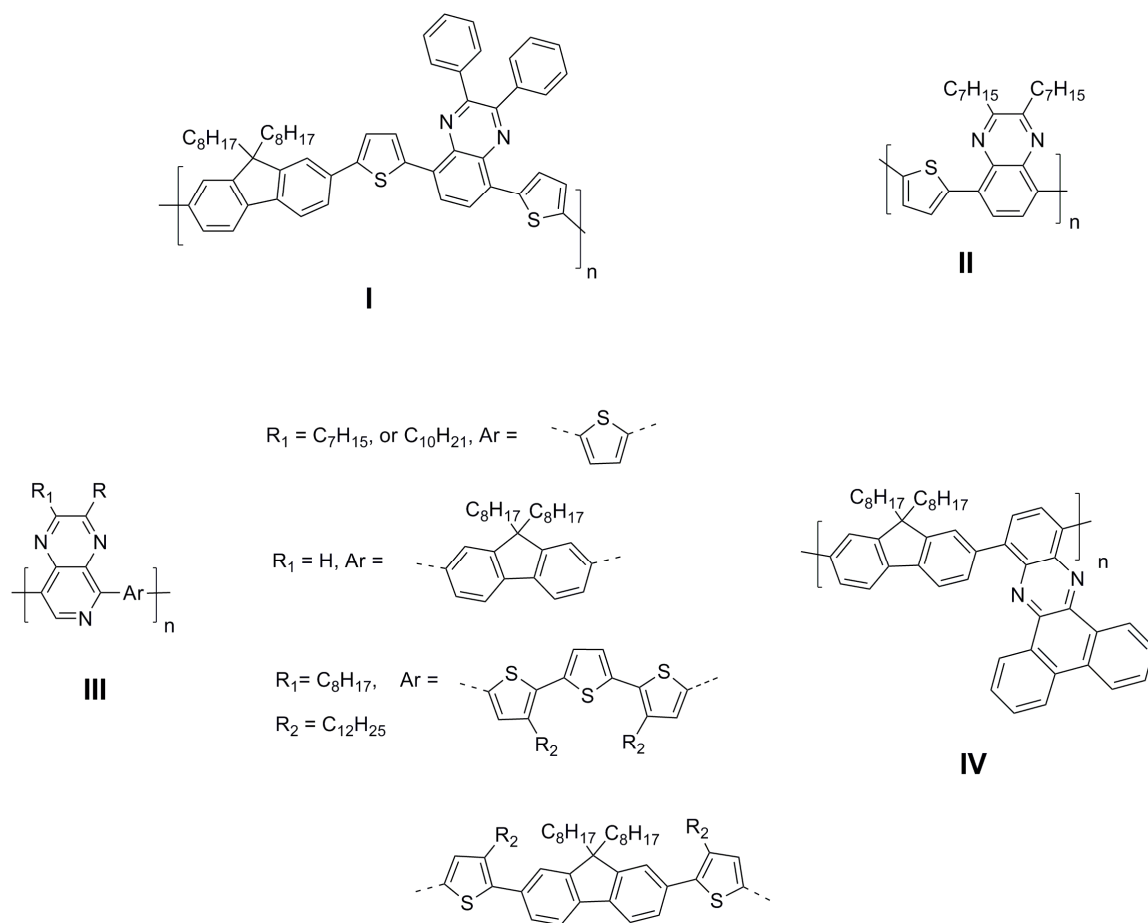


**Figure 5.1** Structures of some polymers discussed in the text.

Dibenzo[*a,c*]phenazine and dibenzo[*f,h*]pyrido[4,3-*b*]quinoxaline can be considered to

be extended quinoxaline and pyridopyrazine, respectively. Small molecules based on those moieties have been found to exhibit liquid crystalline behavior, and were found easily be  $\pi$ - $\pi$  stacked in the solution.<sup>11,12</sup> Only one example (polymer **IV** in Figure 5.1) of a conjugated polymer in which dibenzophenazine linked through 10- and 13-positions has been reported. The polymer was used for OPV fabrication in conjunction with PCBM; however, only a very low power conversion efficiency (0.005%) was obtained with this polymer, possibly in part due to the poor coverage of the solar spectrum (absorption maximum at *ca.* 450 nm).<sup>13</sup> There is no literature report of dibenzopyridoquinoxaline-containing conjugated polymers to the best of our knowledge.

This chapter describes the synthesis and characterization of soluble copolymers based on an *N*-aryl DTP donor, and quinoxaline or pyridopyrazine acceptors. In view of the poor solubilities previously found for the polymers containing dialkyl quinoxaline and pyridopyrazine, the aryl group on the DTP moiety is functionalized with three long-chain alkoxyl groups. Dibenzo[*a,c*]phenazine and dibenzo[*f,h*]pyrido[4,3-*b*]quinoxaline have also been incorporated in the copolymers in order to study the effects of the extended conjugation on the acceptor moieties. The optical and electronic properties of the copolymers are compared. In addition, fabrication of OFETs and OPVs from the polymers is described, along with more detailed study of selected OPV devices based on one of the copolymers blended with PCBM.

## 5.2 Synthesis

The structures of the target polymers in this chapter are shown in Figure 5.2. Details of the monomer and polymer synthesis, especially optimizations of the conditions for some of the polymerizations, will be discussed in the following sub-sections.

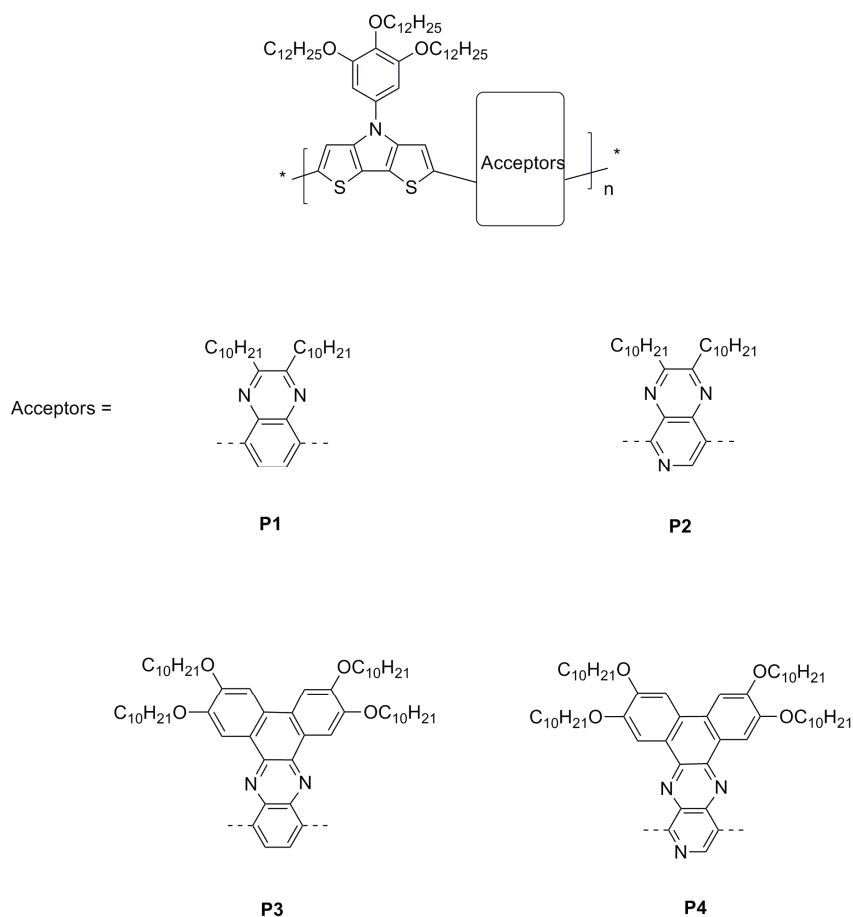
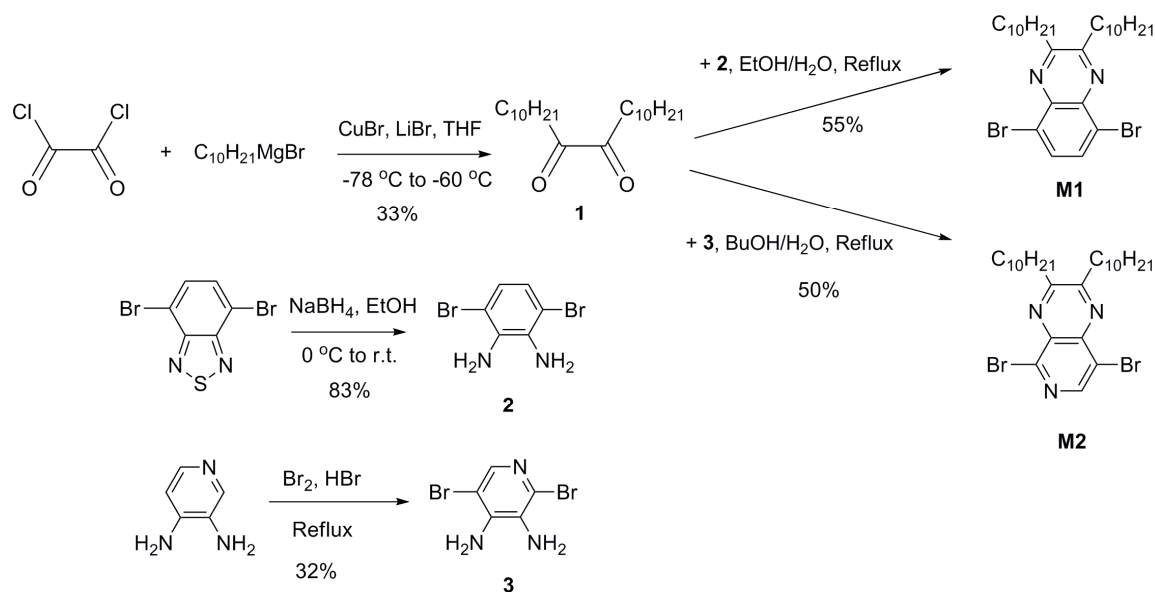


**Figure 5.2** Structures of the target polymers in Chapter 5.

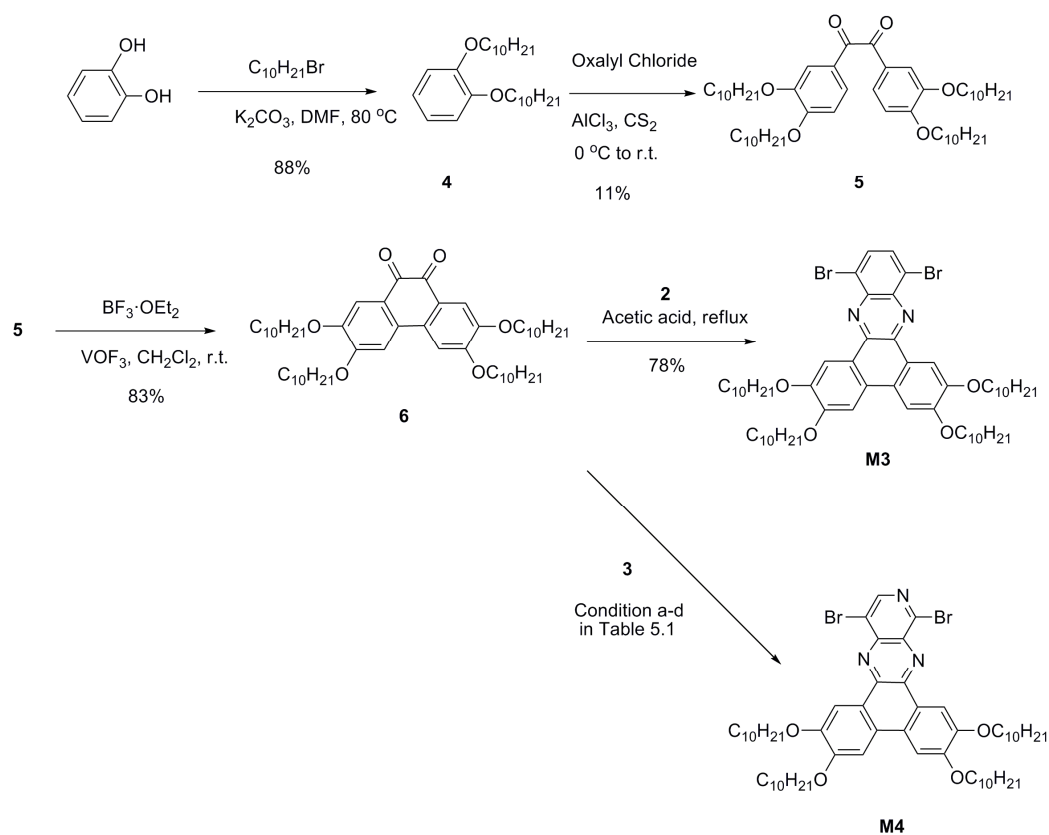
### *Monomer Synthesis*

The 2,6-di(tributylstannyl) derivative of *N*-(3,4,5-tri-*n*-dodecyloxyphenyl)-DTP, previously described in Chapter 4, was also used in the copolymers in this chapter in

order to obtain moderate to high molecular weights, and solution-processable materials in Stille coupling with dibromo derivatives of the acceptors. A distannyl *N*-octyl DTP derivative was used in the copolymers earlier, however, the trial polymerizations were not successful, as will be discussed in detail in the section of polymer synthesis. The acceptor monomers were synthesized using known procedures for identical compounds or close analogues,<sup>7,14</sup> as shown in Scheme 5.1 and 5.2. The syntheses of monomers **M1-3** were straightforward; however, the preparation of the acceptor **M4** was successful only after several attempts using different conditions. From Table 5.1, it can be seen that the combination of acetic acid/ethanol works best for this specific reaction, and the reaction using microwave irradiation gave a higher yield compared to the reaction using conventional heating.



**Scheme 5.1** Synthesis of **M1-2**.



**Scheme 5.2** Synthesis of **M3-4**.

**Table 5.1** Reaction condition and results for preparation of **M4**

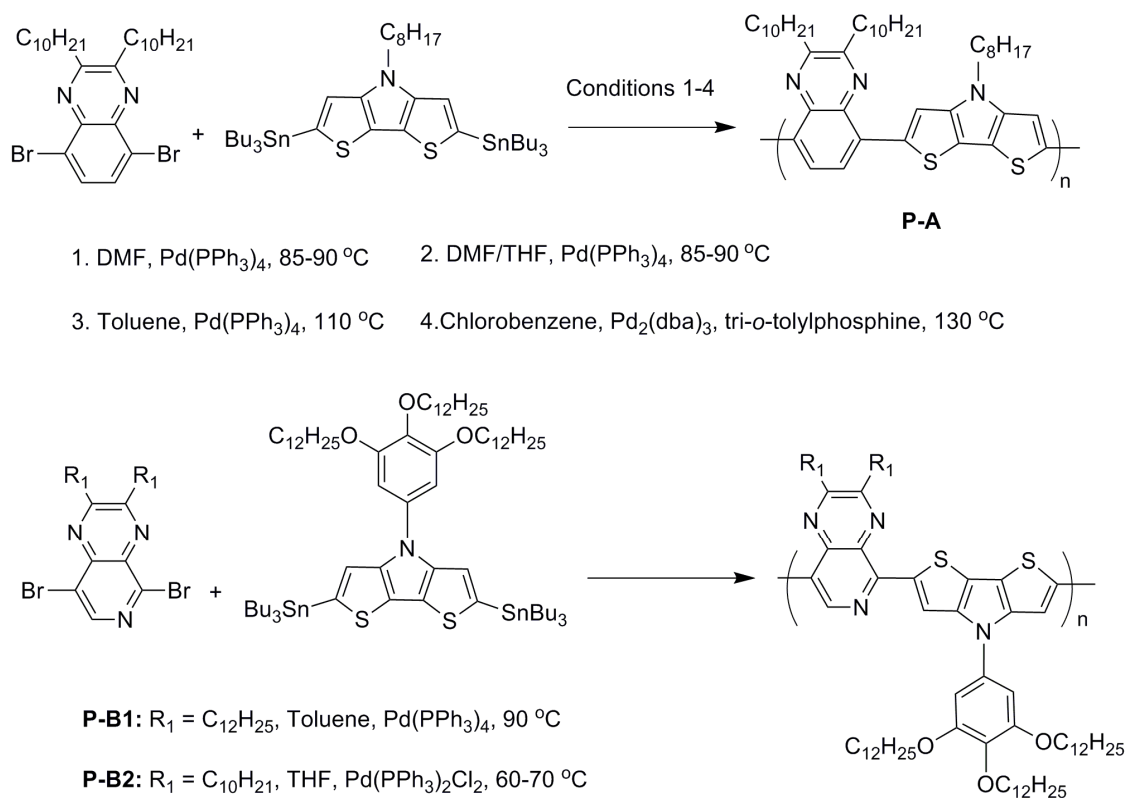
No. of the conditions	Reaction Conditions	Reaction Results
a	Ethanol/ $\text{H}_2\text{O}$ , reflux	Starting materials recovered
b	Acetic Acid, reflux	Unidentified product obtained along with the disappearance of starting materials
c	Acetic acid/ethanol, reflux	Desired product obtained in 20% yield
d	Acetic acid/ethanol, microwave irradiation	Desired product obtained in 65% yield

### Polymer Synthesis

In general, a careful choice of polymerization reaction parameters, such as catalyst (and ligand)/solvent combination, temperature, and the nature of the monomers, is

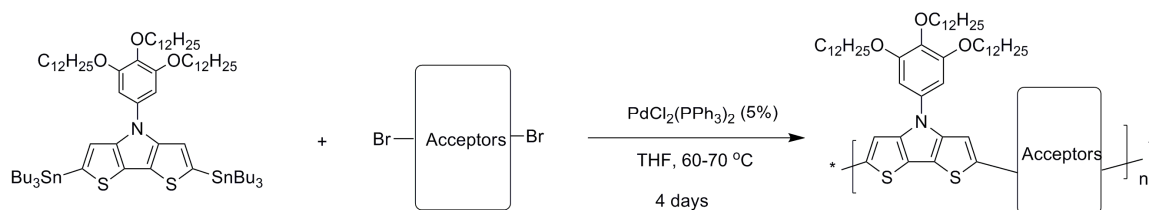
required to achieve high molecular weights (MW) and high yields in cross-coupling polycondensations. However, optimal coupling conditions vary with individual monomers, and the optimized conditions are often obtained only after an extended “trial and error” investigation.<sup>15</sup> In order to obtain solution-processable polymers with high MW, variations of the donor monomer and optimizations of the reaction conditions were carried out for Stille polymerizations of distannyl DTP derivatives and dibromo derivatives of the acceptors (Scheme 5.3). Initially, several polymerizations (**P-A** in Scheme 5.3) of the *N*-octyl DTP distannyl monomer with a dibromo derivative of didecyl-quinoxaline were attempted (collaborative work with the Jenekhe group at UW). Although there were variations in term of molecular weights when using different solvent/catalyst combinations, only very low molecular weights oligomers ( $M_w = 4\text{k-}6\text{k}$  in THF, DP <10) were obtained, or, at least, only low molecular weight fractions were soluble in the solvents used for GPC characterization. The majority of the products obtained from those reactions were insoluble in common organic solvents, such as chloroform, THF and toluene. Therefore, *N*-(3,4,5-tri-*n*-dodecyloxyphenyl)-DTP was used in the hope of improving solubility of the copolymers. The use of this alternative DTP monomer can dramatically improve the solubility of the copolymers; however, the MW (or DP) of the copolymer **P-B1** remains low ( $M_w = 13\text{k}$ , PDI = 1.4 in toluene, DP  $\approx$  7) even using the solvent/catalyst combination (toluene/ Pd(PPh<sub>3</sub>)<sub>4</sub>) that worked best in **P-A** series. Inspired by the high molecular weights obtained in the copolymers in Chapter

4, the THF/ Pd(PPh<sub>3</sub>)<sub>2</sub>Cl<sub>2</sub> combination was used and much higher molecular weights (or larger DP) (M<sub>w</sub> = 103k, PDI = 1.8 in toluene, DP ≈ 47) were obtained for the structurally similar polymer (**P-B2**, also **P2** in Figure 5.2) than those in **P-B1**. It is also worth noting that the polymerization of **P-B2** (or **P2**) was carried out in a pressure vessel, and the monomers, solvent and catalyst were loaded under inert atmosphere in the glove box and was taken out for heating after sealing the vessel. This could be a contributing factor for obtaining higher molecular weights in the latter polymers due to fewer external factors that can interfere with the reactions in a sealed reaction system.



**Scheme 5.3** Trial polymerizations in Chapter 5.

The copolymers **P1-4** studied in this chapter (Figure 5.2) were prepared using optimized Stille coupling conditions, using the THF/  $\text{Pd}(\text{PPh}_3)_2\text{Cl}_2$  combination in pressure vessels, as shown in Scheme 5.4. The purifications of the copolymers were similar to those for the polymers in Chapter 4 in that multiple precipitations and Soxhlet extractions from several types of solvents were employed; in some cases, further purifications were carried out by running flash column chromatography on silica gel, followed by size-exclusion column chromatography.



**Scheme 5.4** Synthesis of **P1-4**.

The copolymers **P1-4** are readily soluble in many common organic solvents including THF, chloroform, and toluene. Weight-average molecular weights ( $M_w$ ) and polydispersities ( $M_w/M_n$ ) were estimated by gel-permeation chromatography (GPC) against polystyrene standards using toluene as eluent (Table 5.2). The  $M_w$  values for the copolymers vary from 119k to 50k, and it is worth noting that the DP of these copolymers are much more higher than the ones listed in Table 5.2. This is presumably attributed to the improved solubility of the polymers in organic solvents and more

efficient polymerization using optimized conditions. The thermal properties of the polymers were determined by thermal gravimetric analysis (TGA); all of them showed good thermal stability with 5 % wt loss only over 350 °C (see Table 5.3).

**Table 5.2** Yields, molecular weights and thermal properties of the copolymers.

Polymers	Yield	$M_w^a$	$M_w/M_n^a$	$DP^b$	$T_d (^{\circ}C)^c$
<b>P1</b>	93%	119k	3.7	27	364
<b>P2</b>	72%	103k	1.8	47	366
<b>P3</b>	66%	70k	1.8	23	365
<b>P4</b>	75%	50k	2.3	13	376

a. Weight average molecular weight ( $M_w$ ) and polydispersity index ( $M_w/M_n$ ) determined by GPC with toluene as eluent vs. polystyrene standards; b. degree of polymerization,  $DP = M_n/M_0$ ,  $M_{m0}$  is the molecular weight of the repeating unit; c. Temperature at which 5% weight loss is observed using TGA under  $N_2$  at heating rate of 10 °C/min.

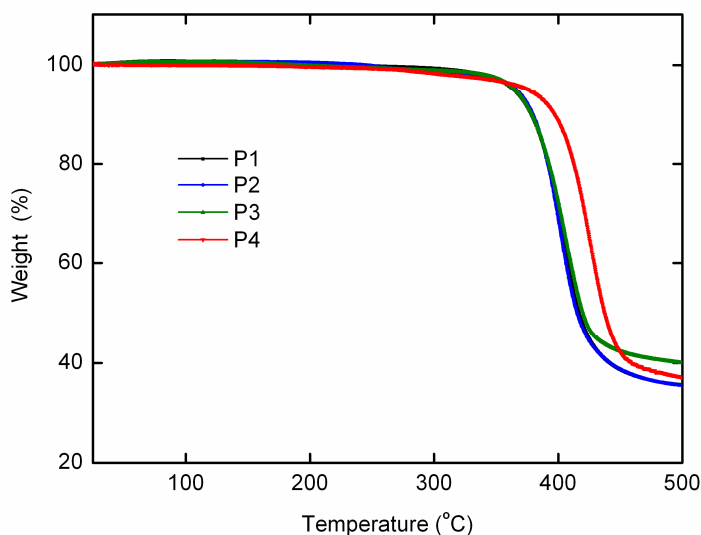


**Figure 5.3** TGA curves of **P1-4**.

### 5.3 Density Functional Theory Calculations of Electronic Structure

Optimized geometries and electronic energy levels were calculated in the gas phase using DFT at the B3LYP/6-31G(d,p) level of theory. Excited state energy calculations were performed at the same level of theory using the time-dependent method (TD-DFT). (obtained by Dr. Joseph Norton in the Brédas group at the Georgia Institute of Technology). Model donor-acceptor oligomers were constructed from DTP donor units coupled with acceptor units containing quinoxaline, pyridopyrazine and their extended analogs. Extended alkyl chains were replaced by methyl groups in the computational studies.

From the schematic illustration of wavefunctions of the oligomers, the LUMO levels of the donor-acceptor oligomers can be seen to be more localized on the acceptor unit while the HOMO levels remain delocalized along the main conjugation path, with only minor extension on the pyrazine ring and even less beyond, when the conjugation becomes extended from quinoxaline (or pyridopyrazine) in **P1** (or **P2**) to dibenzo-phenazine (or dibenzo-pyridoquinoxaline) in **P3** (or **P4**). From the values shown in Table 5.4, it appears that the replacement of C atom in **P1** (or **P3**) to N atom in **P2** (or **P4**) can stabilize both HOMO and LUMO levels, which is consistent with the trend observed in the electrochemical oxidation and reduction potentials in section 5.4, and is consistent with the effect expected on incorporating a more electron-poor atom. The trend showed decreased bandgaps from **P1** to **P2** as expected on the basis of previous studies showing

pyridopyrazine to be a stronger acceptor than quinoxaline in the other D-A copolymers.<sup>7</sup>

Comparisons of the theoretical calculations results with the experimental data will be discussed later in section 3.4.

**Table 5.3** Extrapolated HOMO, LUMO,  $E_g$ , and  $S_1$  transition energies <sup>a</sup>

Polymer	HOMO (eV)	LUMO (eV)	$E_g$ (eV)	$S_1$ (eV)
<b>P1</b>	−4.26	−2.51	1.75	1.46
<b>P2</b>	−4.41	−2.80	1.61	1.42
<b>P3</b>	−4.12	−2.33	1.79	1.47
<b>P4</b>	−4.22	−2.56	1.66	1.38

a. calculated at the B3LYP/6-31G(d,p) level and extrapolated using Kuhn fits

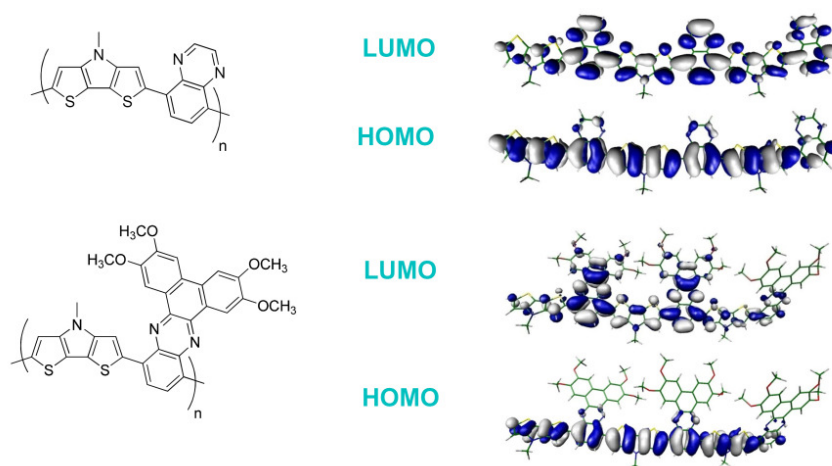


**Figure 5.4** HOMO/LUMO wavefunctions of representative oligomers (n=3).

## 5.4 Optical and Electrochemical Properties

The normalized optical absorption spectra of the polymers in dilute THF solution and thin films are shown in Figure 5.5, and corresponding absorption properties are

summarized in Table 5.4. The copolymers **P1** and **P2** show two prominent absorption bands (one in the range of 390-400 nm and another in the near-IR range). The bands in the range of 390-400 nm do not significantly shift with the acceptor strength; however, the absorption maxima of the lower energy band in the near-IR range are significantly red-shifted from 645 nm in **P1** to 720 nm in **P2**. The lower energy bands in the near-IR range exhibit considerable donor-to-acceptor charge-transfer character, and the significant red-shift in those bands of the two copolymers indicate the order of the electron-accepting strength of those acceptors,  $Qx < PPz$ , which is similar to observations in other quinoxaline/pyridopyrazine-containing D-A copolymers.<sup>7</sup> In thin films, the absorption maxima of these two copolymers are significantly red-shifted compared to those in solution. Besides the two major absorption bands in similar ranges as **P1** and **P2**, **P3** and **P4** have more absorption bands in the range of 300-400 nm compared to **P1** and **P2**. In **P4**, a more structured absorption pattern (maxima at *ca.* 710 and 770 nm) is observed in the low-energy range, which is probably attributed to the vibronic structures (two peaks separated by *ca.*  $1000\text{ cm}^{-1}$ ). When comparing the two copolymers (**P1** and **P3**) with or without extended fused ring on the acceptors, a *ca.* 70 nm red-shift in the low energy bands from **P1** to **P3** with a reduced bandgap in **P3**. The differences from **P1** to **P3** can be explained as the result of extended conjugation on the acceptor moieties. The same trend was also observed from **P2** to **P4** as expected. The absorption bands in the near-IR regime in all these polymers are seen at much lower energy than those obtained

for other structurally similar D-A copolymers containing Qx or PPz. For example, the carbazole-quinoxaline/pyridopyrazine copolymers (polymer **54a** and **54b** in Figure 1.17) have  $\lambda_{\text{max}}^{\text{abs}}$  at *ca.* 510 nm and 550 nm respectively,<sup>7</sup> which is consistent with the expectation that DTP acts as a stronger donor.

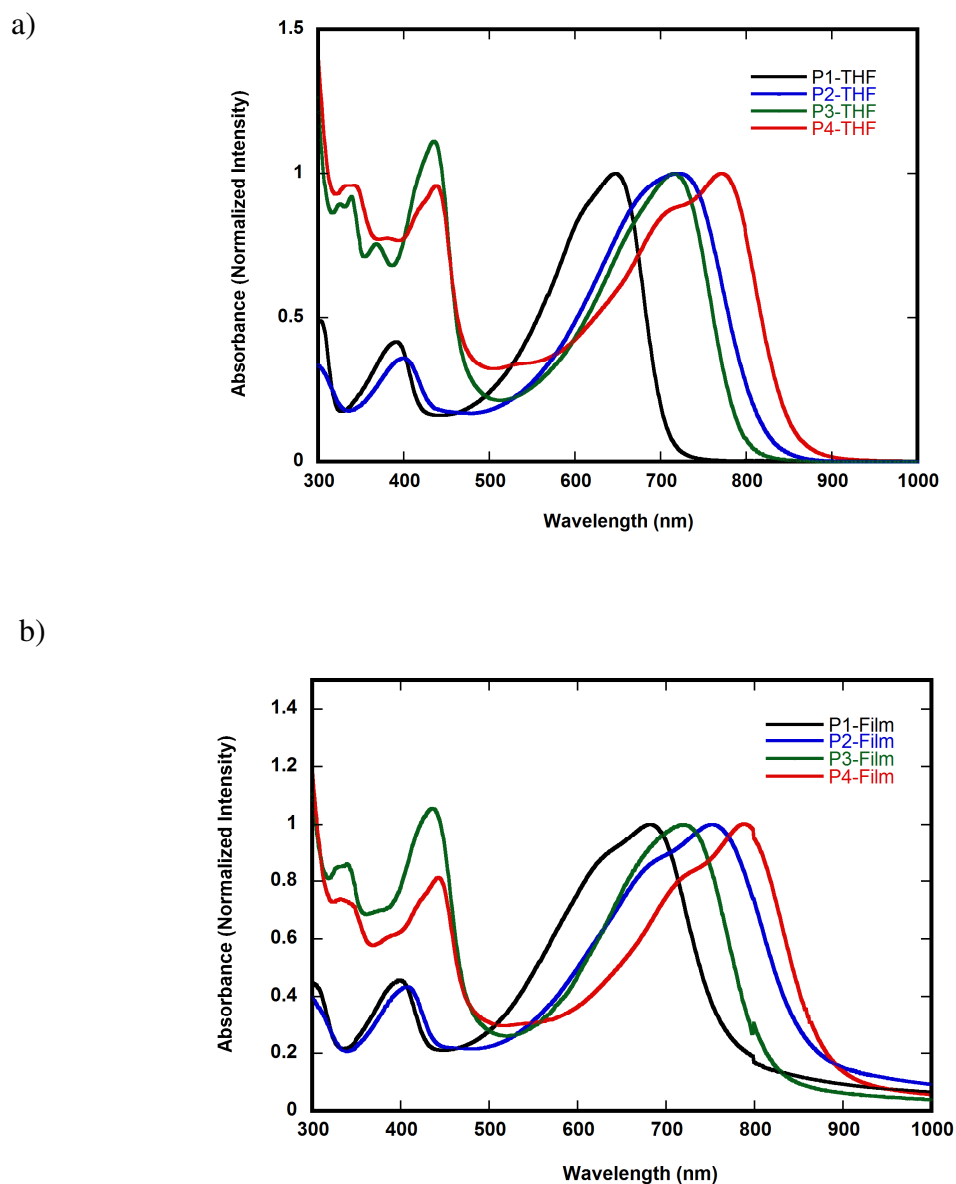


**Figure 5.5** UV-vis-NIR spectra of **P1-4** in (a) dilute THF solution and (b) thin films.

**Table 5.4** Optical and redox properties of the polymers

Polymer	$\lambda_{\max}^{\text{abs}}$ (nm) ( $\epsilon, \times 10^{-4} \text{ M}^{-1} \text{ cm}^{-1}$ or $\alpha, \times 10^{-4} \text{ cm}^{-1}$ )		$E_g^c$ (opt) eV	$E_{\text{ox}}^d$ onset (CV) V	IP <sup>e</sup> (CV) eV	$E_{\text{red}}^d$ onset (CV) V	EA <sup>e</sup> (CV) eV	$E_g^f$ (CV) eV
	Solution <sup>a</sup>	Film <sup>b</sup>						
<b>P1</b>	392 (1.70), 645 (4.68)	400 (2.09), 683 (4.55)	1.61	0.65	5.1	-1.55	2.9	2.2
<b>P2</b>	401 (1.43), 720 (3.87)	408 (1.79), 753 (4.13)	1.43	0.80	5.2	-1.30	3.1	2.1
<b>P3</b>	327 (3.65), 369 (3.06), 435 (4.50), 713 (4.10)	333 (1.92), 374 (1.58), 436 (2.39), 722 (2.26)	1.48	0.69	5.1	-1.36	3.0	2.1
<b>P4</b>	337 (2.77), 438 (2.88), 710 (2.61), 771 (3.02)	343 (2.74), 443 (3.08), 718 (3.08), 785 (3.79)	1.30	0.82	5.2	-1.10	3.3	1.8

a. measured for diluted solution in THF (values of molar extinction coefficients,  $\epsilon$ , in the parentheses); b. measured for thin films spin-coated from toluene solution (values of absorption coefficients,  $\alpha$ , in the parentheses); c. values are optical bandgaps estimated from onset absorption edge in solution; d. Measured in 0.1 M [<sup>n</sup>Bu<sub>4</sub>N]<sup>+</sup>[PF<sub>6</sub>]<sup>-</sup>/acetonitrile solution and reported vs. SCE; e. Values were estimated based on  $\text{IP} = E_{\text{ox}}^{\text{onset}} + 4.4 \text{ eV}$ ,  $\text{EA} = E_{\text{red}}^{\text{onset}} + 4.4 \text{ eV}$ .<sup>16</sup> f.  $E_g$  (CV) is the differences of IP and EA values.

The electrochemical properties of the polymers were investigated by CV using films of the polymers drop-cast from solution onto platinum working electrodes. The values of oxidation and reduction potentials as well as IP and EA are summarized in Table 5.4. Representative oxidative and reductive CV curves of the copolymers are shown in Figure 5.6. The electrochemical oxidation and reduction onsets ( $E_{\text{ox}}^{\text{onset}}$  and  $E_{\text{red}}^{\text{onset}}$  vs. SCE) were also used to obtain estimates of solid-state IP and EA according to  $\text{IP} = E_{\text{ox}}^{\text{onset}} + 4.4 \text{ eV}$ ,  $\text{EA} = E_{\text{red}}^{\text{onset}} + 4.4 \text{ eV}$ ;<sup>16</sup> the electrochemical band gaps were obtained from the

difference between the  $E_{\text{ox}}^{\text{onset}}$  and  $E_{\text{red}}^{\text{onset}}$ . The IP values of the polymers are in the range of 5.1-5.2 eV, and EA values are in the range of 2.9-3.3 eV. Both the IPs and EAs of **P2** and **P4** containing pyridopyrazine are somehow lower compared to the values in their quinoxaline analogues, **P1** and **P3**, respectively; this is consistent with the similar observation in other copolymers containing pyridopyrazine or quinoxaline<sup>7,10</sup> as well as the trend from the theoretical calculation in section 5.3, suggesting the order of electron-accepting strengths is Qx < PPz. Also the extension of the acceptor moieties in **P3** and **P4** affects the reduction potentials, leading to the EA values with *ca.* 0.1-0.2 eV differences from **P1** (or **P2**) to **P3** (or **P4**). The increase in ease of reduction in the polymers is consistent with the trends of red-shifts in their low-energy bands, and provides further evidence for the orders of electron-accepting strengths.

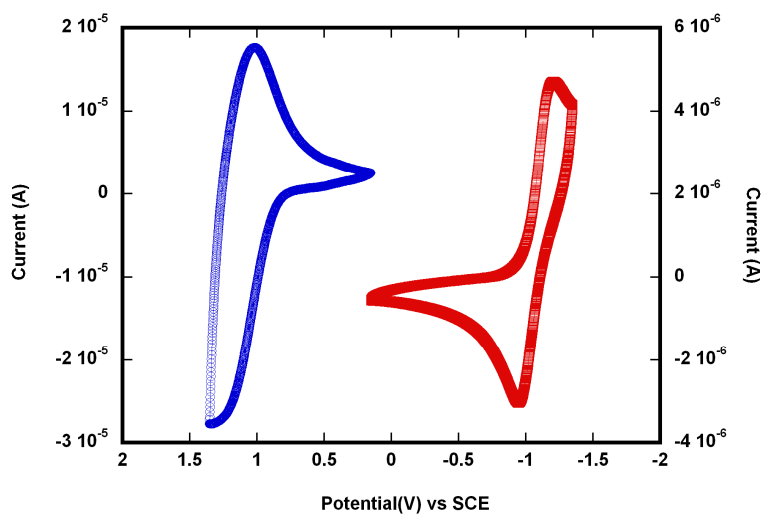


**Figure 5.6** Oxidative (blue line) and reductive (red line) CV of **P4** film at a scan rate of 50 mV/sec.

Comparing the values from optical and electrochemical data, in general they follow the same trends: decreased bandgaps were observed from **P1** (or **P3**) containing Qx to **P2** (or **P4**) containing PPz; similar observation was found from **P1** (or **P2**) to **P3** (or **P4**) when the conjugation was extended on the acceptor moieties. The theoretical calculations (section 5.3) suggest the bandgaps in the polymers containing PPz are smaller than the ones containing Qx, which is consistent with the experimental data; however, they also suggest that the extension of the acceptors leads to a slight increase in bandgaps, whereas experimentally a slightly decrease is found. The inconsistencies between theoretically predicted values and those obtained experimentally are possibly due to effects that changes in both molecular geometry and the environment between the gas phase and condensed phase. Specifically, since the calculations were performed in the gas phase, effects such as solvent or solid-state effects are neglected.

## 5.5 Field-Effect Transistor Characteristics

Charge-carrier transport in the copolymers were explored directly by investigating their use as the active layer in top-contact OFETs fabricated from gold source/drain electrodes and SiO<sub>2</sub> as a gate dielectric layer. Devices are fabricated and tested in the Kippelen group at the Georgia Institute of Technology. Field-effect mobilities ( $\mu$ ) and threshold voltages ( $V_T$ ) were measured in the saturation regime from the saturation region

current equation for a standard MOSFET, using the highest slope of the  $|I_{DS}|^{1/2}$  vs.  $V_{GS}$  plot:

$$I_{DS} = \frac{1}{2} \mu C_i \frac{W}{L} (V_{GS} - V_T)^2 \quad (5.1)$$

where  $C_i$  is the capacitance per unit area of the gate dielectric [ $\text{F}/\text{cm}^2$ ], and  $W$  (width) and  $L$  (length) are the dimensions of the semiconductor channel defined by the source and drain electrodes of the transistor. Characteristics of OFETs based on copolymers **P1-3**, including mobilities ( $\mu$ ), threshold voltages ( $V_T$ ), and current on/off ratios ( $I_{on}/I_{off}$ ), are summarized in Table 5.5.

**Table 5.5** Field-effect transistor characteristics of **P1- 4**.

Polymers	$\mu_h$ ( $\text{cm}^2/\text{Vs}$ )	$V_T$ (V)	$I_{on}/I_{off}$
<b>P1</b>	$1.20 (\pm 0.18) \times 10^{-4}$	- 9.34 ( $\pm 0.78$ )	$10^3$
<b>P2</b>	$2.30 (\pm 0.30) \times 10^{-4}$	- 8.20 ( $\pm 3.60$ )	$5 \times 10^2$
<b>P3</b>	$2.94 (\pm 0.08) \times 10^{-4}$	- 8.36 ( $\pm 0.85$ )	$10^3$
<b>P4</b>	$1.0 (\pm 0.1) \times 10^{-5}$	- 13.6 ( $\pm 3.9$ )	$1 \times 10^2$

Representative output and transfer characteristics of an OFET ( $W/L = 1000 \mu\text{m}/25 \mu\text{m}$ ) with one of the copolymers **P3** are shown in Figure 5.7. The devices based on **P1-P3** showed typical p-channel field-effect transistor characteristics with mobilities of the order of  $10^{-5}$  to  $10^{-4} \text{ cm}^2/(\text{Vs})$ , which are comparable with those reported for other D-A copolymers containing quinoxaline or pyridopyrazine.<sup>7-9</sup> Again, as with devices based on the other DTP-based copolymers in other chapters, low on/off ratios of the devices are

possibly due to adventitious doping by air. The relatively lower mobility in **P4** is possibly due to the smaller DP (DP  $\approx$  13) in this polymer than those found in the other polymers in this series (DP  $\approx$  23-47).

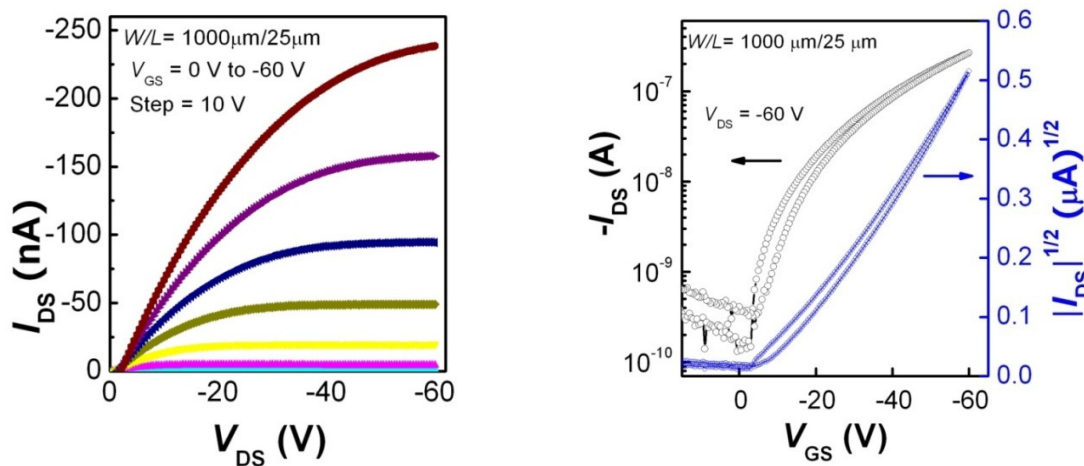


**Figure 5.7** Output (left) and transfer (right) and characteristics of an OFET of **P3**.

## 5.6 Photovoltaic Cell Characteristics

Bulk heterojunction photovoltaic devices were fabricated in the Kippelen group at the Georgia Institute of Technology based on blends of the polymers **P1-4** with the soluble fullerene PCBM; the device performances are summarized in Table 5.6. The performance of devices with different polymers is summarized in Table 5.7, and representative J-V characteristics of the devices based on **P3** are shown in Figure 5.8, and.

The optimum weight ratios for different combinations of donors and PCBM have been varied, for examples, the best ratio for P3HT/PCBM is 1:1 (or 1:0.8), whereas that for

MDMO-PPV/PCBM is 1:4.<sup>17,18</sup> From table 5.7, it can be seen that when the weight ratios of **P3** and PCBM is 1:3, the power conversion efficiency can be increased to 1.4%. The relatively high  $V_{oc}$  combined with relatively large  $J_{sc}$  and  $FF$  in the devices based on **P3**/PCBM (1:3) lead to better performance compared to those for the devices using other compositional ratios. However, in the blends of **P4** and PCBM, devices based on **P4**/PCBM (1:6) gave better efficiency than the other devices using other ratios. These results further support previous suggestions in the literature<sup>19</sup> that the optimum mixing ratios for polymer / PCBM blends can vary significantly with the choice of polymer.

**Table 5.6** Photovoltaic cell performance of **P1-4** blended with PCBM.

Polymers <sup>a</sup> (X: PCBM weight ratio)	$V_{oc}$ (mV)	$J_{sc}$ (mA/cm <sup>2</sup> )	$FF$	$\eta$ <sup>b</sup> (%)
<b>P1</b> (1:1)	439 ± 3	2.20 ± 0.10	0.44 ± 0.01	0.57 ± 0.02
<b>P2</b> (1:1)	468 ± 5	1.71 ± 0.29	0.33 ± 0.01	0.37 ± 0.07
<b>P3</b> (2:1)	544 ± 3	1.23 ± 0.02	0.35 ± 0.01	0.31 ± 0.01
<b>P3</b> (1:1)	579 ± 4	2.12 ± 0.08	0.42 ± 0.01	0.76 ± 0.02
<b>P3</b> (1:2)	594 ± 9	2.68 ± 0.06	0.49 ± 0.01	1.00 ± 0.10
<b>P3</b> (1:3)	626 ± 7	2.69 ± 0.03	0.61 ± 0.02	1.40 ± 0.07
<b>P3</b> (1:4)	624 ± 5	1.87 ± 0.13	0.66 ± 0.03	1.00 ± 0.10
<b>P3</b> (1:5)	624 ± 5	1.67 ± 0.03	0.64 ± 0.03	0.87 ± 0.05
<b>P3</b> (1:6)	624 ± 26	2.27 ± 0.02	0.57 ± 0.12	1.10 ± 0.28
<b>P4</b> (3:1)	634 ± 37	0.38 ± 0.01	0.24 ± 0.01	0.08 ± 0.01
<b>P4</b> (1:1)	496 ± 18	0.88 ± 0.02	0.25 ± 0.01	0.16 ± 0.06
<b>P4</b> (1:3)	527 ± 42	1.82 ± 0.03	0.35 ± 0.01	0.48 ± 0.03
<b>P4</b> (1:6)	705 ± 14	2.14 ± 0.04	0.33 ± 0.02	0.71 ± 0.05

a. processing solvents for the blends films is chlorobenzene; b. power conversion efficiencies  $\eta$  was calculated using the equation 1.11 using a broadband light source with  $P_{in} = \sim 71\text{-}74$  mW/cm<sup>2</sup>.

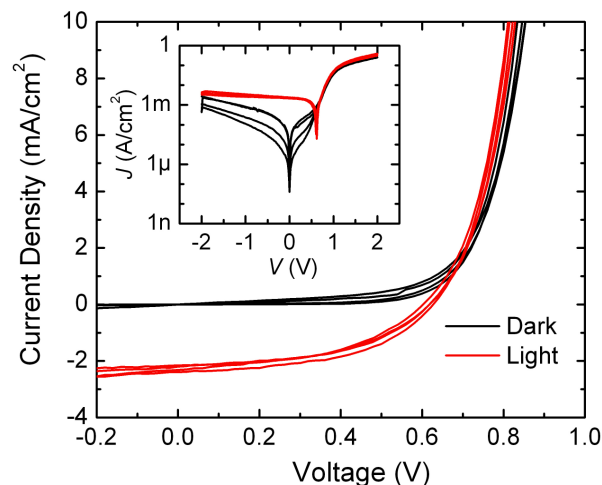


**Figure 5.8** Representative  $J$ - $V$  characteristics of multiple cells measured in the dark (dashed line) and under illumination (solid line) for films of PCBM blended with **P3** in a 1:3 weight ratio. (Inset shows the same data in a semilogarithmic plot)

In order to better understand the origins of the higher efficiency in the 1:3 (w:w) blends of **P3** and PCBM, a morphology study, as well as EQE measurements have been carried out. AFM images of the blends of different weight ratios (1:1, 1:3 and 1:6) were obtained. It is clearly seen that larger domains are observed in the blends of **P3**/PCBM with 1:3 ratio compared to the 1:1 blends, whereas the pattern in the blends of 1:6 ratio looks rather different from that of the other two samples. RMS roughness values for these blends of **P3**/PCBM films are similar: 7.2, 9.2 and 8.6 nm, respectively. The domain size was increased with increasing contents of PCBM (from 1:1 blend to 1:3 blend in this case); the similar observations has also been found in other conjugated polymers, such as MDMO-PPV, blended with PCBM when the weight ratios are varied.<sup>20,21</sup> It is also

suggested in the literature that the larger domain sizes associated with the increasing PCBM contents, often lead to better phase percolation, and thus, better efficiency in the devices.<sup>20,21</sup> It is worth noting that the preferred morphology (with larger domain size evident in AFM images) for **P3**/PCBM blends appears to be different from that (smoothest surface and smallest domain size) for **P1** (DTP with benzothiadiazole) blended with PCBM described in Chapter 4; the differences suggested that it is not possible to draw a general conclusion about favorable morphology for different polymer blends under different conditions on the basis of AFM data alone.

Furthermore, the EQE spectra of the blends of **P3**/PCBM were measured (Figure 5.10). It is clearly seen that EQE was also dramatically improved from 1:1 blend to 1:3 blend, however, the 1:6 blend has a similar spectrum to the 1:3 blend except that it seems a little blue-shifted. This is consistent with the observation in other conjugated polymer blended with PCBM that high EQE value is obtained when the compositional ratio is optimum.<sup>20</sup> Nevertheless, the relatively high EQE value for the 1:3 blend, at least compared to that for the 1:1 blend, could be one of the reasons leading to the best performance in the 1:3 blend.

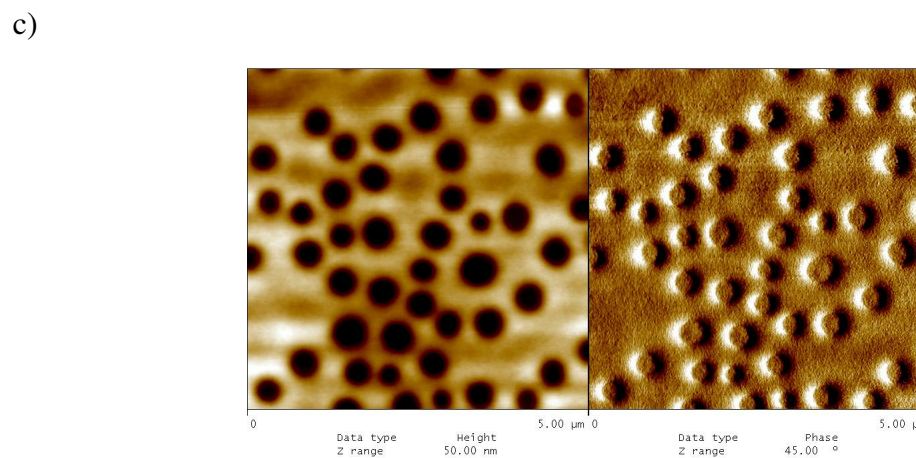
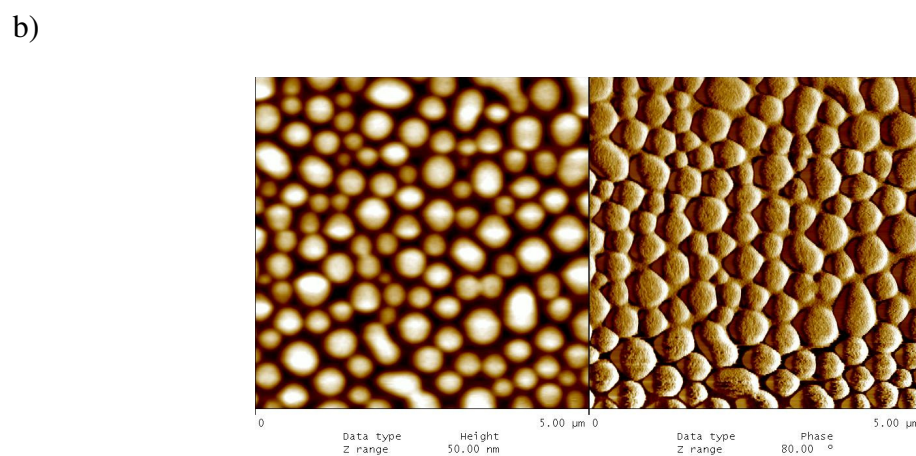
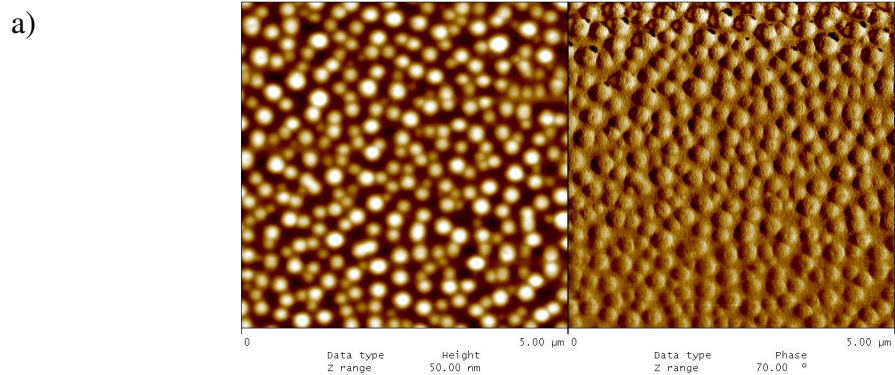


**Figure 5.9** AFM images of **P3/PCBM** blend films (a, 1:1; b, 1:3; c, 1:6) (left, height image, vertical scale is 50 nm for all three images; right, phase image, vertical scale are 70, 80, 45° for a, b and c, respectively)

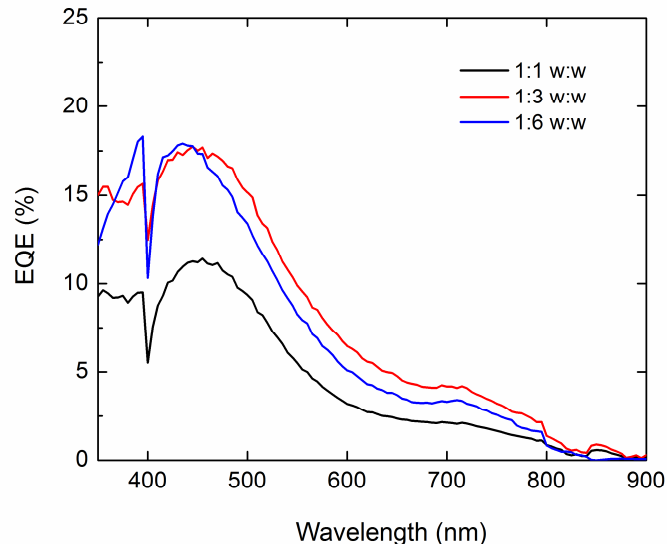


**Figure 5.10** EQE spectra of as a function of wavelength of devices made from **P3**/PCBM blends.

Other factors, such as balanced hole and electron mobilities, may also play important roles in optimizing the efficiencies when varying the weight ratios of polymers and PCBM.<sup>20</sup> Although it is not straightforward to directly link the morphology changes to the device performances, the study of **P3**/PCBM blends with different weight ratios suggested that the compositional ratio of the blends could have influence on the film morphology, external quantum efficiency as well as the OPV power conversion efficiencies of the blends.

## 5.7 Conclusions

A series of D-A copolymers based on dithieno[3,2-*b*:2',3'-*d*]pyrrole donors coupled to quinoxaline/pyridopyrazine-based acceptors have been synthesized and characterized.

Both quantum-chemical calculations and experimental data for these copolymers suggest that the acceptor strengths play an important role in tuning the optical and electrochemical properties of the copolymers. The extended conjugation on the acceptors also has noticeable influences on those properties. Moreover, their potential utilities in OFETs and OPVs were tested. The copolymers functioned as hole-transport materials in OFETs with mobilities up to *ca.*  $3.0 \times 10^{-4} \text{ cm}^2/(\text{Vs})$ . In the OPV devices made from the copolymers/PCBM blends, one of them (**P3**, copolymer of DTP with dibenzo[*a,c*]phenazine) exhibited moderate performance with a power conversion efficiency up to  $1.40 \pm 0.07\%$  from devices after optimization. The study of **P3**/PCBM blends with different weight ratios suggested that the compositional ratio of the blends could have influence on the film morphology, external quantum efficiency as well as the OPV power conversion efficiencies of the blends; this may provide useful information for the further studies of solar cells of DTP-based polymers. In summary, the current study indicated that optical and electronic properties of this series of D-A copolymers can be easily manipulated through the acceptor strength and/or the conjugation on the acceptors, and also they have potentials to be used in device applications, such as OFETs and OPVs.

## 5.8 Experimental Section

### Materials.

Unless stated otherwise, starting materials were purchased and were used without further purification. The synthesis of 2,6-bis(tri-*n*-butylstannyl)-*N*-(3,4,5-tris(*n*-dodecyloxy)phenyl)-dithieno[3,2-*b*:2',3'-*d*]pyrrole was described in the experimental section of Chapter 2. Compounds **3** and **6** were initially provided by Qing Zhang in the Marder group and then scaled-up using literature procedures.<sup>7,22</sup>

### Characterizations.

<sup>1</sup>H NMR and <sup>13</sup>C NMR spectra were measured on a Varian Mercury 300 MHz or a Bruker 400 MHz. The microwave used was a CEM Discover Labmate. Mass spectra were measured on a VG Instruments 70-SE using the electron impact (EI) mode or on an Applied Biosystems 4700 Proteomics Analyzer using MALDI mode. Elemental analyses were carried out by Atlantic Microlabs using a LECO 932 CHNS elemental analyzer. Gel permeation chromatography (GPC) analysis for **P-A** were performed on a Waters 1515 gel coupled with UV and RI detectors using tetrahydrofuran as eluent against polystyrene standards. GPC analysis for **P-B** and **P1-4** were performed on a Waters styragel HR 4, 3, and 1, columns coupled with a Waters 2410 Refractive Index detector and 2690 separations module, using toluene as eluent, against polystyrene standards, and a flow rate of 1mL/min. UV-vis absorption spectra were recorded on Varian Cary 500 UV/Vis/near-IR spectrophotometer. Cyclic voltammetry experiments of polymers were

carried out using a BAS 100B electrochemical analyzer using 0.1 M [<sup>n</sup>Bu<sub>4</sub>N]<sup>+</sup>[PF<sub>6</sub>]<sup>-</sup> in acetonitrile as electrolyte. The Ag<sup>+</sup>/Ag (AgNO<sub>3</sub>) reference electrode was calibrated at the beginning of the experiments by running cyclic voltammetry using ferrocene as the internal standard. The potential values obtained in reference to Ag<sup>+</sup>/Ag electrode were then converted to the saturated calomel electrode (SCE) scale, assuming the values of [FeCp<sub>2</sub>]<sup>+0</sup> = 0.40 V in 0.1 M [<sup>n</sup>Bu<sub>4</sub>N]<sup>+</sup>[PF<sub>6</sub>]<sup>-</sup>/acetonitrile solution.<sup>23</sup> Thermogravimetric analysis (TGA) analysis was conducted with a NETZSCH thermogravimetric analyzer (model STA 449C) under a nitrogen flow at a heating rate of 10 °C/min. AFM images were taken on a Digital Instruments NanoScope™ Scanning Probe Microscope and obtained from Séverine Coppée in the Kippelen group at the Georgia Institute of Technology.

**Docosane-11,12-dione (1).**<sup>24</sup> LiBr (6.4 g, 73 mmol) in dry THF (*ca.* 20 mL) was added to a stirred suspension of CuBr (5.2 g, 36 mmol) in dry THF (*ca.* 20 mL) to form a pale green suspension. This mixture was then cooled to -78 °C. The 1-decylmagnesium bromide solution (35 mL, 1.0 M in diethyl ether) was slowly added to the LiBr/CuBr suspension in *ca.* 4 h, followed by an addition of oxalyl chloride (2.3 g, 18 mmol) dropwise. The temperature of the reaction was kept at *ca.* -60 °C during the additions and stirred for another 1h after adding oxalyl chloride while keeping the similar temperature. The reaction mixture was allowed to warm to room temperature and quenched with

saturated aqueous  $\text{NH}_4\text{Cl}$ . The organic layer was separated and the aqueous layer extracted repeatedly with ethyl acetate, and all the solvents were removed under reduced pressure. The residue was subjected to column chromatography (silica gel, eluent: hexanes: ethyl acetate: 98:2) and a pale yellow solid (2.0 g, 33 %) was obtained. GC-MS:  $m/z$ , 338 ( $\text{M}^+$ ).

**3,6-Dibromobenzene-1,2-diamine (2).** To a suspension of 4,7-dibromobenzo[*c*][1,2,5]thiadiazole (5.0 g, 17 mmol) in EtOH (70 mL),  $\text{NaBH}_4$  (11.4 g, 300 mmol) was added portionwise at 0 °C, and the mixture was stirred for 20 h at room temperature. After reaction,  $\text{H}_2\text{O}$  was added, and the mixture was extracted with  $\text{Et}_2\text{O}$ . The organic phase was washed with saturated aq. NaCl solution. After evaporation under reduced pressure, a white solid (3.7 g, 83%) was obtained.  $^1\text{H}$  NMR (300 MHz,  $\text{CDCl}_3$ ):  $\delta$  6.83 (s, 2H), 3.87 (s, br, 4H). The  $^1\text{H}$  NMR spectrum was consistent with that reported in the literature.<sup>14</sup>

**2,5-dibromopyridine-3,4-diamine (3).** To a three-neck 100 mL round-bottom flask, 2,3-diaminopyridine (3.0 g, 28 mmol) and 150 mL of 48% hydrobromic acid were added. Then bromine (4.6 mL, 89 mmol) was added dropwise. The reaction mixture was refluxed for 4 h and cooled to room temperature. The yellow solid was precipitated out and filtered after the addition of a saturated aq. solution of  $\text{Na}_2\text{S}_2\text{O}_3$ . The obtained solid

was heated to reflux for 30 min in saturated aq.  $\text{Na}_2\text{CO}_3$  solutions. Then it was collected by filtration and recrystallized from a methanol/ethanol mixture to give a yellow powder (2.4 g, 32%).  $^1\text{H}$  NMR (300 MHz, Acetone- $d_6$ ):  $\delta$  7.64 (s, 1H), 5.53 (s, br, 2H), 4.64 (s, br, 2H). The  $^1\text{H}$  NMR spectrum was consistent with that reported in the literature.<sup>7</sup>

**1,2-Bis(*n*-decyloxy)benzene (4).**<sup>22</sup> A mixture of 1,2-dihydroxybenzene (11 g, 0.10 mol), 1-decylbromide (53 g, 0.24 mol), potassium carbonate (41 g, 0.30 mol), and DMF (300 mL) were stirred at 80 °C for 2 days. After the reaction, water was added, and reaction mixture was extracted with ether. The organic layer was separated, and all the solvents were removed under reduced pressure. The crude product was purified by recrystallization from an acetone-methanol mixture. A white solid (34 g, 88%) was obtained. GC-MS:  $m/z$ , 390 ( $\text{M}^+$ ).

**1,2-Bis(3,4-bis(*n*-decyloxy)phenyl)ethane-1,2-dione (5).** 1,2-Bis(*n*-decyloxy)benzene (7.8 g, 20 mmol) was dissolved in carbon disulfide (*ca.* 70 mL), then cooled to 0 °C.  $\text{AlCl}_3$  (2.8 g, 21 mmol) was added slowly, then a solution of oxalyl chloride (1.5 g, 12 mmol) in carbon disulfide (*ca.* 10 mL) was added dropwise. The reaction mixture was stirred overnight. The resulting mixture was poured into ice and extracted with dichloromethane, and all the solvents were removed under reduced pressure. The residue was purified by column chromatography (silica gel,  $\text{CH}_2\text{Cl}_2$  as eluent), and was

recrystallized from acetone. The obtained solid was subjected to another column chromatography (silica gel, CH<sub>2</sub>Cl<sub>2</sub> as eluent). A yellow solid (0.90 g, 11%) was obtained. <sup>1</sup>H NMR (300 MHz, CDCl<sub>3</sub>):  $\delta$  7.54 (d,  $J$  = 2.1 Hz, 2H), 7.41 (dd,  $J$  = 8.7, 2.1 Hz, 2H), 6.82 (d,  $J$  = 8.7 Hz, 2H), 4.03 (t,  $J$  = 6.6 Hz, 8H), 1.82 (m, 8H), 1.44-1.24 (m, 56H), 0.86 (t,  $J$  = 6.6 Hz, 12H). The <sup>1</sup>H NMR spectrum was consistent with that reported in the literature.<sup>22</sup>

**2,3,6,7-Tetrakis(*n*-decyloxy)phenanthrene-9,10-dione (6).** To a stirred solution of 1,2-bis(3,4-bis(*n*-decyloxy)phenyl)ethane-1,2-dione (1.3 g, 1.5 mmol), vanadium oxyfluoride (0.65 g, 4.5 mmol), and anhydrous dichloromethane (40 mL), boron trifluoric etherate (0.46 g, 3 mmol) were added. The reaction mixture was stirred for 30 min at room temperature. Then it was poured into citric acid solution, and extracted with dichloromethane; all the solvents were removed under reduced pressure. The residue was subjected to column chromatography (silica gel, CH<sub>2</sub>Cl<sub>2</sub> as eluent) and a red solid (1.1 g, 83%) was obtained. <sup>1</sup>H NMR (300 MHz, CDCl<sub>3</sub>):  $\delta$  7.52 (s, 2H), 7.09 (s, 2H), 4.17 (t,  $J$  = 6.6 Hz, 8H), 4.05 (t,  $J$  = 6.6 Hz, 8H), 1.86 (m, 8H), 1.44-1.24 (m, 56H), 0.86 (t,  $J$  = 6.6 Hz, 12H). The <sup>1</sup>H NMR spectrum was consistent with that reported in the literature.<sup>22</sup>

**5,8-Dibromo-2,3-di-*n*-decylquinoxaline (M1).** The title compound was synthesized in a similar fasion to the ananlgous diphenyl compound.<sup>14</sup> Docosane-11,12-dione(0.55 g, 1.6

mmol) and 3,6-dibromobenzene-1,2-diamine (0.87 g, 3.2 mmol) were added to 100 mL 3-neck flask; an ethanol/water mixture (30/3 mL) was added, and the reaction mixture was refluxed overnight. After the reaction mixture was cooled down to room temperature, the resulting white precipitate was collected by filtration, and recrystallized from ethanol. A white solid (0.50 g, 55%) was obtained.  $^1\text{H}$  NMR (300 MHz,  $\text{CDCl}_3$ ):  $\delta$  7.79 (s, 1H), 3.05 (t,  $J = 7.5$  Hz, 4H), 1.91 (quint,  $J = 7.5$  Hz, 4H), 1.46-1.24 (m, 28H), 0.86 (t,  $J = 6.8$  Hz, 6H).  $^{13}\text{C}\{^1\text{H}\}$  NMR (100 MHz,  $\text{CDCl}_3$ ):  $\delta$  158.3, 139.3, 131.9, 123.3, 34.8, 31.9, 29.6 (two peaks separated by 0.04 ppm), 29.5 (two peaks separated by 0.04 ppm), 29.3, 27.8, 22.7, 14.1. HRMS (EI)  $m/z$  calcd. for  $\text{C}_{28}\text{H}_{44}\text{N}_2\text{Br}_2$  ( $\text{M}^+$ ): 566.1895; Found: 566.1871. Elemental Analysis: (Calculated) C, 59.16; H, 7.80; N, 4.93; (Found): C, 59.26; H, 7.99; N, 4.84.

**5,8-Dibromo-2,3-di-*n*-decyl-pyrido[3,4-*b*]pyrazine (M2).**<sup>8,10</sup> Docosane-11,12-dione (0.48 g, 1.4 mmol) and 2,5-dibromopyridine-3,4-diamine (0.58 g, 2.2 mmol) were added to 100 mL 3-neck flask, and a butanol/water mixture (30/3 mL) was added, then refluxed overnight. After the reaction mixture was cooled to room temperature, the resulting white precipitate was collected by filtration and recrystallized from ethanol. A white solid (0.40 g, 50%) was obtained.  $^1\text{H}$  NMR (300 MHz,  $\text{CDCl}_3$ ):  $\delta$  8.66 (s, 1H), 3.08 (t,  $J = 7.5$  Hz, 2H), 3.07 (t,  $J = 7.5$  Hz, 2H), 1.89 (m, 4H), 1.46-1.24 (m, 28H), 0.86 (t,  $J = 6.8$  Hz, 6H).  $^{13}\text{C}\{^1\text{H}\}$  NMR (75 MHz,  $\text{CDCl}_3$ ):  $\delta$  163.2, 160.5, 146.4, 145.7, 142.5, 136.0, 120.1, 35.1,

34.9, 31.9, 29.6, 29.5 (two peaks separated by 0.08 ppm), 29.4 (two peaks separated by 0.04 ppm), 29.3, 27.5, 22.7, 14.1 (8 C missing presumably due to overlapping peaks). HRMS (EI)  $m/z$  calcd. for  $C_{27}H_{43}N_3Br_2$ : 567.1824; Found: 567.1848. Elemental Analysis: (Calculated) C, 56.95; H, 7.61; N, 7.38; (Found): C, 57.05; H, 7.46; N, 7.36.

**10,13-Dibromo-2,3,6,7-tetrakis(*n*-decyloxy)dibenzo[*a,c*]phenazine (M3).**

2,3,6,7-Tetrakis(*n*-decyloxy)phenanthrene-9,10-dione (0.35 g, 0.42 mmol), 3,6-dibromobenzene-1,2-diamine(0.30 g, 1.1 mmol), and acetic acid (30 mL) were added to 100 mL 3-neck flask, and then the reaction mixture was refluxed overnight. After the reaction mixture was cooled to room temperature, 50 mL water was added, the resulting yellow precipitate was collected by filtration. The crude product was recrystallized from dichloromethane/acetone mixture. A yellow solid (0.35 g, 78%) was obtained.  $^1H$  NMR(300 MHz,  $CDCl_3$ ):  $\delta$  8.75 (s, 2H), 7.92 (s, 2H), 7.62 (s, 2H), 4.32 (t,  $J$  = 6.6 Hz, 4H), 4.26 (t,  $J$  = 6.6 Hz, 4H), 1.98 (m, 8H), 1.65-1.24 (m, 56H), 0.86 (t,  $J$  = 6.8 Hz, 12H).  $^{13}C\{^1H\}$  NMR (100 MHz,  $CDCl_3$ ):  $\delta$  152.5, 149.4, 142.6, 139.2, 131.8, 127.1, 123.8, 122.9, 109.3, 106.2, 69.6, 69.0, 31.9, 29.7 (two peaks separated by 0.03 ppm), 29.6 (two peaks separated by 0.09 ppm), 29.4, 29.2, 26.2 (two peaks separated by 0.04 ppm), 22.7, 14.1 (7C missing presumably due to overlapping peaks). MS (MALDI):  $m/z$  1063 ( $M^+$ ). Elemental Analysis: (Calculated) C, 67.78; H, 8.53; N, 2.63; (Found): C, 67.91; H, 8.61; N, 2.56.

**10,13-dibromo-2,3,6,7-tetrakis(*n*-decyloxy)dibenzo[*f,h*]pyrido[4,3-*b*]quinoxaline**

**(M4).**

2,3,6,7-Tetrakis(*n*-decyloxy)phenanthrene-9,10-dione-3,6-dibromobenzene-1,2-diamine (0.40 g, 0.50 mmol), 2,5-dibromopyridine-3,4-diamine (0.20 g, 0.75 mmol), acetic acid (0.5 mL), and ethanol (3 mL) were added to a 10 mL sealable vial, heated to 150 °C for *ca.* 25 min (standard mode, run time: 5 min, hold time: 20 min,  $P_{\max} = 110$  psi,  $\text{Power}_{\max} = 100$  W). The reaction mixture was cooled to room temperature, and then irradiated for another *ca.* 25 min using the same conditions as described above. The same reaction was carried out for another batch with the same amounts of starting materials and solvents. The reaction mixture from two vials were combined, and washed with aq.  $\text{NaHCO}_3$  solution. Then the organic phase was separated, and all the solvents were removed under reduced pressure. The crude product was purified by column chromatography (silica gel,  $\text{CH}_2\text{Cl}_2$  as eluent), a orange solid (0.66 g, 65%) was obtained.  $^1\text{H}$  NMR (300 MHz,  $\text{CDCl}_3$ , 0.01 M):<sup>23</sup>  $\delta$  8.70 (s, 1H), 8.54 (s, 1H), 8.51 (s, 1H), 7.47 (s, 1H), 7.45 (s, 1H), 4.25 (m, 8H), 1.99 (m, 8H), 1.63-1.30 (m, 56H), 0.90 (t,  $J = 7.8$  Hz, 12H).  $^{13}\text{C}\{^1\text{H}\}$  NMR (75 MHz,  $\text{CDCl}_3$ ):  $\delta$  153.4, 152.9, 149.5, 149.3, 146.5, 155.5, 145.2, 143.9, 141.6, 135.5, 128.2, 127.1, 122.2, 121.8, 120.2, 109.3, 109.0, 105.7, 105.5, 69.4, 69.3, 68.9, 31.9, 29.8, 29.7 (two peaks separated by 0.06 ppm), 29.6, 29.4, 29.3 (two peaks separated by 0.04 ppm), 29.2, 26.2 (two peaks separated by 0.03 ppm), 22.7, 14.1.

(24 C missing presumably due to overlapping peaks) MS (MALDI):  $m/z$  1064 ( $M^+$ ).

Elemental Analysis: (Calculated) C, 66.59; H, 8.43; N, 3.95; (Found): C, 66.74; H, 8.43; N, 3.93.

**P1.** To a pressure vessel were added 2,6-bis(tri-*n*-butylstannyl)-*N*-(3,4,5-tris(*n*-dodecyloxy)phenyl)-dithieno[3,2-*b*:2',3'-*d*]pyrrole (0.98 g, 0.70 mmol), 5,8-dibromo-2,3-di-*n*-decylquinoxaline (**M1**) (0.40 g, 0.70 mmol), dry THF (30 mL), and  $\text{PdCl}_2(\text{PPh}_3)_2$  (0.025 g, 0.04 mmol) in a  $\text{N}_2$ -filled glove box. The vessel was sealed after the additions and taken out of the glove box. The solution was stirred at 60-70 °C for 4 days. The solution was washed with aq. KF solution, and extracted with chloroform. Then the organic layer was separated, concentrated under reduced pressure, and dropped in methanol (*ca.* 500 mL), and the solid was filtered. The crude product was purified by Soxhlet extraction with methanol, acetone and hexanes each for 1 day. The obtained solid was re-dissolved into chloroform, and was precipitated into methanol again, a black solid (0.80 g, 93%) was obtained.  $^1\text{H}$  NMR (300 MHz,  $\text{CD}_2\text{Cl}_2$ ):  $\delta$  8.16 (br, 2H), 7.02-6.76 (br, 4H), 4.05 (br, 6H), 3.12 (br, 4H), 2.10–1.12 (br, 92 H), 0.91 (br, 15H). Elemental Analysis: (Calculated) C, 77.11; H, 10.20; N, 3.46; (Found) C, 76.57; H, 10.07; N, 3.42.

**P2.** To a pressure vessel were added 2,6-bis(tri-*n*-butylstannyl)-*N*-(3,4,5-tris(*n*-dodecyloxy)phenyl)-dithieno[3,2-*b*:2',3'-*d*]pyrrole (0.93 g, 0.67 mmol), 5,8-dibromo-2,3-di-*n*-dodecyl-pyrido[3,4-*b*]pyrazine (**M2**) (0.38 g, 0.67 mmol), dry THF (30 mL), and PdCl<sub>2</sub>(PPh<sub>3</sub>)<sub>2</sub> (0.024 g, 0.04 mmol) in a N<sub>2</sub>-filled glove box. The vessel was sealed after the additions and taken out of the glove box. The solution was stirred at 60-70 °C for 4 days. The solution was washed with aq. KF solution, and extracted with toluene. Then the organic layer was separated, and all the solvents were removed under reduced pressure. The obtained solid was dissolved into THF (*ca.* 20 mL), and was dropped into methanol (*ca.* 500 mL), and the solid was filtered. The crude product was purified by Soxhlet extraction with methanol, acetone and hexanes each for 1 day. The obtained solid was re-dissolved into chloroform, and was precipitated into methanol again. The solid after filtration was run through the silica gel plug using THF as eluent, followed by a SEC column chromatography (SX-1 bio-beads, THF as eluent). The solution was concentrated, and precipitated from methanol, a black solid (0.58 g, 72%) was obtained. <sup>1</sup>H NMR (300 MHz, CD<sub>2</sub>Cl<sub>2</sub>): δ 8.90-9.10 (br, 1H), 7.62 (br, 1H), 7.28 (br, 1H), 6.80-7.02 (br, 2H), 4.10 (br, 6H), 3.16 (br, 4H), 2.10–1.12 (br, 92 H), 0.91 (br, 15H). Elemental Analysis: (Calculated) C, 76.06; H, 10.11; N, 4.61; (Found) C, 75.11; H, 10.02; N, 4.34.

**P3.** To a pressure vessel were added 10,13-dibromo-2,3,6,7-tetrakis(*n*-decyloxy)dibenzo[*a,c*]phenazine (**M3**) (0.50 g, 0.47 mmol), 2,6-bis(tri-*n*-butylstannyl)-*N*-(3,4,5-tris(*n*-dodecyloxy)phenyl)-dithieno[3,2-*b*:2',3'-*d*]pyrrole (0.65 g, 0.47 mmol), dry THF (25 mL), and PdCl<sub>2</sub>(PPh<sub>3</sub>)<sub>2</sub> (0.017 g, 0.03 mmol) in a N<sub>2</sub>-filled glove box. The vessel was sealed after the additions and taken out of the glove box. The solution was stirred at 60-70 °C for 4 days. The solution was washed with aq. KF solution, and extracted with toluene. Then the organic layer was separated, concentrated under reduced pressure. The concentrated solution was dropped into methanol (*ca.* 500 mL); the resulting solid was filtered. The crude product was purified by Soxhlet extraction with methanol, acetone and hexanes each for 1 day. The solution extracted from hexanes was concentrated under reduced pressure, and dissolved into chloroform, and was precipitated into methanol again; a black solid (0.53 g, 66%) was obtained. <sup>1</sup>H NMR (300 MHz, THF-*d*<sub>8</sub>): δ 9.36 (br, 2H), 8.50-7.80 (br, 6H), 7.15 (br, 2H), 4.62-4.02 (br, 14H), 2.00-1.02 (br, 124 H), 0.90 (br, 21H). Elemental Analysis: (Calculated) C, 77.28; H, 10.20; N, 2.46; (Found) C, 76.83; H, 10.06; N, 2.49.

**P4.** To a pressure vessel were added 10,13-dibromo-2,3,6,7-tetrakis(*n*-decyloxy)dibenzo[*f,h*]pyrido[4,3-*b*]quinoxaline (**M4**) (0.44 g, 0.42 mmol), 2,6-bis(tri-*n*-butylstannyl)-*N*-(3,4,5-tris(*n*-dodecyloxy)phenyl)-

dithieno[3,2-*b*:2',3'-*d*]pyrrole (0.59 g, 0.42 mmol), dry THF (30 mL), and PdCl<sub>2</sub>(PPh<sub>3</sub>)<sub>2</sub> (0.015 g, 0.02 mmol) in a N<sub>2</sub>-filled glove box. The vessel was sealed after the additions and taken out of the glove box. The solution was stirred at 60-70 °C for 4 days. The solution was washed with aq. KF solution, and extracted with chloroform. Then the organic layer was separated, concentrated under reduced pressure. The concentrated solution was dropped into methanol (*ca.* 500 mL), and the solid was filtered. The crude product was purified by Soxhlet extraction with methanol, acetone and hexanes each for 1 day. The solution extracted from hexanes was concentrated under reduced pressure, and was precipitated into methanol again. The solid after filtration was run through the silica gel plug using THF as eluent, followed by a SEC column chromatography (SX-1 bio-beads, THF as eluent). The solution was concentrated, and precipitated from methanol, a black solid (0.53 g, 75%) was obtained. <sup>1</sup>H NMR (300 MHz, THF-*d*<sub>8</sub>): δ 9.42 (br, 1H), 8.80 (br, 2H), 8.40-6.80 (br, 4H), 6.70 (br, 2H), 4.62-3.86 (br, 14H), 2.00-1.10 (br, 124 H), 0.90 (br, 21H). Elemental Analysis: (Calculated) C, 76.53; H, 9.90; N, 3.28; (Found) C, 75.69; H, 9.90; N, 3.25.

### **Fabrication and Characterization of Thin Film Transistors.**

OFETs were fabricated and tested by Shree Prakash Tiwari in the Kippelen group at the Georgia Institute of Technology. OFETs were fabricated on heavily doped n-type silicon substrate (also serves as gate electrodes) with 200 nm thick thermally grown SiO<sub>2</sub>

as the gate dielectric, in top contact configuration. Ti/Au (10 nm/100 nm) metallization on the backside of the substrate was done to enhance the gate electrical contact. Firstly, the substrates were cleaned by O<sub>2</sub> plasma for 3 min. Surface treatment (with 5mM in toluene) was done by soaking the substrates in the *n*-butyl-trichlorosilane (BTS) or *n*-octyl-trichlorosilane (OTS) solution for 17 h in a N<sub>2</sub>-filled dry box. The substrates were rinsed with toluene, and annealed at 60 °C for 5 minutes. The capacitance of the BTS or OTS treated SiO<sub>2</sub> was about 16.2 nF/cm<sup>2</sup>. A thin layer of organic semiconductor was formed on the substrates by spin coating with a solution (10 mg/mL) in chlorobenzene. To remove solvent, the films were annealed at 90 °C for 30 minutes. 50 nm-thick Au was deposited through a shadow mask to act as top source/drain electrode. The prepared devices were post-annealed at 130 °C for 35 minutes inside N<sub>2</sub> glove box.

### **Fabrication and Characterization of Photovoltaic Cells.**

Photovoltaic cell were fabricated and tested by Jaewon Shim in the Kippelen group at the Georgia Institute of Technology. An ITO-coated glass (Colorado Concept Coating LLC) Si substrate, with resistivity of ~15Ω/sq, serves as an anode electrode. The ITO/Glass substrate was cleaned by immersing in the de-ionized water with detergent and rinsed with de-ionized water in an ultrasonic bath for 20 min, followed by ultrasonic cleaning using acetone and isopropanol for 20 min each sequentially. Nitrogen was used to dry the substrates after each of the last three baths. Next, SiO<sub>x</sub> (300 nm) is deposited on

cleaned ITO surface by electron beam deposition (AXXIS, Kurt J. Lesker) at a rate of 5 Å/S under the  $3.3 \times 10^{-7}$  Torr at room temperature. Prior to deposition of the hole conducting layer, the ITO/glass substrate with SiO<sub>x</sub> was cleaned with isopropanol through ultrasonication for 10 minutes and the surface was prepared by exposure to air plasma for 3 min. PEDOT:PSS (Baytron P VP AI 4083 PE FL) serving as a hole conductor was filtered through 0.45µm-pore-PVDF filters and spin-coated on the substrate at the speed of 5000 rpm for 1 min followed by 140 °C annealing step for 10 min in the atmosphere. The next fabrication step was solution-based film deposition. The mixtures of polymers/PCBM with different weight ratios were dissolved in chlorobenzene at the concentration of 20 mg/mL without any filtration. The solution was then spin-coated on to the active region at 1000 rpm and 1000 rpm for 1 min to give a film of 80-90 nm thickness. Each film deposition step was performed in the M-Braun nitrogen glove box. The substrate was loaded on the shadow mask for cathode and taken into thermal evaporation (SPECTROS, Kurt J. Lesker) connected with the glove box. And 200 nm Al electrode was deposited on the top of the active region at a rate of 10-20 nm/S under the  $5.0 \times 10^{-8}$  Torr at the room temperature. The sample was then annealed at 150°C for 25 minutes. Electrical properties were measured with a source meter (2400 Keithley) controlled by a LabVIEW program under nitrogen environment. For testing solar cell properties under illumination, filtered light from a 175 W Xenon lamp (ASB-XE-175EX, CVI) was used for broad light source with an irradiance of ~71-74 mW/cm<sup>2</sup>.

## 5.9 References

- (1) Gadisa, A.; Mammo, W.; Andersson, L. M.; Admassie, S.; Zhang, F.; Andersson, M. R.; Inganäs, O. *Adv. Funct. Mater.* **2007**, *17*, 3836.
- (2) Huo, L. J.; Tan, Z. A.; Wang, X.; Zhou, Y.; Han, M. F.; Li, Y. F. *J. Poly. Sci. Poly. Chem.* **2008**, *46*, 4038.
- (3) Kitazawa, D.; Watanabe, N.; Yamamoto, S.; Tsukamoto, J. *Appl. Phys. Lett.* **2009**, 95.
- (4) Lai, M. H.; Chueh, C. C.; Chen, W. C.; Wu, J. L.; Chen, F. C. *J. Poly. Sci. Poly. Chem.* **2009**, *47*, 973.
- (5) Liu, C. L.; Tsai, J. H.; Lee, W. Y.; Chen, W. C.; Jenekhe, S. A. *Macromolecules* **2008**, *41*, 6952.
- (6) Tsai, J. H.; Chueh, C. C.; Lai, M. H.; Wang, C. F.; Chen, W. C.; Ko, B. T.; Ting, C. *Macromolecules* **2009**, *42*, 1897.
- (7) Blouin, N.; Michaud, A.; Gendron, D.; Wakim, S.; Blair, E.; Neagu-Plesu, R.; Belletete, M.; Durocher, G.; Tao, Y.; Leclerc, M. *J. Am. Chem. Soc.* **2008**, *130*, 732.
- (8) Wu, P. T.; Kim, F. S.; Champion, R. D.; Jenekhe, S. A. *Macromolecules* **2008**, *41*, 7021.
- (9) Champion, R. D.; Cheng, K. F.; Pai, C. L.; Chen, W. C.; Jenekhe, S. A. *Macromol. Rapid Commun.* **2005**, *26*, 1835.
- (10) Lee, B. L.; Yamamoto, T. *Macromolecules* **1999**, *32*, 1375.
- (11) Gao, B. X.; Wang, M.; Cheng, Y. X.; Wang, L. X.; Jing, X. B.; Wang, F. S. *J. Am. Chem. Soc.* **2008**, *130*, 8297.
- (12) Lavigueur, C.; Foster, E. J.; Williams, V. E. *J. Am. Chem. Soc.* **2008**, *130*, 11791.
- (13) Ashraf, R. S.; Hoppe, H.; Shahid, M.; Gobsch, G.; Sensfuss, S.; Klemm, E. *J. Poly. Sci. Poly. Chem.* **2006**, *44*, 6952.
- (14) Edelmann, M. J.; Raimundo, J. M.; Utesch, N. F.; Diederich, F.; Boudon, C.; Gisselbrecht, J. P.; Gross, M. *Helv. Chim. Acta* **2002**, *85*, 2195.
- (15) Babudri, F.; Farinola, G. M.; Naso, F. *J. Mater. Chem.* **2004**, *14*, 11.
- (16) Micaroni, L.; Nart, F. C.; Hummelgen, I. A. *J. Solid State Electrochem.* **2002**, *7*, 55.
- (17) Reyes-Reyes, M.; Kim, K.; Carroll, D. L. *Appl. Phys. Lett.* **2005**, *87*, 3.
- (18) Thompson, B. C.; Frechet, J. M. J. *Angew. Chem. Int. Ed.* **2008**, *47*, 58.
- (19) Hoppe, H.; Niggemann, M.; Winder, C.; Kraut, J.; Hiesgen, R.; Hinsch, A.; Meissner, D.; Sariciftci, N. S. *Adv. Funct. Mater.* **2004**, *14*, 1005.
- (20) van Duren, J. K. J.; Yang, X. N.; Loos, J.; Bulle-Lieuwma, C. W. T.; Sieval, A. B.; Hummelen, J. C.; Janssen, R. A. J. *Adv. Funct. Mater.* **2004**, *14*, 425.
- (21) Yang, X. N.; van Duren, J. K. J.; Janssen, R. A. J.; Michels, M. A. J.; Loos, J. *Macromolecules* **2004**, *37*, 2151.
- (22) Mohr, B.; Enkelmann, V.; Wegner, G. *J. Org. Chem.* **1994**, *59*, 635.
- (23) Connelly, N. G.; Geiger, W. E. *Chem. Rev.* **1996**, *96*, 877.
- (24) Kenning, D. D.; Mitchell, K. A.; Calhoun, T. R.; Funfar, M. R.; Sattler, D. J.; Rasmussen, S. C. *J. Org. Chem.* **2002**, *67*, 9073.

## CHAPTER 6

### CONCLUSIONS

The research described in this thesis was focused on dithienopyrrole-based materials. The objectives of the research were: to synthesize a range of conjugated oligomers and polymers; to understand the structure-property relationships for these materials; and to assess their utility in organic electronic devices (OFETs, OPVs *etc*). The main focus of this thesis is on the synthesis, characterization, and properties of DTP-based copolymers - donor-donor copolymers in Chapter 3 and donor-acceptor copolymers in Chapters 4-5 - but the synthesis and characterization of a few oligomers and homopolymers were also described in Chapter 2.

In order to obtain solution-processable polymers with moderate to high molecular weights, efforts were paid to synthesize pure monomers and identify appropriate coupling methodologies, purification procedures as well as appropriate substituent patterns enabling facile solution processability of the materials. As described in section 3.2, the distannyl DTP derivatives can be obtained analytically pure after optimization of reaction conditions and careful purification; this is the first and important step to obtain polymers with moderate to high molecular weights. Stille coupling was used for the preparation of the polymers in Chapter 3-5, mainly due to the ease of synthesis and purification of distannyl DTP derivatives; the choice is also related to the results of trial polymerizations

mentioned in section 3.2. The low solubility of some polymers in common organic solvents was found to lead to problems in the purification and characterization of these materials. Although *N*-octyl or dodecyl-DTP-based donor-donor copolymers described in Chapter 3 are readily soluble in many medium-polarity organic solvents, the attempts to prepare soluble donor-acceptor copolymers in Chapter 4 and 5 based on *N*-alkyl DTPs were not successful. Use of a distannyl derivative of an alternative *N*-tri(alkyloxy)phenyl DTP can dramatically improve the solubility of the resulting polymers. It is also found that many factors, such as the choice of catalysts and solvents, and varying degrees of air exclusion, can affect the molecular weights of the resulting polymers, as described in section 5.2. It is worth noting that the degree of polymerization of the copolymers in Chapter 4 and 5 are much higher than the ones described in the trial polymerizations in section 5.2, as well as those of analogous polymers, such as **52a** in Figure 1.16, reported in the literature. This is presumably attributed to the improved solubility of the polymers in organic solvents and more efficient polymerization using optimized conditions.

After successful synthesis of these polymers, their structure-property relationships have been studied. Both optical and electrochemical properties of the polymers can be tuned by choosing different comonomers. In the case of donor-donor copolymers (copolymerized with thiophene, bithiophene, and fluorene), the absorptions,  $E_g$ , and estimated ionization potentials have slight variations when the co-monomers with DTP were varied. On the other hand, the optical and electrochemical properties of the

donor-acceptor copolymers in Chapter 4 and 5 were strongly influenced by the acceptors. The low-energy absorption bands in these copolymers have considerable donor-to-acceptor charge-transfer character, and when DTP is coupled with a very strong acceptor (benzobisthiadiazole), this band maximum is found at *ca.* 1.2  $\mu\text{m}$ , making this material one of the lowest bandgap solution-processible polymers reported to date. Both quantum-chemical calculations and the electrochemical properties of these copolymers suggest that the HOMO energy is only weakly dependent upon the choice of the acceptors, while the LUMO energy and the energy of the low-energy absorption band is strongly influenced by the acceptors, especially in the case of the copolymers in Chapter 4.

The potential utilities of these polymers in OFETs and OPVs were tested. For the OFET devices based on these copolymers, most of them only exhibited p-channel characteristics. One of the donor-donor copolymers (DTP with bithiophene) has shown relatively high hole mobility (up to  $4.8 \times 10^{-2} \text{ cm}^2/(\text{Vs})$  under ambient conditions), whereas the example with the strongest acceptor (benzobisthiadiazole) exhibited ambipolar field-effect characteristics. However, many OFET devices based on these materials exhibited relatively low on/off ratios ( $10^2$ - $10^3$ ). These on-off ratios (and in some cases values of the threshold voltage) are presumably due to adventitious aerial doping; the DTP materials are rather easily oxidized compared to many other thiophene-based materials according to electrochemical data. Bulk heterojunction

photovoltaic devices were fabricated based on blends of the polymers with PCBM. The unoptimized power conversion efficiencies of the polymers blended with PCBM were relatively low (<1%), however, after optimizations, efficiencies up to 1.4% were obtained in blends based on the selected polymers. It was found that in the blends based on one of the donor-donor copolymers (DTP with bithiophene), power conversion efficiency was dramatically increased upon annealing, and the increased crystallinity of the blends after annealing was supported by the morphology studies from AFM and XRD. Optimizations of the OPV devices were also carried out by varying the weight ratio with PCBM, as well as changing the solvents. The optimal performance based on the copolymer of DTP coupled with benzothiadiazole was obtained when spin-coated using chlorobenzene and blended with PCBM in a 1:3 weight ratio. Morphology differences were observed using AFM when the blends were processed from different solvents. A 1:3 weight ratio was also found to be the optimum ratio for the blends for one polymer (DTP with dibenzo[*a,c*]phenazine) in Chapter 5, and the compositional ratio of the blends influence the film morphology, external quantum efficiency, as well as the OPV power conversion efficiencies of the blends. However, OPV devices based on the blends of another polymer (DTP with dibenzopyridoquinoxaline in Chapter 5) with PCBM with 1:6 weight ratio gave better performance than the other measured devices based on the same materials with other ratios. All these studies could provide useful information for the further studies of solar cells based on DTP-containing polymers. Devices based on the copolymers

containing thiadiazolo[3,4-*g*]quinoxaline and benzobisthiadiazole exhibited very low efficiencies, presumably due to the mismatched energy levels with PCBM; however, they might act as active components in tandem cells due to their broad absorbance in the near-IR.

These polymers might have utilities in other applications. For example, spectroelectrochemical measurements of the copolymers in Chapter 4 indicated they can be either electrochemically p-doped or n-doped at moderate potentials, suggesting that the polymers could have potential use in electrochromic devices. These materials may also be useful for optical limiting in the near-IR region via a charge-transfer mechanism in combination with a suitable acceptor, or through other mechanisms. Furthermore, some of donor-acceptor copolymers in Chapter 4 and 5, because they have broad absorption in the near-IR, they may have potentials to be candidate materials used as near-IR photodectors.

In Chapter 2, DTP-based oligomers (two dimers and a trimer) along with a homopolymer were synthesized by Pd-catalyzed couplings and characterized in both their neutral and chemically oxidized forms. The extended conjugation along the DTP main chain can alter their optical and electronic properties. Also a DTP homopolymer was successfully synthesized by electropolymerization, the changes in the spectroelectrochemistry of the electro-polymerized DTP homopolymer is very similar as that observed in the homopolymer synthesized by Stille coupling upon chemical

oxidization; this suggested that both chemical and electrochemical methods can lead to similar degree of oxidation in the DTP homopolymers. Similarity of radical cation spectra for trimer and for polymer, but different from that for dimer, suggests that a polaron is delocalized over *ca.* three DTP repeat units. Future work can be continued to study the delocalization of the radical cations in these compounds by other techniques, such as Electron Paramagnetic Resonance.

The research in this thesis provides some useful information for the future work on DTP-based materials, and, more generally, electron-rich thiophene-based conjugated polymers. DTP is a relatively electron-rich moiety that more easily to be oxidized than many analogous thiophene building blocks of comparable conjugation length, such as bithiophene and dithienothiophene; incorporation of this electron-rich moiety into conjugated oligomers and polymers has both advantages and disadvantages. Due to the strong electron-donating ability, the incorporation of this building block into donor-acceptor copolymers often leads to the formation of low-energy absorption bands that are seen at longer wavelengths than in structurally similar copolymers using other donors, such as thiophene, carbazole, and fluorene. The better coverage of the solar spectrum may allow them to be good candidates as electron donors in organic solar cells in conjunction with PCBM. As seen in the OPV results in this thesis, moderate performance were achieved for some optimized devices, and the power conversion efficiencies of the devices may be further improved by further optimization, such as using

the C<sub>70</sub> analogue of PCBM, or annealing. More D-A copolymers based on DTPs can be designed if careful consideration is given to the relative energy levels of the new materials and PCBM. Even though some of the polymers in this thesis may not be suitable for solar cells in conjunction with PCBM due to the mismatching energy levels with PCBM, it is very possible that they can be used in other applications. For example, they may serve as materials for near-IR photodetectors due to their absorbance in the near-IR regions. They may also be useful in non-linear optical applications, such as optical limiting. On the other hand, these materials suffer limitations for certain electronic applications. Based on the results from OFET devices, the devices made from these DTP-containing polymers often have low on/off ratios, presumably due to aerial oxidation due to their low ionization potentials. However, DTP-based oligomers may be an alternative choice that can take advantages of the fused-thiophene structure, but not suffer from the issue from the low ionization potentials of the polymers.

To be more general, the research described in this thesis could be broadly useful for the future design and synthesis of conjugated polymers for organic electronics. First of all, the synthetic efforts shown here indicated that many factors, such as substituents, reaction conditions and environments can affect the molecular weights of the polymers and, thus, the optical and electronic properties of the materials. Therefore, extended and systematic “trial and error” study will be necessary for each new series of conjugated polymers. The research in this thesis showed that the copolymerization with different co-monomers was

an effective approach to finely tune the optical and electronic properties of the resulting polymers; therefore, specific properties can be obtained by careful choices of the building blocks or modifications of the substituents. However, it is difficult to control or predict the occurrences of aggregation effect or interchain interactions in the polymers, especially in the solid states. More attention should be paid to studying the morphology changes of the thin films under different conditions, eg. with or without annealing. In order to utilize the materials in practical applications in OFETs and OPVs, more careful consideration is needed regarding to the relative energy levels of the materials and the work functions of the electrodes, or the energy levels of the other materials in conjunction with, such as PCBM. Moreover, the study in this thesis indicated that morphology changes have been observed when altering the weight ratios of the polymers and PCBM, or changing the processing solvents, or upon annealing. Although it is difficult to directly link the morphology changes to the device performance, more detailed and thorough studies of the morphology obtained under different conditions will be useful to understand deeply the solid-state electronic properties of the polymers. Furthermore, the applications of these polymers are not limited to organic electronics. They could have potential applications in other devices, such as electrochromic devices, or photodetectors, but structural modifications may be needed to meet the materials requirements for those applications.

## List of Publications

1. Zhang, X.; Steckler, T. T.; Dasari, R. R.; Hwang, J.; Ohira, Shino; Potscavage, W.; Tiwari, S. P.; Coppée, S.; Ellinger, S.; Barlow, S.; Brédas, J. L.; Kippelen, B.; Reynolds, J. R.; Marder, S. R.. “Dithienopyrrole-based donor-acceptor copolymers: low band-gap materials for charge transport, photovoltaics and electrochromism”, *J. Mater. Chem.*, accepted.
2. Steckler, T. T.; Zhang, X.; Hwang, J.; Honeyager, R.; Ohira, S.; Zhang, X.; Grant, A.; Ellinger, S.; Odom, S. A.; Sweat, D.; Tanner, D. B.; Rinzler, A. G.; Barlow, S.; Brédas, J. L.; Kippelen, B.; Marder, S. R.; Reynolds, J. R.. “A spray-processable, low bandgap, and ambipolar donor-acceptor conjugated polymer”, *J. Am. Chem. Soc.*, **2009**, *131*, 2824.